DEEP SEISMIC EVIDENCE OF LATE MIDDLE
PROTEROZOIC RIFTING BENEATH THE
KALAHARI, WESTERN BOTSWANA

BRIAN H. HOFFE

Deep Seismic Evidence of Late Middle Proterozoic Rifting Beneath the Kalahari, Western Botswana

by

Brian H. Hoffe

A thesis submitted to the

School of Graduate Studies

in partial fulfilment of the

requirements for the degree of

Master of Science

Department of Earth Sciences
Memorial University of Newfoundland

April 1996

St. John's   Newfoundland

ABSTRACT

The full processing of seven reconnaissance, deep seismic reflection profiles recorded in western Botswana reveal the presence of a single, deep basin with a relatively uniform fill of 12 to 15 km of sedimentary rocks underlain by a mid to lower crust which shows considerable structure and reflectivity. Much of western Botswana falls within the broad physiographic region known as the Kalahari where much of the bedrock geology is concealed by Cretaceous to Recent Kalahari sands making regional tectonic interpretations difficult. Potential field data suggested the existence of deep sedimentary basins which prompted the Government of Botswana, with assistance from Petro-Canada International Assistance Corporation (PCIAC), to acquire approximately 1,000 km of 12 to 15 fold deep seismic reflection data in the western Kalahari region to evaluate its petroleum potential. A followup well drilled to a total depth of approximately 4 km along one of these profiles showed that a majority (> 2 km) of the rocks are sedimentary and of late Proterozoic (Ghanzi?) to early Cambrian (Nama) age. The stratigraphic break between the rocks of the Nama Group and those of the Permo-Carboniferous - Jurassic Karoo Supergroup is marked by a major unconformity and represents a considerable hiatus ($\approx$ 200 - 300 Ma). The gross lithologic nature of "bright" mid to lower crustal reflectors is explored in a qualitative fashion by examining possible correlations between the potential field anomalies and these zones of increased reflectivity. These seismic data also indicate the possible presence of large-scale extensional structures suggestive of continental rifting.

ISBN   0-612-17603-7

Canadä

These extensional structures, along with an ^{40}Ar-^{39}Ar date of 1,071.7 ± 11.1 Ma from a gabbroic body forming part of the Kalahari Line, and a series of continental rift sequences exposed along the northern and western fringes of the Kalahari region, all provide evidence of a widespread late Middle Proterozoic rifting event affecting much of the Kalahari region. This rifting may have marked the disassembly of a proposed Proterozoic supercontinent.

ACKNOWLEDGEMENTS

TABLE OF CONTENTS '

LIST OF TABLES

LIST OF FIGURES

1 INTRODUCTION

1.1 Location

Botswana is a landlocked nation located in the centre of the south African subcontinent and has international boundaries with South Africa, Zimbabwe, Zambia and Namibia. The location of Botswana and its boundaries with neighbouring southern Africa nations is illustrated in Figure 1.1. The country covers an area of approximately 582,000 km² with much of it falling within the physiographic region known as the Kalahari - part of a continental plateau of generally low relief which extends from Angola and Zambia in the north. As a consequence, much of the geology of Botswana's western region is concealed by the sands of the Kalahari making regional tectonic interpretations difficult. What is known of the geology has largely been derived from structural, sedimentological and geochronological studies of sparse and isolated outcrop and regional scale geophysical surveys, particularly aeromagnetic.

1.2 Geological Setting

The general geological setting of Botswana is illustrated in Figure 1.2. It is essentially defined by a core of Archean cratonic nuclei represented by gneisses, granitoids and greenstones of the Kaapvaal and Zimbabwe Provinces which are separated by the Limpopo Province, an intervening mobile belt, also of Archean age. These Archean provinces are surrounded by Proterozoic and younger Palaeozoic fold belts of the Namaqua and Damara Provinces. Late Permian tectonism associated initially with
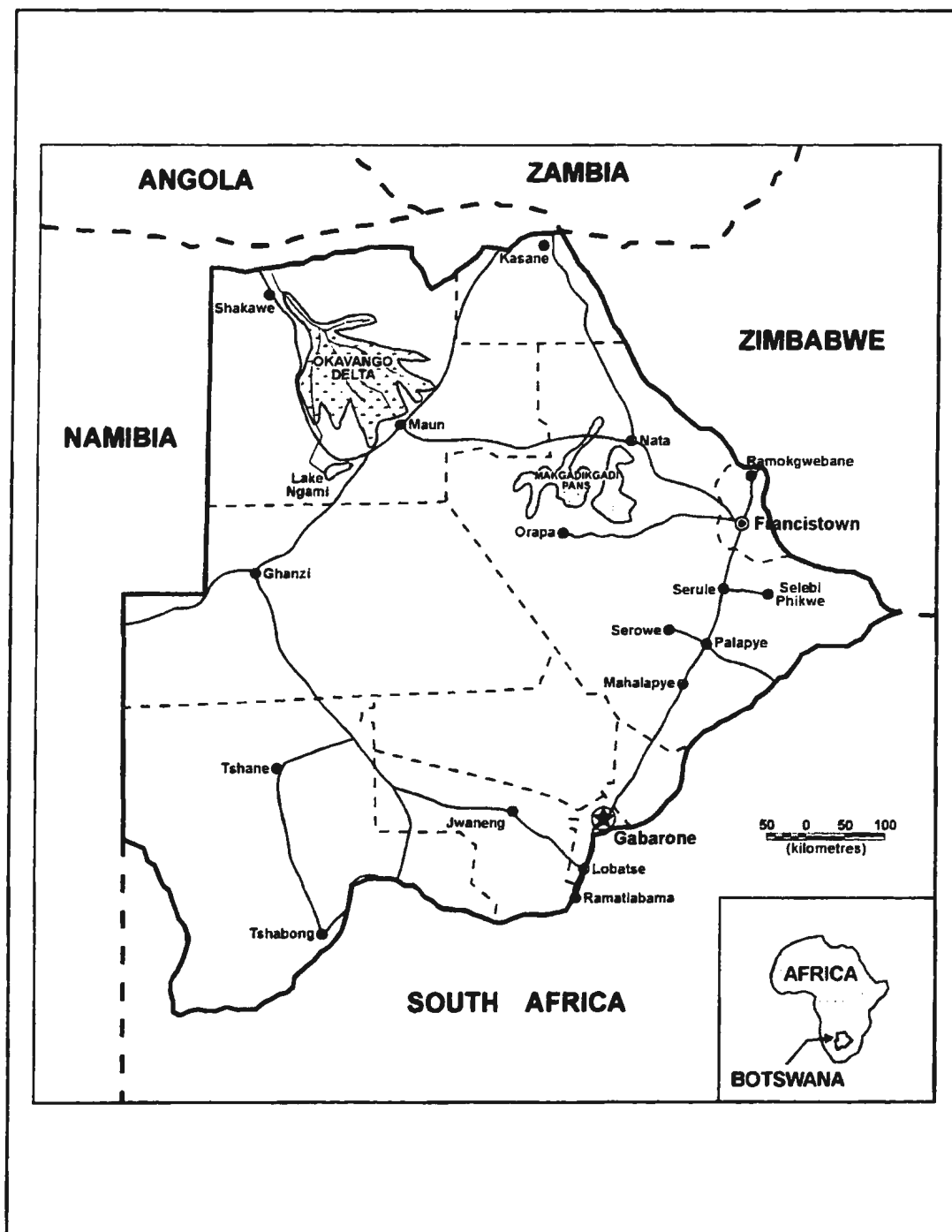
Figure 1.1   Location map of Botswana showing its general geography and international boundaries with neighbouring southern Africa nations.

Figure 1.2   Map outlining the general geology of southern Africa and the location of the seismic reflection profiles in Botswana (after Hall *et al.*, 1990).

LEGEND

☐ Late Mesozoic - Recent Sediments

☐ Late Paleozoic - Mesozoic Cover

☐ Paleozoic Fold Belts

☐ Proterozoic Fold Belts

☐ Archean Cratonic Nuclei

Kalahari Cover

Zimbabwe Province

Ghanzi-Chobe Fold Belt

Damara Province

Limpopo Province

Kaapvaal Province

Kheis Subprovince

Namaqua Province

Karoo Cover

100 0 100 200
(kilometres)
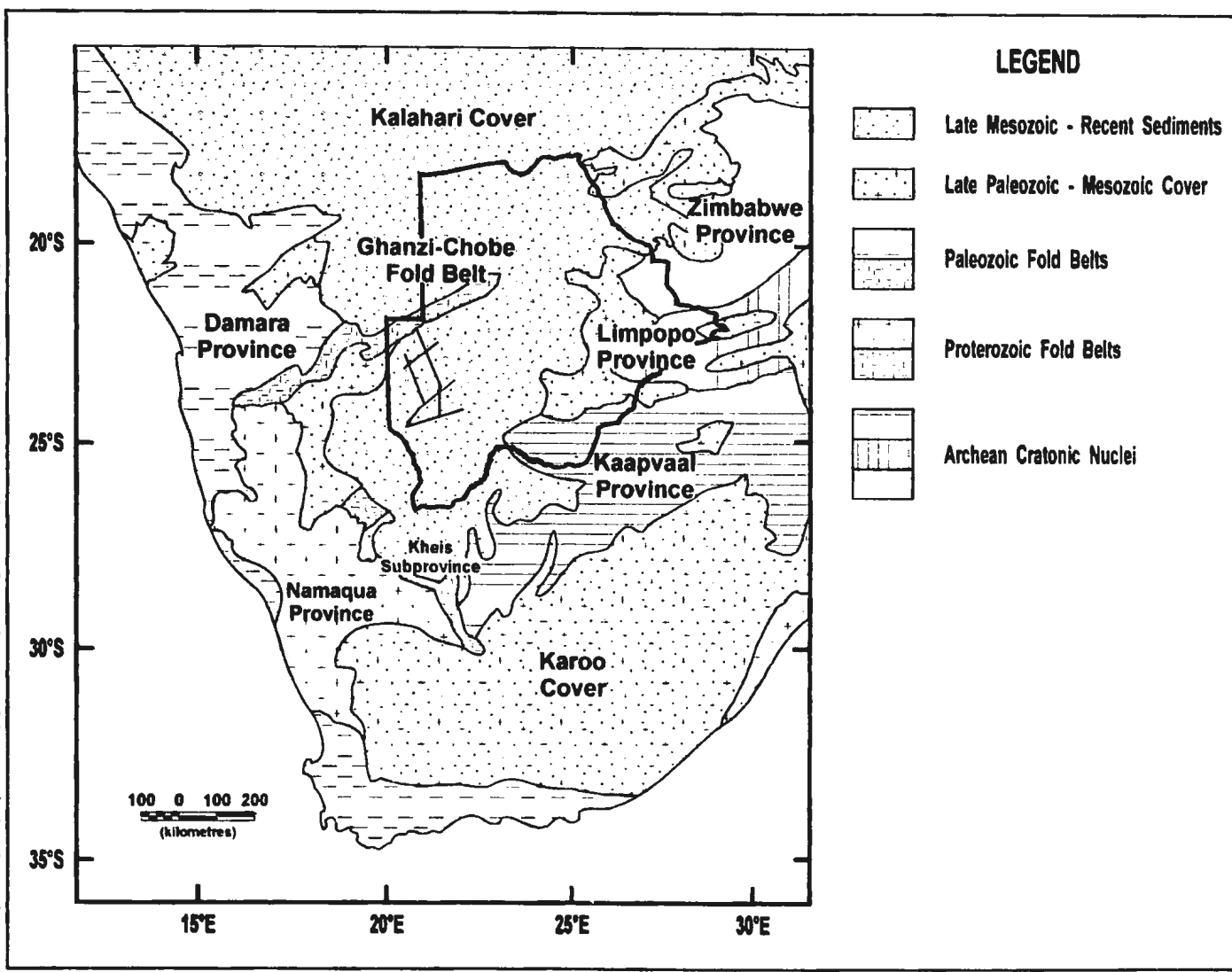
convergence at the edge of the Gondwanan continent, followed by the Jurassic to Cretaceous breakup of Gondwana which led to the creation of the South Atlantic and Indian Oceans, resulted in widespread Permo-Carboniferous to Jurassic Karoo sedimentation in the continental interior terminated by extensive mafic volcanism (Hall *et al.*, 1990; Bally *et al.*, 1989). This was followed by late Cretaceous to Recent deposition of the extensive and undeformed cover of the Kalahari Basin. It is this Mesozoic to Recent Karoo and Kalahari sedimentary cover which extensively masks the older rocks of western Botswana making the use of geophysical methods essential tools in exploring the pre-Karoo, subsurface geology of the Kalahari region.

1.3   Previous Work

The 1975-77 National Reconnaissance Aeromagnetic Survey of Botswana was one of the first regional geophysical surveys of the Kalahari in western Botswana. A significant and important outcome of this survey was the recognition of the Kalahari Line (**K-K'** of Figure 2.2), a relatively narrow, north-south magnetic lineament characterized by strong, positive anomalies and great lateral continuity (Reeves and Misener, 1988; Reeves and Hutchins, 1982; Reeves, 1978). With the knowledge of an early Proterozoic fold and thrust belt exposed farther to the south in the northern Cape Province of South Africa, initial interpretations of the aeromagnetic data from the Kalahari Line suggested that it represented a suture marking the Proterozoic collision of an oceanic "plate" to the west with a continental "plate" to the east (Reeves, 1978). Based on this interpretation, the

strong positive anomalies associated with the Kalahari Line would be the result of the obduction onto, and preservation of oceanic material on, an ancient continental margin during collision. Thus the Kalahari Line would represent the westernmost edge of the Archean Kaapvaal craton which is exposed or buried at shallow depth to the east.

West of the Kalahari Line the magnetic anomaly pattern is characterized by a sequence of pronounced linear, SW-NE trending anomalies with wavelengths of 50 km or more which terminate against this prominent north-south feature. This anomaly pattern would imply the deep burial (> 10 km) of magnetic basement beneath a non-magnetic cover. Reeves (1978) originally proposed the existence of two separate and distinct basins west of the Kaapvaal craton possibly separated by a basement high, as suggested by the change in amplitudes of the magnetic and gravity anomaly patterns, within the region of 23° 30'S. He named the northernmost basin the Ncojane Basin and the one farther to the south the Nosop Basin. Although both basins were thought to contain thicknesses of non-magnetic sediment in the range of 10-15 km, the Nosop Basin was distinguished from the Ncojane Basin by the highly magnetic character of the basement rocks forming its floor.

This interpretation encouraged the Government of Botswana, with assistance from Petro-Canada International Assistance Corporation (PCIAC), to collect approximately 1000 km of 12 to 15 fold multichannel seismic reflection data within this region in 1987 and 1988. The location of these seismic lines is indicated in Figure 1.2. The reconnaissance seismic reflection survey was designed to evaluate the basins' petroleum potential with a main objective of determining the overall thickness of the sediments and

any stratigraphic boundaries and/or intrabasinal structure (Hall *et al.*, 1989). Indeed, the distinctive aeromagnetic anomaly pattern of the Nosop/Ncojane basins played a major role in the siting of the seismic lines which were sited to provide regional coverage of both basins and the postulated basement high that separated them.

Preliminary interpretations of these deep seismic data by Wright and Hall (1990) and Hall *et al.* (1990) suggested that the Kalahari Line does not mark the western limit of the Kaapvaal craton. Seismic lines orientated along the SW-NE strike of the major aeromagnetic anomalies reveal thinning of the sedimentary section northeastwards approaching the Kalahari Line and clearly display a thickening of the crust eastwards across the Kalahari Line. Based on these observations, Wright and Hall (1990) interpreted the Kalahari Line as representing a hinge line for sedimentary deposition that might be associated with either an Archean or Proterozoic rifted margin of the Kaapvaal craton. East of the Kalahari Line the craton retained its original thickness, while to the west, the craton was thinned by rifting so that an extended Kaapvaal crust underlies the basin area. Another important recognition derived from the seismic data was that only one large basin of relatively uniform depth (12 to 15 km), rather than the two separate basins originally interpreted by Reeves (1978), exists west of the Kalahari Line (Hall *et al.*, 1990; Wright and Hall, 1990).

1.4   Purpose and Scope

The focus of this thesis is the full processing of all seven deep reflection seismic lines

recorded within the Nosop/Ncojane region and a re-examination of their interpretation within the "known" regional tectonic framework of this enigmatic area of the south African subcontinent. Although the quality of the initially processed lines used for the earlier interpretations (Hall *et al.*, 1990; Wright and Hall, 1990) is quite good, full processing was carried out with inclusion of the shallower data (< 5 s TWT) which, until recently, was proprietary as it formed part of the confidential assessment of the regional petroleum potential. Also, as part of the processing, phase-shift migrations of all seven lines were performed which, in the past, has proven to be difficult due to the lines' crossing closely-adjacent structures of different strike (Hall *et al.*, 1990). These migrations have been most helpful in better imaging some of the more complex structures present in the deep seismic data and worked particularly well in enhancing structures associated with a buried fold and thrust belt which is present on one of the deep seismic lines. In addition to the processing, a wealth of geological information obtained from a deep exploratory borehole ($\approx$ 4,000 m total depth) drilled along one of the seven reflection profiles has recently become available through open files. This has provided several geological constraints for this interpretation which were unavailable in previous interpretations.

Of primary concern to this present interpretation is the examination of the possible link between the nature of the basement magnetization, indirectly expressed by the magnetic anomaly patterns, and zones of "bright" basement reflectors seen in the deep seismic data. The primary rationale for this reconnaissance seismic reflection programme

was to evaluate the petroleum potential of two, *presumed*, major basins rather than the single, large basin the deep seismic data later revealed. It was the magnetic anomaly pattern in the region of 23° 30'S which made Reeves (1978) suggest possible closure of the Ncojane Basin to south. If indeed the anomaly pattern present in this region is generated by the deep basement, then the seismic data indicate that it must be due to lateral magnetisation contrasts within the basement itself rather than to structural relief on its top surface. Alternatively, the anomaly pattern may be associated with the presence of magnetic material within the sedimentary section itself. These ideas are explored in a qualitative fashion within the present interpretation.

1.5   Methodology

Chapter 2 provides the geological setting of western Botswana, beginning with a discussion of its lithostratigraphy. A tentative tectonostratigraphic chart is presented and is used to summarize the spatial and temporal relationships between the major structural provinces of the "greater" western Botswana region. This is followed by a discussion of the Proterozoic structures found in the rocks presented in the tectonostratigraphic chart. Finally, a possible scenario for the fragmentation of a postulated Late Proterozoic supercontinent with focus on the southern Africa region is presented. This provides an insight into the gross tectonics that were at play during this critical time period in the evolution of the southern Africa subcontinent.

Chapter 3 introduces the deep seismic reflection data set and describes, in some detail,

the processing sequence utilized for its processing. The theory behind each of the processors is very briefly summarized and, in some cases, the algorithm employed by a processor is discussed to provide a better understanding of its exact function. The final unmigrated, time and depth migrated sections are presented.

Chapter 4 deals with the interpretation of the seismic data beginning with the geological information derived from the deep exploratory borehole drilled along one of the seismic profiles. This information is used to place constraints on the ages and thicknesses of various stratigraphic units present in the uppermost part ($\leq$ 4 km) of the basin. This is followed by a general description of the dominant patterns of reflectivity common to all of the seismic lines with the stronger and more laterally coherent reflection events being systematically labelled. The main structural and stratigraphic features evident on each of the lines are then described (with reference to the previously labelled reflectors) and the similarities and differences between these features is discussed. The possible link between the highly reflective zones seen in the basement and the anomaly patterns apparent in the aeromagnetic data is then explored in a qualitative way. Also, detailed gravity data collected within this area are presented and its relationship to the deep seismic and aeromagnetic data is discussed. Finally a synthesis of all the geological and geophysical information previously outlined is presented. The synthesis offers possible scenarios for the lithostratigraphic content of both the sedimentary basin and underlying basement as well as for the geological evolution of the area as a whole.

Chapter 5 provides a synopsis of the major findings.

2 GEOLOGICAL SETTING

Southern Africa is divided into a number of geological provinces based on geographical identity and the age of the last "major" tectonothermal event that is recorded by isotope geochronology. There are three Archean and three Proterozoic provinces and these are illustrated in Figure 2.1. How exactly they are defined and where and what their boundaries are, are matters of current debate and research. Nevertheless, they provide a useful first approach to understanding the tectonic development of southern Africa. Recognition of these provinces and their boundaries is particularly difficult in southwestern Botswana because the widespread cover of young Karoo and, especially, recent Kalahari sand limits exposure of older rocks, leading to reliance on sparse outcrop, a few wells and interpretation of potential field data.

The Kaapvaal, Limpopo and Zimbabwe Provinces are of Archean age and represent stable continental nuclei onto which subsequent provinces have accreted. The Early Proterozoic Kalahari Province evolved along the western flanks of the Archean provinces between 2,000 and 1,700 Ma. The Middle Proterozoic Namaqua Province is a broad region of high grade metamorphism which extends for some 2,000 km across the southern flank of the Kaapvaal Province and has a 1,200 to 900 Ma metamorphic-plutonic history. The Late Proterozoic to Early Palaeozoic Damara Province forms part of the southernmost extension of the Pan-African cycle ($\approx$ 1,000 to 500 Ma) of tectonothermal crustal reorganization and consists of a north to northwest-trending coastal branch as well as a northeast-trending intracratonic arm (Henry *et al.*, 1990).
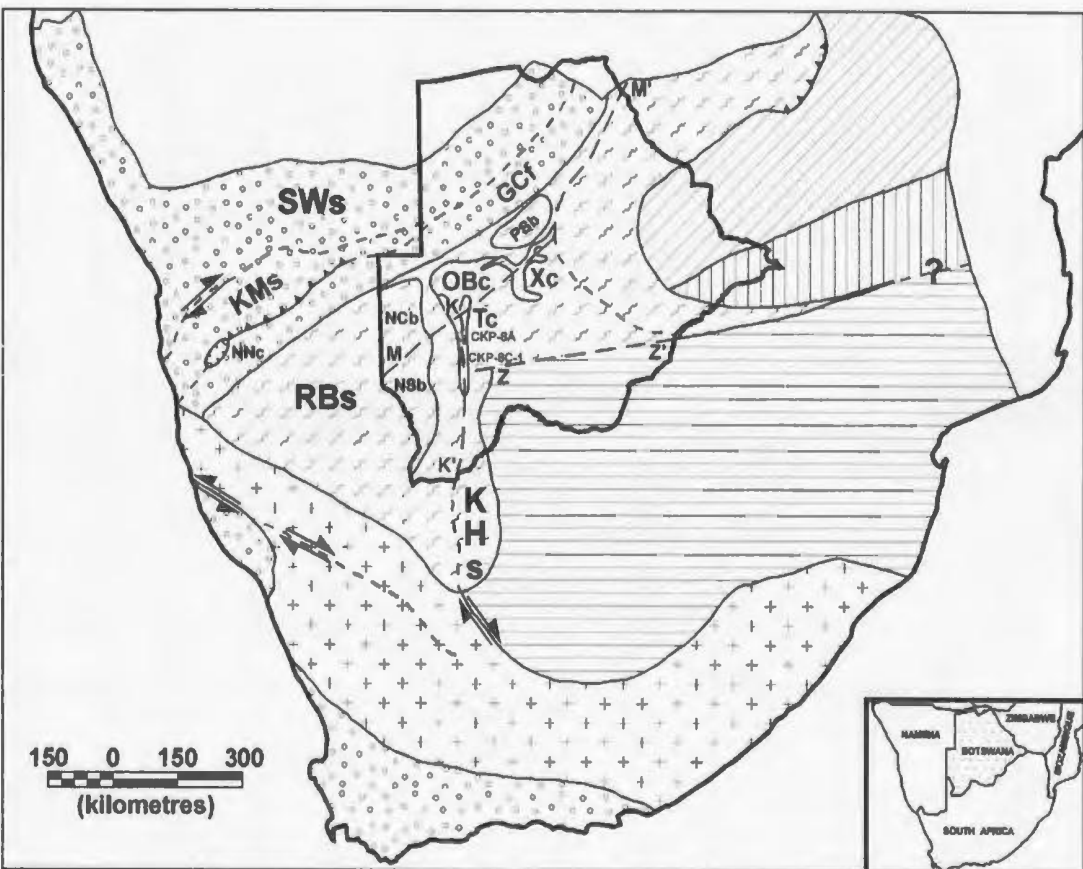
LEGEND

Late Proterozoic - Early Paleozoic

Damara Province

KMs = Khomas Subprovince
SWs = Swakop Subprovince
NNc = Naukluft Nappe Complex
GCf = Ghanzi-Chobe Fold Belt

Middle Proterozoic

Namaqua Province

Early Proterozoic

Kalahari Province

KHs = Kheis Subprovince
NCb = Ncojane Basin
NSb = Nosop Basin
OBc = Okwa Basement Complex
PSb = Passarge Basin
RBs = Rehoboth Subprovince
Tc = Tshane Mafic Complex
Xc = Xade Mafic Complex

Archean

Kaapvaal Province

Limpopo Province

Zimbabwe Province

Geophysical Lineaments

K-K' = Kalahari Line
M-M' = Makgadikgadi Line
Z-Z' = Zoetfontein Fault
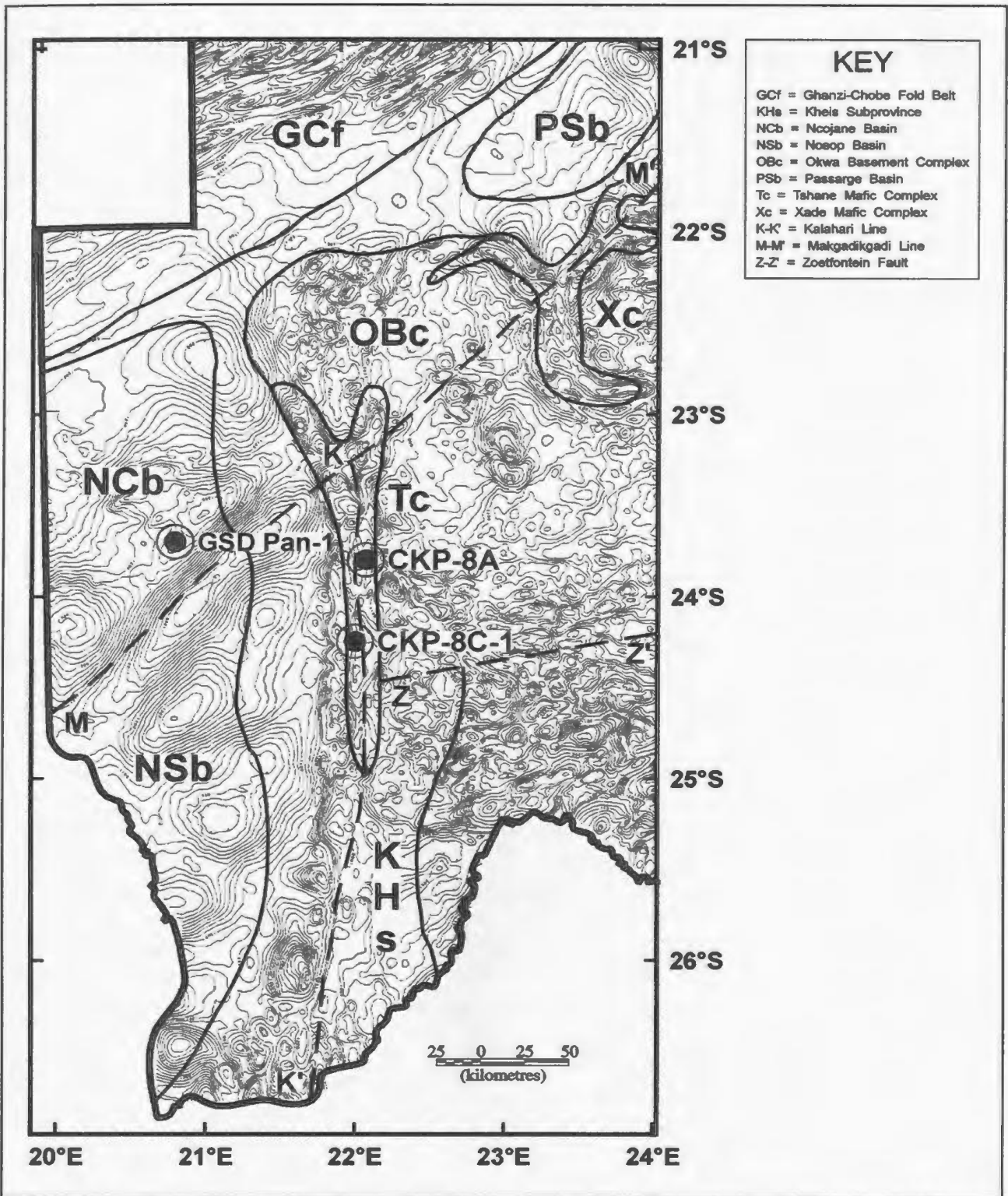
Figure 2.2   Total intensity aeromagnetic anomaly map of southwestern Botswana. Note the change in character of the anomalies west of the Kalahari Line (**K-K'**).

The primary foci of this thesis are the Proterozoic provinces of southwestern Botswana which, for the most part, are obscured by rocks of the Cenozoic "Kalahari Beds" and the Late Paleozoic to Middle Mesozoic Karoo Supergroup. However, the qualitative interpretation of regional geophysical surveys, particularly aeromagnetic, has led to the division of the basement into a number of tectonic elements on the basis of distinct geophysical character (Reeves, 1978; Hall *et al.*, 1989). The aeromagnetic data for western Botswana, as well as the interpreted structural elements and the discontinuities that separate them, are illustrated in Figure 2.2.

2.1   Stratigraphy

Figure 2.3 presents a tentative tectonostratigraphic chart for western Botswana and environs. This chart provides a generic synthesis of the geology contained within the greater western Botswana region from the Kaapvaal Province in the southeast to the Damara Province in the northwest. More importantly, however, it is helpful in providing a pictorial summary of the crustal evolution which occurred within this broad region of the southern African subcontinent.

Brief descriptions of the lithostratigraphy contained within each of the structural provinces of the greater western Botswana region are now presented from oldest to youngest with possible correlations between these regions also discussed.
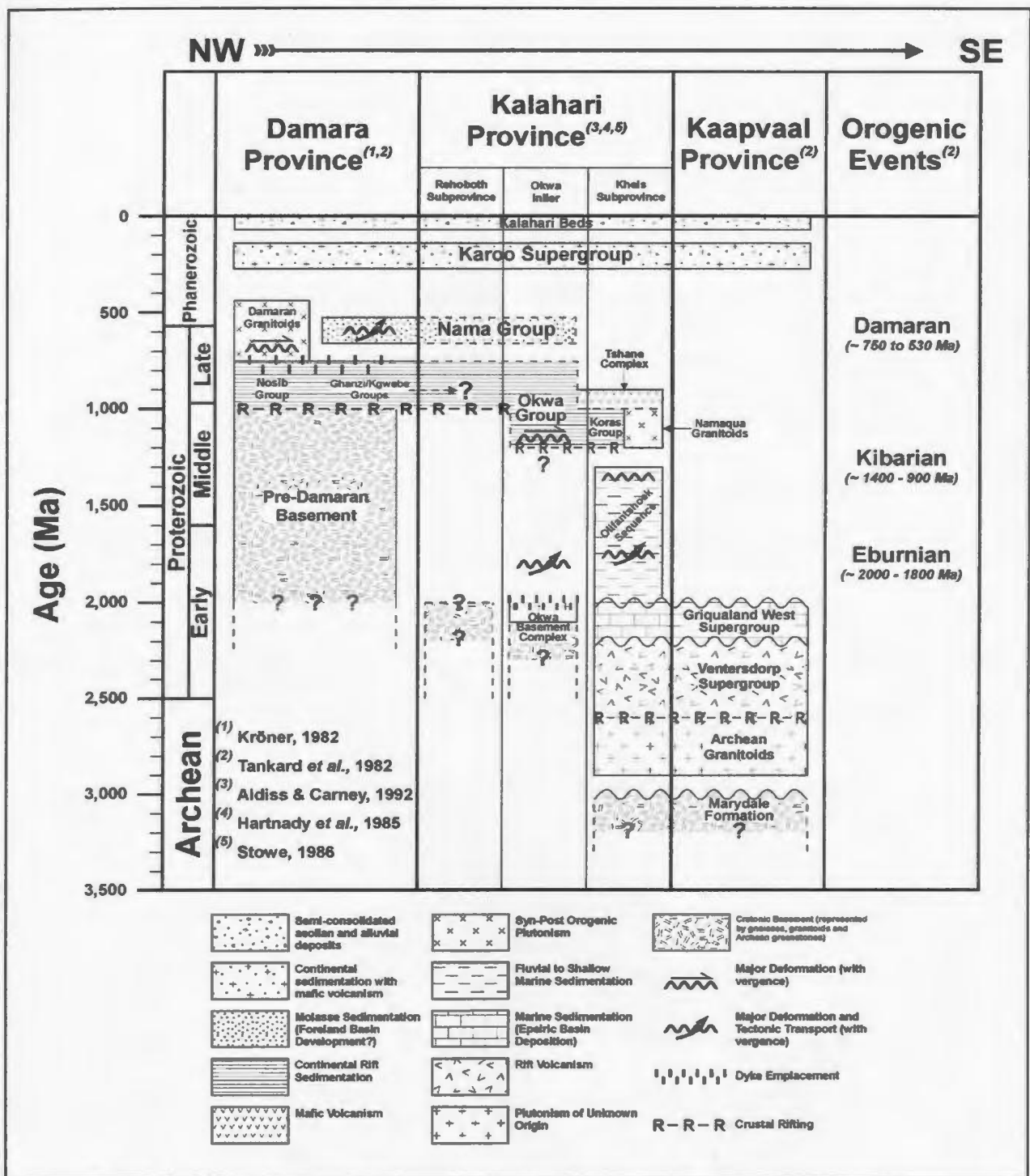
Figure 2.3 Tentative tectonostratigraphic chart for western Botswana and environs. Note the northwest younging of the crust from the Kaapvaal Province to the Damara Province.

2.1.1 Archean

The Marydale Formation is an Archean greenstone belt and represents the oldest unit exposed in the Kaapvaal Province and the adjoining Kheis Subprovince (**KHs** of Figures 2.1 and 2.2) of the northern Cape Province of South Africa. Where exposed, the thickness of the Marydale Formation is estimated to be about 8 km. Pb-Pb radiometric dating of this greenstone belt has yielded an age of 3,000 Ma (Tankard *et al.*, 1982). Late Archean granitoids intrude the Marydale greenstones and the oldest of these has been dated at 2,900 Ma (Burger and Coertze, 1973).

2.1.2 Early Proterozoic

The Ventersdorp Supergroup is a volcano-sedimentary sequence which nonconformably overlies the Archean granitoids in both the Kaapvaal Province and the Kheis Subprovince. The Ventersdorp succession exceeds 8 km in thickness and is primarily comprised of basaltic, dacitic and rhyolitic lavas (> 2 km) interbedded with agglomerate, subgreywacke and conglomerate, and subordinate shale and limestone (Tankard *et al.*, 1982). U-Pb radiometric ages determined from the Ventersdorp Supergroup fall into two groups clustered around 2,300 Ma and 2,500 to 2,700 Ma, respectively (Van Niekerk and Burger, 1978).

Overlying the Ventersdorp Supergroup unconformably are the rocks of the Griqualand West Supergroup. The thickness of the Griqualand West Supergroup is estimated to be 4.5 km and is thought to have been deposited in a vast epeiric basin, covering at least 5.0

$\times$ 10^5 km^2 of the Archean Kaapvaal Province (Tankard *et al.*, 1982). The lithology of the Griqualand West Supergroup is represented by a basal quartz arenite grading into dolomite, banded iron-formation with slate and laminated mudstone, capped by andesitic tuff and lava. Sedimentation and volcanism probably initiated after 2,300 Ma and had ceased by about 2,100 Ma.

A large percentage of the Kheis Subprovince within Botswana (**KHs** of Figure 2.2) is buried beneath Kalahari and Karoo cover but isolated exposures and borehole data show a belt of tightly folded metasedimentary rocks associated with the Olifantshoek Sequence which extend southward into the northern Cape Province of South Africa (Hartnady *et al.*, 1985; Levin, 1981; Reeves, 1978). The Olifantshoek Sequence consists primarily of quartzites, phyllites and amphibolites which are separated from the underlying rocks by a major disconformity (SACS, 1980). Because of the intense folding and thrusting within this metasedimentary succession, the total thickness of the Olifantshoek Sequence is uncertain (Stowe, 1986). The age of this sequence and also the age of the main metamorphism is broadly constrained between the 2,000 Ma Hartley Formation lavas near its base, and the overlying 1,300 Ma Wilgenhoutsdrif Group (Stowe, 1986; Barton and Burger, 1983). These rocks are thought to have been deposited in fluvial to shallow marine settings which may have existed parallel to the Kaapvaal Province during the Early to Middle Proterozoic.

The Okwa Basement (**OBc** of Figures 2.1 and 2.2) was first defined wholly geophysically by Reeves (1978). Recent geological studies by Aldiss (1988) and Aldiss

and Carney (1992) of isolated exposures of outcrop along the Okwa dry river valley, referred to as the *Okwa Inlier*, have revealed an Early Proterozoic crystalline basement complex, termed the Okwa Basement Complex, unconformably overlain by cover sequences ranging from Middle Proterozoic through to earliest Paleozoic of the Okwa and Nama Groups.

Felsites and sericitic quartzites of the Okwa Basement Complex were intruded by varied granites between 2,100 and 2,000 Ma (Aldiss and Carney, 1992). The Eburnian orogeny at ≈ 1,800 Ma transformed these granites to augen gneisses and, indeed, the most widespread lithologic association exposed in the Okwa Inlier is between the megacrystic granites and gneisses. Aldiss and Carney (1992) contended that the Okwa Basement Complex is a piece of Early Proterozoic crust which was accreted to the Archean craton at about 1,800 Ma, probably adjacent to the epicratonic sediments associated with the Olifantshoek Sequence of the Kheis Subprovince.

Because of the extensive cover of the relatively undeformed late Proterozoic - early Paleozoic Nama Group, Permo-Carboniferous to Jurassic Karoo Supergroup and recent Kalahari sand, the lithologic nature and age of the basement forming the enigmatic Rehoboth Subprovince is unknown (Hartnady *et al.*, 1985).

Pre-Damaran basement is exposed along the margins and as large inliers scattered throughout much of the Damara Province. In northern areas, the basement is represented by supracrustal metamorphic suites, by gneisses and granitoids and by an anorthositic intrusive suite (Tankard *et al.*, 1982). In the central and southern areas, largely

allochthonous Damara metasediments rest on gneisses and other supracrustal metamorphic suites. The basement rocks generally yield radiometric ages that suggest resetting during the time span of two periods of pre-Damara tectonism: these are the Eburnian ($\approx$ 2,000 Ma) and Kibarian ($\approx$ 1,400 to 900 Ma) (Tankard *et al.*, 1982).

2.1.3 Middle Proterozoic

Overlying the Olifantshoek Sequence in the Kheis Subprovince are the rocks of the Koras Group which consists of a succession of calc-alkaline lavas and immature sediments deposited in graben-like depressions which developed shortly after the cessation of folding in the underlying Olifantshoek Sequence (SACS, 1980; Aldiss, 1988). Total thickness of the Koras Group is estimated to be 8 km (Borg, 1988) and U-Pb radiometric dating of quartz porphyry lavas from this volcano-sedimentary sequence have yielded ages of 1085 $\pm$ 80 Ma to 1180 $\pm$ 74 Ma (SACS, 1980). The Koras Group is also nonconformably floored, in some areas, by granitoids and radiometric dating of these rocks have yielded ages of 1,000 to 1,200 Ma which are typically Namaquan (Tankard *et al.*, 1982).

Situated directly north of the Kheis Subprovince, the Tshane Complex (Tc of Figures 2.1 and 2.2) is one of the larger mafic complexes of western Botswana. Originally defined from the regional aeromagnetic data, this distinctive and extensive magnetic feature associated with the larger Kalahari Line (K-K' of Figures 2.1 and 2.2) was drilled to depths at which the causative bodies were believed to be located (Hutchins and Reeves,

1980; Meixner and Peart, 1984).

On the southern portion of Tshane Complex at latitude 24° 14'S, borehole CKP-8C-1 (location shown on Figures 2.1 and 2.2) encountered a pre-Karoo, layered gabbroic body at a depth of approximately 800 m. This gabbro was overlain by a well-developed and essentially complete succession of the Karoo Supergroup. Meixner and Peart (1984) classified this body as a probable cumulate gabbro or gabbroic norite. ^{40}Ar - ^{39}Ar dating of this gabbro yielded an age of 1,071 ± 11 Ma and these radiometric dating results are further discussed in Chapter 4.

Borehole CKP-8A (location shown on Figures 2.1 and 2.2) situated further north at latitude 23° 50'S encountered rocks of the lower Karoo Supergroup resting on basalt at a depth of approximately 250 m. Below this contact, sandstones are interbedded with chilled basalt flows and below 300 m these basalts grade downward into dolerite. Meixner and Peart (1984) believed the dolerite represented the top portion of a differentiated body, continuous with depth, containing higher magnetic concentrations (relative to the overlying basalts) to a depth of at least 1 km below the surface.

The lower Okwa Group of the Okwa Inlier consists of pale-coloured felsites, red sandstones, siliceous siltstones and mudstones together with felsic lapilli tuffs. During Mid-Proterozoic times, the felsic tuffs and red sandstones of the lower Okwa Group were intruded by dolerite sills, and a contemporary northeasterly dyke swarm intruded the basement granitoids of the Okwa basement Complex (Aldiss and Carney, 1992). The upper Okwa Group rests unconformably on the lower Okwa Group and is comprised of

a heterogeneous red bed assemblage and this sequence grades from pebbly arkosic sandstone to medium-grained feldspathic sandstone, and interlaminated mudstone and wacke. Aldiss and Carney (1992) estimated the thickness of the Okwa Group to be in excess of 800 m and the age of the lower Okwa Group is constrained between that of the main basement metamorphic event, at ≈ 1,800 Ma (Eburnian), and ages yielded from K-Ar determinations of the basement gneisses which suggest an isotopic re-setting event at ≈ 1,150 Ma (Kibarian).

Aldiss (1988) and Aldiss and Carney (1992) assigned the uppermost units exposed in the Okwa Inlier to the widespread and younger Nama Group. The Nama Group, as exposed in the Okwa Inlier, consists of red breccias and conglomerates, gently dipping laminated fine sandstones and siltstones displaying, in places, cross lamination. The Nama Group is a late Proterozoic to early Paleozoic sequence (SACS, 1980) and its thickness within the Okwa Inlier is estimated to be approximately 100 m.

2.1.4 Late Proterozoic

On the southern margin of the Damaran Province, the Ghanzi-Chobe fold belt (GCf of Figure 2.1 and 2.2) consists of a sequence of folded, Late Proterozoic sedimentary rocks and forms a northeast trending structural ridge. This topographic feature is referred to as the Ghanzi ridge and extends northeastward into Botswana from the Namibian border for some 350 km.

The volcano-sedimentary rocks of the Kgwebe Group outcrop intermittently along

strike of the Ghanzi ridge. The Kgwebe Group is composed of massive porphyries and felsites interstratified with sandstones, minor conglomerates, tuffaceous sediments and vesicular diabases (Thomas, 1973). The porphyries and felsites are fine-grained, flow banded and flow brecciated indicating an extrusive origin. The associated sediments are predominantly tuffaceous being comprised of green, brown and purple feldspathic and epidotic sandstones and siltstones and conglomerates containing recognizable porphyry fragments. Due to the sparsity of outcrop of Kgwebe Group along the Ghanzi ridge, the total thickness of this volcano-sedimentary sequence is uncertain.

Overlying the rocks of the Kgwebe Group, possibly unconformably (Ratsoma *et al.*, 1991) is the Ghanzi Group. This unconformity is not thought to represent a major hiatus but rather is regarded as being related to a syn-rift (Kgwebe) phase and a thermal subsidence phase (Ghanzi) of a pre-Damaran basin (Ratsoma *et al.*, 1991). The thickness of the Ghanzi Group is estimated to be 13 km and consists of over 90% of medium-grained arkosic sandstones. The remaining 10% is composed of intercalations, which are never more than 50 m thick, of mudstones, siltstones and limestones. Sedimentary structures such as slumping and current bedding preserved within the sandstones indicate a shallow-water, fluviatile depositional environment for the Ghanzi sediments. A maximum age for the Ghanzi Group sediments is derived from radiometric dating of the quartz feldspar porphyries of the underlying Kgwebe Group. The Rb-Sr isochron yielded an age of 821 ± 43 Ma (Key and Rundle, 1981) with the scatter being attributed to a "resetting" event which occurred at about 650 to 700 Ma. Key and Rundle (1981)

proposed that the Damaran orogeny was responsible for this isotopic resetting.

Deposition of the Nosib Group began at about 1,000 to 900 Ma with the infilling of grabens produced in rifted continental crust with up to 6 km of clastic sediments and minor amounts of volcanic rock (Tankard *et al.*, 1982). Three parallel grabens trending northeast have been recognized in the intracontinental branch of the Damara Province and each was approximately 50 to 70 km wide and 200 km long. Arkosic arenites, which are locally conglomeratic, have been attributed to fluvial or shallow marine infilling of the Nosib grabens. Marine incursions in later Nosib times resulted in the formation of impure carbonates and anhydrite, now metamorphosed to calc-silicate rocks (Tankard et al., 1982). A minimum age for this continental rift sequence is derived from radiometric dating of acid volcanics present in the upper Nosib Group. The Rb-Sr isochron from these volcanics yielded an age of 840 ± 12 Ma (Kröner, 1982).

It has been suggested that the Ghanzi Group rocks exposed farther south in the Ghanzi ridge could be correlative with the Nosib Group (K. Hoffman, 1989). Similarly, Aldiss and Carney (1992) suggested that the upper Okwa Group could be the same age as the Nosib Group, and its lateral continuation in Botswana, the Ghanzi Group.

2.1.5 Phanerozoic

The Nama Group is a late Proterozoic to early Paleozoic sequence that extends over much of the Kalahari Province and into the Damaran Province. Its predominant lithologies are quartzites, limestones, sandstones and shales (SACS, 1980). Its stratigraphy has been

described in detail by Germs (1972, 1974 and 1983) and has been subsequently divided informally into three subgroups. The lowermost Kubuis Subgroup includes basal transgressive clastics which are capped by distinctive black limestones. The succeeding Schwartzrand Subgroup is dominated by arenaceous and argillaceous clastics, although limestone does form an important constituent of this subgroup. The uppermost unit of the Schwartzrand follows a significant unconformity. Then, following another unconformity, the uppermost Fish River Subgroup forms a thick redbed sequence of conglomerates, sandstones and mudstones. It is this unconformity, along with the molasse sedimentation of the uppermost Fish River Subgroup, that is suggestive of convergence and foreland basin development as indicated in the tectonostratigraphic chart of Figure 2.3.

Lawrence (1989), referring to the work of Germs (1983), uses lithostratigraphic and facies relationships as a key in providing depositional patterns and subsidence, and the relative importance of the craton *versus* the rising Damara orogen as a sediment source for a developing foreland basin. Kubuis Subgroup facies relationships show fluvial systems building westwards from the craton into a marine foredeep. Schwartzrand Subgroup depositional patterns show a broad conformity with those of the Kubuis, except that fluvial or fan-delta sedimentation from the rising orogen to the north becomes increasingly important. In the Fish River Subgroup, sedimentation was dominated by fluvial systems building out southwards from the rising orogen.

The Vreda 281 #1 deep borehole situated 30 km west of the Botswana border in Namibia at about latitude 24° 15'S intersected 833 m of Nama Group clastics overlain by

781 m of lower Karoo sediments and 105 m of the Kalahari beds (Wilson, 1964; Meixner and Peart, 1984). Also, the deep exploratory borehole, PCIAC-GSD Masetlheng Pan-1 drilled at latitude 23° 42'S (location shown in Figure 2.2), along one of the deep seismic profiles, encountered 1,113 m of interpreted Nama sediments beneath an overlying Karoo section (Petro-Canada, 1990).

Between 750 and 530 Ma, the central area of the Damara Province underwent polyphase folding and voluminous (> 50% of the area) intrusions of syntectonic and posttectonic granitoids (Tankard *et al.*, 1982). Some of these Damaran granitoids may have been derived from partial melting of sediments and basement granitoid gneisses during high temperature medium P/T metamorphism. Initial Sr and Nd isotope ratios of posttectonic diorite and granites indicate that their magmas were derived both directly from the upper mantle and by melting of material with a previous crustal history (Hawkesworth *et al.*, 1981).

The lithostratigraphy of the Karoo Supergroup in Botswana has been formalised by Smith (1984) and is comprised of stratiform consolidated sedimentary rocks capped by Jurassic basaltic lavas. The sedimentary rocks consist of arenaceous deposits that accumulated in a continental environment during the Late Paleozoic to Middle Mesozoic (Permo-Carboniferous to Jurassic). The deposition of the Karoo sediments was controlled by a crustal downwarp of the Kalahari craton associated with the breakup of the Gondwana supercontinent (Farr *et al.*, 1981) and were laid down in a number of subbasins. The final phase of Karoo sedimentation was terminated by the voluminous

Jurassic outpouring of basaltic magma with acid volcanism continuing into the Early Cretaceous (Tankard *et al.*, 1982). The total thickness of Karoo sediments in Botswana is uncertain, but Farr *et al.* (1981) estimated a maximum thickness of 1,000 m. In southwestern Botswana, the PCIAC-GSD Masetlheng Pan-1 stratigraphic test borehole penetrated 1,162 m of Karoo sediments with 283 m of this interval represented by dolerite with shale interbeds (Petro-Canada, 1990).

Overlying much of the Karoo Supergroup in southwestern Botswana are the aerially extensive Tertiary to Recent unconsolidated and semi-consolidated aeolian and alluvial deposits of the Kalahari beds. In the Ghanzi ridge area, the Kalahari beds attain a thickness of 30 m (Litherland, 1982) and the PCIAC-GSD Masetlheng Pan-1 borehole situated some 100 to 150 km farther south encountered 109 m of Kalahari beds (Petro-Canada, 1990).

2.2 Structure

The geological history of the southern African subcontinent stretches far back in time to a limit presently fixed at approximately 3.8 billion years and the most recent comprehensive summary of the geology of this region is given by Tankard *et al.* (1982). Most of this extensive geological history is Precambrian and an overview of the course of geologic events in southern Africa indicates that the crust passed through a well-defined sequence of evolutionary stages.

A period of Archean crustal development gave rise to crystalline massifs represented

by the Kaapvaal, Limpopo and Zimbabwe Provinces (Figure 2.1). This was followed by a period of Early Proterozoic supracrustal development in which the Archean basement was buried beneath a largely sedimentary cover. Several Proterozoic orogens in the southern and western parts of the subcontinent resulted in older crystalline rocks and their supracrustal cover being reworked tectonically, with geosynclinal deposits accumulating and massive granitoid intrusions emplaced by partial melting of older crust and by additions from the mantle. The Paleozoic Gondwana era ushered in a period of aborted rifting and unparalleled continental sedimentation throughout the Gondwanan supercontinent, of which southern Africa formed the hub. Cretaceous fragmentation of Gondwana was preceded by Jurassic continental rift volcanism and injection of diamondiferous kimberlites, carbonatites and other alkaline intrusions. Late Mesozoic and Cenozoic sedimentation was restricted to the newly formed margins of the stable subcontinent and depressed areas of the interior. The following discussion focuses on Proterozoic structures found in the rocks of the Kaapvaal, Kalahari and Damara Provinces presented in the tectonostratigraphic chart of Figure 2.3.

2.2.1 Eburnian Orogeny

The Eburnian Orogeny is broadly constrained between 1,800 and 2,000 Ma (Tankard *et al.*, 1982). It appears to be focussed on the N-S Kheis Subprovince of the northern Cape Province of South Africa, where at least five major thrust sheets are recognized within and beneath the Olifantshoek Sequence which are separated by mylonites (Stowe,

1986). The thrusting was directed eastwards and large-scale recumbent folds display eastwards tectonic vergence, towards the older craton.

The Eburnian Orogeny transformed the granites of the Okwa Basement Complex to produce augen gneisses. Eburnian deformation was also accompanied by metamorphism of pre-tectonic mafic dykes in the epidote amphibolite facies and sporadic exposures of deformed metadolerites and metadiorites also occur within the megacrystic granitoids of the Okwa Basement Complex (Aldiss, 1988; Aldiss and Carney, 1992). This orogeny thus appears to be related to easterly accretion of the Early Proterozoic Kalahari Province onto the Archean Kaapvaal Province.

2.2.2 Kibarian Orogeny

Following Eburnian tectonism, rocks of the Okwa Basement Complex and the lower Okwa Group were affected by a second and rather less ductile compressional deformation associated with the Kibarian Orogeny which occurred between 1,400 and 900 Ma (Tankard et al., 1982). Kibarian structures occur in the lower Okwa Group and are comprised of NE-SW trending upright folds and associated coarse fracture cleavage with subvertical mineral lineation and this deformation is believed to have occurred at ≈ 1,150 Ma (Aldiss and Carney, 1992). Previous Eburnian foliations in the Okwa Basement Complex are folded and cross-cut by mylonite zones produced by later Kibarian tectonism. The metadolerite dyke swarm and sills lack the main foliation of the basement gneisses, and therefore post date the most pervasive phase of Eburnian deformation

affecting the Okwa Basement Complex. However, these dykes and sills are fractured, brecciated and locally mylonitised and is probably related to Kibarian deformation. This would imply that the Kibarian compressional event was preceded by a tensional phase, when the northeasterly dykes were emplaced (Aldiss and Carney,1992). The compressional event appears to represent a phase of SE-directed accretion of the Kalahari Province onto the Kaapvaal craton.

2.2.3 The Damara Orogeny

Published tectonic models for the Damara Orogeny (750 to 530 Ma) fall broadly within two groups (Hawkesworth *et al.*, 1986). In the first, structural and metamorphic asymmetry across the orogen and the presence of a possible ophiolite fragment has suggested that a limited ocean (500-800 km) developed between the southern Kalahari craton and the northern Congo craton which was later subducted along the leading edge of the Congo craton via an Andean-type collision (Burke *et al.*, 1977; Barnes and Sawyer, 1980; Kasch, 1983). The second group of tectonic models invokes some form of intracontinental rift or aulacogen which was also a zone of high mantle heat flow (Martin and Porada, 1977; Kröner, 1982). These models highlight the intracratonic nature of the orogen, the suggested stratigraphic continuity across it and the palaeomagnetic evidence for little relative movement between the Kalahari and Congo cratons.

The Khomas and Swakop Subprovinces (**KMs and SWs** of Figure 2.1) constitute the intracratonic branch of the Damara Province with the Ghanzi-Chobe fold belt forming its

southern margin. The southern Khomas Subprovince contains a deeply exhumed, southeasterly vergent fold and thrust belt, including an outlier klippe, the Naukluft Nappe Complex (**NNc** of Figure 2.1), and a variety of deeper thrust system elements such as duplex structures, antiformal stacks and tectonic windows. This Naukluft Nappe Complex is comprised of five major, south-verging thrust nappes which have been subsequently subdivided lithostratigraphically (Tankard *et al.*, 1982). The Nama Group serves as an autochthonous foundation for the nappe complex and probable stratigraphic equivalents to it are found within the complex itself.

The Ghanzi-Chobe fold belt of Botswana is generally considered to be part of the southern margin of the Damara Province and the rocks which comprise it are believed to have been deformed during the Damaran Orogeny (750 - 530 Ma) which produced large open folds with axes trending southwest to northeast (Aldiss and Carney, 1992; Ratsoma *et al.*, 1991; Borg, 1988). Within this fold belt, Damaran deformation has thrown Kgwebe and Ghanzi Group rocks into a regional scale NE trending fold and thrust belt. On the extreme NE flank of the Ghanzi ridge, the belt has the form of a narrow anticlinorium cored by Kgwebe Group rocks. This anticlinorium is comprised of a series of large scale tight folds which can be traced over tens of kilometres along the strike of the fold belt (Ratsoma *et al.*, 1991). These major folds have upright or steep NW-dipping axial planes and horizontal or gently plunging axes. Farther southwest along strike of the Ghanzi ridge in the vicinity of the Botswana-Namibia border, the folds have a more open, asymmetrical style and extend southwestwards into Namibia where Nama Group rocks have been

preserved in synclinal cores (Ratsoma *et al.*, 1991).

There are several important unanswered questions regarding the relationship of Proterozoic to Archean provinces in this area of Botswana. Of special relevance to this thesis is that the basement of the Proterozoic is unknown - it is not clear whether there is reworked Archean core or whether the Proterozoic blocks are relatively juvenile.

With the stratigraphy and structure of the greater western Botswana region now adequately introduced, the following section examines what role the south African subcontinent may have played in the evolution of a proposed Late Proterozoic supercontinent.

2.3   Global Relevance

2.3.1   A Late Proterozoic Supercontinent?

It has been postulated that the period of Earth history encompassing 700 to 500 Ma witnessed the fragmentation of a Late Proterozoic supercontinent (Dalziel, 1991; Hoffman, 1991; Moores, 1991). This idea stemmed from the observation that rifting and continental breakup occurred contemporaneously around the margins of Laurentia (North America and Greenland), Baltica (Baltic shield and Russian platform), Siberia and parts of Gondwanaland. However, due to the lack of sufficient palaeomagnetic data, the spatial relationship of this hypothetical supercontinent with the continents forming Gondwanaland (South America, Africa, Arabia, India, Antarctica and Australia)   is unclear for this geologic interval. An alternate means of establishing former linkages between separated
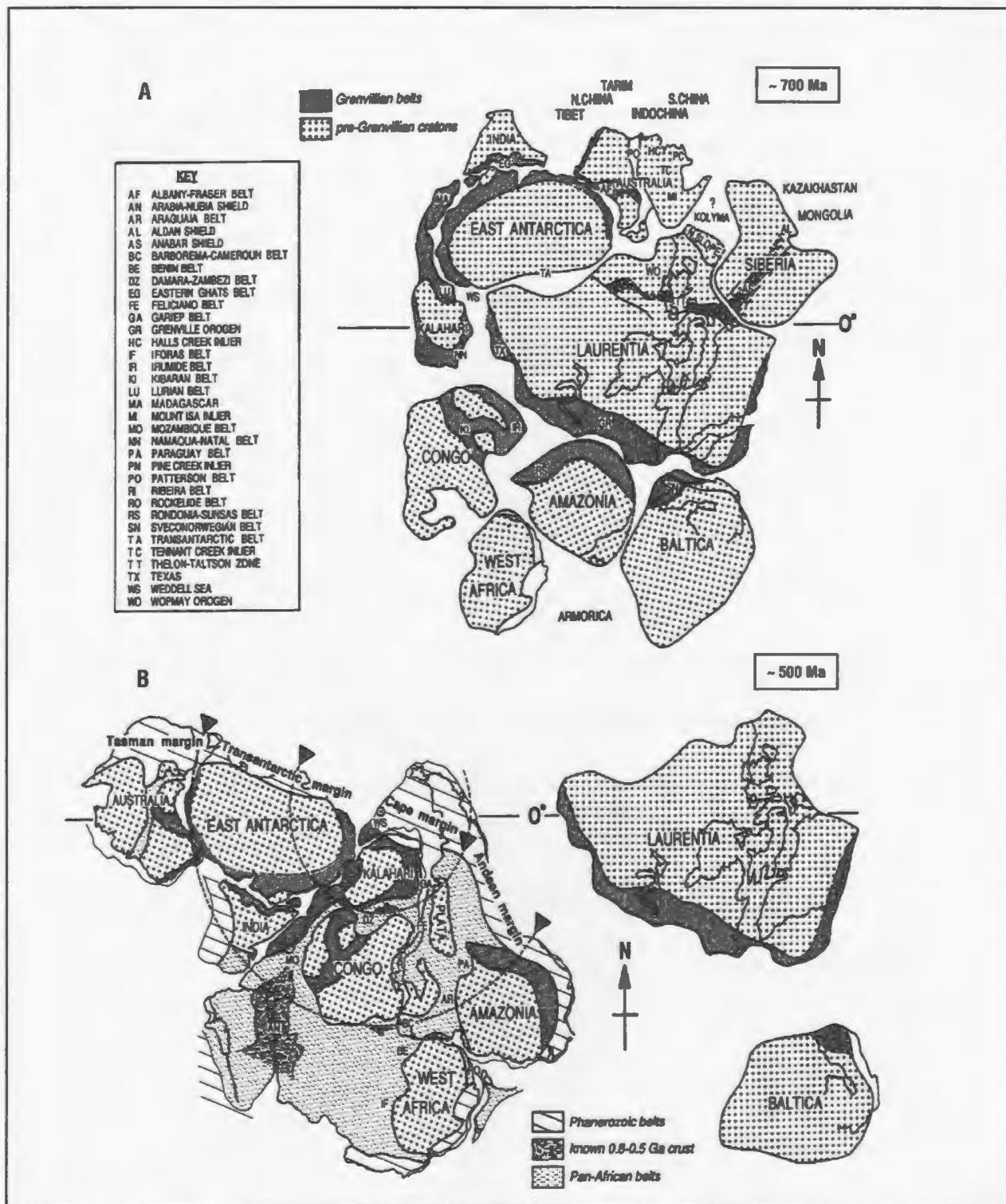
Figure 2.4 (A) Reconstruction of the proposed Late Proterozoic supercontinent and (B) Late Cambrian paleogeography after the breakout of Laurentia (after Hoffman, 1991).

continents is through the correlation of Precambrian orogenic belts that were once presumed continuous but that are now truncated at modern or ancient continental margins. Based on such evidence, Hoffman (1991) presented a qualitative model for the breakup of a Late Proterozoic supercontinent centred on Laurentia and the subsequent assembly of Palaeozoic Gondwanaland. In comparison, reconstructions presented by Dalziel (1991) and Moores (1991) focus more on the hypothesis that the Laurentian and East Antarctic-Australian cratons were once continuous in the late Precambrian and that their Pacific margins formed a conjugate rift pair. As such, their reconstructions do not specifically address the positions of the constituent cratons which comprise the present day African continent, relative to Laurentia, during this late Precambrian period. Thus, for the purposes of this thesis, Hoffman's model is presented and his reconstructions are illustrated in Figure 2.4.

Hoffman (1991) uses age of orogeny as evidence as to which continents may have been adjacent and south of Laurentia before the opening of the Iapetus Ocean, if east Gondwanaland (India-Australia-Antarctica) did indeed separate from western Laurentia. The Appalachian and Ouachita margins of southern Laurentia are confined to areas affected by Grenvillian orogeny, a major compressional event which affected much of Laurentia between 1,300 and 1,000 Ma. Thus cratons which are bordered by Grenvillian belts are better candidates to have been conjugate to southern Laurentia than those like the West African craton that lack Grenvillian belts. Grenvillian belts marginal to cratons in Gondwanaland include the Rondonia-Sunsas belt (**RS** of Figure 2.4) of the Amazonia

craton, the Irumide and Kibaride belts (**IR** and **KI** of Figure 2.4) of the Congo craton and the Namaqua-Natal belt (**NN** of Figure 2.4) of the Kalahari craton. The observation that Grenvillian rocks in both the Namaqua-Natal belt and southern Laurentia have isotopic ages that cluster around 1,400 Ma further supports the reconstruction of Figure 2.4(**A**). Thus, the cratons that are most likely to have been conjugate to eastern and southern Laurentia in the Late Proterozoic are Baltica, Amazonia, Congo and Kalahari.

Hoffman (1991) proposed that Gondwanaland was assembled through a rotational collapse of its constituent cratons. This assembly is implied by the separation of Australia-Antarctica and Amazonia-Baltica from western and eastern Laurentia respectively and could have been achieved by counter-clockwise rotation of Australia-Antarctica and dextral translation (with or without clockwise rotation) of Amazonia, relative to Laurentia (with Baltica left behind). He points out that available palaeomagnetic data are compatible with the implied rotation and with the large-scale convergence between east and west Gondwanaland, possibly lasting until the late Cambrian. Rotation about a pole near the Weddell Sea (**WS** of Figure 2.4) would account for the dominantly transcurrent motion observed in east to northeast trending belts of Pan-African (800 to 500 Ma) age. Such belts would approximate small circles of rotation. For instance, the Damara-Zambezi belt (**DZ** of Figure 2.4) shows geological evidence for dominantly sinistral transcurrent shear and palaeomagnetic evidence for a 35° clockwise rotation for the Kaapvaal craton with respect to the Congo craton (Hartnady *et al.*, 1985; Renne *et al.*, 1990).

Orthogonal to the Damara-Zambezi belt is the Mozambique belt (**MO** of Figure 2.4)

which welds east and west Gondwanaland. The Mozambique belt also provides strong geological evidence to support a pole of rotation near the Weddell Sea. Although the southern limit of the Mozambique belt is uncertain, some workers (Kaźmin, 1988) have envisaged that this Late Proterozoic collision zone extends between the Kalahari and east Antarctic cratons. Others (Sacchi *et al.*, 1984; Cadoppi *et al.*, 1987) have interpreted the southernmost extremity of the belt as essentially Grenvillian in age: this would imply that the Kalahari craton belongs to east Gondwanaland and the collision zone between east and west Gondwanaland is translated from the Mozambique belt to the Gariep belt (**GA** of Figure 2.4) by way of the Damara-Zambezi belt. Consequently, the Damara-Zambezi belt should have experienced net dextral rather than sinistral transcurrent shear.

Thus, according to Hoffman (1991), the final assembly of Gondwanaland must postdate the breakout of Laurentia for the proposed scenario to be viable. This requirement constitutes a clear test of the model. Rifting had begun in western Laurentia by 780 Ma (P. Hoffman, 1989) and in eastern Laurentia by 600 Ma (Williams and Hiscott, 1987). A minimum age for continental breakup of 620 to 560 Ma is inferred from the onset of long-lived thermal subsidence along both margins (Bond *et al.*, 1984) and stratigraphic evidence suggest an Early Cambrian rift-to-drift transition. However, no equivalents of the Late Proterozoic Beardmore and Pampean orogenies that affected the Transantarctic and Andean margins respectively can be found in the Cordillera and Appalachians. This implies, if these orogenies are correctly dated, that east and west Gondwanaland had separated from Laurentia before the end of the Proterozoic. The age

of consolidation of east and west Gondwanaland is also uncertain. Subduction of oceanic lithosphere below the Arabian-Nubian shield ended at 640 to 620 Ma. To the southeast, however, a terminal collision of latest Cambrian age (510 to 500 Ma) has been postulated between an active margin in northeast Somalia and east Gondwanaland. Thus, the scenario proposed by Hoffman (1991) may or may not be viable depending on which set of age estimates is confirmed.

The Kalahari craton forms a major structural province of the western Botswana region and its position within the postulated Late Proterozoic supercontinent may have important implications for the tectonic evolution of the southern Africa subcontinent. The south, central portion of Laurentia, the "proto" North American craton, is the present day site of the Mid-continent rift system (MRS). This continental rift system is 1,110 to 1,090 Ma in age and marine seismic reflection data from the Great Lakes has revealed an extraordinary thickness (> 30 km) of volcano-sedimentary rocks (Behrendt *et al.*, 1988). Similarly, within the greater western Botswana region, significant thicknesses of volcano-sedimentary rocks of continental rift affinity associated with the Koras, Okwa and Ghanzi/Kgwebe Groups as previously described in this chapter also provide evidence of a late Middle Proterozoic rifting event affecting much of the southern Africa region (Aldiss and Carney, 1992; Borg, 1988). The juxtaposition of the Kalahari and Laurentia cratons of Hoffman's proposed reconstruction suggest that the North American Mid-continent rift and the similar aged rift affecting the southern Africa subcontinent may represent preserved portions of the same precursory and widespread late Middle Proterozoic continental rifting event which marked the breakout of Laurentia from this Proterozoic supercontinent. These ideas are expanded further in Chapter 4 which deals

with the interpretation of the seismic data. Chapter 3 now follows which describes the acquisition and processing of the western Botswana deep seismic reflection data set.

3 SEISMIC REFLECTION DATA

3.1 Introduction

In 1987 and 1988 Petro-Canada International Assistance Corporation (PCIAC), through Sonics Exploration Limited, collected about 1,000 km of 12 to 15 fold multichannel reflection seismic data for the Government of Botswana. The seismic lines were sited so as to provide regional coverage in both the Nosop-Ncojane basin located in southwest Botswana and the Passarge Basin farther to the northeast. The locations of the seismic lines recorded in the Nosop-Ncojane basin are indicated in Figure 3.1.

The primary objective of these surveys was to determine the overall thickness of the sediments and any stratigraphic boundaries and/or intra-basinal structure. A recording time of 8 s was originally proposed to meet this objective but a 15 s record time was finally decided on so that the deep crustal structure could be investigated in order to provide a better understanding of the regional tectonic framework of this part of southern Africa. Such deep seismic data would be valuable in providing insight into the tectonic setting of the region and to constrain possible models for basin evolution.

3.2 Acquisition Parameters

The acquisition parameters used to collect the reflection seismic data in western Botswana are summarized in Table 3.1. A *DFS-V* seismic acquisition system was utilized and the data were recorded in *SEG-B* format using a 2 ms sample rate with a total record length of 15 s. The recording array consisted of a symmetrical split spread of 120
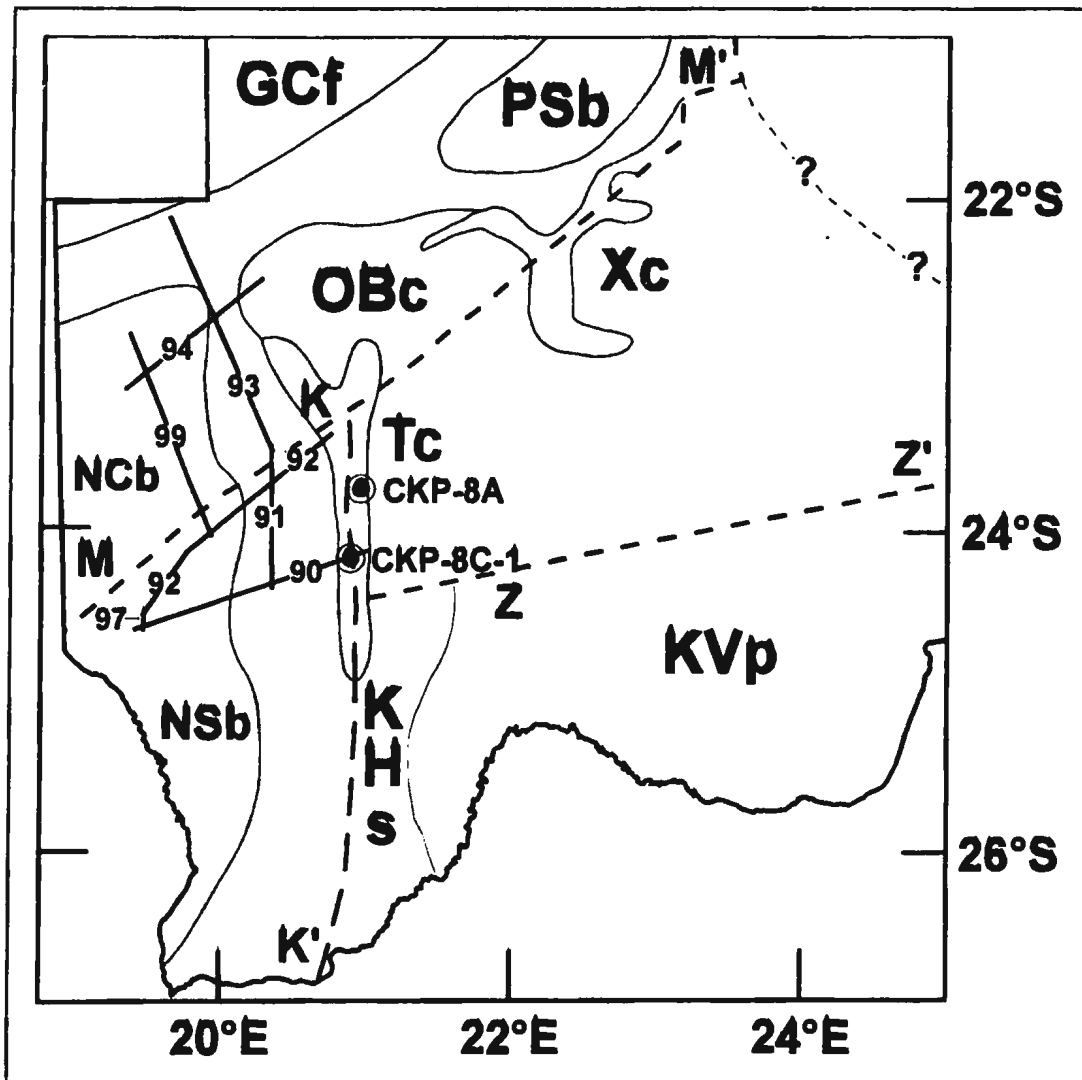
Figure 3.1   Location of western Botswana seismic profiles in relation to major tectonic elements (after Reeves, 1978; Meixner & Peart, 1984; Aldiss & Carney, 1992).

geophone groups spaced at 50 m intervals with a 150 m gap at the shot point giving a total spread length of approximately 6 km. The source used was dynamite and typically consisted of 12 kg shots split among 6 holes, each 6 m in depth. Shotpoints were placed at either 200 m intervals for 15 fold coverage or 250 m intervals for 12 fold coverage.

Table 3.1. Acquisition parameters for western Botswana seismic profiles (after Hall *et al.*, 1990).

Geophone Groups	*Geospace* 10 Hz phones, 18 per group, spaced at 5.88 m (100 m total group length).
Spread	120 groups at 50 m interval for a total spread length of 6,050 m, symmetrical split, 150 m gap at shotpoint.
Source	Dynamite, typically 6 x 2 kg in 6 m holes, shots at 200 m interval (15 fold) or 250 m interval (12 fold).
Recording	*DFS-V, SEG-B*, 2 ms sample rate, 15 s record length (line 99 recorded to 20 s), 8 Hz low-cut filter at 18 dB/octave, 128 Hz high-cut filter at 72 dB/octave

3.3   Processing

The processing sequence used on this deep reflection seismic data set is outlined in Table 3.2. All data were processed solely by the author on a *CONVEX C1* mini-supercomputer using Texaco's *STARPAK* software (Texaco, 1989). The right to use these data was obtained from the Government of Botswana by Memorial University's Centre for Earth Resources Research. The data had been previously demultiplexed from the original field tapes by PCIAC to *SEG-Y* format.

In the following sections, brief descriptions of the *STARPAK* processors used in the processing of the western Botswana deep seismic data set are provided.

3.3.1   Geometry

One of the first essential steps in seismic processing is to define the shooting and recording geometry of the line and to assign relevant geometry information to the

Table 3.2. General processing sequence for western Botswana seismic profiles; All seismic data were processed solely by the author.

Geometry Definition & Application
Processing Line Definition, Common Midpoint (CMP) Binning & Application
Field Statics Definition & Application
CMP Gathering
Velocity Analysis
Normal Moveout (NMO) Correction
Front Mute Determination
Spectral Balancing
Standard Mean Stack
Migration(s)
Coherency Filtering
Trace Arraying & Summing
Low Pass Filter
Gain Control
Display: High Bias - Variable Area

recorded traces. This was accomplished through the use of the *STARPAK* processor :**GEOM**.

The survey data (provided by PCIAC in *SEG-P* format) describing the geographic locations and elevations of stations is combined with the information provided in the observer's logs which describe the positioning of sources and receivers relative to the stations and to each other. This allows the precise determination of the source, receiver and midpoint coordinates for each trace. This and other geometry information related to the traces and stations are stored in a database (defined by processor :**DBAS**) for use by subsequent processors.

Processor **:GMAP** was used to apply the geometry information defined by **:GEOM**; i.e. to fill the relevant portions of the trace header and to kill or reverse polarity of bad traces identified by visual inspection of all shot gathers.

3.3.2 Processing Line and Binning

Multichannel seismic data is recorded in the common shot or shot-receiver domain whereas seismic data processing is conventionally performed in the common midpoint (CMP) or midpoint-offset domain (Yilmaz, 1987). The sorting of the data into the CMP domain essentially groups individual traces associated with a common midpoint between various shot and receiver locations. This sorting process is presented schematically in Figure 3.2. It is this grouping of traces which make up the CMP gather.

The acquisition of multichannel seismic data can sometimes result in the spatial scattering of the common midpoints; this is particularly true for seismic data acquired along crooked lines. A common solution to this scattering is to extend the definition of the common midpoint to cover a small area which is often referred to as a "bin" (Hatton *et al.*, 1986). Processor **:PROC** was used to define the "processing line" which is essentially a line along the earth's surface along which the common midpoint bins (defined by **:BIND**) will be located.This processing line can be different from the acquisition line (defined in **:GEOM**), especially for crooked lines. However, in the case of the western Botswana data, the survey lines were exceptionally straight and the processing lines generally coincided with the acquisition lines.
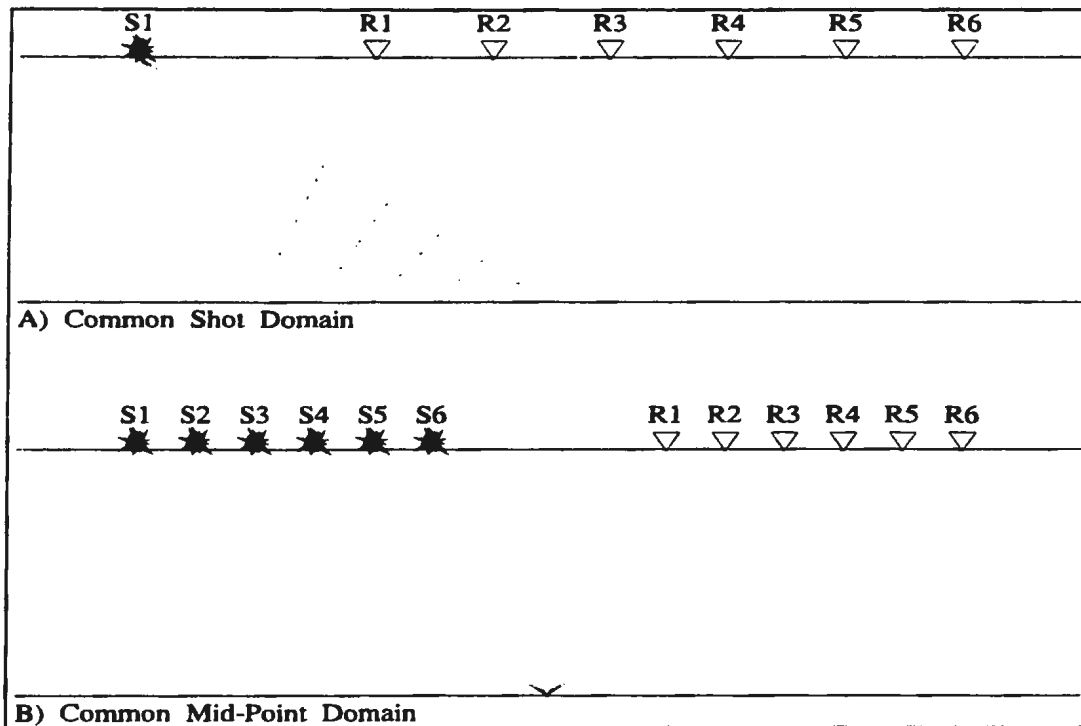
Figure 3.2 Raypath differences between A) common shot domain where data is recorded and B) common midpoint domain where data is normally processed (after Yilmaz, 1987).

:**PROC** defines a series of points along the surface which are connected by straight line segments and these points are referred to as "nodes". These nodes and their coordinates comprise the processing line description which is then stored in the database. :**PROC** allows three different ways to specify these node coordinates and, for this data set, the processing verb **AUTO** was used to automatically derive a smoothly varying processing line which is, in some sense, a "best fit" to the midpoints.

Processor :**BIND** accesses the geometry and processing line information previously generated by :**GEOM** and :**PROC** and contained within the database. From this, it defines bin position, size, shape and orientation and determines the trace-bin correspondence (i.e.

which traces fall into which bins). An important consideration of the binning process is to choose a bin size and shape at a point along the processing line which gives a sufficiently large bin population of source-receiver common midpoints (CMPs) without being large enough to reduce spatial resolution (Hatton *et al.*, 1986). The bins are rectangular in shape and are equally spaced and centred along the processing line. The coordinates of the bin corners and the trace-bin correspondence are then stored in the database for later access by subsequent processors.

Processor **:BINA** applies the bin information stored in the database to the trace headers in preparation for CMP gathering.

3.3.3 Field Statics

:FSIN was the first of three processors used in the field statics correction sequence **:FSIN → :FSCA → :FSAP**. It is used to define a near surface model consisting of one or more layers with a thickness and velocity specified for each. A model is defined by use of the verb **MODEL** and, in the case of this data set, consisted of:

1) Surface elevations specified in **:GEOM** retrieved automatically from the database by **:FSIN**.

2) A single layer defined by the shot depth and uphole time specified in **:GEOM** also retrieved automatically from the database.

3) Replacement velocity.

4) Replacement datum.

The layer is built from the surface down with its base being located at the buried shot locations and the layer velocity is determined from the shot depths and uphole times. This layer information is then stored in the database for subsequent use by the other field statics processors.

:FSCA is then employed for the calculation of the field statics corrections from the information previously stored in the database by :GEOM and :FSIN. The time shifts are calculated in a two step process:

A) *Calculation of Stripping Time*. This is the travel time from the surface through the defined layer or, in this case, simply the uphole time.

B) *Calculation of Replacement Time*. This is the travel time from the base of the defined layer to the desired datum (using the replacement velocity, SUBVEL, specified in :FSIN).

The replacement time minus the stripping time is the field static correction. A negative correction shifts the trace earlier in time and a positive correction shifts the trace later in time.

:FSAP is the application phase of the field statics correction sequence. It applies the field statics corrections to the data traces and the static shift is applied to the nearest sample.

3.3.4 CMP Gathering

With the trace headers now containing relevant geometry information, processor

:GATHER was used to sort the data from the common shot domain to the common midpoint (CMP) domain (see Figure 3.2).

The sorting of traces into the CMP domain utilizes the data redundancy inherent in the seismic acquisition technique to improve the signal-to-noise (S/N) ratio. This redundancy is achieved by using multiple sources per trace, n_S, multiple receivers per trace, n_R and multiple offset coverage of the same subsurface point, n_F, during the field operation. Given the total number of elements in the recording system, $N = n_S \cdot n_R \cdot n_F$, the S/N ratio is theoretically improved by a factor of $\sqrt{N}$ (Yilmaz, 1987). This is based on the assumptions that the reflection signal on traces of a CMP gather are identical and that the random noise is uncorrelated from trace to trace. However, in practice, these assumptions rarely hold and the improvement in the S/N ratio gained by stacking is somewhat less than $\sqrt{N}$.
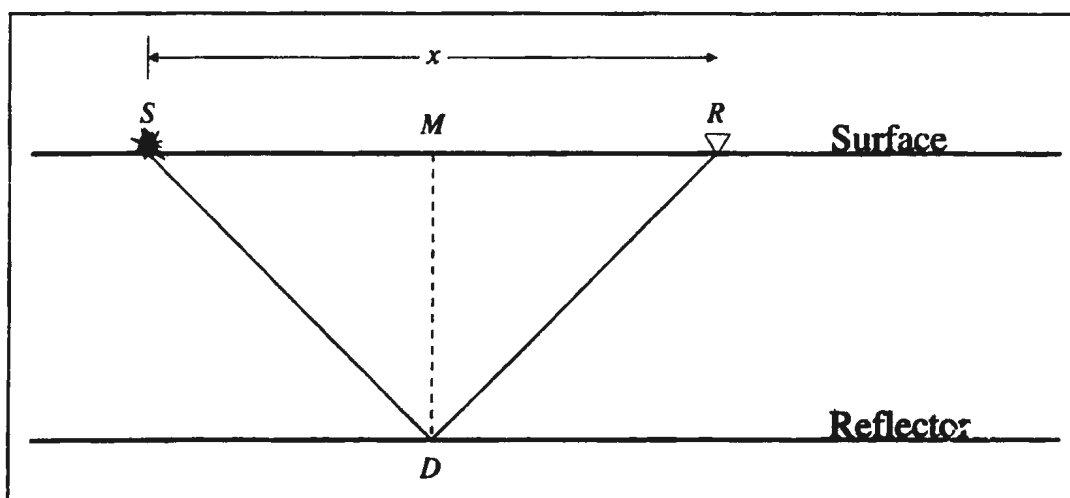

Figure 3.3 Raypath geometry for a single horizontal reflector (after Yilmaz, 1987).

3.3.5   Velocity Analysis and Normal Moveout (NMO) Correction

Figure 3.3 illustrates the simple case of a single horizontal reflector. At a given midpoint location M, the traveltime along the raypath from shot position S to depth point D, then back to receiver position R is $t(x)$. It can be demonstrated (Dix, 1955) that this traveltime equation expressed as a function of shot-receiver offset can be written as:

$$t^2(x) = t^2(0) + \frac{x^2}{v^2} \tag{3.1}$$

where x is the distance or offset between the source and receiver positions, v is the velocity of the medium above the reflecting interface, and $t(0)$ is twice the traveltime along the vertical path MD (Yilmaz, 1987). Equation 3.1 describes a hyperbola and this traveltime curve is schematically depicted in Figure 3.4. The difference between the two-way travel time at a given offset $t(x)$ and the two-way zero-offset time $t(0)$ is called the normal moveout or NMO (see Figure 3.4). When offset x and two-way travel times $t(x)$ and $t(0)$ are known, the velocity v can be computed from Equation 3.1.

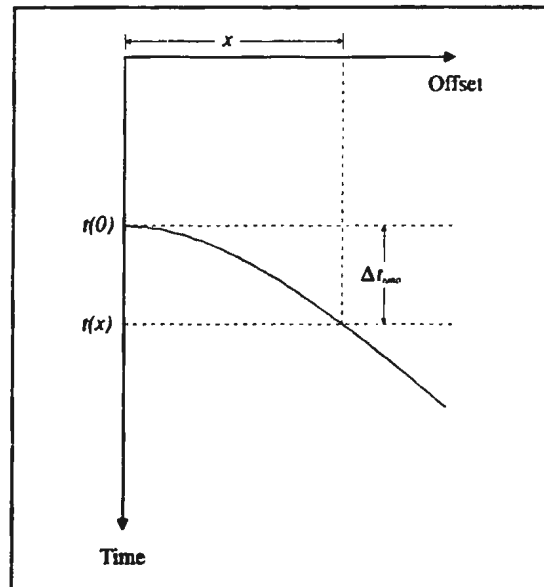Normal moveout is the one basis for

Figure 3.4   Traveltime curve associated with a single horizontal reflector. The apex of the hyperbola is located at zero-offset (after Yilmaz, 1987).

velocity determination from seismic data. Once the NMO velocity v_{nmo} is determined, the traveltimes can be corrected to remove the effects of offset. Traces in the NMO-corrected gather can then be summed to obtained a stacked trace at that particular CMP location. For the western Botswana data set, two different methods of stacking velocity determination were employed.

The first and probably the simplest method of velocity determination was the use of constant velocity stacks (CVS). This was accomplished by using processor :VFANAL. In this method, 25 adjacent multi-trace CMP records were corrected for normal moveout over a range of constant velocities (2600, 3000, 3800, 4400, 5000, 5400 and 6000 m/s), stacked and then displayed. A typical velocity analysis from this data set is displayed in Figure 3.5. These stacked records were then studied to determine which velocity yielded the largest amplitude and/or coherence of the various reflection events seen within the section. From this examination, a set of time-velocity pairs were obtained which constituted an optimum stacking velocity function at that particular CMP location and "neighbourhood". These velocity functions were later used for normal moveout correction in subsequent processing. These CVS analyses were carried out at every 200 CMP locations along each of the seismic lines.

The second method, which was run concurrently with the CVS method (i.e. within the same processing run), used velocity spectra. This was done through the use of processor :MERVEL. The velocity spectrum at a particular CMP location was combined with the corresponding CVS on the display in order to aid in more accurate picking of the time-
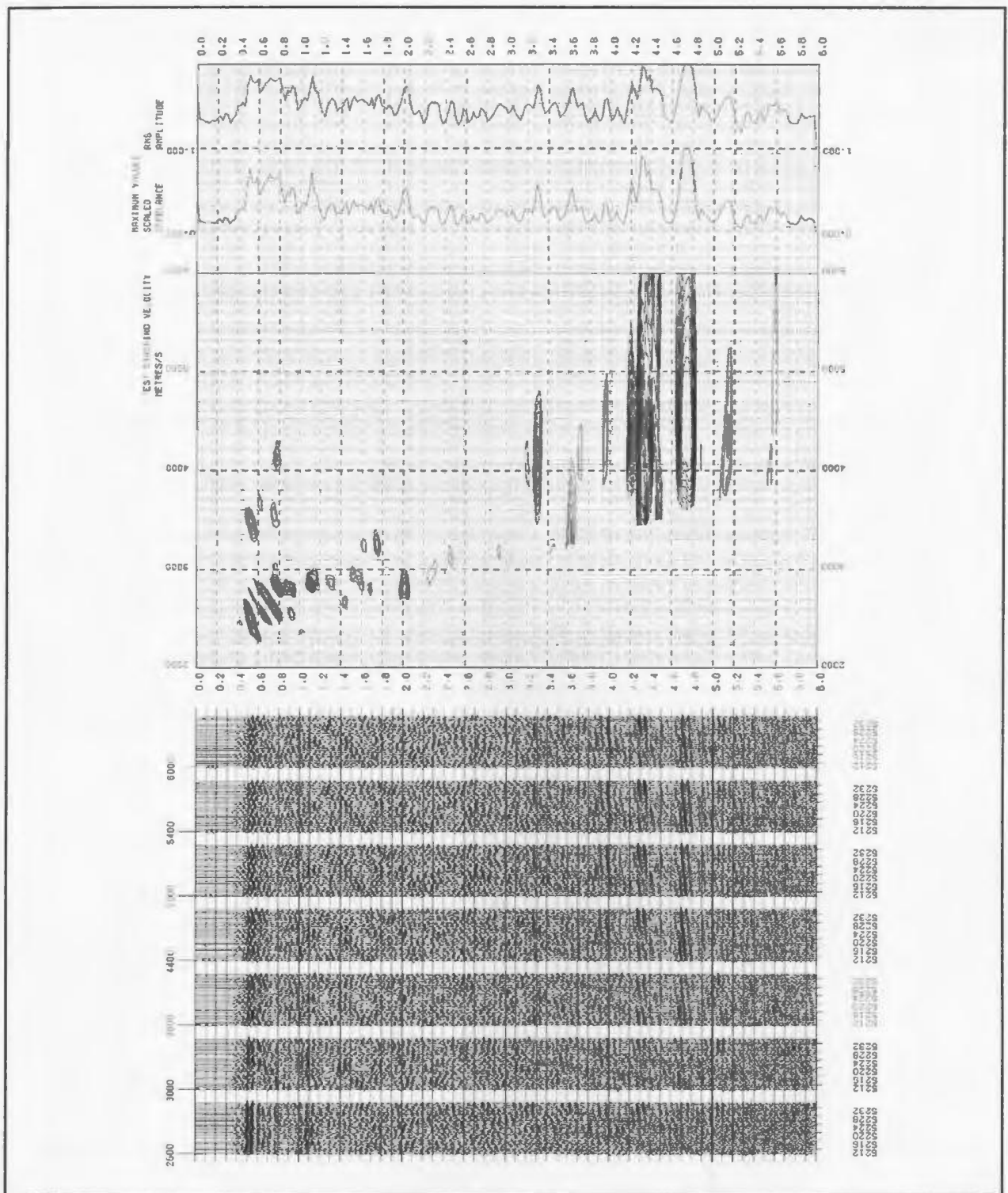
Figure 3.5 Typical velocity analysis from the western Botswana deep seismic data set containing both constant velocity stacks (CVS) and velocity spectra.

velocity pairs. The spectrum or contour plot of Figure 3.5 is essentially a measure of how well a hyperbolic trajectory of some trial curvature, dependent upon t_0 and v_{nmo}, fits the CMP data itself at a particular time t (Hatton *et al.*, 1986). The measure of fit or "coherence" used by processor :MERVEL is called the *semblance* and is expressed as:

$$Semblance = \frac{\sum_{i=1}^{N}\left[\sum_{j=1}^{M} a_{ij}\right]^2}{M\sum_{i=1}^{N}\sum_{j=1}^{M} a_{ij}^2} \tag{3.2}$$

where a_{ij} is the amplitude of time sample i on trace j within the CMP gather. It should be noted that $0 < Semblance < 1$, with perfect correlation corresponding to 1.

Whereas the CVS method utilized 25 adjacent CMP records for stacking, the velocity spectra produced by :MERVEL used only 5 adjacent CMPs for its analysis. The velocity increment used for the semblance calculation was 50 m/s with the calculation confined between low velocity limits of 2,000 to 4,000 m/s from 0 to 6 s respectively and a high velocity limit of 6,000 m/s, also from 0 to 6 s (see Figure 3.5). Also, only semblance values between 0.4 and 0.9 were contoured and plotted on the final spectrum display.

3.3.6 Front Mute Determination

An undesirable side-effect of NMO correction is frequency distortion, particularly for shallow events and at large offsets (Yilmaz, 1987). This distortion is referred to as *NMO stretch*. Since the aim of the NMO correction is to shift all reflections to their respective zero-offset times, a waveform with dominant period T is stretched so that its period after

correction, T', is somewhat greater. This frequency distortion of the waveform shifts events to lower frequencies and can be expressed quantitatively as:

$$\frac{\Delta f}{f} = \frac{\Delta t_{nmo}}{t(0)} \tag{3.3}$$

where f is the dominant frequency, Δf is change in frequency and Δt_{nmo} is the difference between $t(x)$ and $t(0)$ of Equation 3.1 (Yilmaz, 1987).

Because of the stretched waveform at large offsets, stacking all traces of the NMO corrected CMP gather will severely damage shallow events. This problem is solved by muting the most-stretched zones in the gather prior to stacking. For the western Botswana data set, determination of these front mutes was done by displaying every 200th NMO corrected CMP gather along each of the line and then manually picking time-offset pairs which defined the undesirably-stretched zones. These front mutes are then linearly interpolated between these control points and applied to the NMO corrected data via the use of processor :MUTE prior to stacking.

3.3.7 Spectral Balancing

Immediately prior to stacking, the data were spectrally balanced by way of processor :AFBAL. This processor designs non-overlapping narrow-band trapezoidal filters in the frequency domain based on user input. These narrow-band filters, when applied in the frequency domain, separate the trace into its spectral components. It is worthy to note that in order for spectral balancing to provide effective whitening, the bandwidth of the

seismic data should be ≥ 2 octaves.

The user specifies an upper and lower frequency and the number of filters to use within this frequency range. The input trace is then filtered in the frequency domain and the filtered results are then Fourier transformed to the time domain, balanced in the same manner as processor :GAIN, (processor description to follow in a subsequent section) and then summed. The result is a trace that is both spectrally whitened over the frequency range specified and temporally balanced. It should be noted that this processor operates on each trace independently.

To determine an appropriate frequency range to balance over, a series of bandpass filters were applied to a portion of the stacked section and then displayed in order to ascertain the dominant reflection frequencies contained within the data. These filter panels are displayed in Figure 3.6. Pass bands of 10 to 20 Hz, 20 to 40 Hz, 30 to 60 Hz and 40 to 80 Hz were used and based upon the examination of the filtered results, it was decided to spectral balance the data from 5 to 45 Hz using 3 pass bands. The pass band of each filter in the frequency domain has a width = [4×{45 - 5}]/[{3×3}+1] or 16 Hz. The first node of the first filter is the lower frequency and the next filter node begins at the first node of the previous filter plus [(3×5)/4] or 15 Hz. Table 3.3 lists the nodes of the three filters used. For temporal balancing of the data upon completion of the filtering, a fixed length sliding window of 1 second was used for calculation of the gain function that is applied to all samples in the trace from the first to last sample.
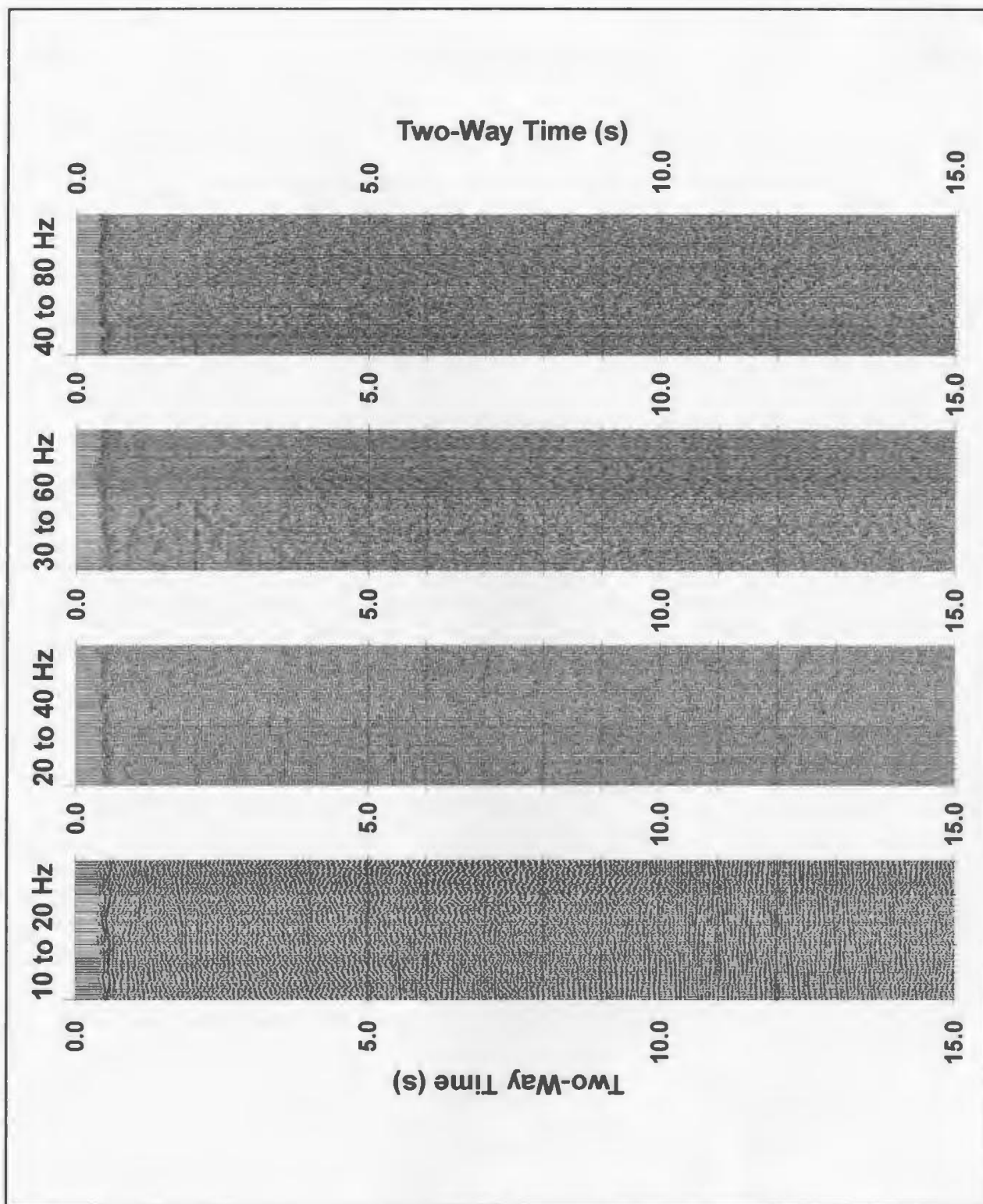
Figure 3.6   Filter panels of the western Botswana deep seismic data set displayed with pass bands of 10 to 20 Hz, 20 to 40 Hz, 30 to 60 Hz and 40 to 80 Hz.

Table 3.3 Filter nodes (Hz) of the three filters used in the spectral balancing of the western Botswana deep seismic data set.

Filter	0% Pass	100% Pass	100% Pass	0% Pass
1	5	9	17	21
2	17	21	29	33
3	29	33	41	45

3.3.8 Stacking

Processor :**STACK** was used to output a single "stacked" trace for each CMP record input. Data samples on all traces within the record are summed at each time and this result is then divided by the number of values summed (excluding muted zones on the front of each trace). This process is known as *standard mean stacking*.

The stacking process is a very simple but powerful tool for improving the signal-to-noise ratio of seismic reflection data. Each time sample of a single trace from the common mid-point gather can be regarded as an estimate of the primary reflected signal at a particular two-way travel time, contaminated by random noise (Hatton *et al.*, 1986). The redundancy of the information inherent in the seismic recording technique can be used to reduce the error in this estimate by taking a statistical average. The most commonly used estimator is the mean.

After correction of the data for normal moveout, the mean sample value at each two-

way travel time can be calculated. Defining the amplitude of the ith time sample of the jth trace to be a_{ij}, the mean will be given by:

$$A_i = \frac{1}{M}\sum_{i=1}^{N}\sum_{j=1}^{M} a_{ij} \qquad (3.4)$$

where N is the total number of time samples per trace and M is the total number of traces contained within each CMP gather. This summation or stacking of traces in Equation 3.4 is normalised by the factor $1/M$ which results in the signal having the correct amplitude after the stack. If each trace after normal moveout correction is thought of as containing the same amount of signal plus the addition of Gaussian noise, the signal-to-noise improvement in the stacking process should be $\sqrt{M}$. The final unmigrated time stacks for lines 90, 91, 92, 93, 94, 97 and 99 are presented in Section 3.4.

3.3.9 Migration

Migration moves or "migrates" dipping reflectors into their true subsurface positions and collapses diffractions, thereby delineating detailed subsurface features such as fault planes (Yilmaz, 1987). Thus the goal of migration is to make the stacked section appear similar to a geological cross-section along the seismic line. The migration process can produce both a migrated time section (displayed in two-way travel time) and a migrated depth section (displayed in depth) which are referred to as time migration and depth migration respectively.

These data were migrated using the Landmark/ITA *INSIGHT* poststack processing

package. The primary motivation for the switch from *STARPAK* to *INSIGHT* for migration purposes was the much wider variety of migration algorithms offered by the *INSIGHT* software. All of the western Botswana seismic lines, except for line 99, were time migrated to their maximum record length, 15 s, and depth migrated to 45 km. Line 99, due to its longer record length, was time migrated to 20 s and depth migrated to 60 km.

The algorithm that was chosen to migrate the western Botswana data was the Gazdag phase-shift implementation of a frequency-wavenumber migration which produces both a time and depth migrated section. This method involves a coordinate transformation from frequency (the transform variable associated with the input time axis) to vertical wavenumber (the transform variable associated with the output depth axis), while keeping the horizontal wavenumber unchanged (Yilmaz, 1987).

Fourier transform methods in migration were introduced by Stolt (1978). Gazdag (1978) published his work on the phase-shift method which led to a further understanding of wave field extrapolation in the transform domain. As pointed out by Yilmaz (1987), frequency wavenumber (f-k) migration is not easily explained from a physical view point and referred to the work of Chun and Jacewitz (1981) as providing good insight into the principles of f-k migration.

Figure 3.7 presents a flowchart of the phase shift method. Downward continuation involves a pure phase-shifting operation $\exp(-ik_z z)$ and, at each depth step, z, a new extrapolation operator with the velocity defined for that z value is computed (Yilmaz,

Input Zero-Offset Section
$P(x, z = 0, t)$

2-D Forward Fourier Transform
$P(k_x, z = 0, \omega)$

Apply the phase shift, $\exp(-ik_z z)$,
to downward continue the surface data

Compute P at new z ←—— $P(k_x, z, \omega)$

Sum over the frequency;
(This is the imaging principle, $t = 0$)
$P(k_x, z, t = 0)$

Inverse Fourier transform in x
$P(x, z, t = 0)$
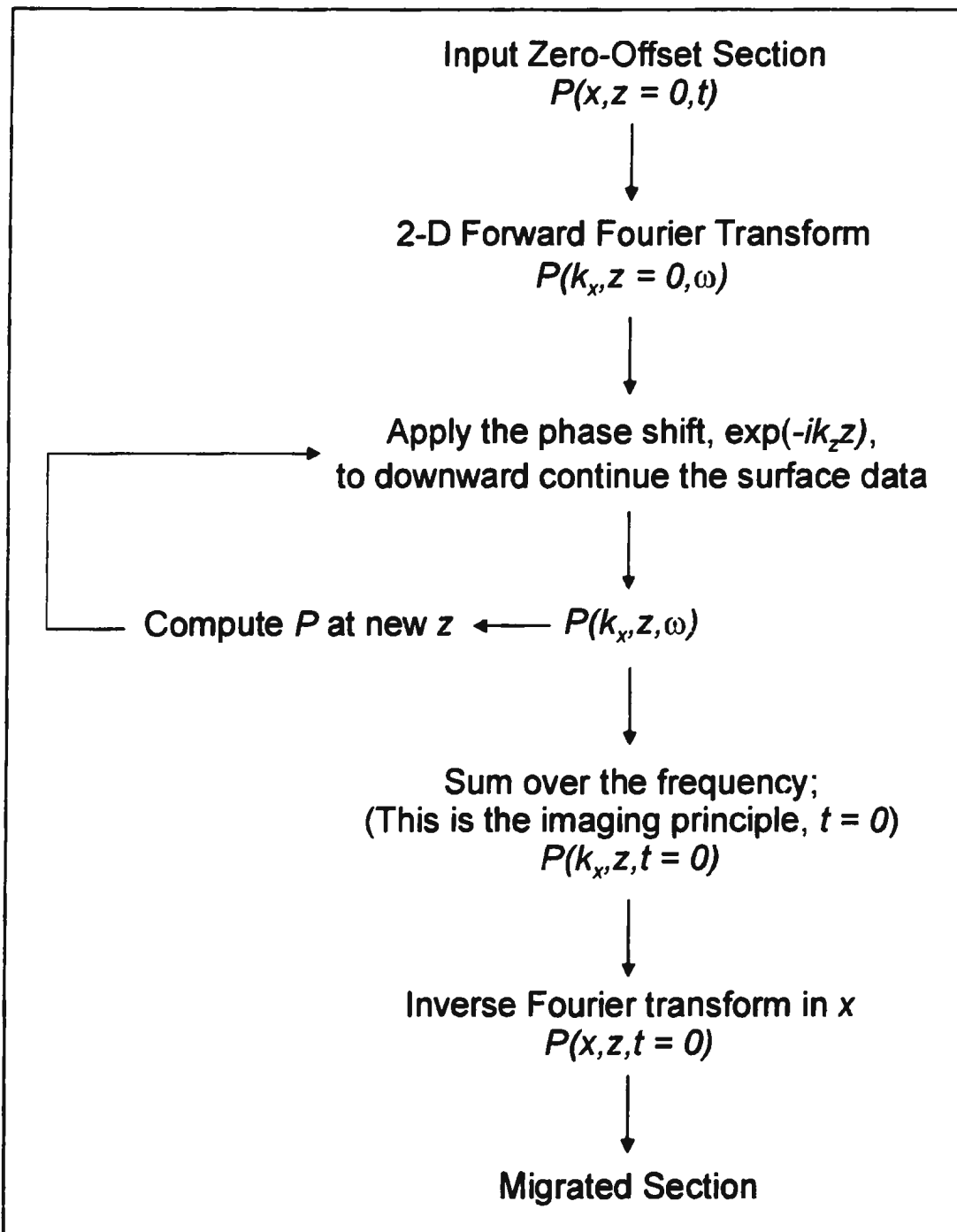
Migrated Section

Figure 3.7   Flowchart for Gazdag's phase-shift method of migration (after Yilmaz, 1987).

1987). As for any other migration, the imaging principle (t = 0) needs to be invoked at each extrapolation step to obtain the migrated section. The imaging principle refers to the fact that the wavefront shape at t = 0 corresponds to the reflector shape for the wave field generated by an exploding reflector (Yilmaz, 1987). The imaging condition t = 0 is met by summing over all frequency components of the extrapolated wave field at each depth step. The procedure of downward continuation and imaging is repeated until the entire wave field is migrated.

The *INSIGHT* phase-shift migration algorithm, **PSMIG_FAST**, requires the definition of a number of time-frequency bands which are used to define a range of frequencies to migrate for a given time. Since the data had been previously spectrally balanced between 5 and 45 Hz, a single frequency band of 5 to 45 Hz was chosen for the entirety of the record to migrate over.

The phase-shift method can only handle vertically varying velocities. To enable the tying of all seven depth migrated sections at their respective cross-overs, a constant depth step or depth sampling interval, Δz, was required. This could only be accomplished by using a single velocity function for the migration of all seven seismic profiles. As such, in order to utilize a migration velocity function which provided a certain degree of geologic control, integrated two-way sonic times and corresponding depths were picked from the adjusted sonic log of the stratigraphic test well drilled on line 99 (labelled "GSD Pan-1" on Figures 3.27 - 3.29).

Since the adjusted sonic log did not extend entirely to the surface, it was necessary

to perform first break refraction analyses of a few shot gathers centred about the well location in order to provide near surface velocity-depth information. These refraction analyses along with the time-depth picks from the sonic log allowed the compilation of an interval velocity function for the well interval.

To tie this function with deeper (> 2 s TWT) velocity information, interval velocities were converted to RMS (root-mean-square) values using the following equation (Dix, 1955):

$$V_{rms} = \left(\frac{\sum_{i=1}^{n} V_i^2 t_i}{\sum_{i=1}^{n} t_i} \right)^{\frac{1}{2}} \tag{3.5}$$

where V_i and t_i being respectively the interval velocity in, and the travel time through, the ith layer. These RMS velocities were then combined with velocity picks from a conventional velocity analysis (as described in Section 3.3.5) performed at the well location to produce a final velocity function used for the migrations. This RMS velocity function is illustrated in Figure 3.8. The final time and depth migrations for all the profiles are presented in Section 3.4

3.3.10 Coherency Filtering

With the migrations completed, the data was moved back to *STARPAK* to perform coherency filtering. This was achieved by using processor :CANE which is a spatial coherency filter. The filtering is accomplished by stacking sub-windows of data from
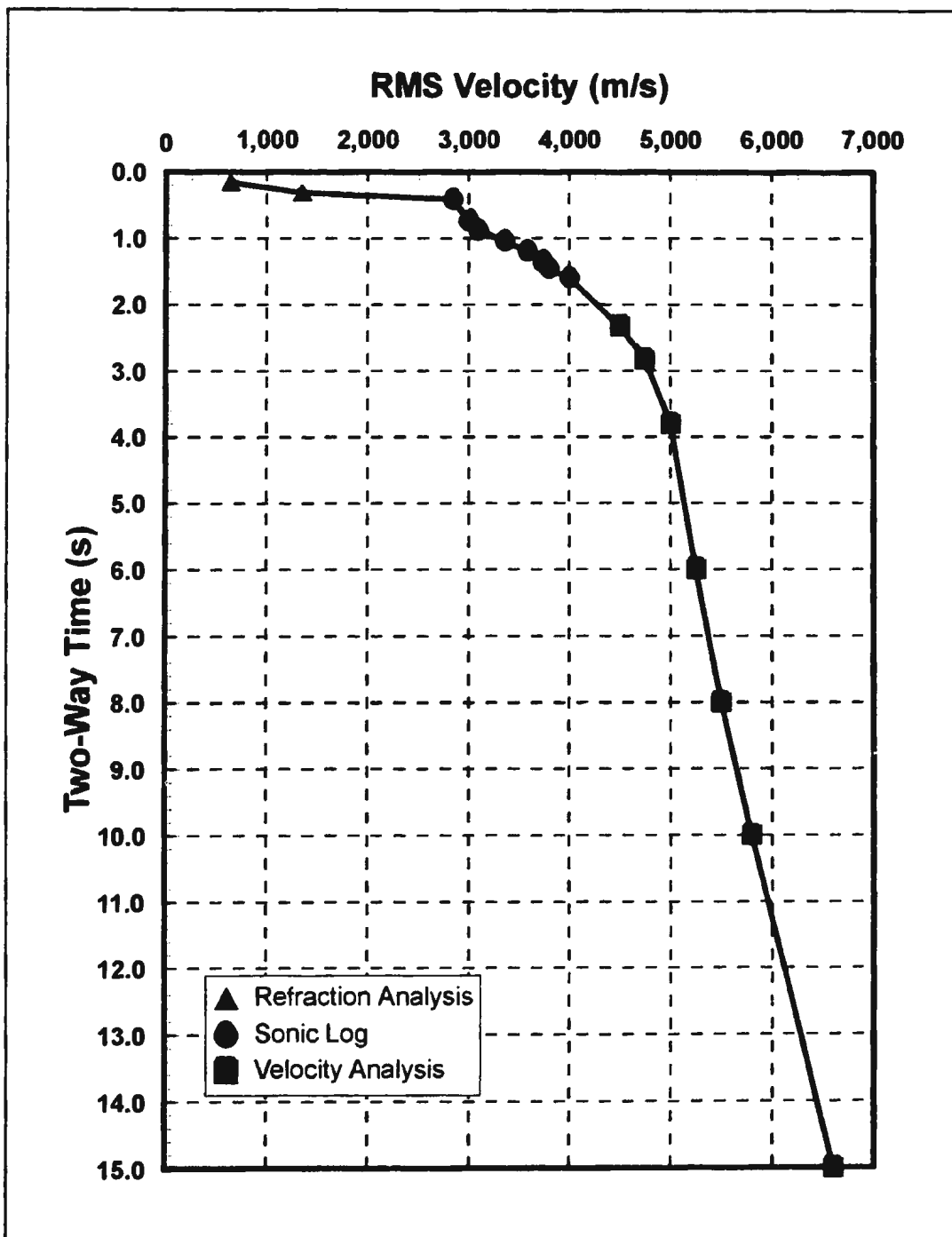
Figure 3.8   RMS velocity function used to migrate all seven deep seismic reflection profiles from the Nosop Basin, western Botswana.

several adjacent traces. By properly time aligning these sub-windows with the reference or current trace, an optimum coherence stack is obtained and undesirable noise is suppressed.

:CANE crosscorrelates a sub-window of the current trace with corresponding sub-windows on a selected number of adjacent traces centred on the current trace. The largest peak of each crosscorrelation is searched for, within a limited temporal range. The corresponding trace sub-windows are then shifted by the peak lag times, weighted, stacked and then tapered. The resulting sub-stacks are summed, at the appropriate times, to form the output trace. The sub-window is moved down the trace in steps of half the sub-window's length between the selected start and end times. The crosscorrelation length is chosen to just include events of desirable dip and is expressed as ms/trace.

A trace window of nine adjacent traces, a time sub-window of 120 ms and a crosscorrelation of 8 ms/trace was used for both the unmigrated and time migrated stacks. A smaller rather than larger trace window was opted for as the data were to be later trace-mixed and summed. Lateral "smearing" of the trace energy prior to these steps should be minimized. Also, a crosscorrelation length of 8 ms/trace was chosen as this number would encompass the range of time dips seen in the unmigrated and time migrated sections.

For the depth migrations, because the sampling interval was no longer in terms of ms but rather m, the sub-window length was chosen to include the same number samples that were used for the time sections. This was also true for the choice of crosscorrelation length.

3.3.11 Trace Mixing and Summing

Processor :ARRAY was used to perform an array simulation on the stacked traces. It utilizes a time-invariant weighting function which may be either symmetrical or asymmetrical. The output trace is a linear combination of the input traces in the array multiplied by the weighting function. Normalization of the trace weights is necessary to accommodate for dead traces and for tapering of the edges of the data.

A three weight symmetrical array with weights of 1-2-1 was used to array the unmigrated and migrated stacks. The same number of traces were output as were input with the array moving along the stacked traces in a roll-along fashion. As with the coherency filtering, a small array was opted for to prevent the data from looking highly mixed on final output.

Adjacent arrayed traces were then summed using processor :TSUM. This processor vertically stacks or sums a selected number of adjacent traces. The summed traces are then scaled by the number of live traces in the adjacent trace group. A three adjacent trace sum was used on the arrayed data.

3.3.12 Filtering

Prior to gaining and final display, a low-pass, minimum-phase time domain filter was applied to the unmigrated and time migrated stacks using processor :TIMEFILT. A cut-off frequency of 30 Hz with a 16 dB/octave roll-off was chosen. These parameters were selected based on examination of the filter panels previously generated for design of the

spectral balancing. It was felt that this filter would pass the most dominant frequencies present in the data given the source used and the record length (i.e. predominantly lower frequencies). Also, since the data had been previously spectral balanced, frequencies in this range (5-30 Hz) would have been equalized in terms of their amplitudes.

It should be noted that the depth migrated stacks were not filtered. Since the traces making up the depth migrations were now expressed in terms of depth rather than time, the application of a low-pass time domain filter was questionable and, in the end, avoided.

3.3.13 Gaining

In order to produce a final section which can be interpreted, the trace amplitudes must be somehow balanced so that both high and low energy reflection events can be seen. This was done through the use of processor :GAIN.

A fixed or variable length window slides down the trace one sample at a time. Within this window, the average absolute amplitude of all non-zero amplitudes is calculated as follows:

$$A = \sum_{i=1}^{N} \frac{|a_i|}{N} \tag{3.6}$$

where N is the number of time samples contained within the window and a_i is the amplitude at time sample i. The ratio of the desired output average amplitude to the average amplitude calculated within the window is the gain scalar, S. This gain scalar can be applied to one of two sample locations within the window:

1) If the centre of the window is specified, the scalar S is multiplied by the amplitude a_c of the centre sample of the window.

2) If the bottom of the window is specified, the scalar S is multiplied by the amplitude a_b of the last sample of the window.

In either case, $S \cdot a_c$ or $S \cdot a_b$ represents the balanced amplitude for that particular sample.

A clipping option exists for the centre window option to prevent excessive attenuation of amplitudes in the region of high energy reflections. This clipping option limits the contribution of high energy amplitude events to the computed average by clipping. The clipping level is determined by multiplying the clipping scalar, specified by the clipping scalar verb, by the trace average absolute amplitude within the defined clipping window.

A fixed length window of 1,000 ms and the default average amplitude normalization level of 3,000 were chosen for the amplitude balancing of the unmigrated and time migrated sections. The calculated gain scalar was applied to the centre of the window and, due to the presence of high energy reflections contained within the data, the clip option was chosen with the mandatory clipping window and clipping scalar verbs. The clipping level scalar used was 0.5 with a clipping window length of 3,000 ms and 4,000 ms for line 99 (20 s record). These were selected by running a number of tests by first changing the value of clip scalar and examining the output to determine its optimum value and, using this clip scalar value, altering the clipping window length to determine its optimum value.

For the depth migrated stacks, values of 1,500 ms, 0.5 (dimensionless) and 4,500 ms

were used for the fixed window length, the clip scalar and the clipping window respectively. For line 99 (60 km record length), the values of the fixed window length and the clipping window were increased to 2,000 ms to 6,000 ms respectively.

3.3.14 Trace Display

Processor :PLOT was used for the final display of the stacked sections. For the unmigrated and time migrated sections, the horizontal and vertical scales used for plotting was 16 traces/cm and 2.54 cm/s (0.83 cm/km for the depth sections) respectively. These scales yielded a final display with a 1:1 vertical exaggeration assuming an average velocity of 6 km/second. The mode of display chosen for the traces was variable area positive with the application of a high negative bias. This produced a display with good contrast with the high bias accenting only the most prominent reflections seen within the stacked sections. The plotting direction (CMP numbers increasing right to left vs. left to right) for each stacked section was chosen so that the western end of the line was always situated on the left-hand side of the section and the eastern end on the right.

3.4   Final Processed Sections

The final processed unmigrated time sections and their respective time and depth migrations for lines 90, 91, 92, 93, 94, 97 and 99 are presented in Figures 3.9 through to 3.29 respectively. All seven lines clearly show the presence of a single, extensive sedimentary basin containing 12 to 15 km of strata which thin substantially to the east.

Below this basin, the crust also appears to be highly stratified containing numerous horizontal to sub-horizontal reflectors, some of which are very coherent and exceedingly continuous and traceable for tens of kilometres. In the following chapter, only the depth migrations overlain with simplified line drawings are presented for interpretation and discussion purposes.

It should be noted that the two digit line identities used in this thesis are the last two digits of the first four digits of the line numbers assigned by PCIAC (eg. "90" herein corresponds to 9490-87 in PCIAC reports).

.

97

SW

| 3457 | 3358 | 3259 | 3160 | 3061 | 2962 | 2863 | 2764 | 2665 | 2566 | 24 |
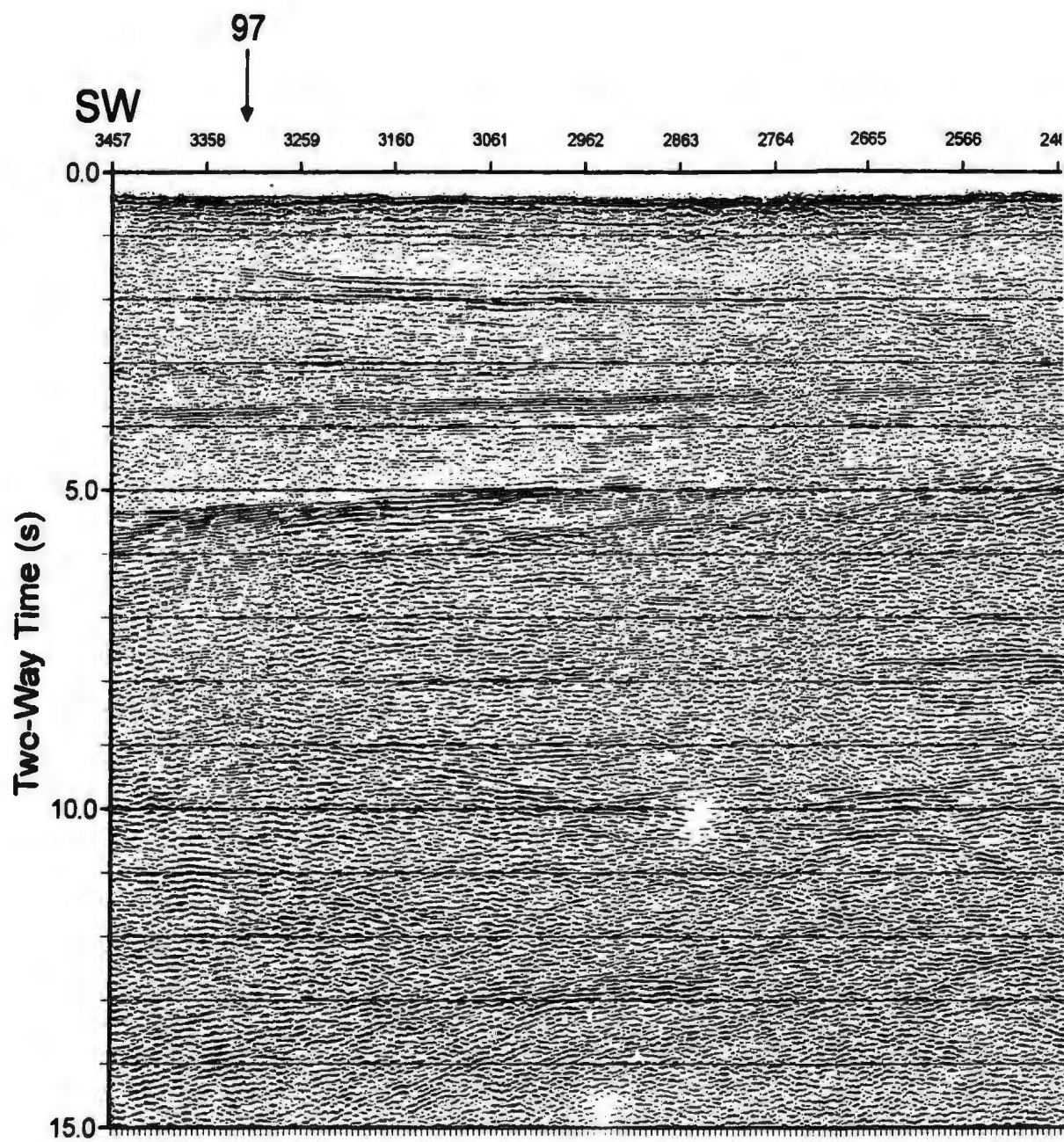
Figure 3.9   Unmigrated time section for Line 90.

91

| 2764 | 2665 | 2566 | 2467 | 2368 | 2269 | 2170 | 2071 | 1972 | 1873 | 1774 | 1675 | 1576 | 1477 | 1378 | 1279 |

91

Figure 3.10 Time migrated section for Line 90.

91

| 1279 | 2368 | 2269 | 2170 | 2071 | 1972 | 1873 | 1774 | 1675 | 1576 | 1477 | 1378 | 1279 | 1180 | 1081 | 982 |

Two-Way Time (s)

NE
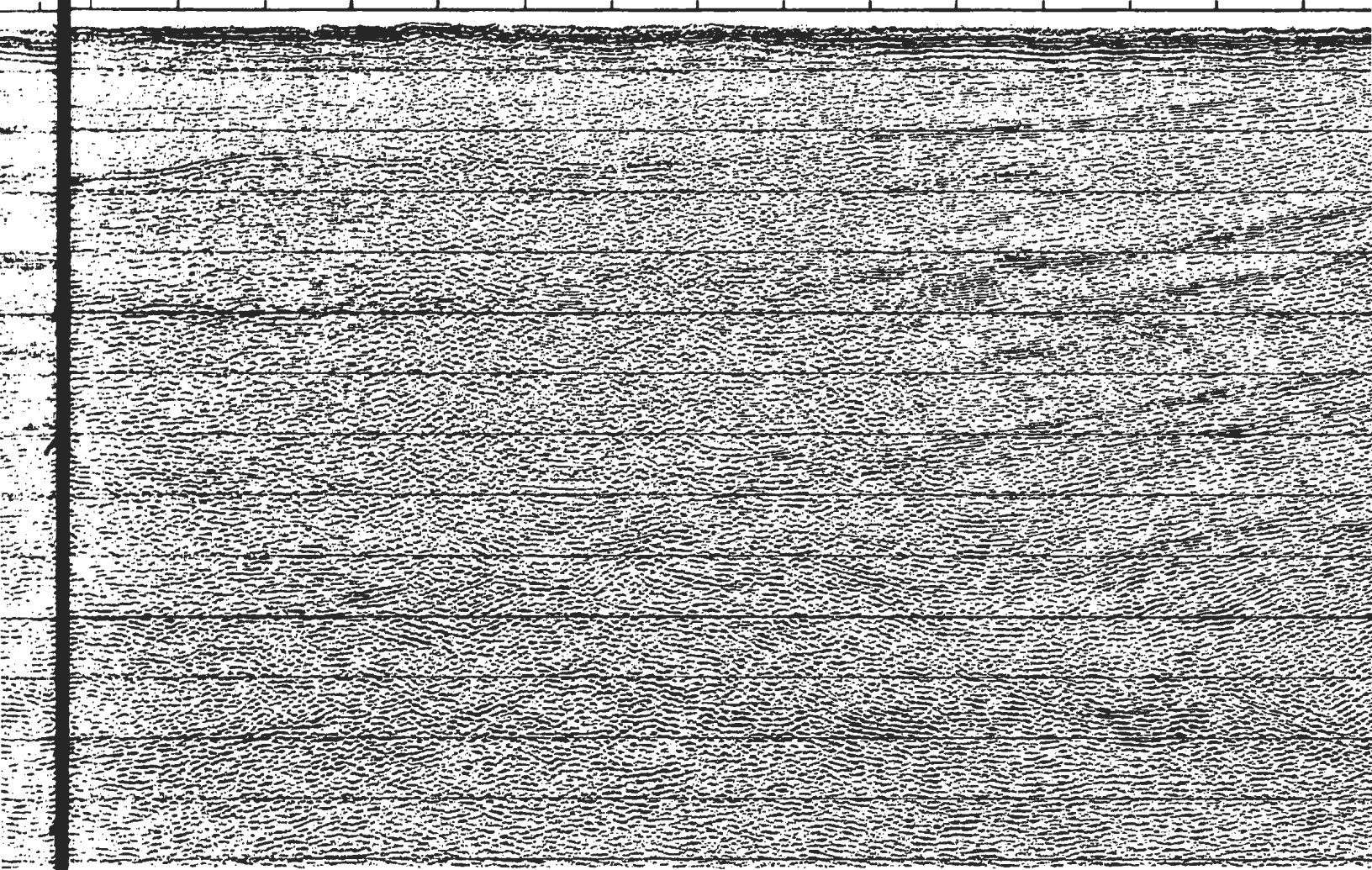
CKP-8C1
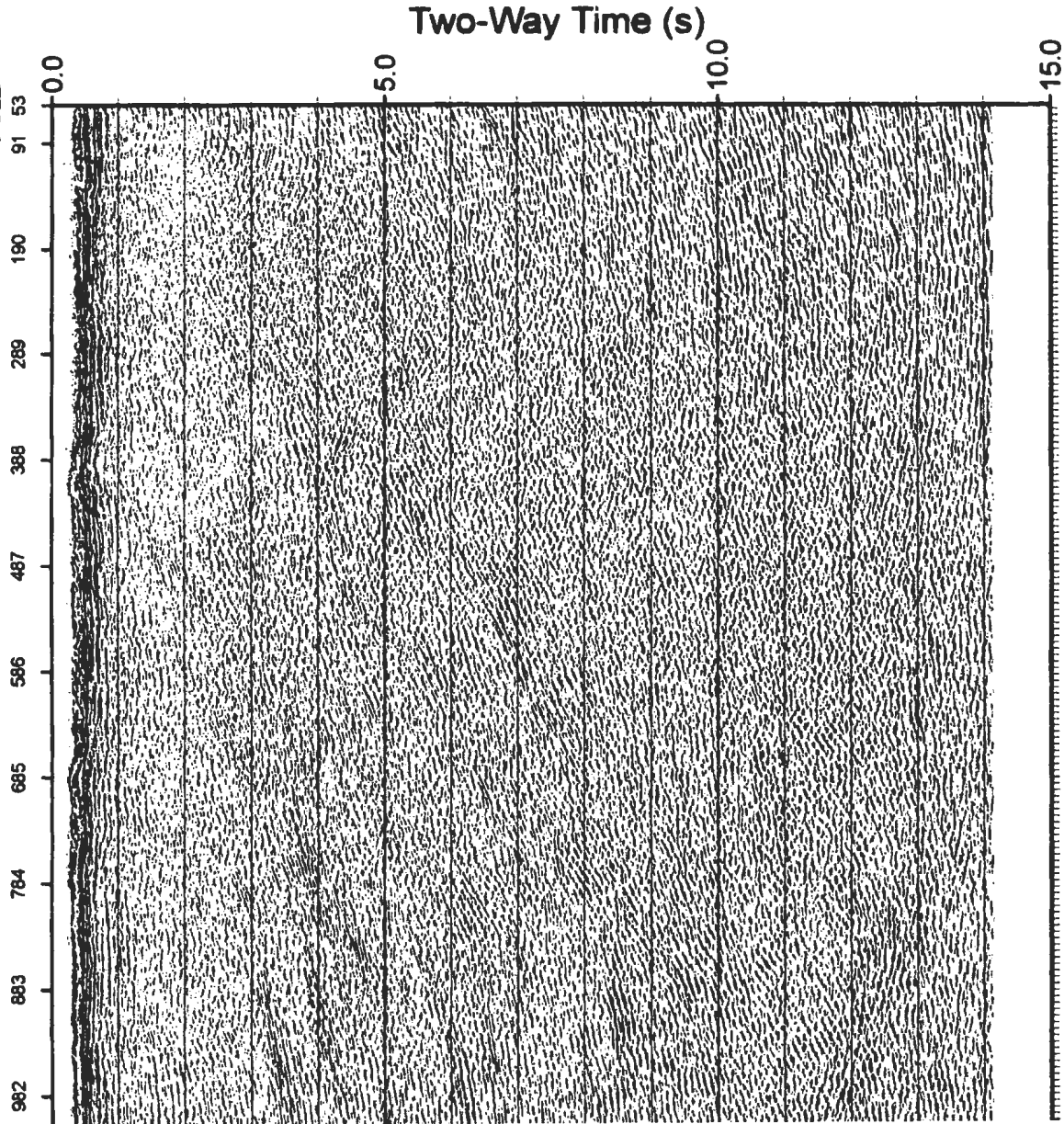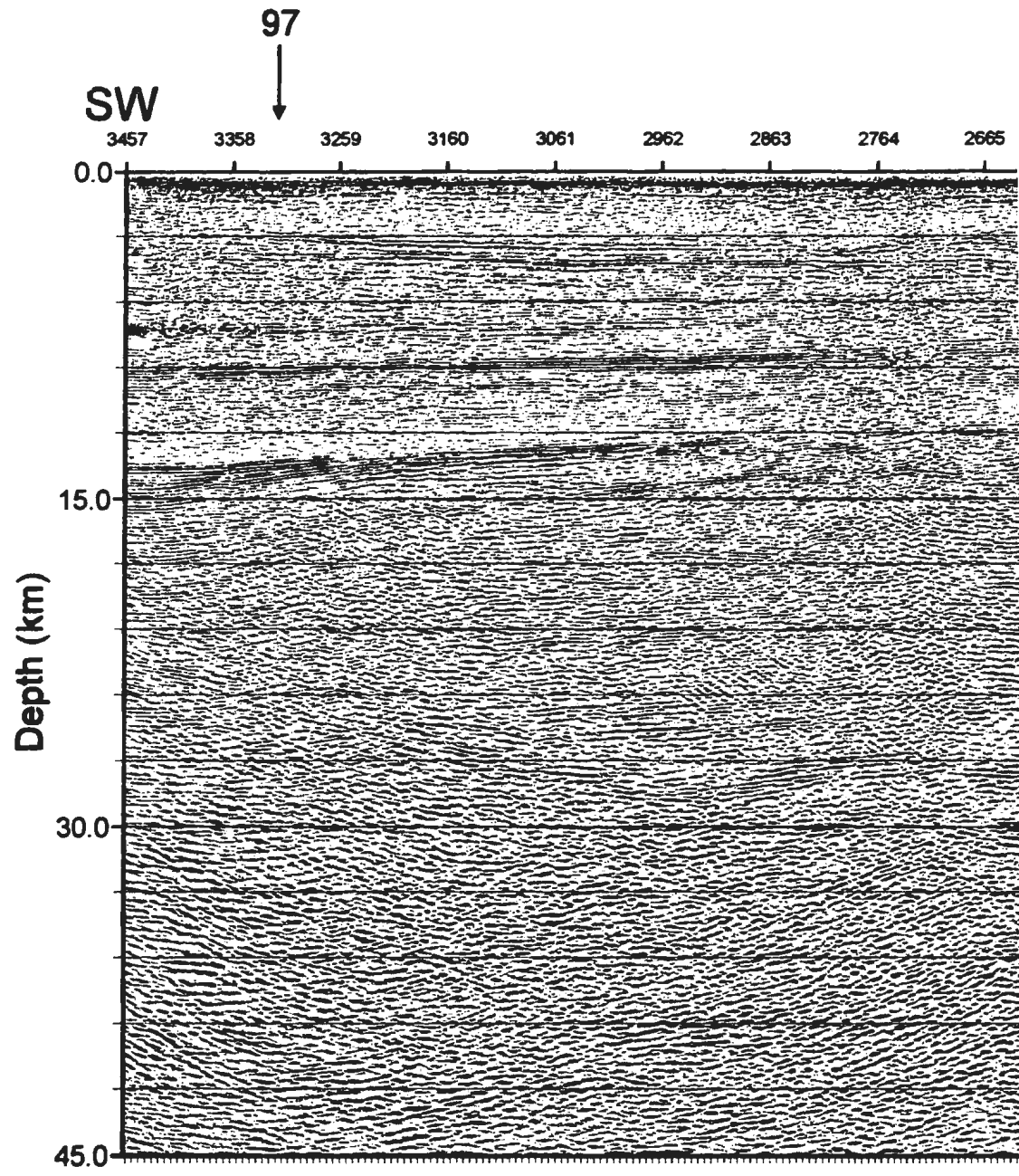
Figure 3.11 Depth migrated section for Line 90.

91

| 2764 | 2665 | 2566 | 2467 | 2368 | 2269 | 2170 | 2071 | 1972 | 1873 | 1774 | 1675 | 1576 | 1477 | 1378 | 1279 | 2368 |
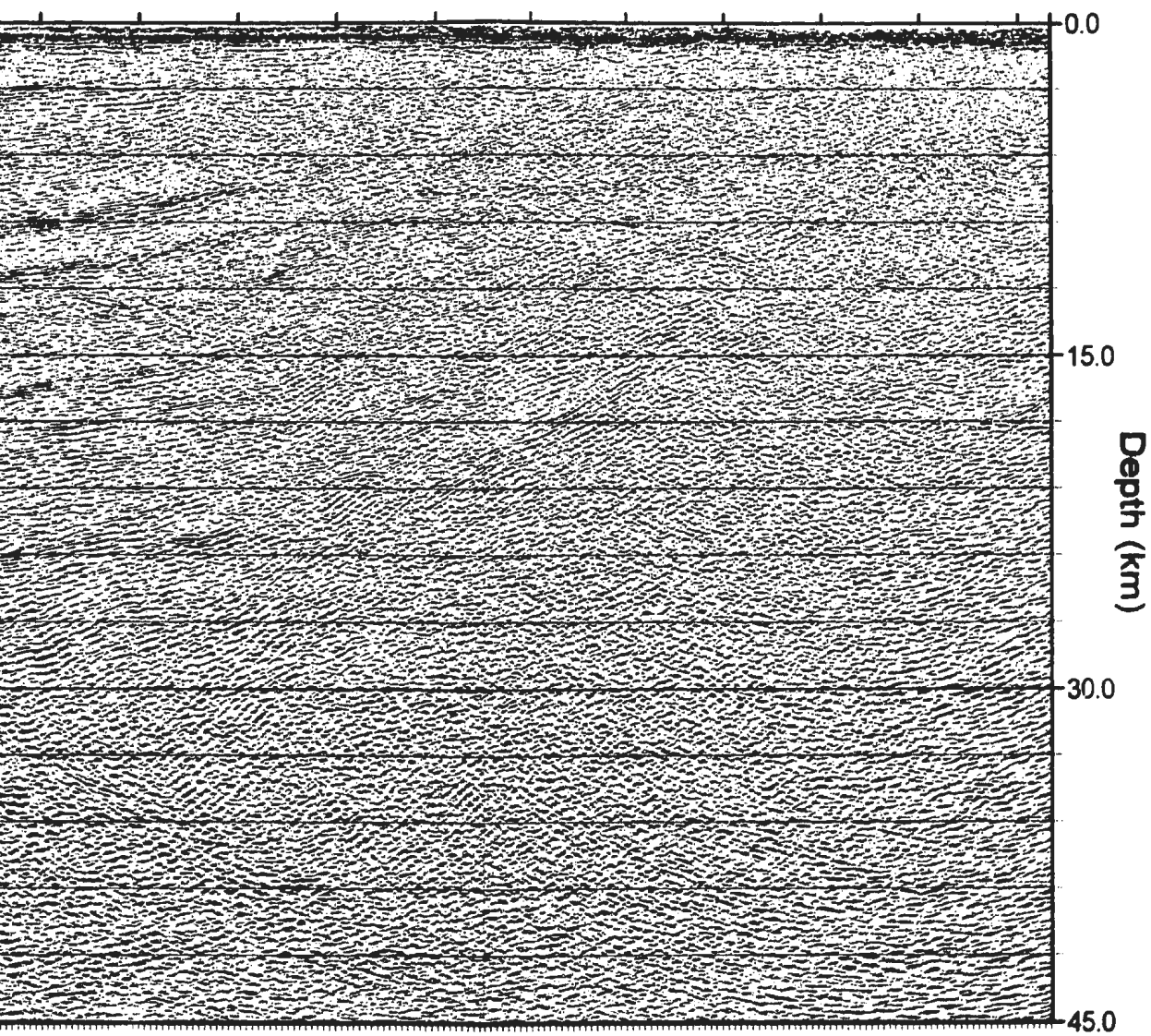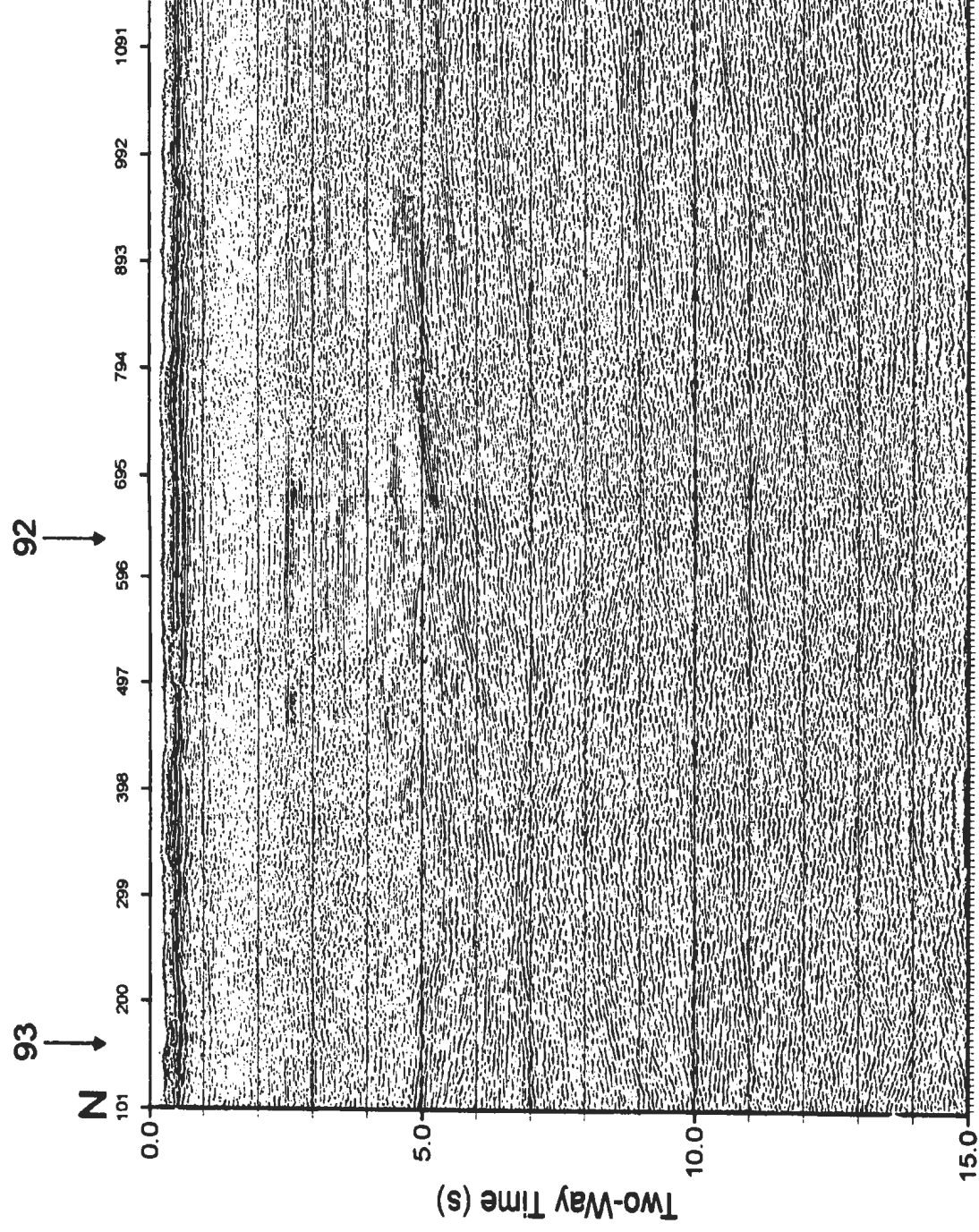
Figure 3.12 Unmigrated time section for Line 91.

Seismic Reflection Data/69

90

S

992   1091   1190   1289   1388   1487   1586   1685   1784   1883   1982   2079

0.0

5.0

Two-Way Time (s)

10.0

15.0
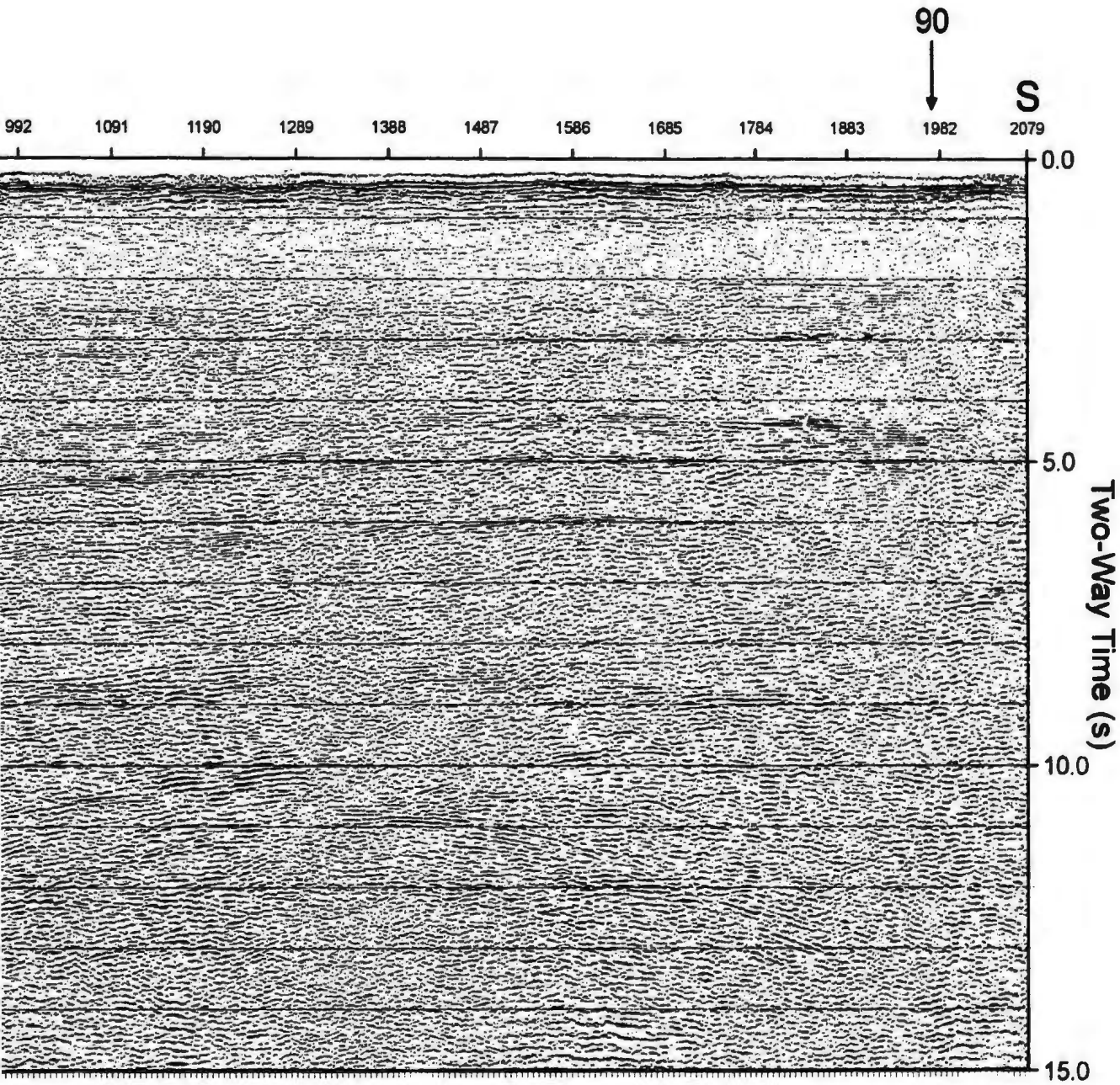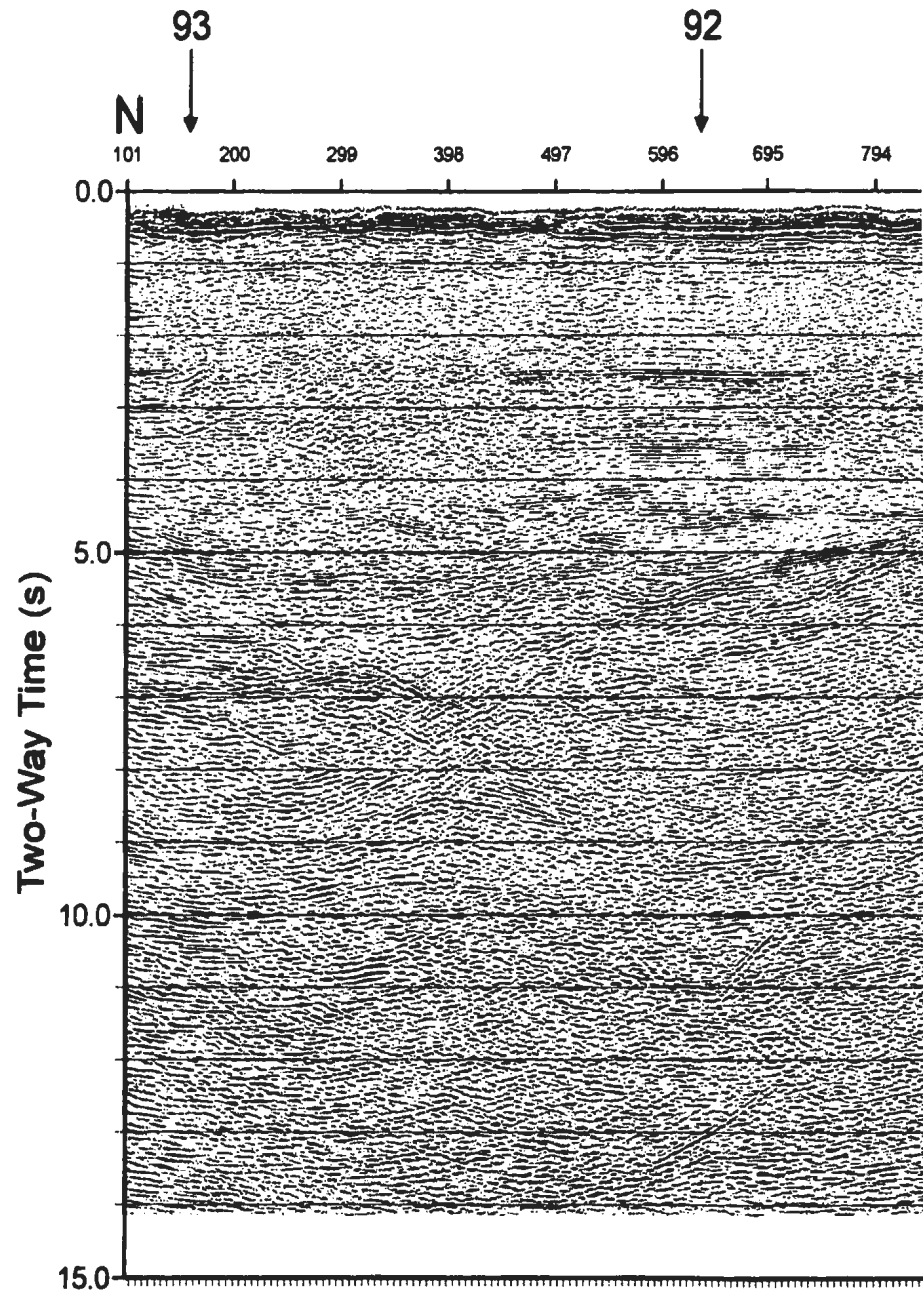
Figure 3.13 Time migrated section for Line 91.
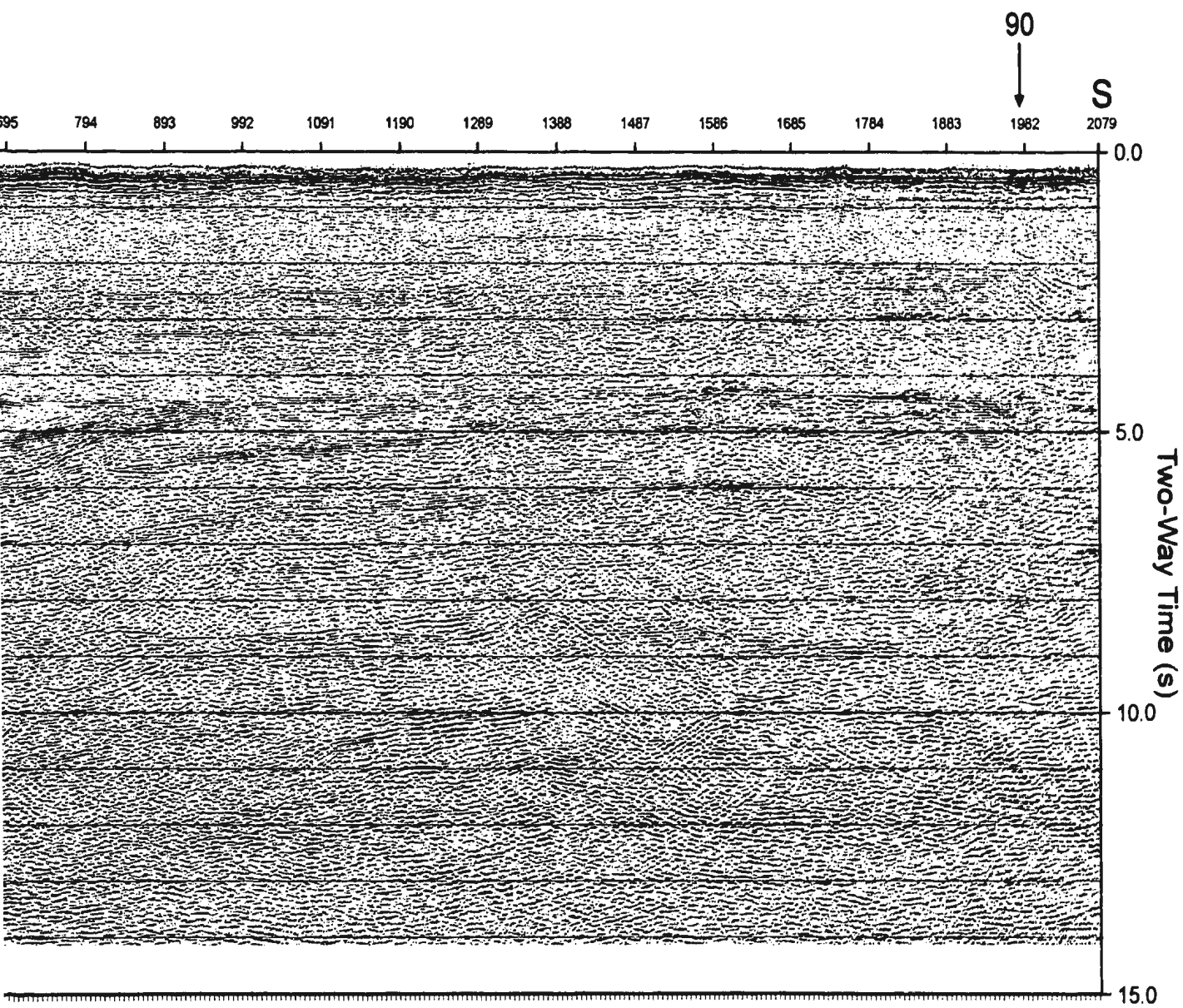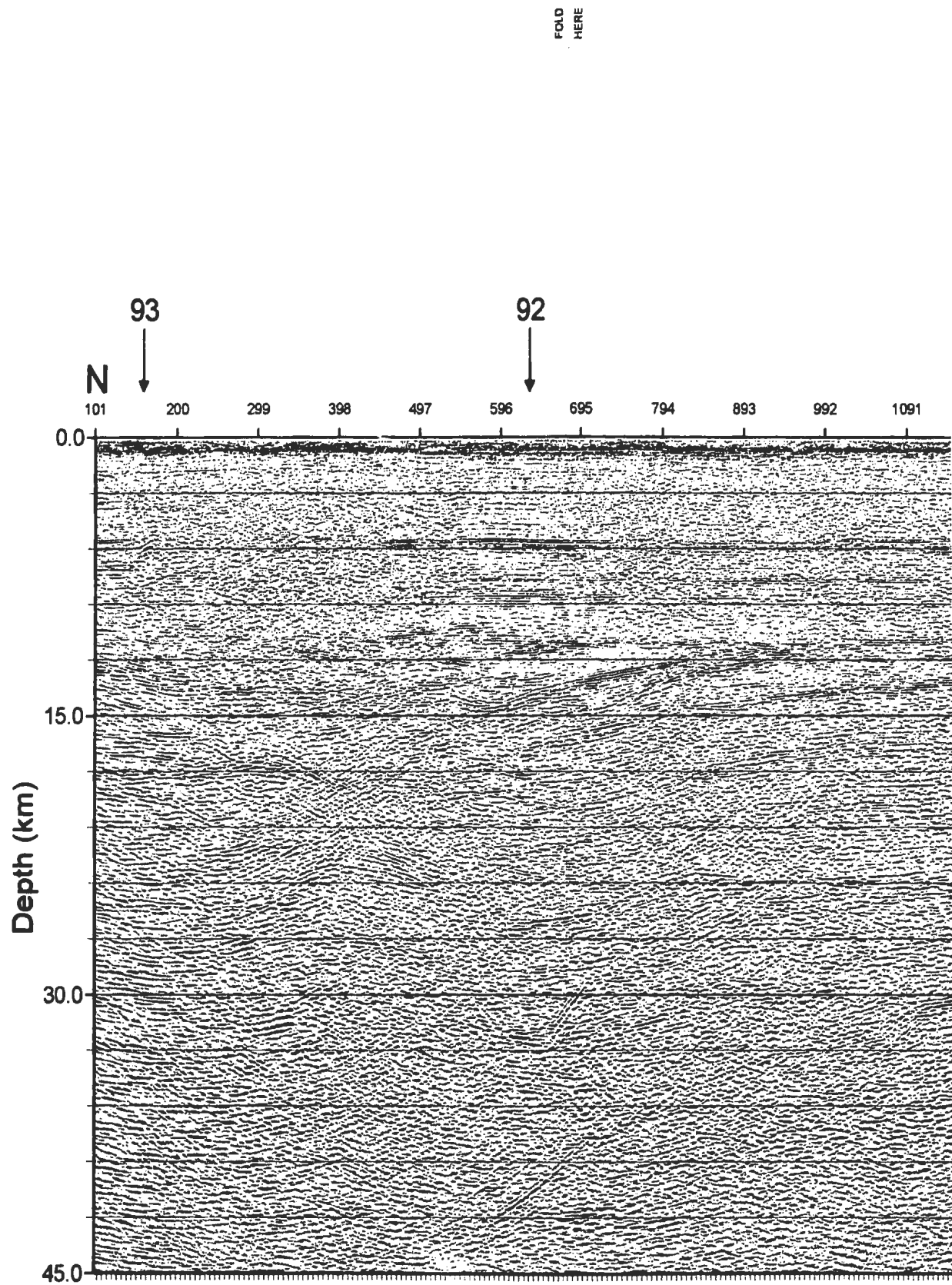
Figure 3.14 Depth migrated section for Line 91.

90

S

| 893 | 992 | 1091 | 1190 | 1289 | 1388 | 1487 | 1586 | 1685 | 1784 | 1883 | 1982 | 2079 |

0.0

15.0

30.0

45.0

Depth (Km)

97

SW ↓

3709 3665   3566   3467   3368   3269   3170   3071   2972   2873   2774   267
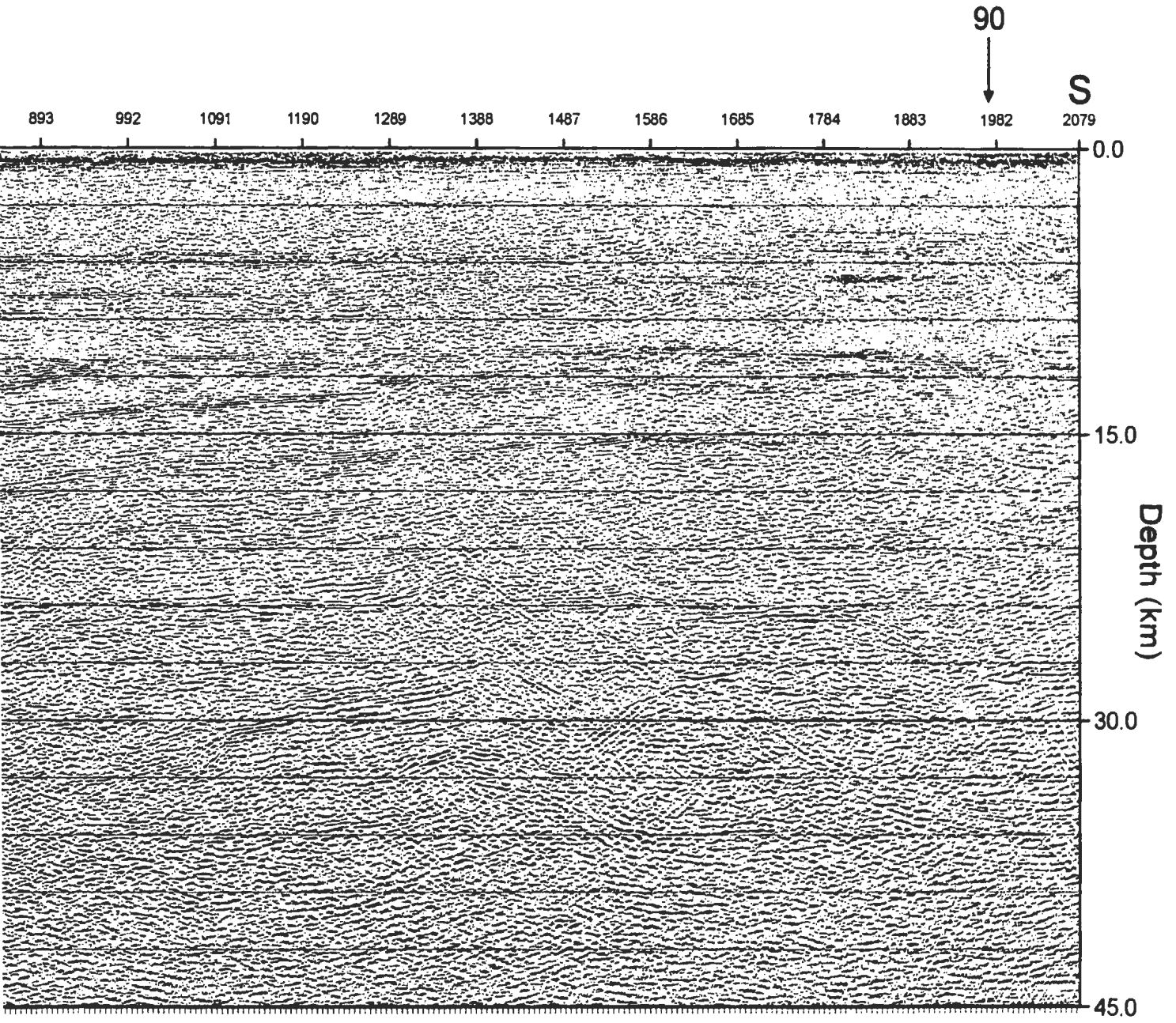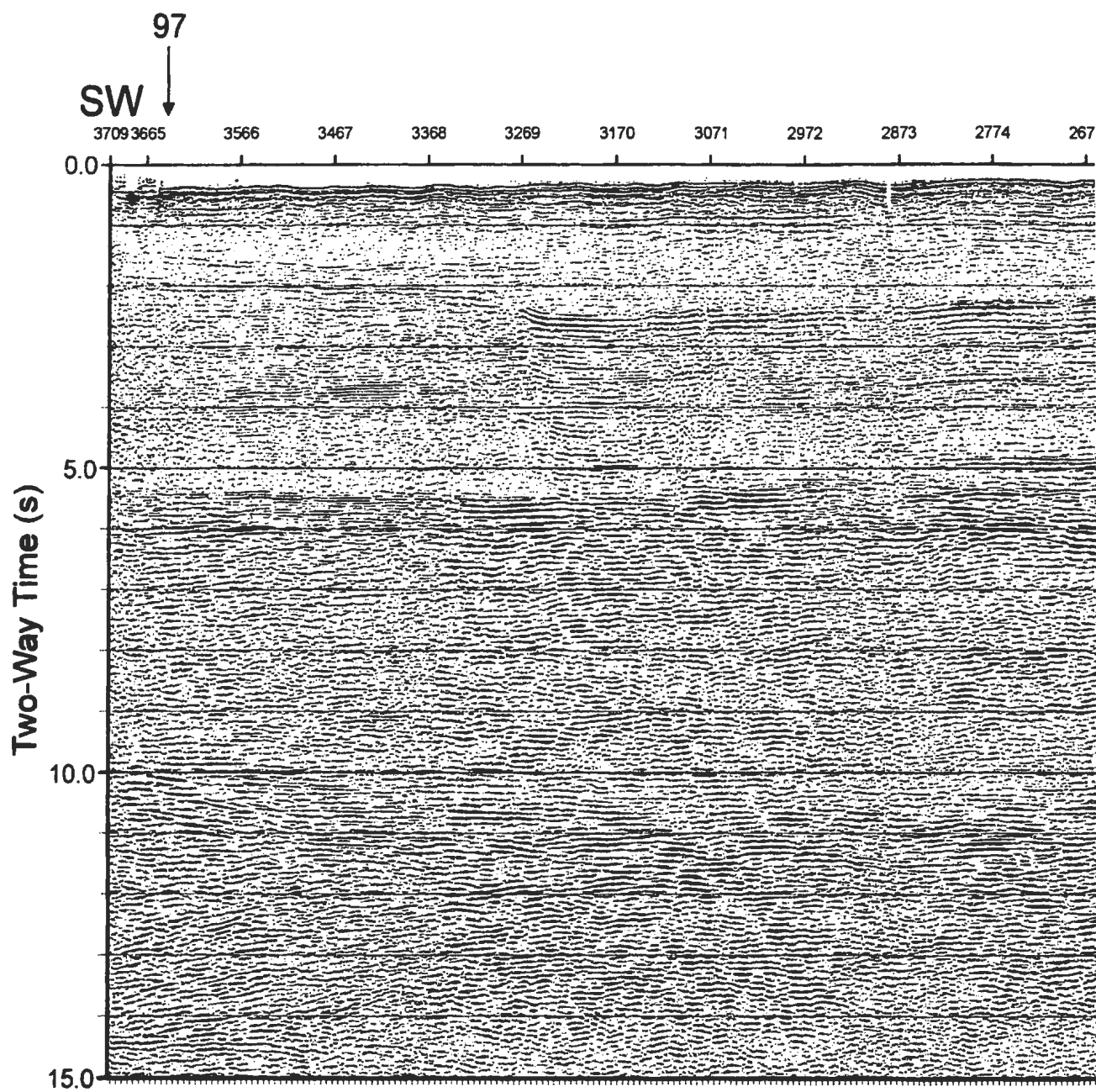
Figure 3.15 Unmigrated time section for Line 92.

99

91

NE

1091	992	893	794	695	596	497	398	299	200	101

0.0

5.0

Two-Way Time (s)

10.0

15.0

97

SW ↓

| 37093665 | 3566 | 3467 | 3368 | 3269 | 3170 | 3071 | 2972 | 2873 | 2774 |

Two-Way Time (s)

0.0

5.0

10.0

15.0
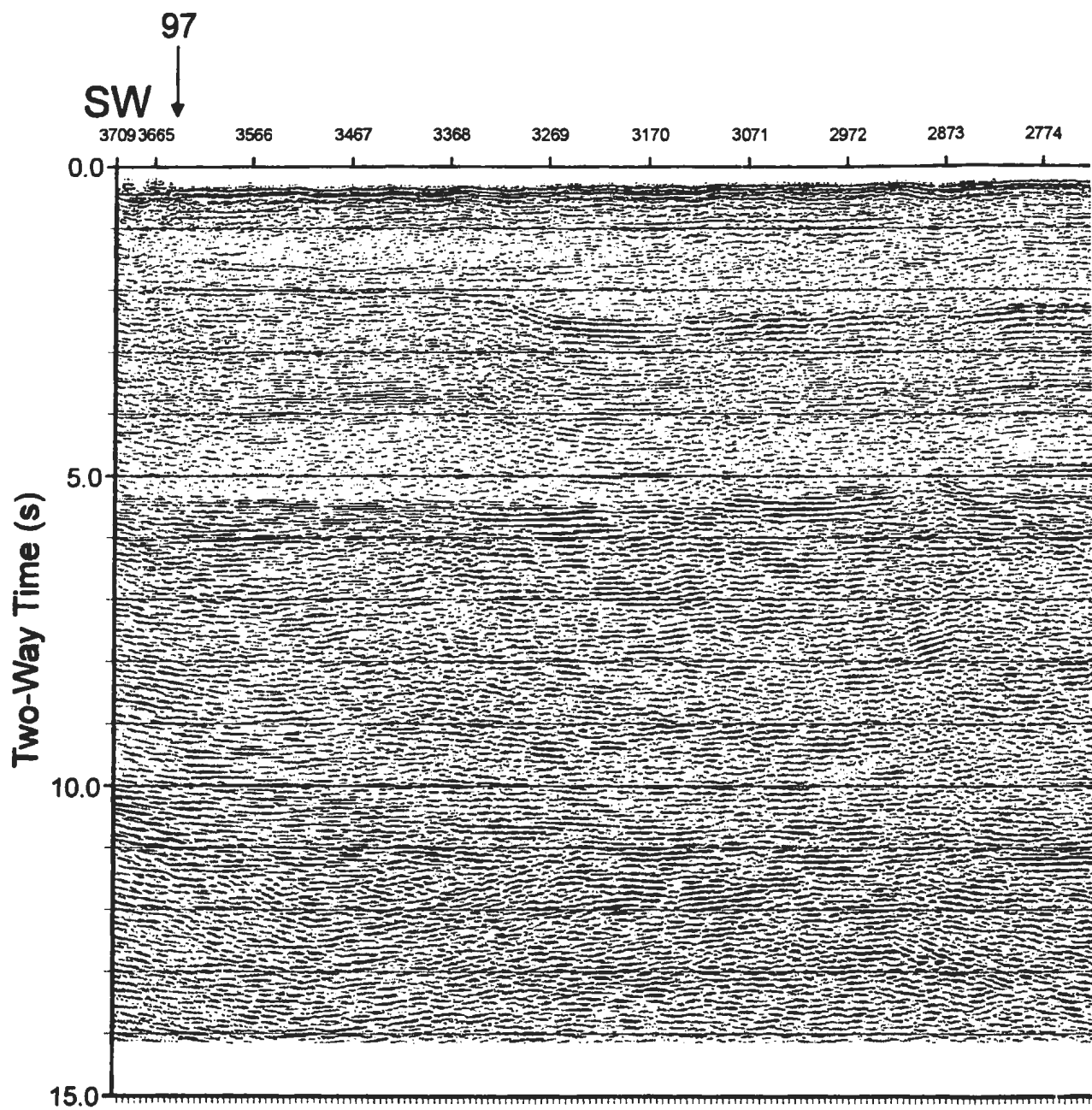
Figure 3.16 Time migrated section for Line 92.

99

| 2675 | 2576 | 2477 | 2378 | 2279 | 2180 | 2081 | 1982 | 1883 | 1784 | 1685 | 1586 | 1487 | 1388 |

99

91

2477   2378   2279   2180   2081   1982   1883   1784   1685   1586   1487   1388   1289   1190
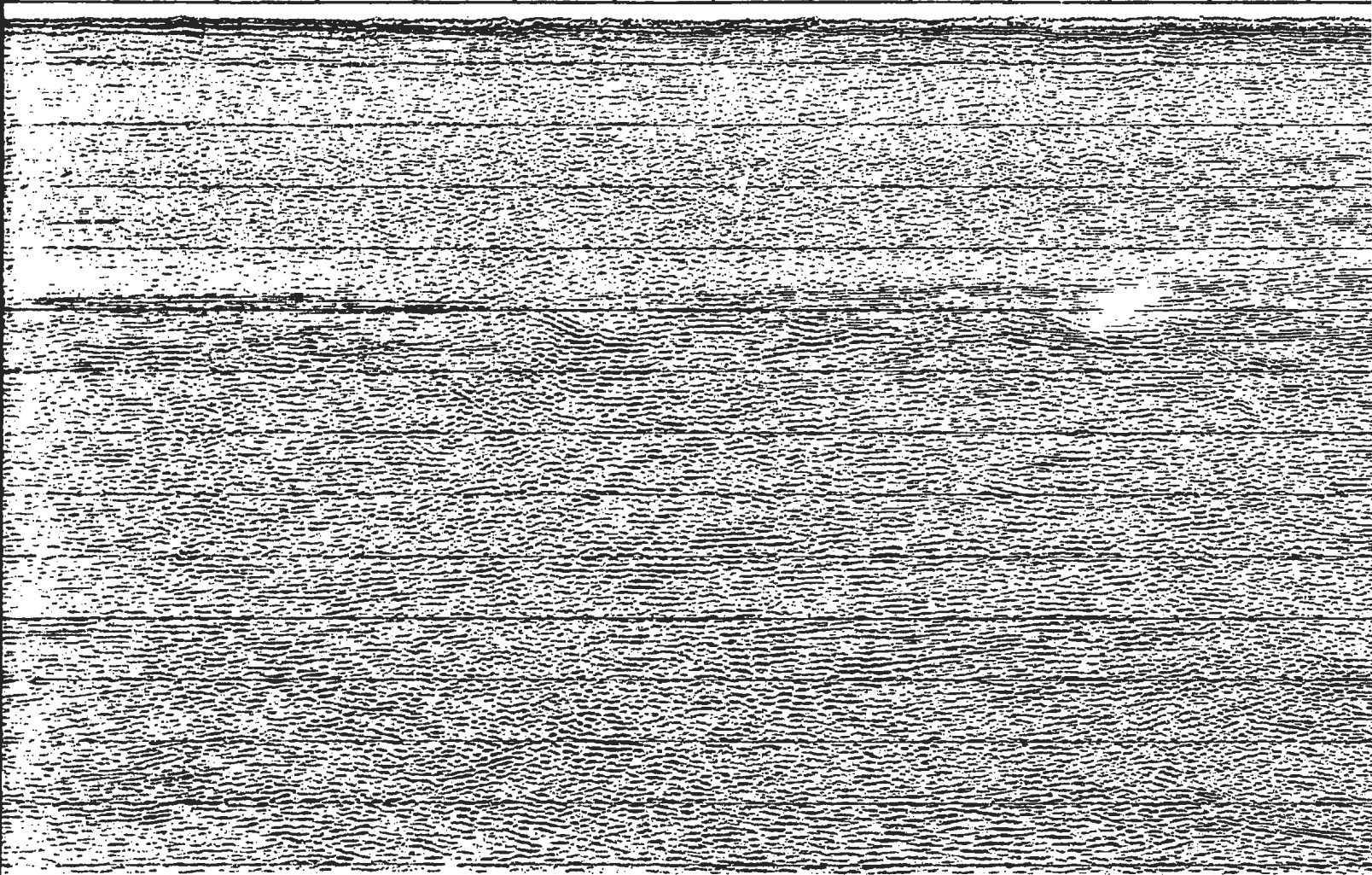
91

NE

1091   992   893   794   695   596   497   398   299   200   101

0.0

5.0

Two-Way Time (s)

10.0

15.0
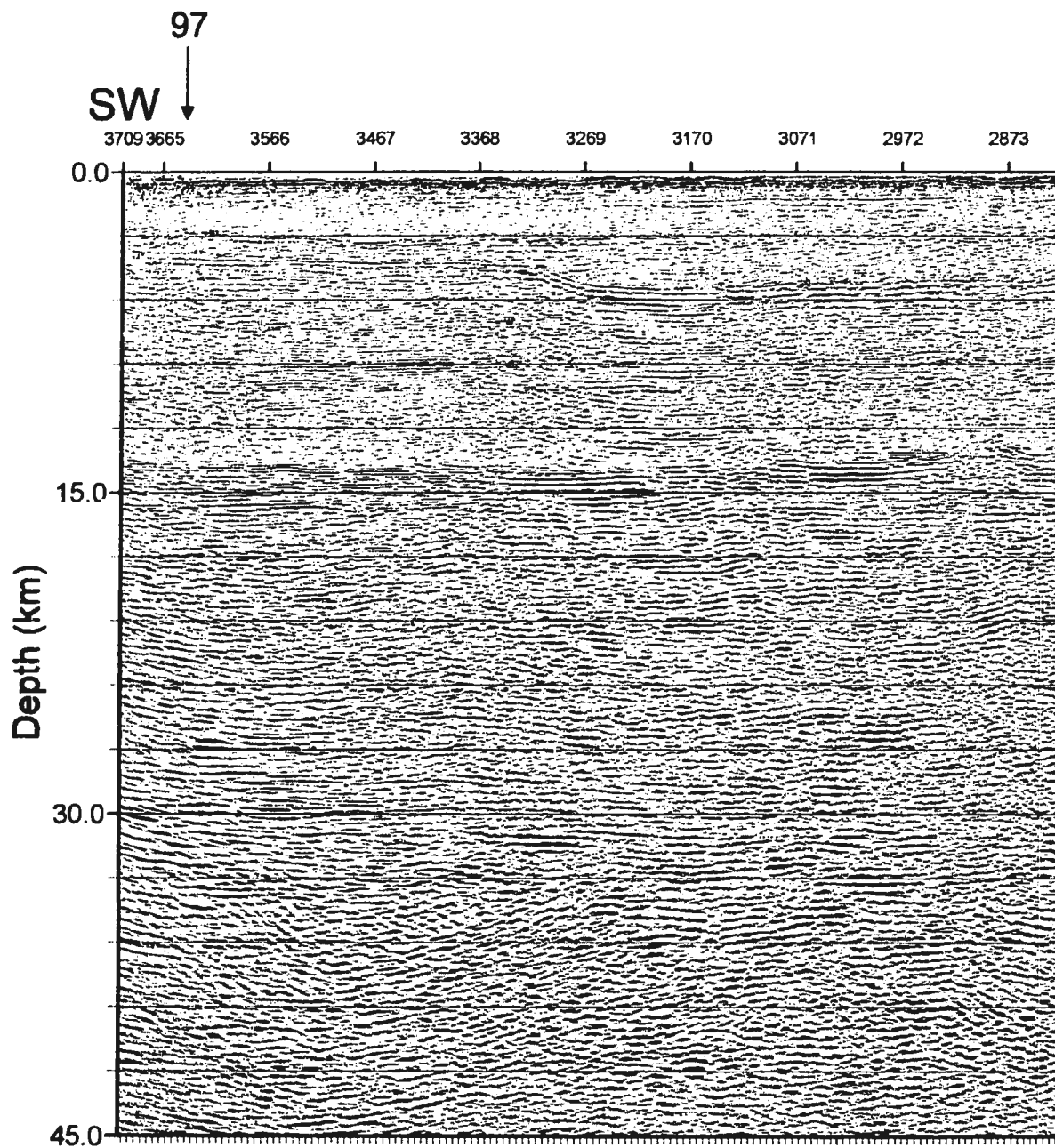
Figure 3.17 Depth migrated section for Line 92.

99

2774	2675	2576	2477	2378	2279	2180	2081	1982	1883	1784	1685	1586	1487	1388

99

91

2378 2279 2180 2081 1982 1883 1784 1685 1586 1487 1388 1289 1190 1091 992 8

1

NE

| 1091 | 992 | 893 | 794 | 695 | 596 | 497 | 398 | 299 | 200 | 101 |

0.0

15.0

30.0

45.0

Depth (Km)

NNW
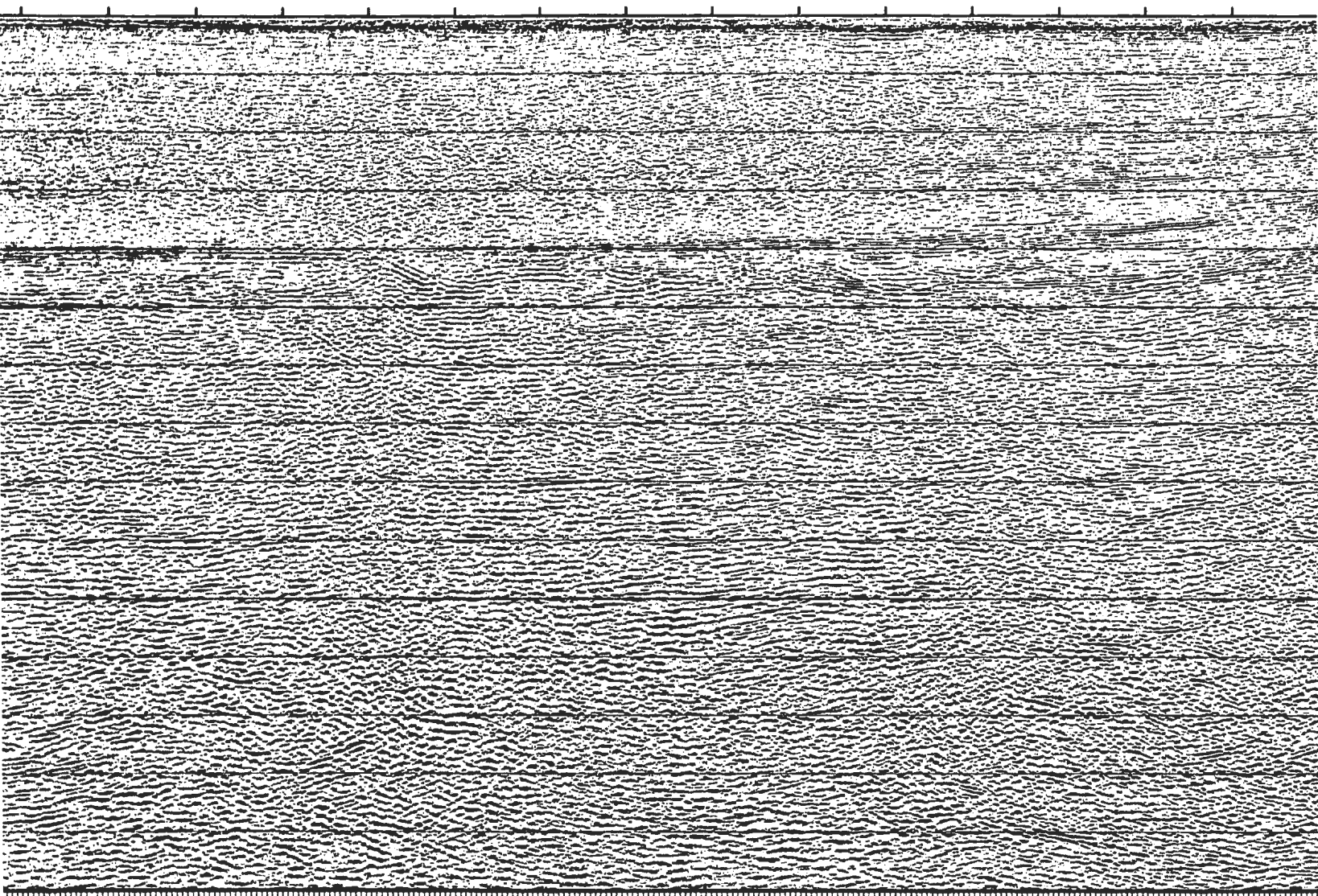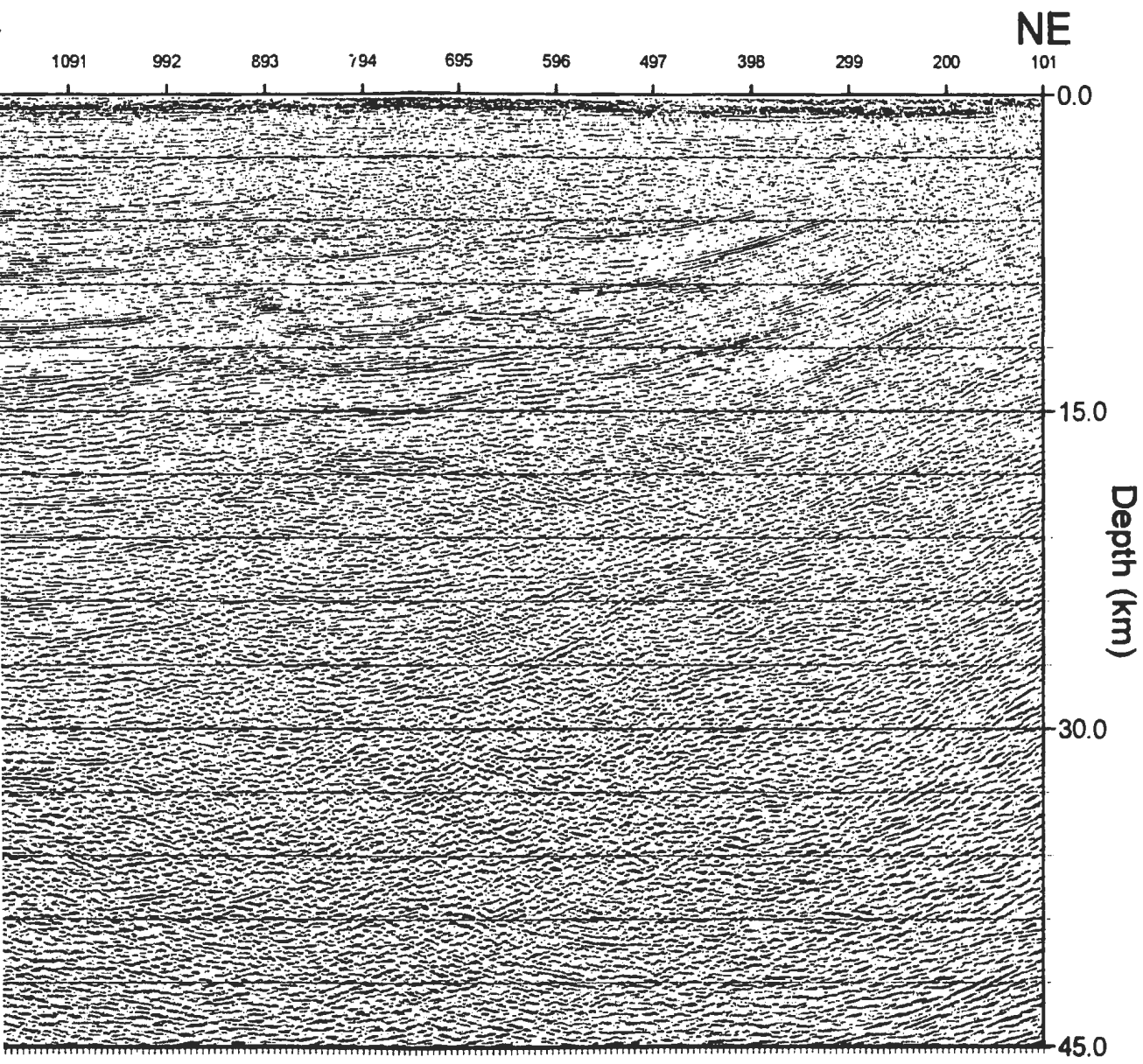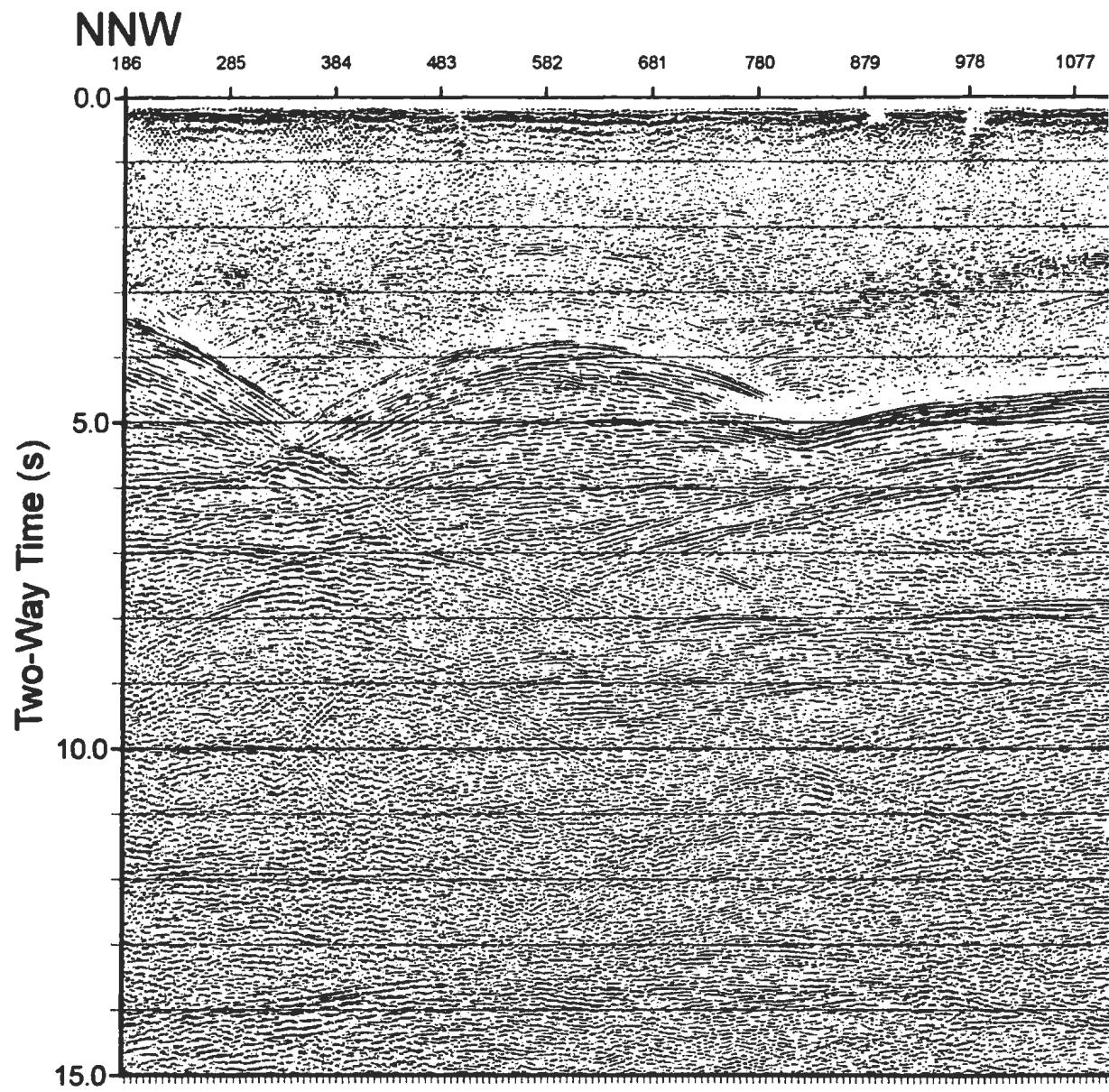
Figure 3.18 Unmigrated time section for Line 93.

94

| 978 | 1077 | 1176 | 1275 | 1374 | 1473 | 1572 | 1671 | 1770 | 1869 | 1968 | 2067 | 2166 | 2265 | 2364 | 246 37 |

94

| 1473 | 1572 | 1671 | 1770 | 1869 | 1968 | 2067 | 2166 | 2265 | 2364 | 2463 | 2562 | 2661 | 2760 |

91

SSE

2760   2859   2958   3057   3156   3255   3354   3453   3552   3651 3697

0.0

5.0

Two-Way Time (s)

10.0

15.0
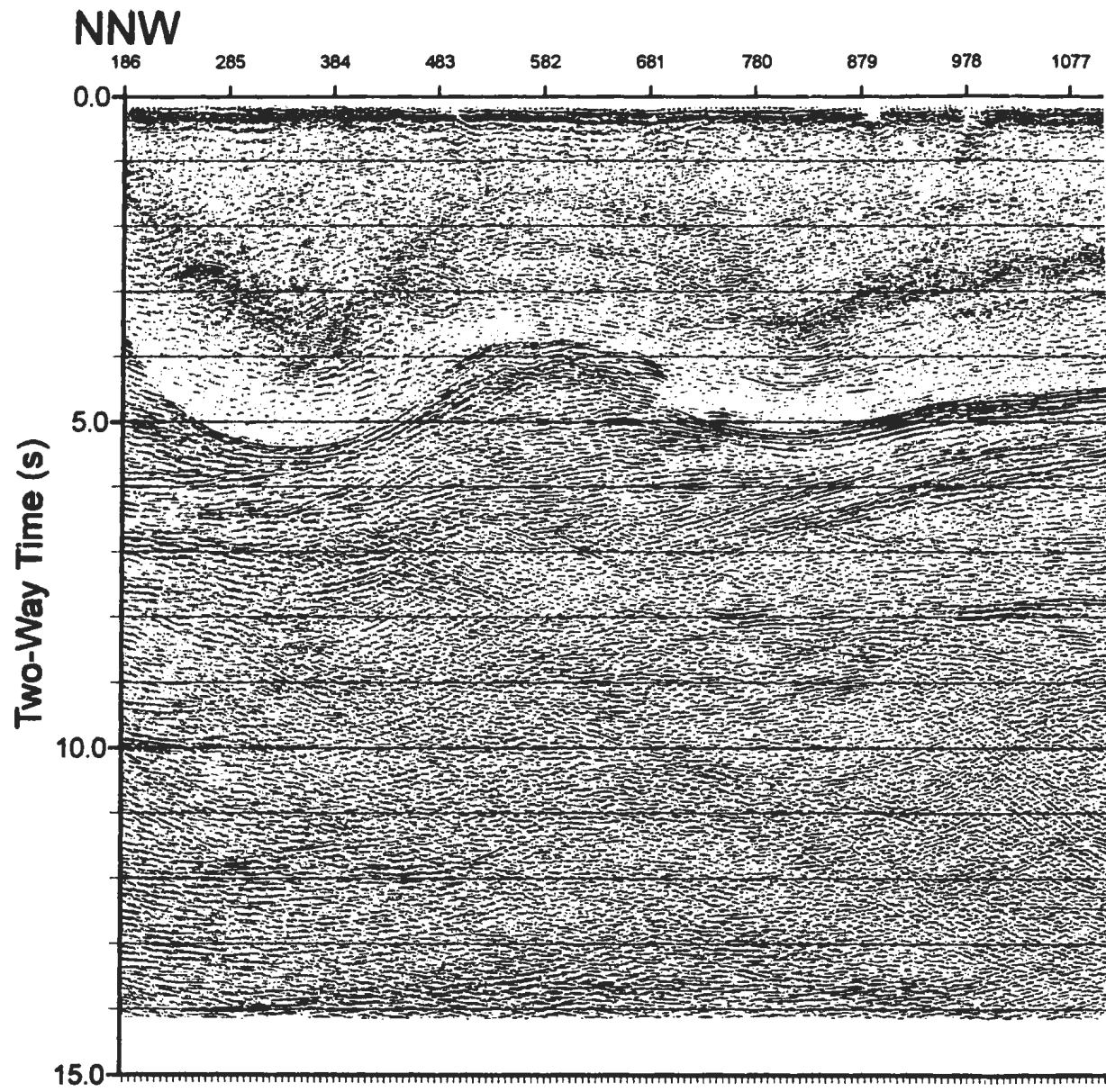
Figure 3.19 Time migrated section for Line 93.

94

| 1077 | 1176 | 1275 | 1374 | 1473 | 1572 | 1671 | 1770 | 1869 | 1968 | 2067 | 2166 | 2265 | 2364 | 246 |

94

1473 1572 1671 1770 1869 1968 2067 2166 2265 2364 2463 2562 2661 2760

Two-Way Time (s)

NNW

| 186 | 285 | 384 | 483 | 582 | 681 | 780 | 879 | 978 | 107 |
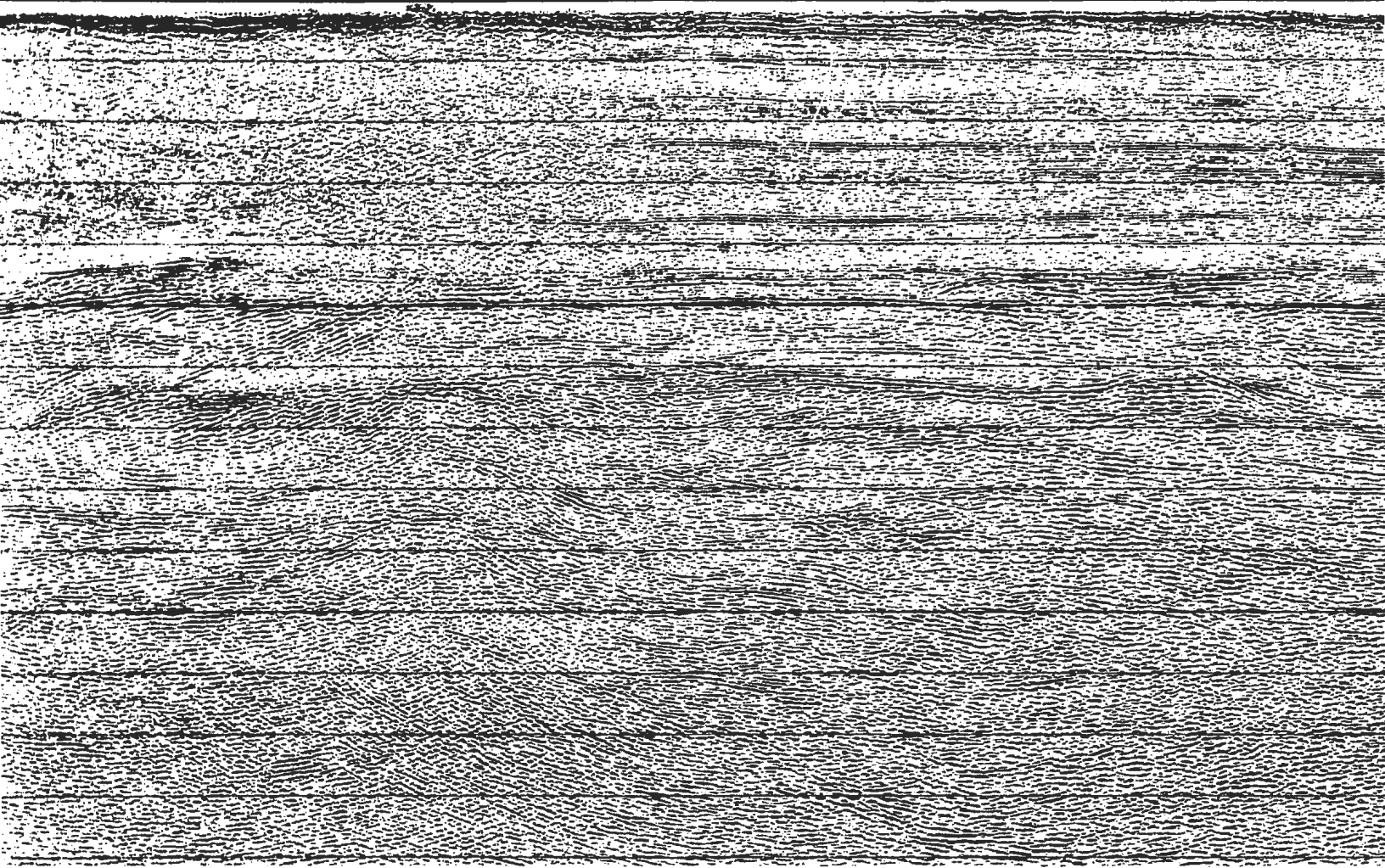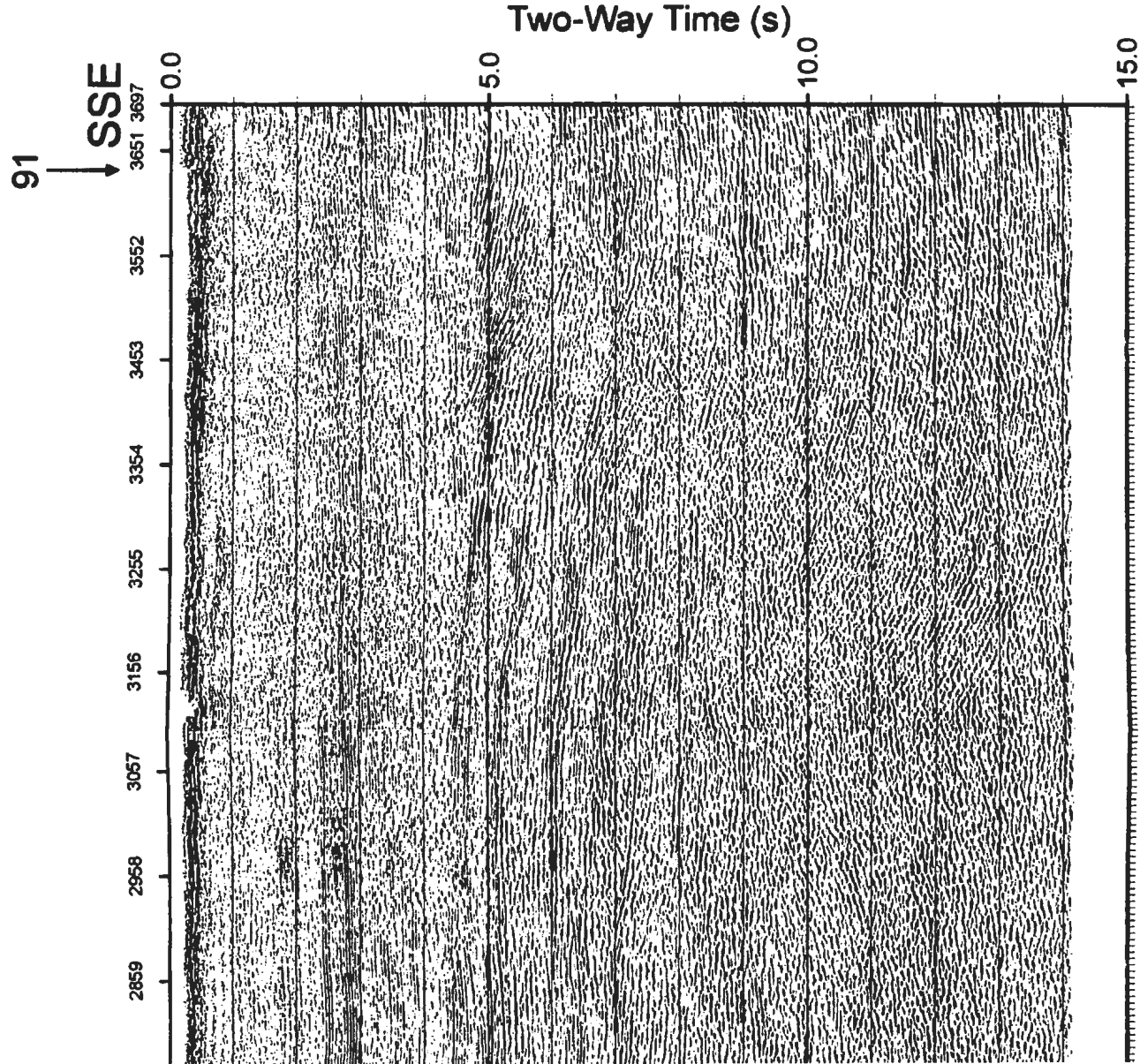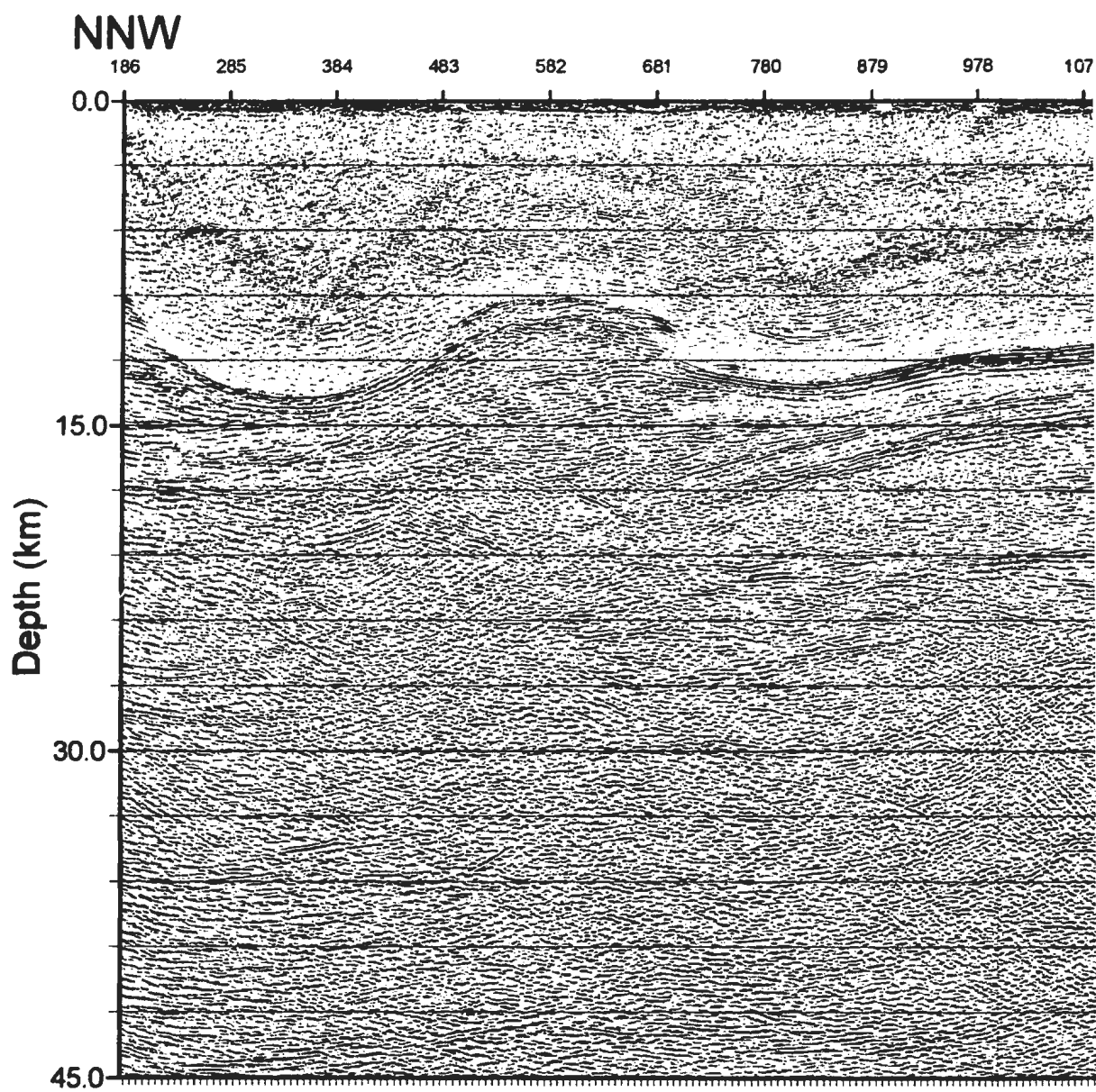
Figure 3.20 Depth migrated section for Line 93.

94

| 1176 | 1275 | 1374 | 1473 | 1572 | 1671 | 1770 | 1869 | 1968 | 2067 | 2166 | 2265 | 2364 |

94

| 1374 | 1473 | 1572 | 1671 | 1770 | 1869 | 1968 | 2067 | 2166 | 2265 | 2364 | 2463 | 2562 | 2661 |

91

↓ SSE

2859   2958   3057   3156   3255   3354   3453   3552   3651 3697

0.0

15.0

Depth (km)

30.0

45.0
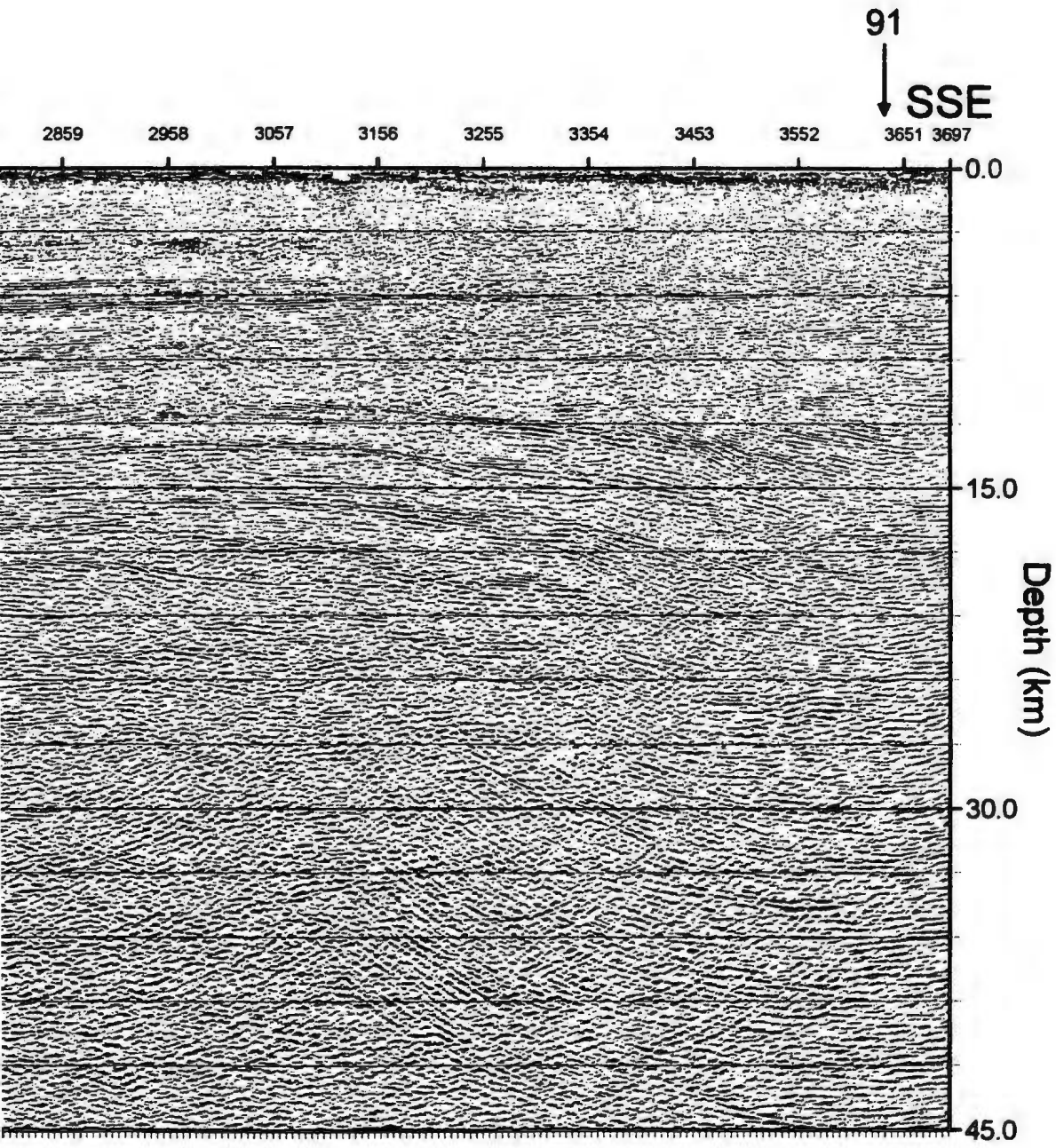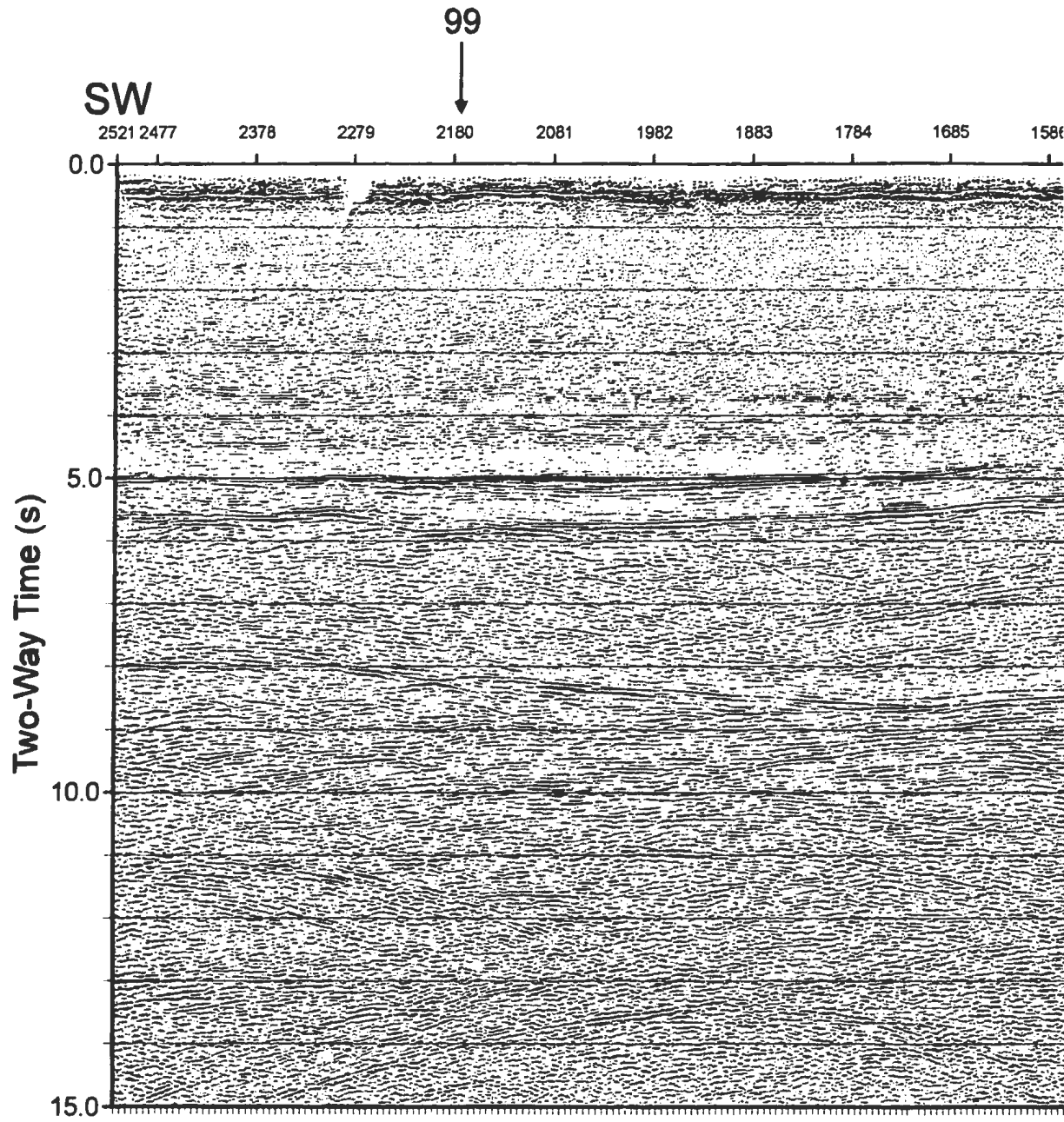
Figure 3.21 Unmigrated time section for Line 94.

93

NE

| 299 | 992 | 893 | 794 | 695 | 596 | 497 | 398 | 299 | 200 | 101 |

0.0

5.0

Two-Way Time (s)

10.0

15.0

Figure 3.22 Time migrated section for Line 94.

Seismic Reflection Data/79 for Line 94.

93

NE

992   893   794   695   596   497   398   299   200   101

0.0

5.0

Two-Way Time (s)

10.0

15.0
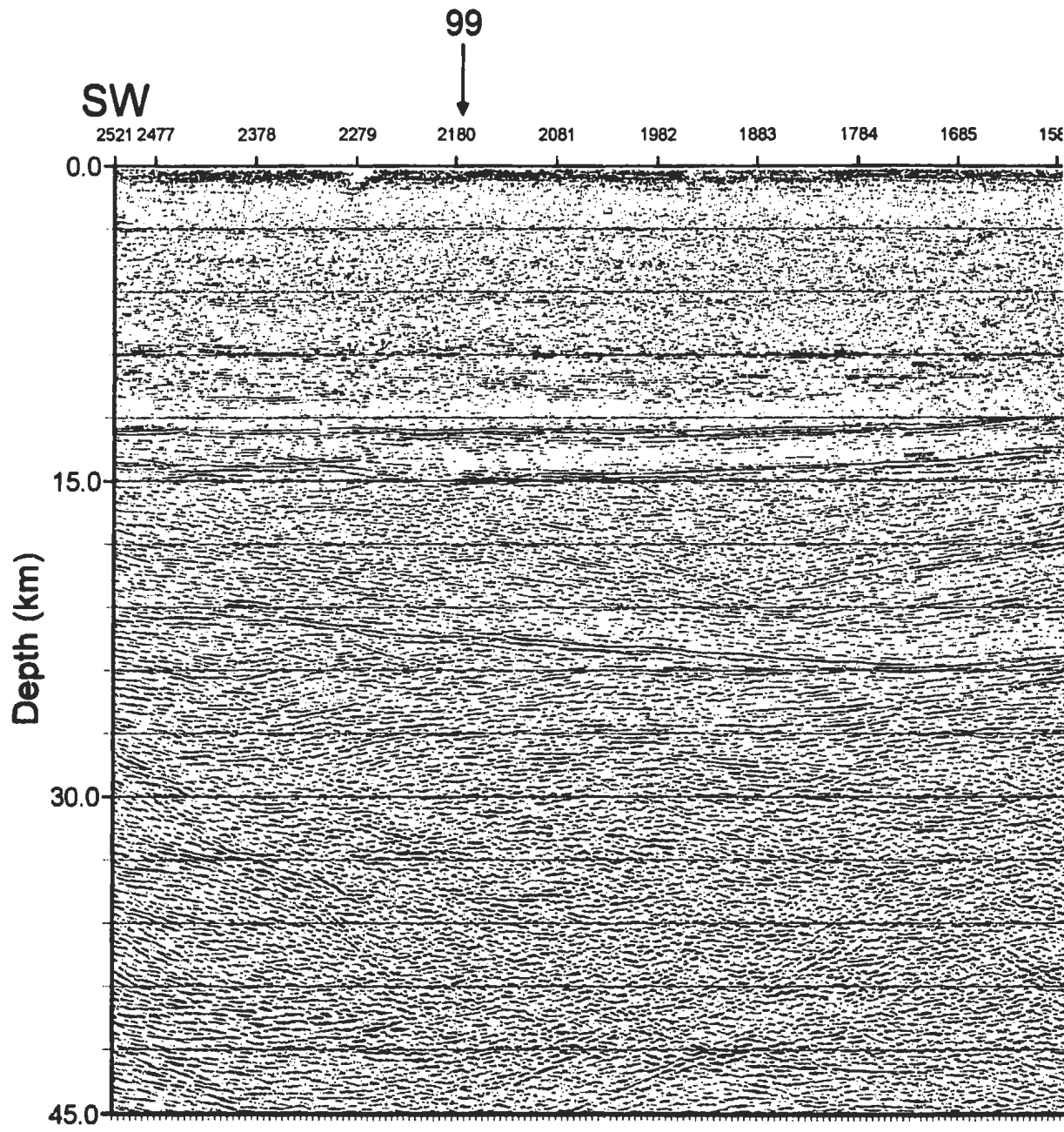
Figure 3.23 Depth migrated section for Line 94.

93

1685   1586   1482   1388   1289   1190   1091   992   893   794   695   596   497   398   299
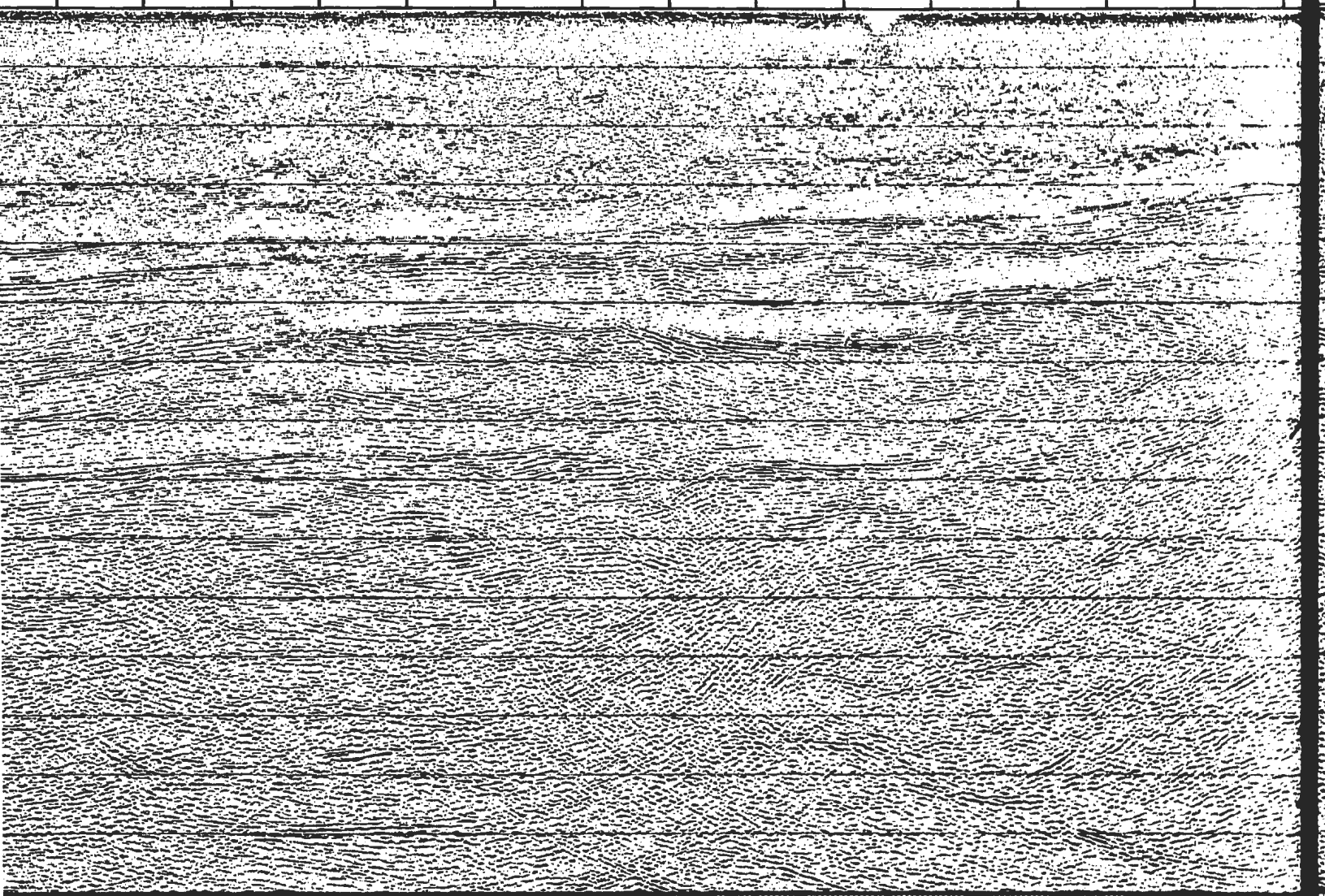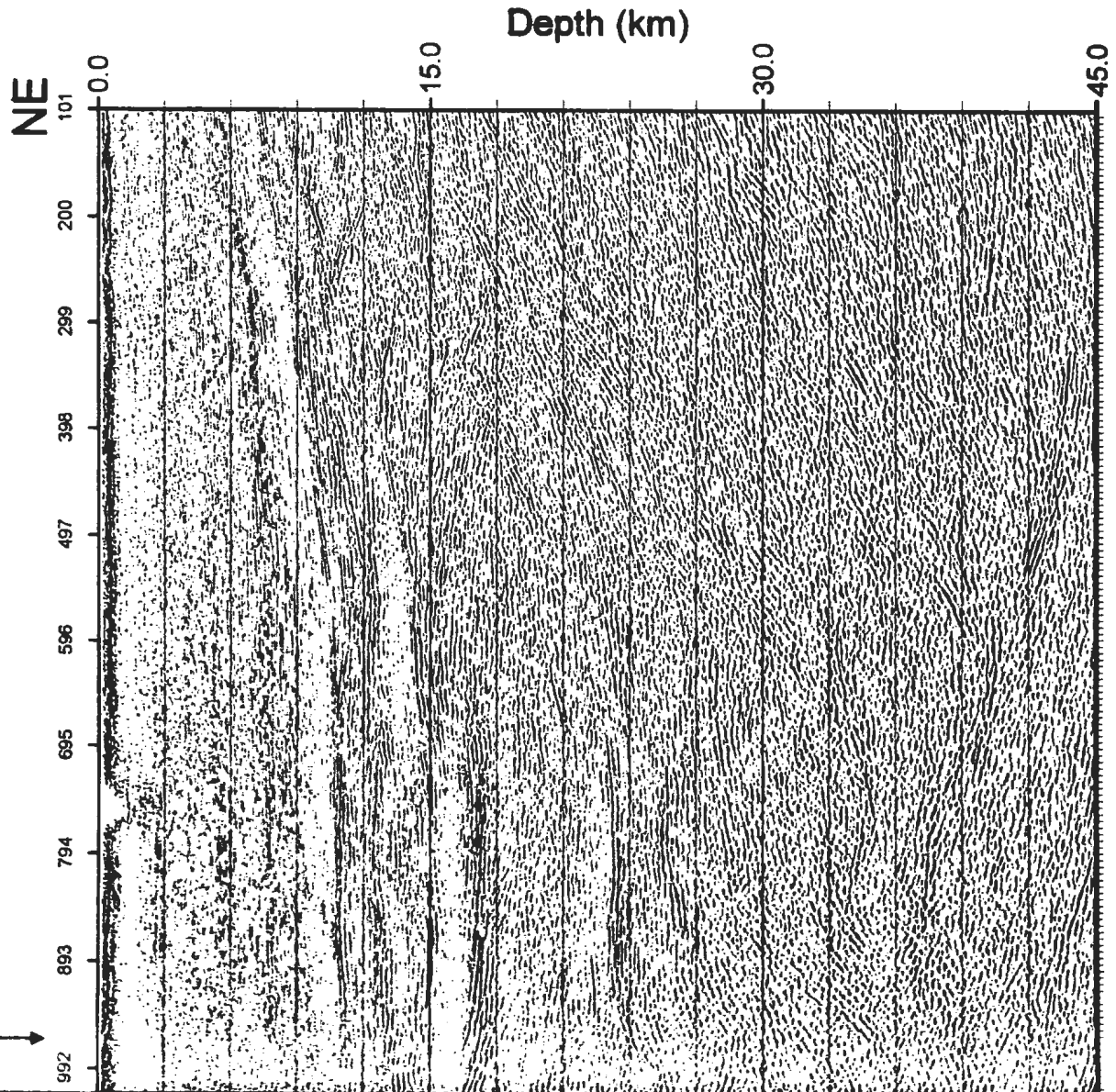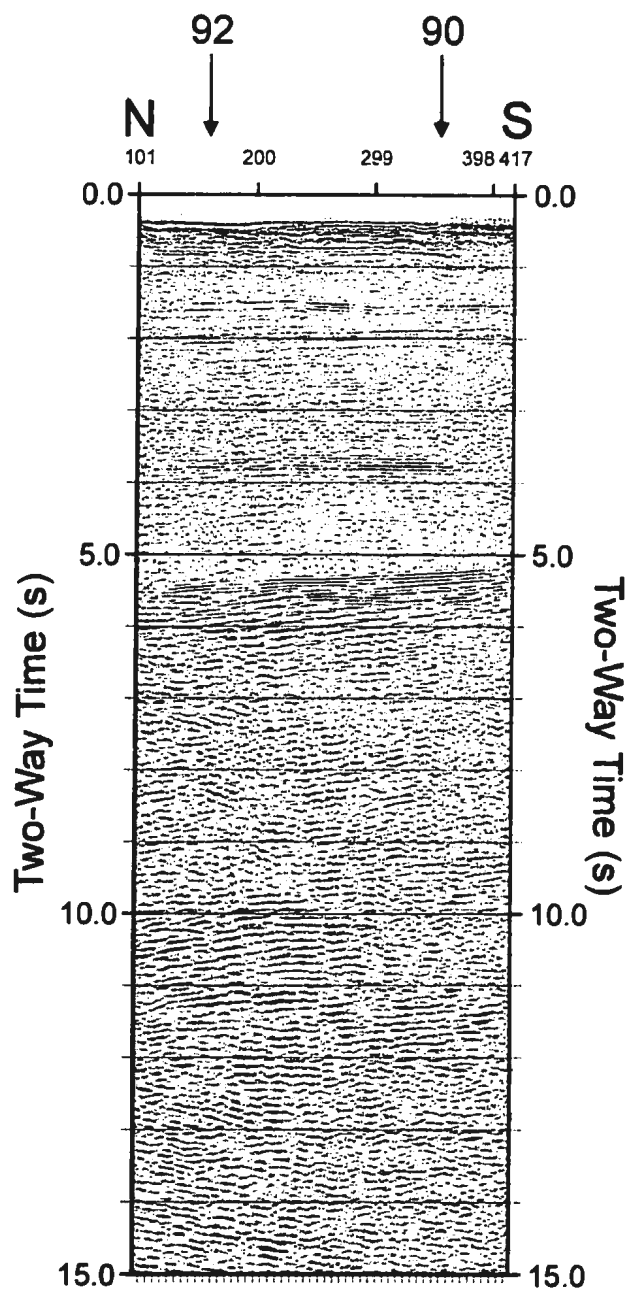
Figure 3.24 Unmigrated time section for Line 97.
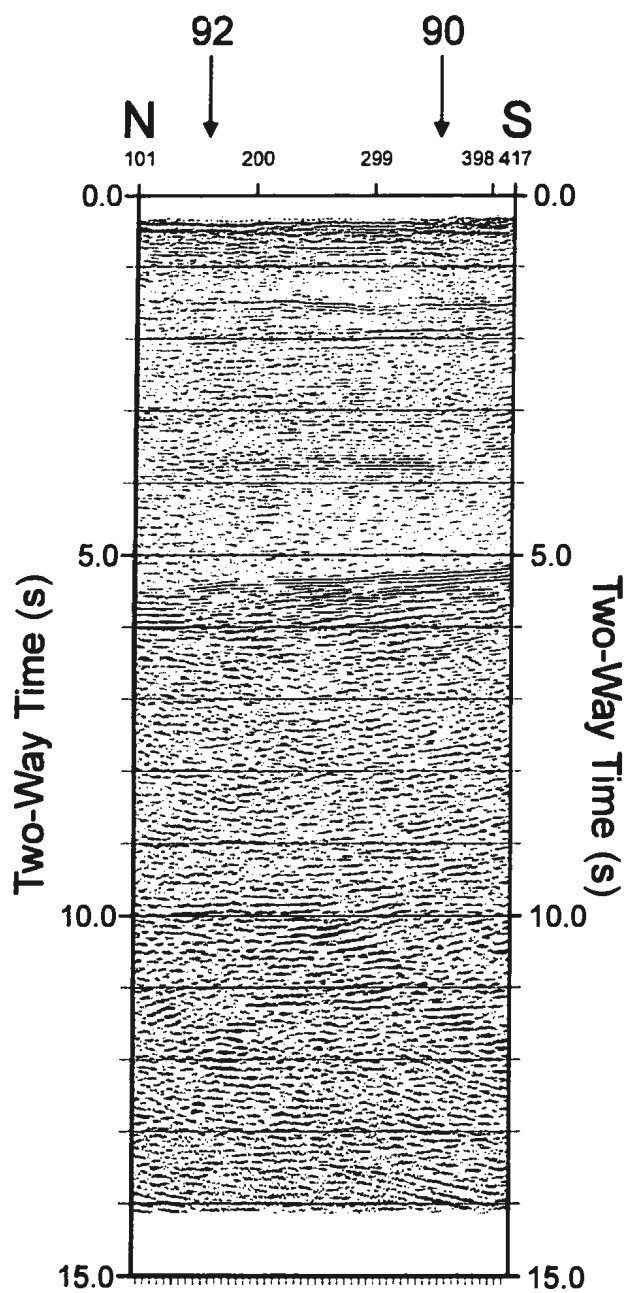
Figure 3.25 Time migrated section for Line 97.
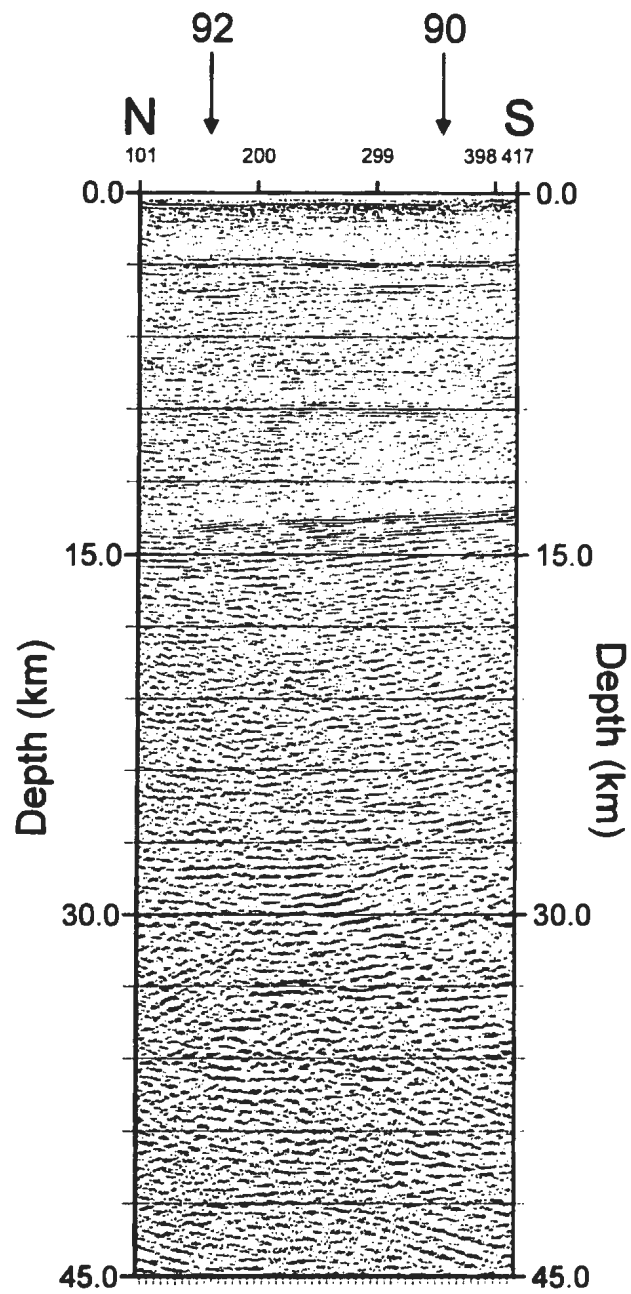
Figure 3.26 Depth migrated section for Line 97.
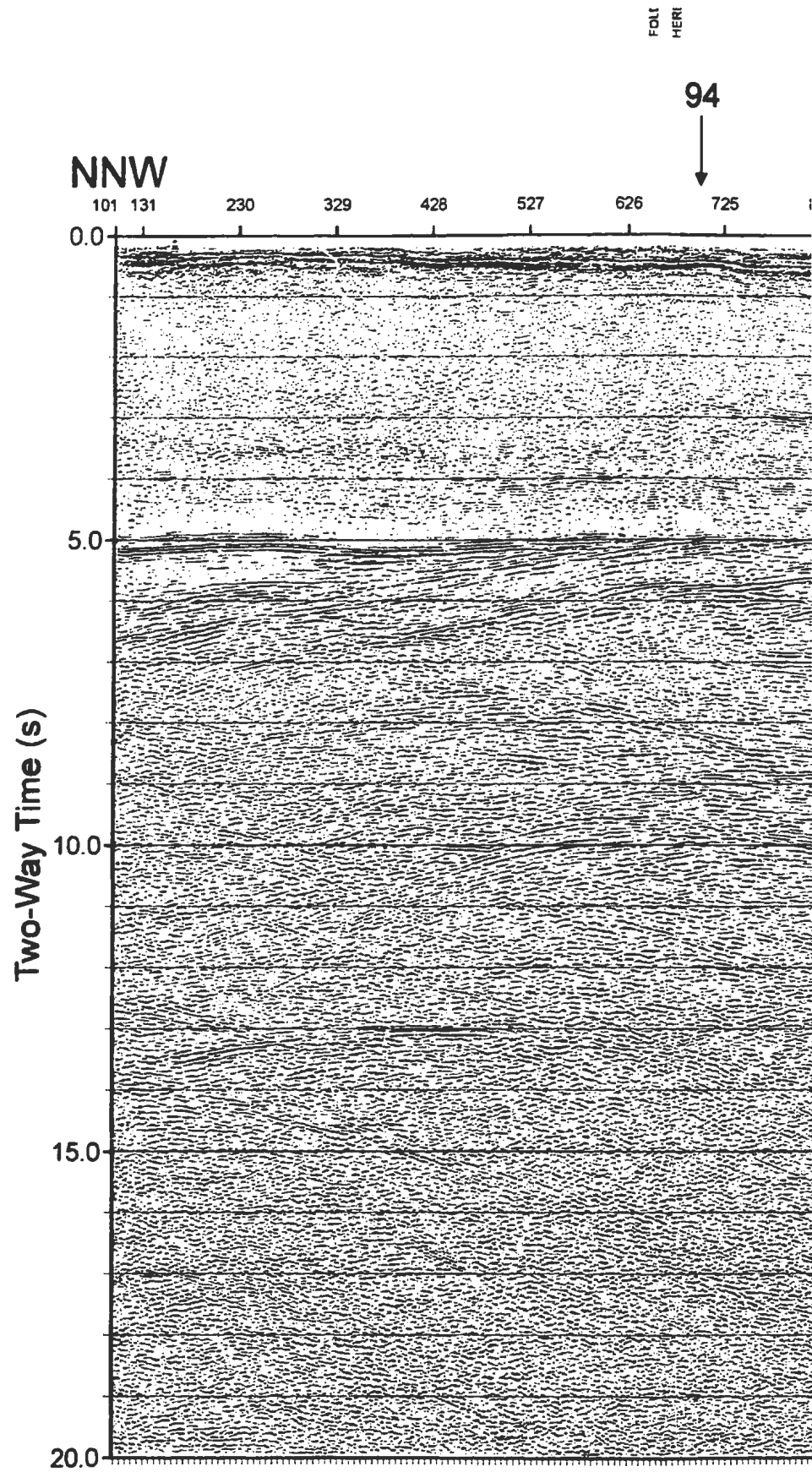
Figure 3.27 Unmigrated time section for Line 99.

725
824
928
1022
1121
1220
1319
1418
1517
1616
1715
1814
1913
2012
2111

GS

GSD PAN-1

2111   1022   1121   1220   1319   1418   1517   1616   1715   1814   1913   2012   2111   2210   2309

94

NNW

Figure 3.28 Time migrated section for Line 99.

94

G
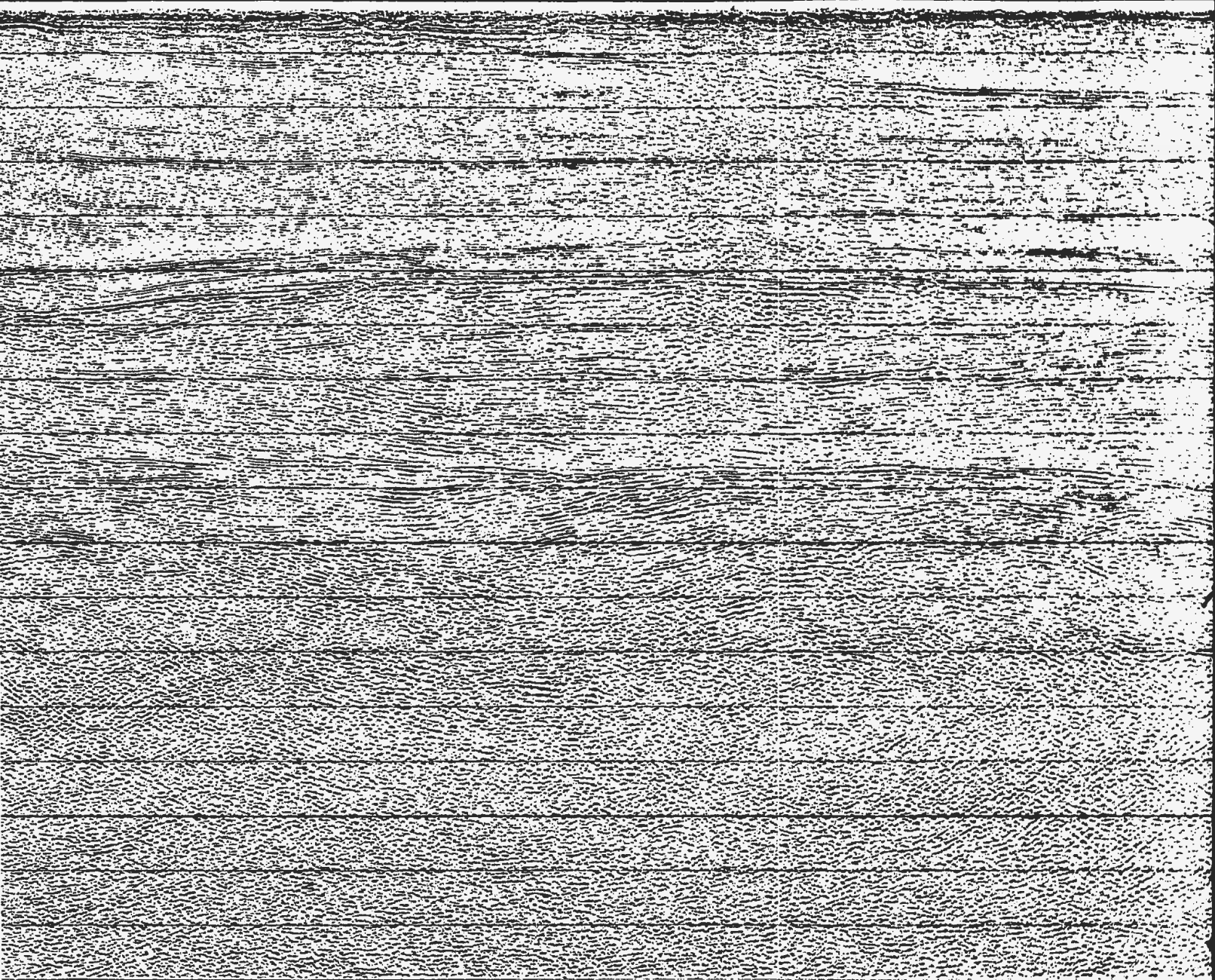
G

| 11 | 1022 | 1121 | 1220 | 1319 | 1418 | 1517 | 1616 | 1715 | 1814 | 1913 | 2012 | 2111 | 2210 | 2309 | 2408 |

92

↓SSE
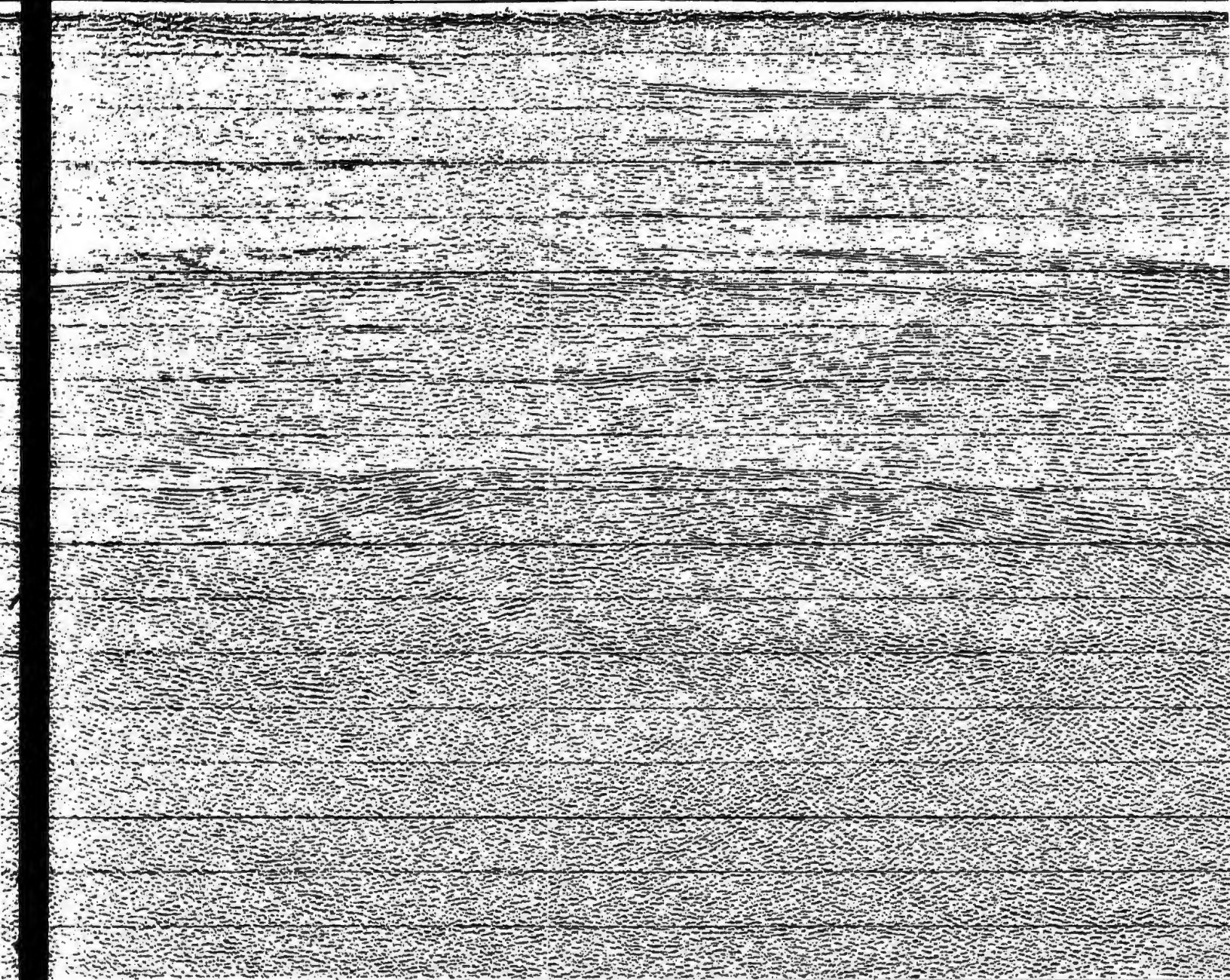
2507   2606   2705   2804   2903   3002   3101

0.0

5.0

Two-Way Time (s)

10.0

15.0

20.0
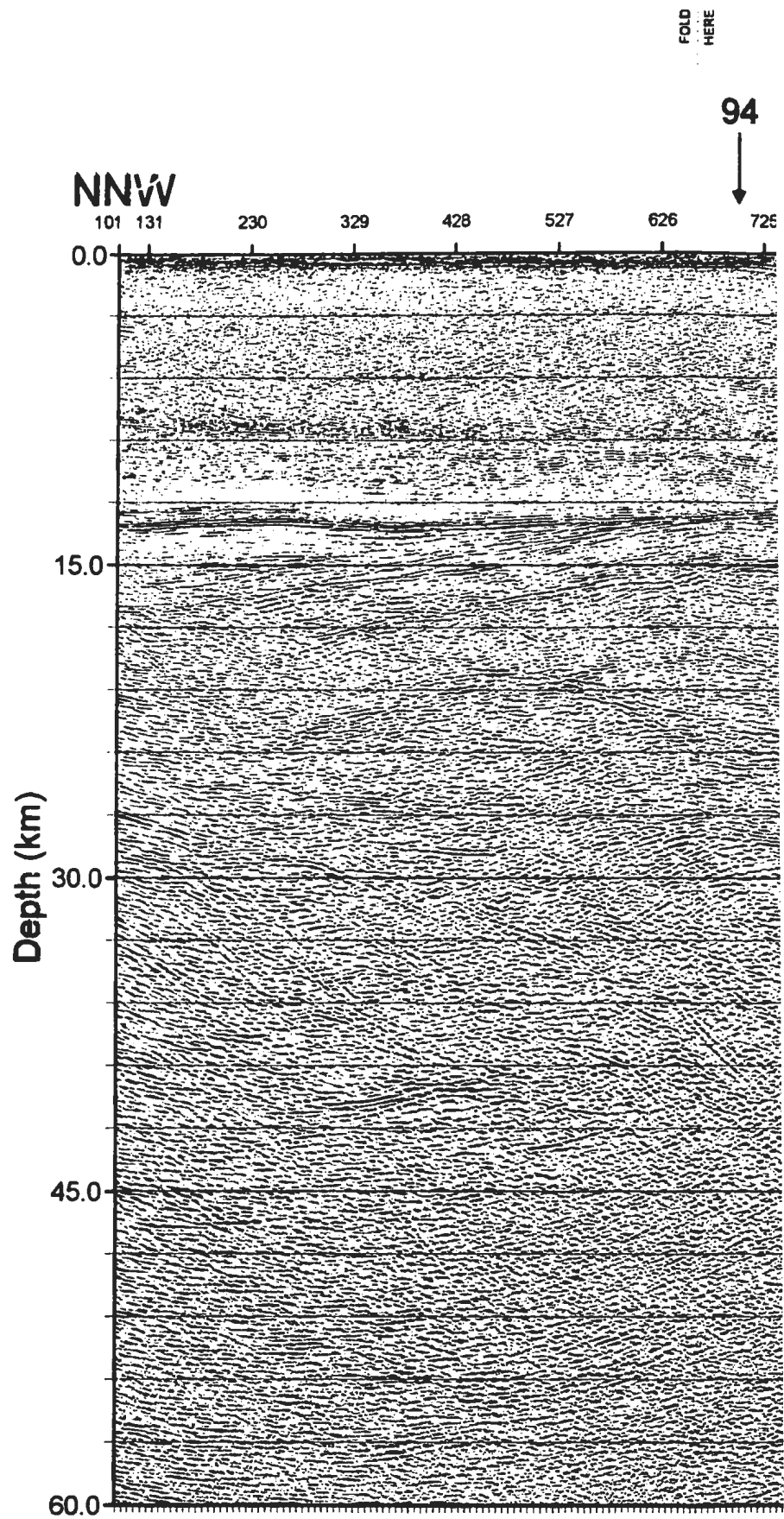
Figure 3.29 Depth migrated section for Line 99.

725 824 928 1022 1121 1220 1319 1418 1517 1616 1715 1814 1913 2012 2111
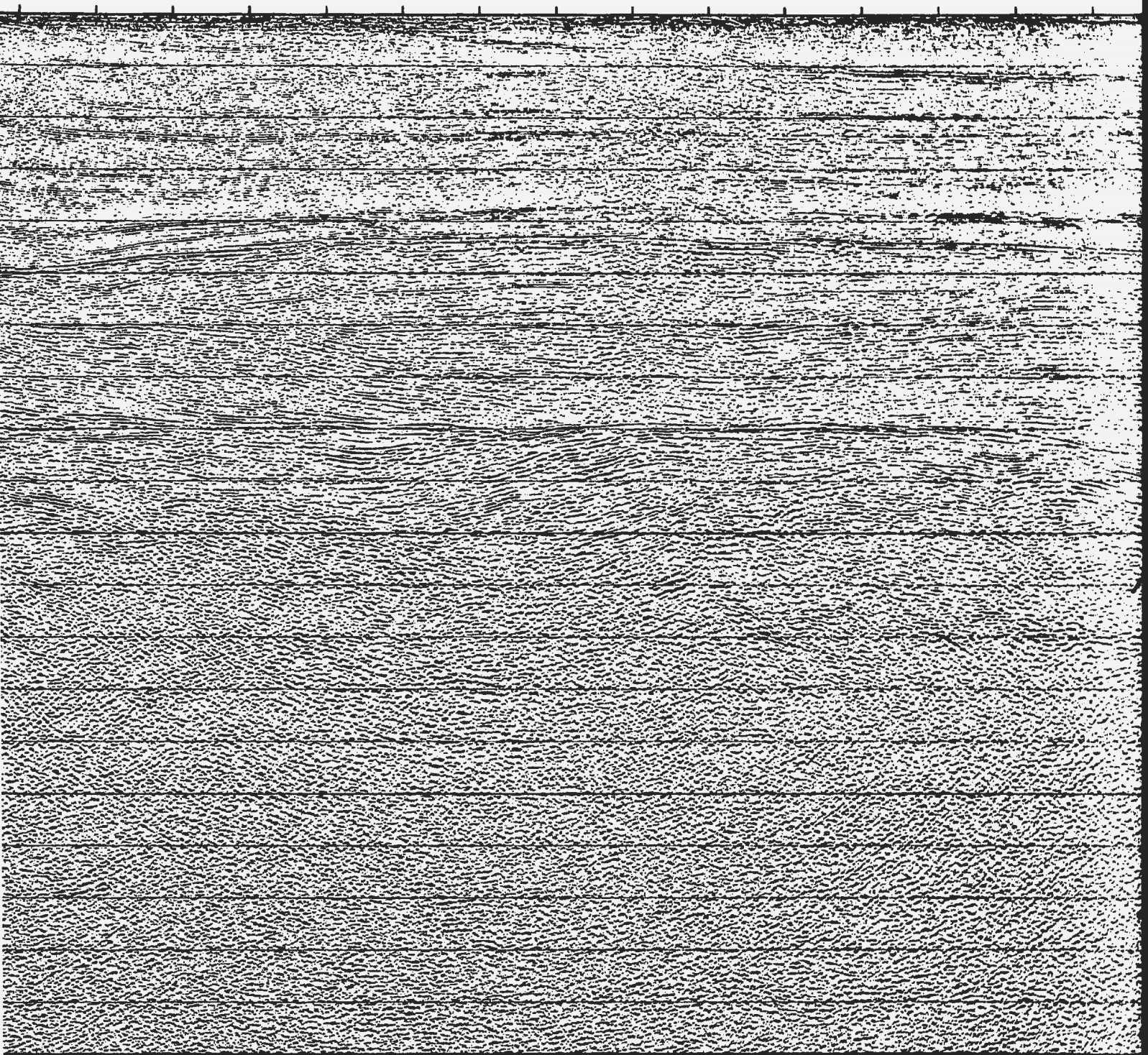
GSD PAN-1

022   1121   1220   1319   1418   1517   1616   1715   1814   1913   2012   2111   2210   2309
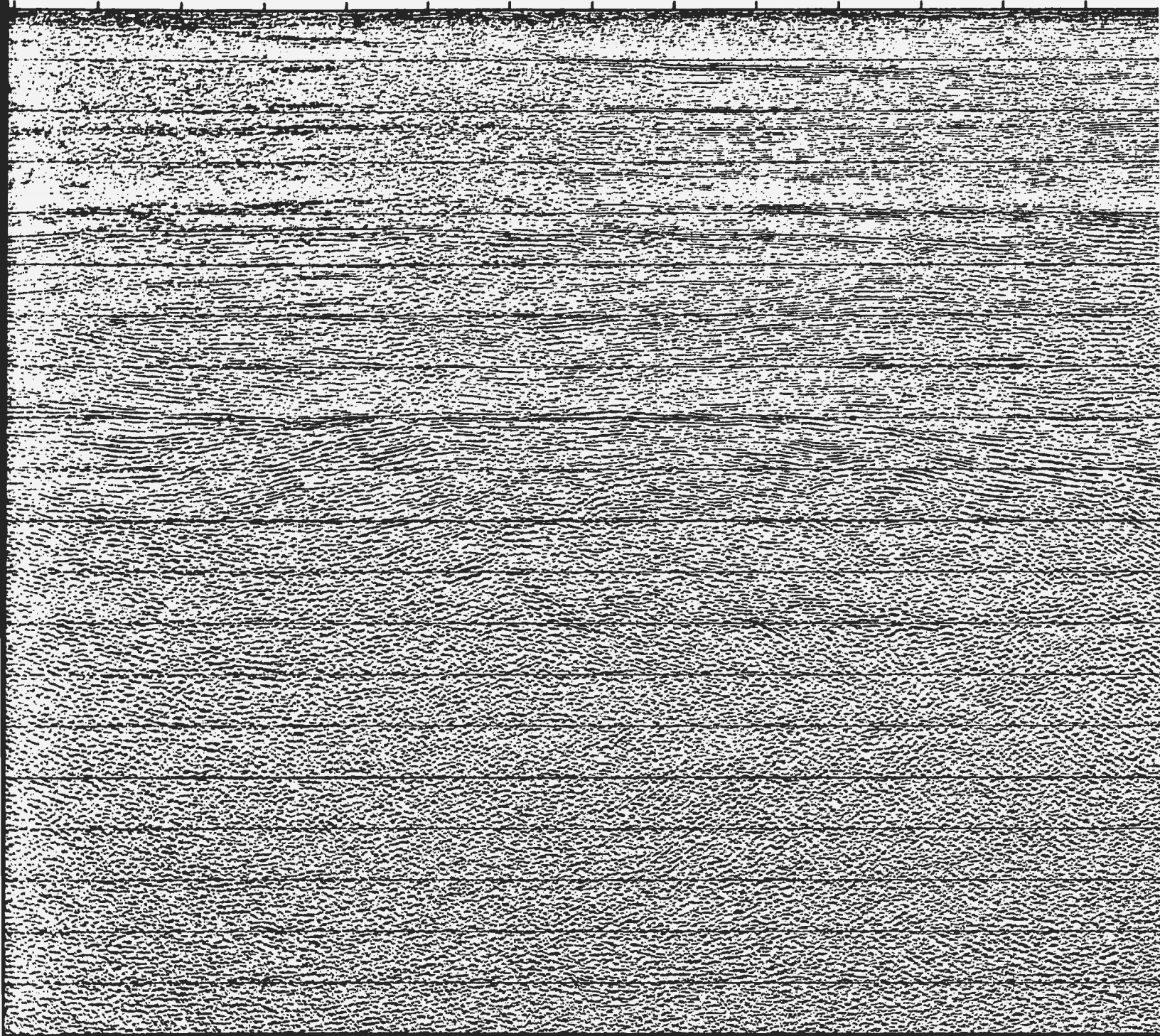
FOLD HERE

FOLD HERE

92

↓SSE

2507   2606   2705   2804   2903   3002   310ɪ

0.0

15.0

Depth (km)

30.0

45.0

60.0

4 INTERPRETATION

4.1 PCIAC-GSD Masetlheng Pan-1

PCIAC-GSD Masetlheng Pan-1 was a s ratigraphic test well designed to evaluate the age and prospectivity of the deeper sedimentary sequences contained within the Nosop Basin (Petro-Canada, 1990). This well was spudded on November 18th, 1989 by Petro-Canada International Assistance Corporation (PCIAC) in cooperation with the Government of Botswana's Geological Survey Department (GSD) and drilled to a total depth of 4,016 m (13,177 ft) which was reached on April 15th, 1990.

The drilling of this stratigraphic well followed from Wasilenkoff's (1988) original interpretation of the 1987-88 regional deep seismic reflection survey of the Nosop Basin. Based on ties to other exploration boreholes farther west in Namibia, he postulated the presence of a thick ($\approx$ 3,000 m) sequence of Palaeozoic sediments concealed between the base of the Karoo Supergroup and the underlying Proterozoic section which he assumed consisted predominantly of Nama Group. In fact, his interpretation of a possible hidden Palaeozoic section existing in the Nosop Basin was largely hinged on extrapolations made to the Vreda-281 well drilled 30 km west of the Botswana/Namibia border and some 75 km southwest from the ends of seismic lines 90 and 92. Wasilenkoff (1988) thought that this "extra" section of Ordovician to Carboniferous rocks were equivalents of the Mulden Group of Namibia, Cape Supergroup of South Africa and the Likupekupe Formation of Zambia.

To test the existence of this additional Palaeozoic section, Wasilenkoff (1988)

Graphic Log	Depth (m)	Lithology	Environment of Deposition	Stratigraphic Unit		Age	
	109			Kalahari Beds		Cret - Rec	
		Dolerite with Shale Interbeds	Intrusive	Ecca Group	KAROO	Early Permian	
	392	Sand - Shale Sequence	Marginal Marine				
	828	Diamictite	Glaciomarine	Dwyka Group		Late Carboniferous	
	939	Sand	Continental				
	1070	Diamictite	Glaciomarine				
	1162			Fish River Subgroup	NAMA GROUP	Vendian	Late Proterozoic - Paleozoic ?
		Arkosic Sandstones with Local Shale Interbeds	Continental Fluvial Braided Stream to Alluvial Fan	Schwarzrand Subgroup			
				Kuibis Subgroup			
	2275			Numees-Hilda Undiff.	GARIEP GROUP	Late Riphean	Proterozoic
	3511	Varved Silts	Glaciomarine?	Kaigas Tillite			
	3592	Gabbro	Intrusive				
	3738	Sand-Shale Seq	Marine	Stinkfontein Formation			
	3843	Sands	Continental Fluvial				
	4016						

Figure 4.1 Geological summary of PCIAC-GSD Masetlheng Pan-1 stratigraphic well showing thicknesses and ages of the various sedimentary sequences encountered (after Petro-Canada, 1990).

recommended that a stratigraphic borehole be drilled at shot point 2193 (labelled "GSD Pan-1" on Figure 4.7) on line 99 (latitude 23° 41' 59.57"S, longitude 20° 51' 08.00E) with a projected depth of 4000 m (13,124 ft). This location was selected in order to test an onlapping reflection close to total projected depth.

The geological summary of the PCIAC-GSD Masetlheng Pan-1 well is presented in Figure 4.1. As indicated by this figure, the test borehole penetrated a sequence of Karoo sediments to a depth of 1162 m (3812 ft) and then passed into a thick succession of Proterozoic aged sediments which have been assigned to the Nama and Gariep Groups (Petro-Canada, 1990). The Proterozoic section located in the lowest portion of the well is comprised of highly indurated arkosic sandstones and an interval of marine sediments is present close to total depth. This deeper marine sequence has been intruded by a gabbro/dolerite which yielded a K-Ar date of 333 ± 17 Ma (lower Carboniferous).

The stratigraphic break at 1162 m marking the top of the Pre-Karoo strata is an obvious major unconformity and represents a large hiatus. This unconformity separates the glaciomarine sediments of the lower Dwyka Group from the well-cemented arkosic sandstones of the Pre-Karoo section. Although being predominantly composed of arkosic sandstones, this Pre-Karoo section also contains local intervals of subarkose, quartzarenite and subquartzarenite. The sandstones below this unconformity are, as stated, generally more indurated and notably more physically compacted than those encountered in the Karoo section (Petro-Canada, 1990). This compaction would seem to suggest a longer and more complex diagenetic history and supports the notion that the unconformity does

indeed represent a large span of missing geological time in which a considerable amount of sediment had been deposited and subsequently removed.

Petro-Canada (1990) correlated the upper half (1,162 - 2,275 m) of the well's Pre-Karoo section with the Nama Group. This was largely based on a biostratigraphic Late Precambrian age (Vendian) determined from a shaley interval at 2,225 m. This biostratigraphic age, along with the close resemblance of these shales with those of the Kubuis Subgroup of the Nama Group in Namibia, combined with the apparent stratigraphic break at 2,275 m suggests lithologic parallels with Nama sedimentation (Petro-Canada, 1990). Exact subdivision of the Nama Group in the predominantly continental sequence lying above the shales is difficult but it may be that the interpreted lithologic break at 1,689 m may relate to the widespread basal unconformity (as identified in Namibia) which separates the uppermost Fish River Subgroup from the lower Nama stratigraphy.

Petro-Canada's (1990) correlation of the lower half (2,275 - 4,016 m) of the Pre-Karoo section with the Gariep Group should be questioned. The Gariep Group represents a sequence of Late Proterozoic to Early Cambrian volcano-sedimentary rocks with exposures along the Atlantic coast and straddling the international boundary between Namibia and South Africa. There are no known occurrences of Gariep Group rocks within Botswana and indeed the known exposures of the Gariep Group just mentioned are some hundreds of kilometres from the Masetlheng Pan-1 well. The decision to correlate the Gariep Group with the deeper Proterozoic sediments encountered in the borehole seems

to be based solely on the statement that "In Botswana **no** sedimentary deposits older than Karoo are known ..." (Petro-Canada, 1990) which is, of course, not true.

A much better and more plausible correlative for the pre-Nama sediments encountered in the PCIAC-GSD Masetlheng Pan-1 stratigraphic well would be the Ghanzi Group. As discussed in Chapter 2, there is abundant outcrop of Ghanzi Group rocks in the extreme northwest corner of Botswana (northern and western international borders with Namibia) which were described in detail by Litherland (1982). These outcrops are situated only some 150 km due north of the Pan-1 borehole and its lithologic character is strikingly similar to the pre-Nama sediments assigned to the Gariep Group also consisting chiefly of arkoses. It is beyond the scope of this thesis to provide a detailed comparison and correlation of the Ghanzi Group rocks with the pre-Nama strata encountered in the borehole. However, it is felt by the author that the lithological descriptions and subsequent discussions of the pre-Nama strata provided in the Petro-Canada report (1990) might have been better served in terms of the Ghanzi Group rather than the Gariep Group.

4.1.1   Well Tie with Depth Migrations

In order to verify the accuracy of the depth migrations, a check was made as to whether the well depths could be tied directly to the migration depths. To illustrate the validity of the ties, Figure 4.2 displays the comparison of the synthetic seismogram generated for the PCIAC-GSD Masetlheng Pan-1 well with portions of the time and depth migrations at the well location on line 99 (SP 2193).
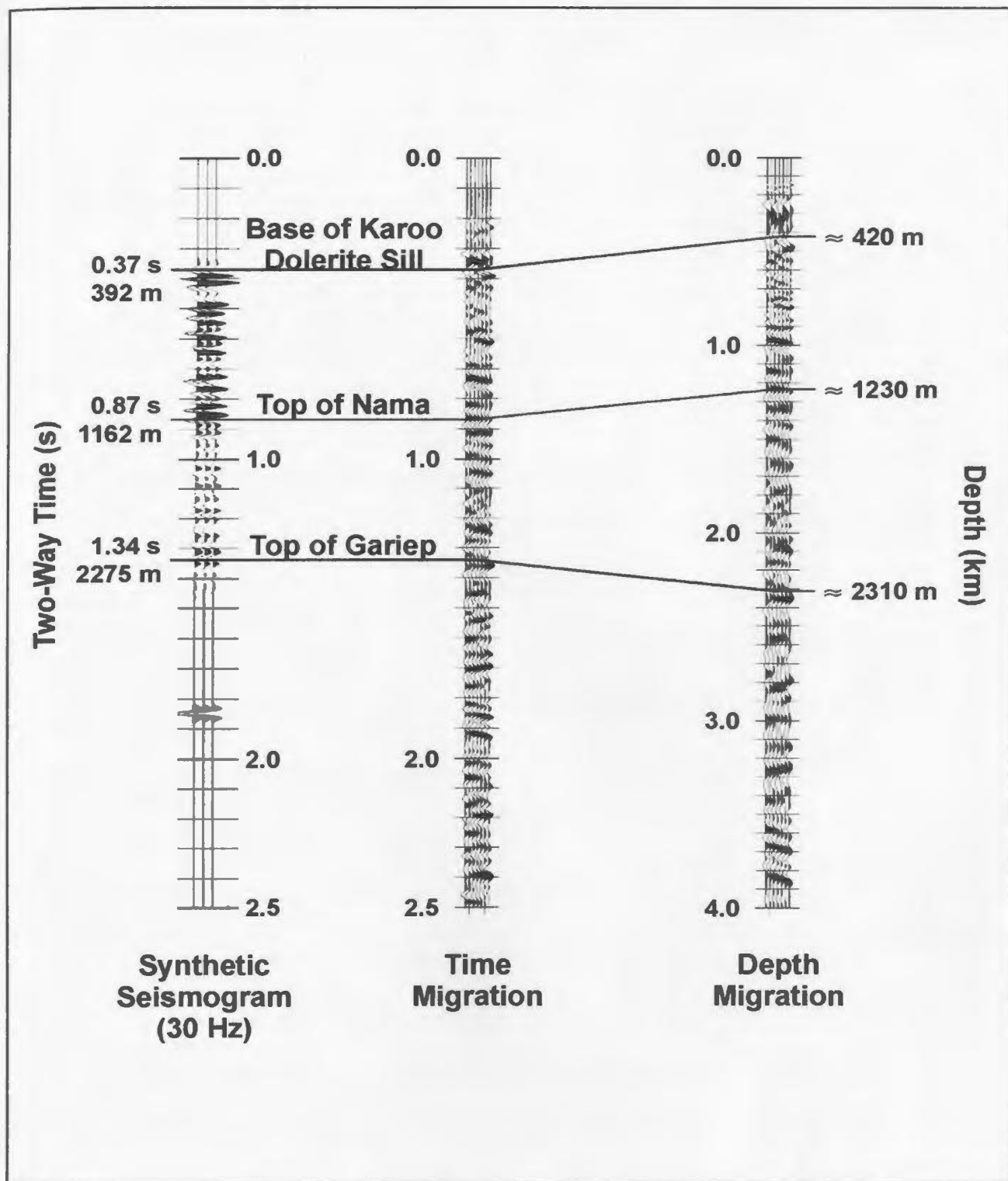
Figure 4.2 Comparison of the synthetic seismogram generated for the PCIAC-GSD Masetlheng Pan-1 stratigraphic well with portions of the time and depth migrations for line 99 at the well location.

Referring to this figure, the synthetic seismogram has annotated along its time axis both the time and depth picks for base of Ecca dolerite (Karoo), top of Nama and Gariep (Ghanzi?) derived for the well. The time picks, according to the Petro-Canada report (1990), were obtained from the correlation of the VSP (vertical seismic profile) data for the well with the actual seismic data itself. This correlation was apparently good and enabled the major reflectors to be identified with some confidence. The depth picks were simply taken from the lithology log for the well. These time picks from the synthetic seismogram are then directly transferred to the time migration and the reflecting events coinciding with these picks are then matched to the same events on the depth migration thus giving the appropriate depth values for the stratigraphic units in question. The depth values yielded from this procedure are annotated along the depth axis of the depth migration for line 99 at the well location.

As is evident from Figure 4.2, there is good correspondence between the major formation depths reported for the well and those provided by the tie to the depth migration. The percent difference between the actual well depths and those derived from the depth migration are 7.2%, 5.9% and 1.5% for base of Ecca dolerite (Karoo), top of Nama and top of Gariep respectively. Thus the depth migrations would appear to be accurate, at least for the stratigraphic interval encompassed by the well, and this depth information can certainly be used for interpretation purposes.

It is important to note that the "shallow" reflection events, labelled A, A1 and A2 (Figures 4.3 to 4.9; discussed in the following sections), picked on the seven seismic

profiles all have depths substantially greater than that penetrated by the stratigraphic test well (i.e. > 4 km). The actual depth extent of the PCIAC-GSD Masetlheng Pan-1 well, labelled "GSD Pan-1" on Figure 4.7, is indicated by the inset located at SP 2193. The picked reflection event which is penetrated by the well, labelled "W" on Figure 4.7, may correspond to Wasilenkoff's (1988) onlapping reflection close to total projected depth ($\approx$ 3,600 m) and appears to be coincident with the younger gabbro/dolerite intrusive which yielded the lower Carboniferous K-Ar date (333 $\pm$ 17 Ma).

4.2   Line Descriptions

Interpreted versions of the depth migrations for lines 90, 92, 94, 93, 99, 91 and 97 are presented in Figures 4.3 to 4.9 respectively. The profiles show a series of clear and correlatable reflection events which have been labelled appropriately. The nature of reflecting events common to all or some of the profiles is first briefly described followed by more detailed descriptions of the structures of each profile in turn.

A common and prominent feature of all seven profiles is the presence of a particularly strong reflector labelled "B" which marks the top of a very reflective sequence and represents the boundary between a deep sedimentary basin some 12 to 15 kilometres thick and a highly reflective and stratified mid to lower crust. Although event B does exhibit some lateral variability along its length, it can be picked with confidence over all of the profiles.

Within the sedimentary basin there are at least two prominent reflectors which can be

correlated with reasonable certainty from profile to profile. These events, labelled "A1" and "A2", like the underlying event B, also exhibit some lateral variability with coherency fading in areas which only allows these reflectors to be picked in a piece-wise fashion. In addition to events A1 and A2 there are reflection events on some of the profiles which are quite prominent but cannot be traced from line to line. These are not labelled and were only traced on the individual profiles to illustrate the "layer-cake" style of the basin's stratigraphy.

Lines 90, 92 and 94, all show a series of clear and strongly dipping reflectors (labelled "K" and "F") at or near their NE terminations. These reflectors, together with reflector B, and many others contained within the sedimentary basin, gradually rise up the section with the separation between them steadily decreasing as the layers thin towards the Kalahari Line.

A significant increase in reflectivity is marked by event "C" which occurs at a depth of 16 to 18 km on a majority of the profiles. The C event marks the start of a zone of reflectivity which varies both in thickness and character from line to line, being rather thin on some of the profiles ($\approx$ 1 km) and having a patchy appearance, to having a thickness of 3 to 5 km and being somewhat more continuous and coherent. Also the dips of individual reflectors comprising this zone vary from horizontal to moderate ($\approx$ 15° - 20°).

Event "D" marks another zone of increased reflectivity occurring at a deeper crustal level ($\approx$ 24 km) on most of the seismic profiles. Like event C, it displays considerable

lateral variability of thickness and internal structure.

Lines 90, 92 and 94 all have SW-NE orientations and structures imaged on these three profiles are described first. This is followed by a description of structures imaged on lines 93 and 99 which have NNW-SSE orientations. Lines 91 and 97 are then described which are tie lines to the above SW-NE and NNW-SSE profiles and both have northerly orientations.

4.2.1   Line 90

Line 90 (Figure 4.3) is the southernmost of the three SW-NE profiles and is the only one which crosses the Kalahari Line to image the easternmost edge of the Nosop Basin. The sedimentary section exhibits uniform layering over a majority of its length but there are some secondary structures which offset the sedimentary reflectors between stations 2368 and 2566. The sedimentary section is rapidly attenuated as the reflectors steeply rise up section to the east and are overstepped by overlying strata near or at the surface between stations 883 and 1477.

As indicated on Figure 4.3 (and Figures 4.10 and 4.11 in rear pocket), line 90 passes over borehole CKP-8C-1 and provides geologic control on the shallow stratigraphy at this location. As mentioned in Chapter 2, borehole CKP-8C-1 was sited on the southern portion of the Tshane Complex, one of the more prominent and extensive magnetic megafeatures of the Kalahari Line. Drilled to a total depth of 795 metres, this borehole penetrated a well-developed, well-preserved and essentially complete succession of the
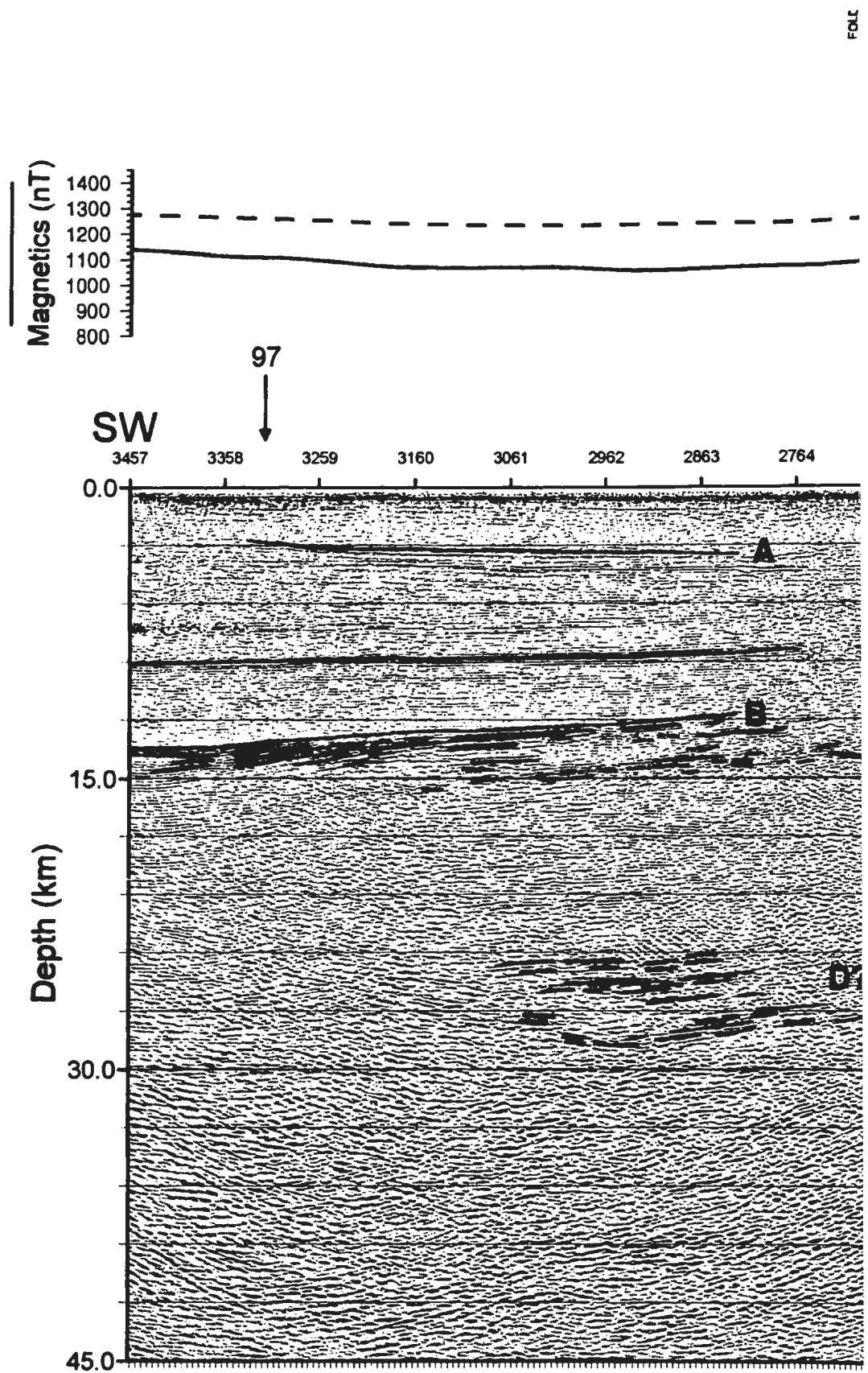
Figure 4.3 Interpreted version of the depth migration for Line 90.

91

Gravity (mgal)

-90
-100
-110
-120
-130
-140
-150

KL
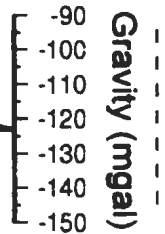
Pre-Karoo Gabbro(s) ?

CKP-8C1

NE

883   784   685   586   487   388   289   190   91 53

0.0

B

F

15.0

F

Depth (km)

30.0

45.0

Karoo Supergroup which rests unconformably upon a pre-Karoo, layered gabbroic body at a depth of 772 metres. The upper contact of this mafic body is not chilled and therefore is not believed to be intrusive into the lower Karoo (Meixner and Peart, 1984).

Thus it is likely that Karoo rocks provide the "pinchout" of the deeper Nosop Basin sediments which rise very close to surface at this locale. The pre-Karoo gabbro encountered in borehole CKP-8C-1 may be imaged on the seismic profile as a series of strong and laterally continuous reflectors evident at the borehole location at a depth of 0.7 to 1 km (see enlargement inset of Figure 4.3). It may be that a majority of the stronger reflectors existing in this region could represent lateral and/or depth equivalents of the mafic body penetrated by borehole CKP-8C-1. This might explain some of the complexity and chaotic nature of the deeper reflectors ($\approx$ 9 to 15 km depth) seen on the northeastern end of this profile.

Probably the most distinguishing feature of the lower crust imaged on line 90, and indeed on the other two SW-NE profiles, is the very notable contrast in reflectivity below the basin and immediately west of the Kalahari Line (indicated by strong, positive magnetic response and labelled "KL" at the NE end of the magnetic profile of Figure 4.3). At this location the reflectivity is stronger and more ubiquitous through the middle and lower crust as evidenced by the presence of the K reflectors. Indeed, the moderate to steep dips of this reflective sequence as well as the presence of a deeper series of reflectors ($\approx$ 24 km), labelled "F" on Figure 4.3, may be indicative of a crustal shear zone at or just below the F event. A complementary dipping event, labelled "M", may represent

an interrelated shear zone at the base of the crust ($\approx$ 33 to 36 km) although its lateral extent is very much limited. A more convincing demonstration of the M event is indicated by the unmigrated section for line 90 presented in Figure 3.9. The form of these two events, along with the thickening of the basin to the southwest, suggests that the crustal basement lying below a majority of the Nosop Basin may be extended or stretched Kaapvaal craton which is known to exist east of the Kalahari Line.

The lower crustal events C and D are not as easily recognizable as on other lines. The two sets of deeper reflectors visible between stations 2368 and 3061 at depths of 21 and 24-30 kilometres respectively are tentatively identified with C and D events. Certainly below the middle portion of the basin on this profile there is little or no change in the reflectivity through the middle and lower crust.

4.2.2 Line 92

Line 92 (Figure 4.4) shows uniform layering in the sedimentary section, broadly defined by the interval of 0 to 15 km, for most of its length. However, similar to line 90, some structure is present within the sedimentary section which seems to be offset between stations 3170 and 3368. On approach to the Kalahari Line the reflectors rise up section and rapid thinning of the sedimentary section occurs over a few tens of kilometres and appears to be equally distributed among the recognizable units. Onlap of the reflectors towards the Kalahari Line is observed, as is some complexity of structure, and, concurring with Hall *et al.* (1990), there appears to be no obvious angular unconformity present to
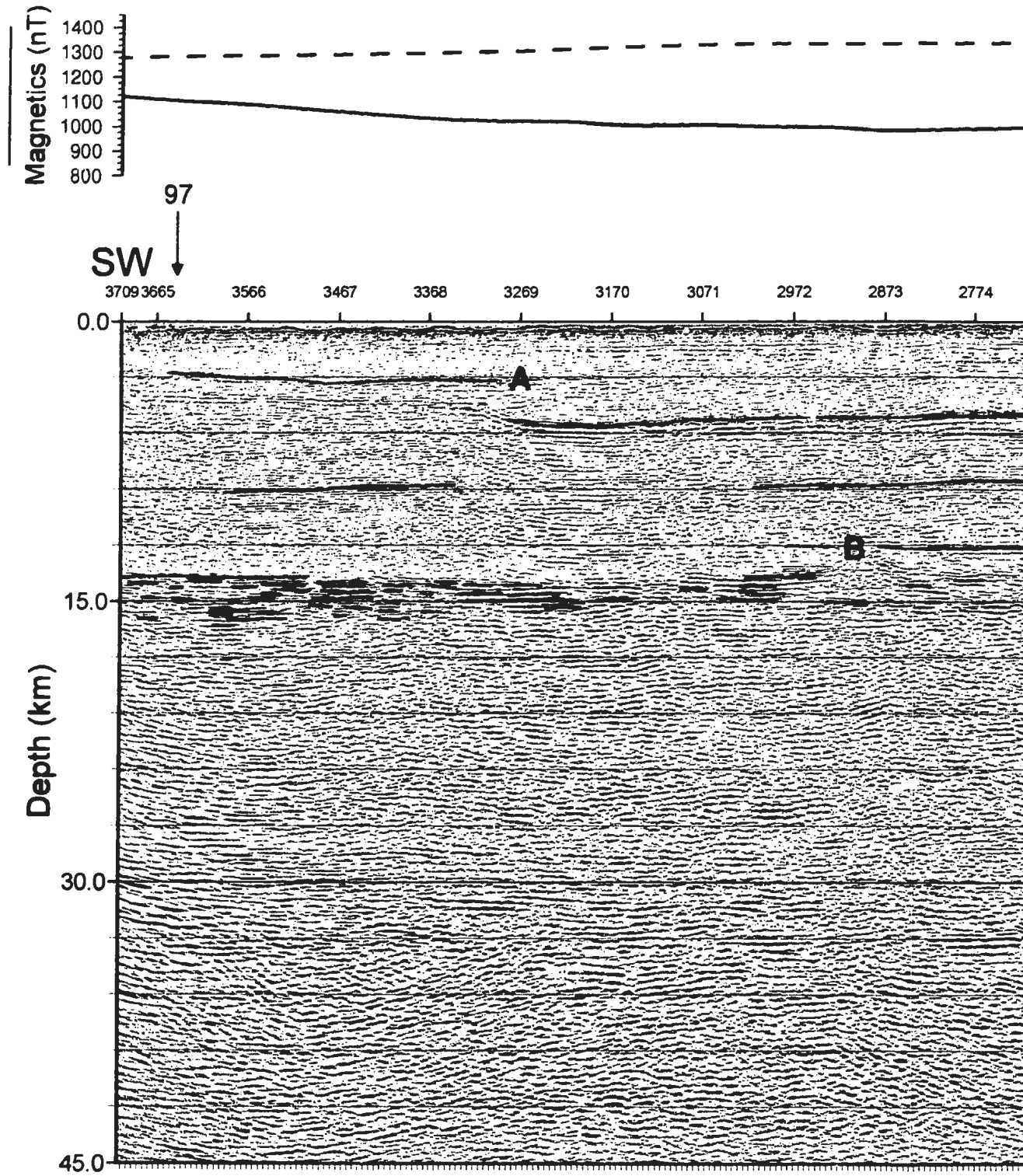
Figure 4.4   Interpreted version of the depth migration for Line 92.

99

| 2675 | 2576 | 2477 | 2378 | 2279 | 2180 | 2081 | 1982 | 1883 | 1784 | 1685 | 1586 | 1487 |
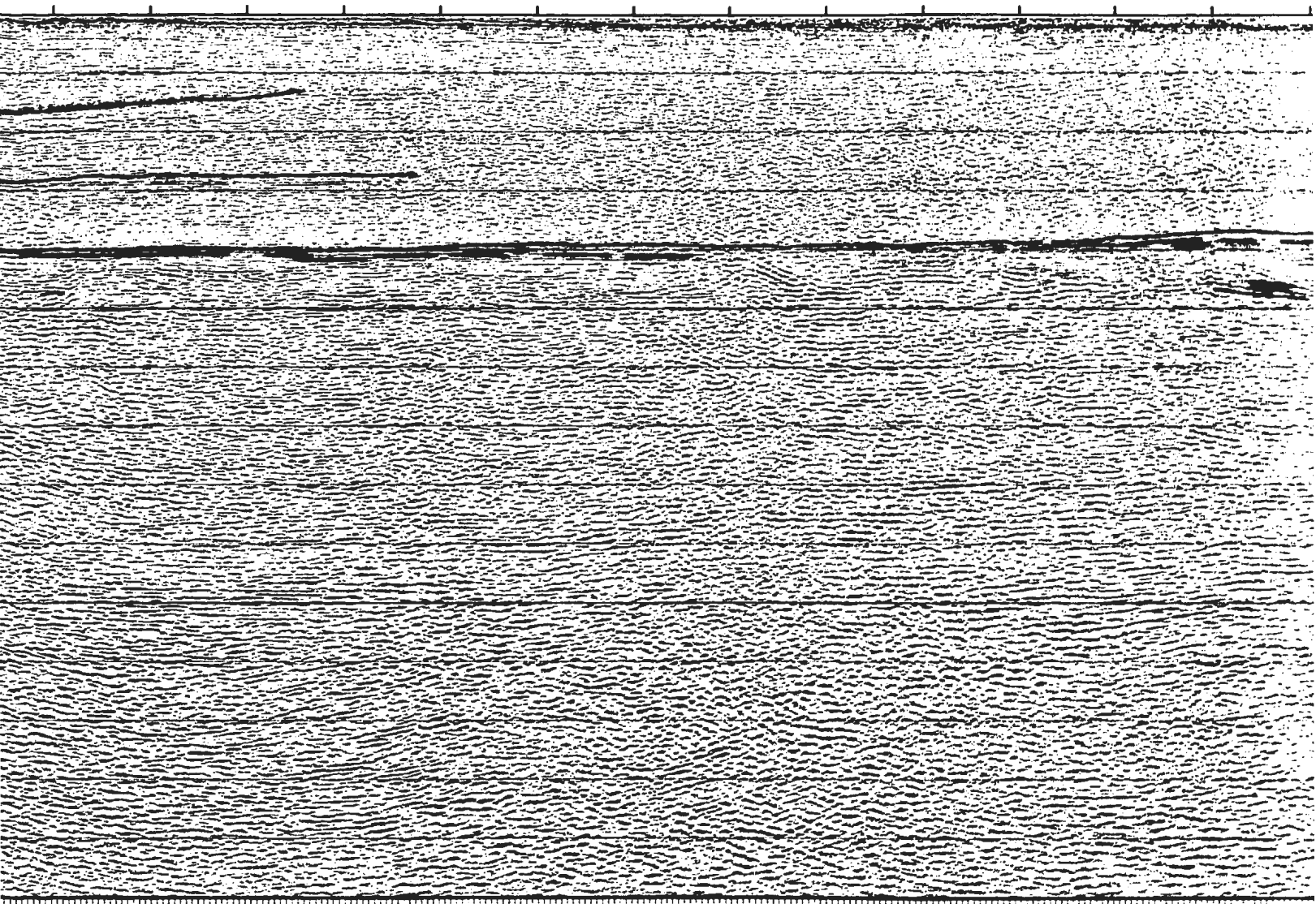
99

91

1388 477   2378   2279   2180   2081   1982   1883   1784   1685   1586   1487   1388   1289   1190
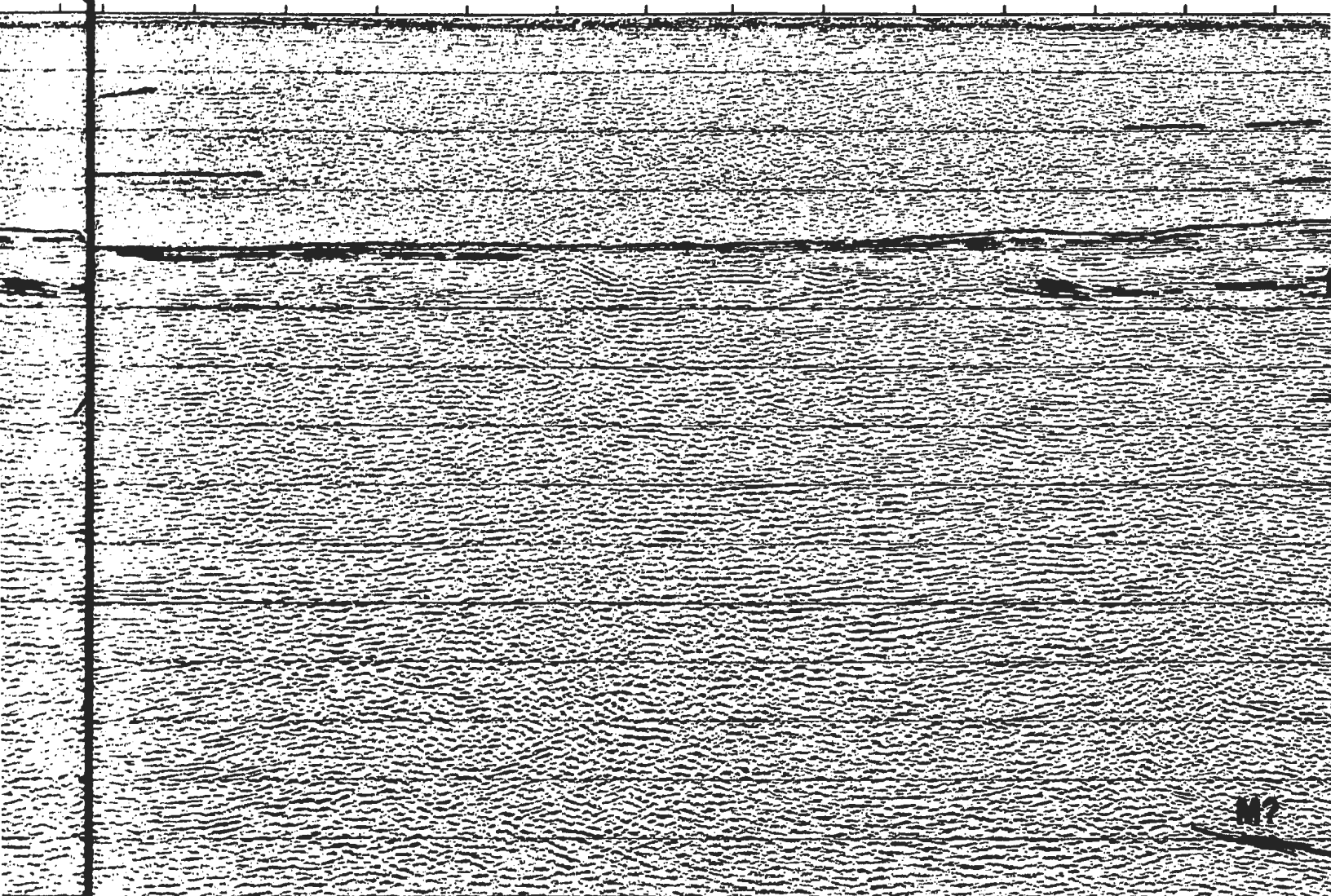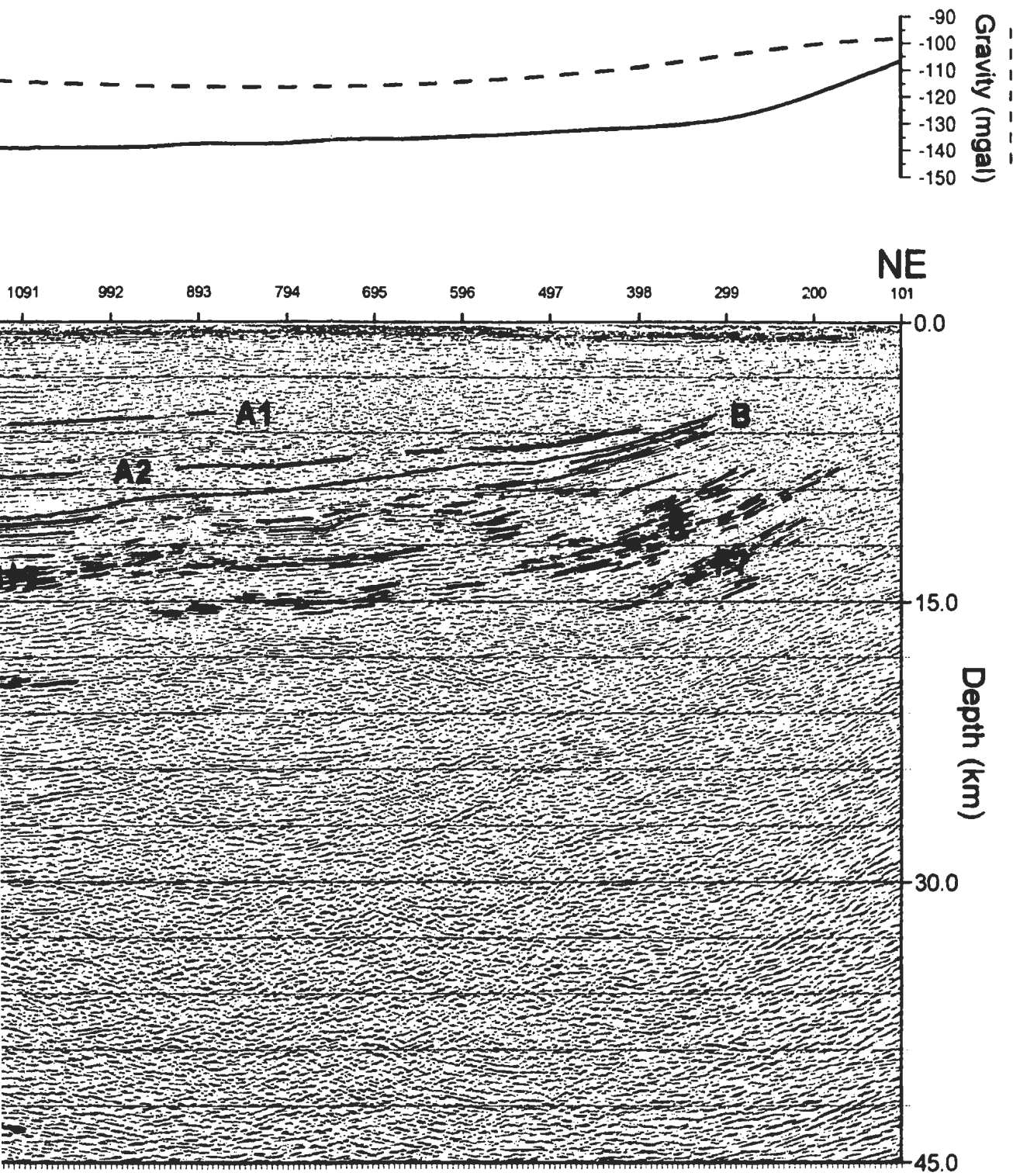
indicate a pulse of deformation rather than a continuous subsidence of the basin.

As with line 90, the clearest deeper crustal feature is the apparent contrast between the reflectivity seen below the main basin and that at the northeastern edge of the profile in the vicinity of the Kalahari Line. The middle and lower crustal sections show a stronger and more pervasive reflectivity at this edge as again indicated by the presence of the K reflective sequence. Also, comparable to line 90, the moderate to steep dips imaged at this end of the line along with another reflective zone lying just below the level of the K reflectors, similarly labelled "F", may be evidence that a crustal shear zone exists at or below the F event. However, it should be noted that the F event on line 92 is much shallower (12 - 15 km vs. 24 km) than on line 90 and, as such, correlating these two events as one should be considered tentative. There is no clear indication of the existence of a complementary shear zone M at or near the base of the crust as with line 90. However, there are two solitary reflectors situated between stations 1091 and 1289 at the very base of the profile (i.e. 45 km) that might be an expression of this possible deep shear zone but it could also be a migration artifact. The presence of the M event is probably better corroborated by examining the unmigrated section of line 92 presented in Figure 3.15.

Another interesting feature of this deep seismic reflection profile is the series of reflectors located below the B reflector (12 - 15 km) near the intersection with line 91 between stations 794 and 1487. This reflective package corresponds well with the B1 package of line 91 and, as such, has been labelled the same. These reflectors appear to

be conformable with the overlying sub-B reflectors but it should be noted that, because of the orientation of line 92, it may represent a near-strike line to the B1 package imaged on line 91. In this case no noticeable dips would be observed in the B1 package of line 92 and an angular relationship of it with the higher B reflector would not be observed.

Unlike line 90, reflectors C and D are not at all discernible on this profile and it would seem that the reflectivity below a majority of the main basin is quite homogeneous and weak with no noticeable change in pattern throughout the mid to lower crust.

4.2.3 Line 94

Line 94 (Figure 4.5) shows all the features of both lines 90 and 92, but they are much more apparent on this profile. However, unlike on the other two profiles, the mid to lower crust beneath the basin away from the Kalahari Line is much more reflective and displays considerable structure. There is obvious thinning of the sedimentary section towards the Kalahari Line and, as with the lines 90 and 92, the presence of the gentle to moderate dipping reflective package, again labelled "K", may indicate the presence of a broad crustal shear zone. However, the picking of event "F", which was done with the other two SW-NE profiles and would mark the approximate location of the shear zone, is difficult. This is because there is no clear indication of a distinct reflective package lying below the K reflectors at a lower crustal level as is evident on lines 90 and 92. Thus the F event was picked to lie at the base of the K reflective package on this profile.

Along with the presence of the K reflectors, there is other strong evidence for the
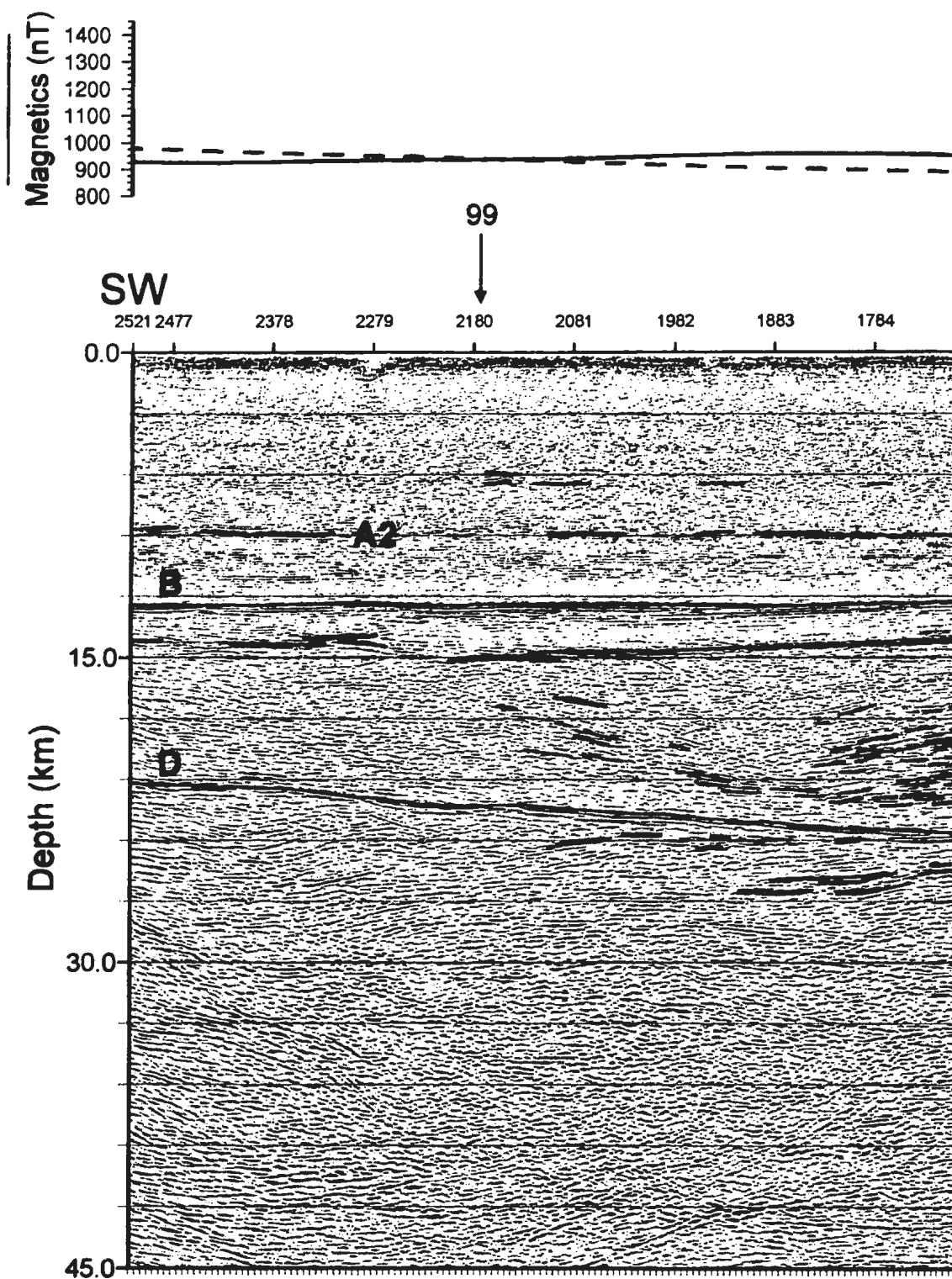
Figure 4.5 Interpreted version of the depth migration for Line 94.

93

| 1685 | 1586 | 1487 | 1388 | 1289 | 1190 | 1091 | 992 | 893 | 794 | 695 | 596 | 497 | 398 | 299 | 92 |
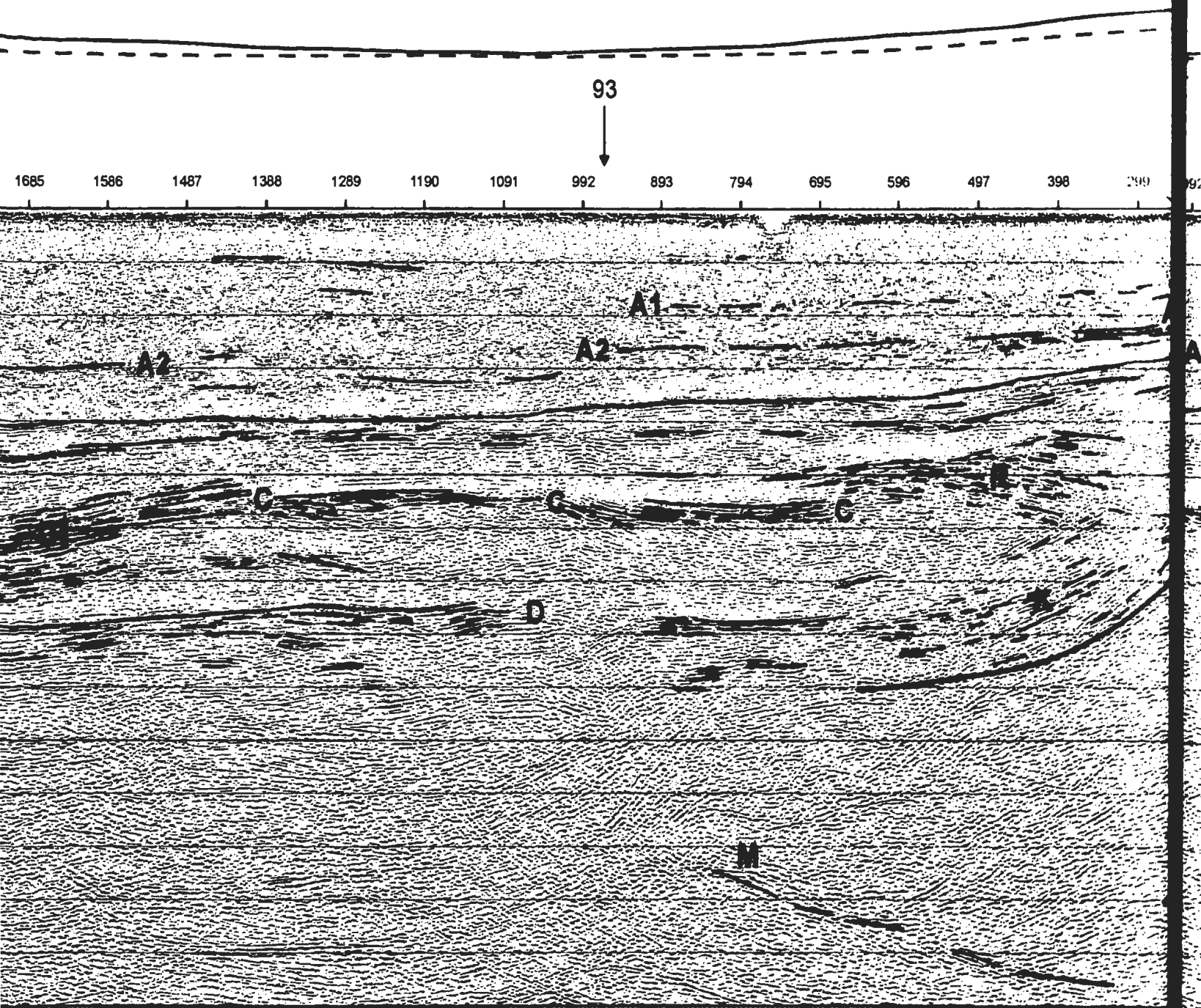
Gravity (mgal)

-90
-100
-110
-120
-130
-140
-150

93

NE

92   893   794   695   596   497   398   299   200   101

0.0

A1

A1

A2

A2

B

15.0

R

C

F

Depth (km)

30.0

M

45.0

existence of a shear or fault zone at the NE end of line 94. A reflective package, labelled "R", which lies above the K package, dips in the opposing direction and appears to be terminated by it. The SW dipping K and F events, along with shape of the complementary dipping R reflectors, are suggestive of a large scale listric fault with development of a rollover against the margin of the craton to the east. This structure along with the complementary dipping event M, which is clearest on this profile, suggests that it was formed by extension of the crustal basement in the east by movement along this shear zone. This implies that the R reflector and its lateral correlatives are part of a sedimentary/volcanic sequence and that the C event may mark the top of crystalline basement.

The C reflective package is very well defined on this profile and it exhibits significant structure along its length. Lying at a depth of 18 to 21 km, its southwestern end is dominated by a thick ($\approx$ 7 km) and extremely coherent series of SW dipping reflectors between stations 1388 and 1883. These reflectors have been labelled "C1" to indicate they may be a subset of the C package although the "stratigraphic" relationship between these two packages is unclear. The underlying D package on this profile is quite striking as its uppermost reflector, which marks the lower crustal layering, can be traced for approximately 70 km (stations 1091 - 2521) from the SW end to the middle part of the profile.

4.2.4 Line 93

Line 93 (Figure 4.6) along with line 99 are two of the profiles which span the Nosop

Basin in a NNW-SSE direction and essentially run parallel to one another. On the

northwest end of these lines, buried structures associated with the Ghanzi - Chobe fold

belt are imaged, most clearly and dominantly on line 93 as the NNW termination of this

profile is much closer to the surface exposures of the Ghanzi Group. The association of

these buried fold and thrust structures imaged on line 93 with those exposed in the

Ghanzi - Chobe fold belt itself is supported by their similar SE structural polarities. In

fact, the start of line 93 falls within one of Litherland's (1982) study areas and is less than

10 km from outcrop of the Ghanzi Group rocks which he described and as outlined in

Chapter 2.

The phase-shift migration has done a reasonably good job in resolving the true form

of the major folds and possible related thrust faults that are a part of the Ghanzi-Chobe

fold belt. The scale of these folds is indeed huge with wavelengths on the order of 25 km

and structural relief of approximately 6 km. The folds appear to be detached on thrust

faults, labelled "F1" to "F3" on Figure 4.6.

Evidence for the existence of these faults is provided by the antiformal feature,

labelled "G1", whose internal reflectors are abruptly terminated by an interpreted fault,

labelled "F1", between stations 681 and 780. Also, the sudden change in dips at the base

of the reflective zone labelled "G2" is further evidence of faulting. Here NNW dips of 15°

- 20° change to horizontal to subhorizontal over a very short depth interval (≤ 1 km)
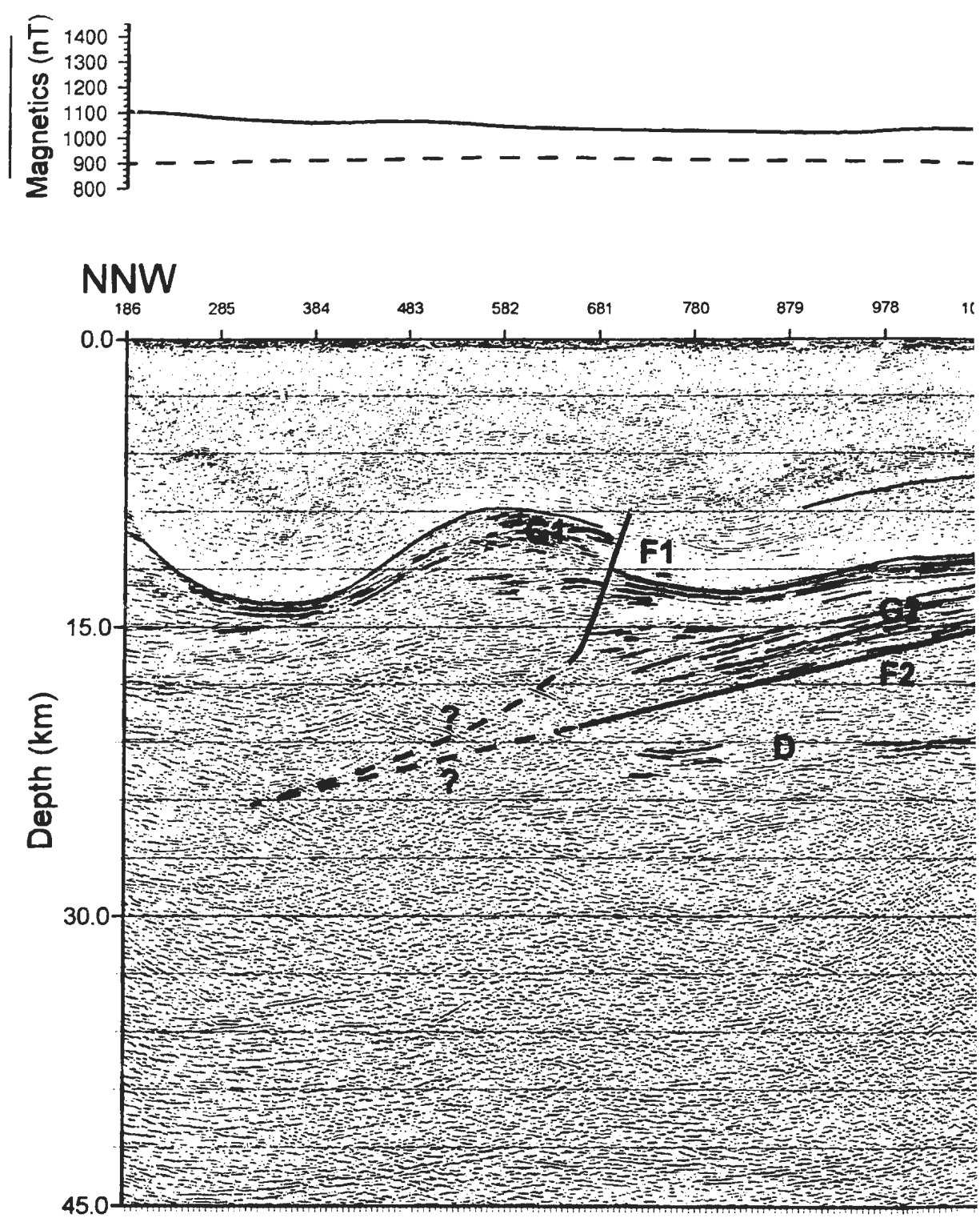
Figure 4.6 Interpreted version of the depth migration for Line 93.
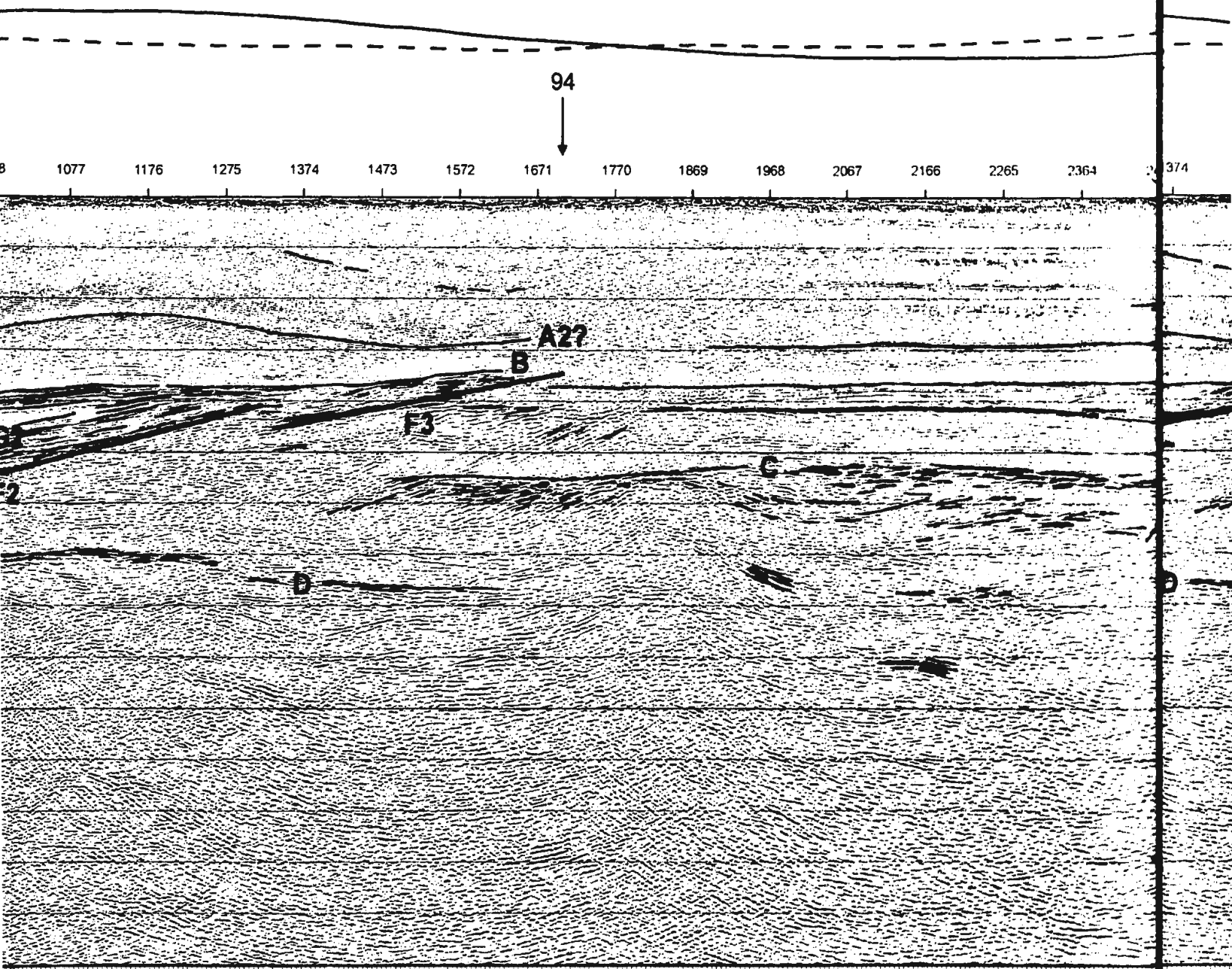
94

| 8 | 1077 | 1176 | 1275 | 1374 | 1473 | 1572 | 1671 | 1770 | 1869 | 1968 | 2067 | 2166 | 2265 | 2364 | 374 |

A2?

B

F3

C

D

D

Gravity (mgal)

-90
-100
-110
-120
-130
-140
-150

91

↓ SSE

| 2661 | 2760 | 2859 | 2958 | 3057 | 3156 | 3255 | 3354 | 3453 | 3552 | 3651 3697 |

0.0

A1

A2

B

15.0

C

30.0

Depth (km)

45.0
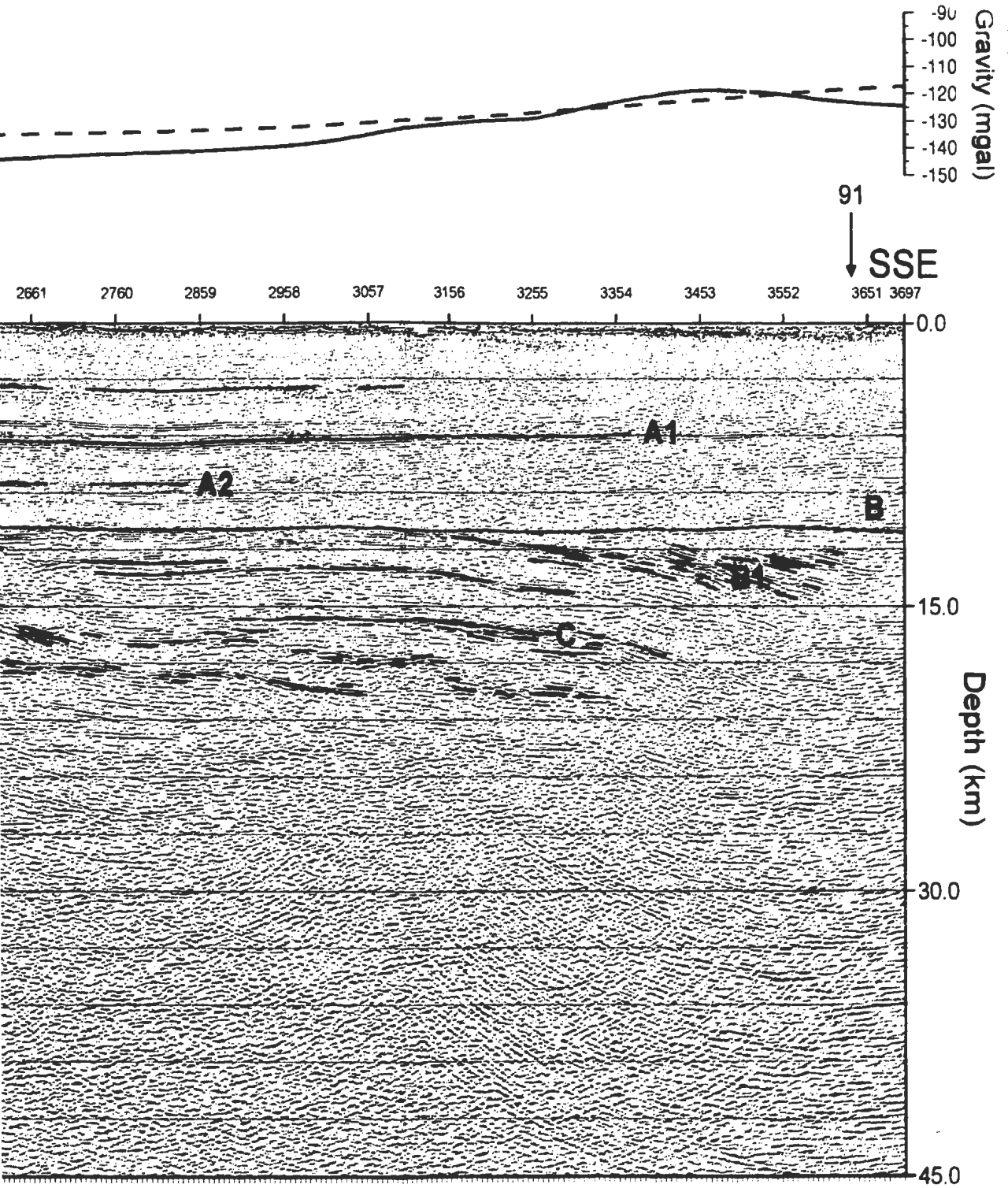
across the "F2" boundary. The G2 reflectors could represent a broad shear zone that is soled by event F2 which resulted from thrust movement during the orogenesis that formed the Ghanzi-Chobe fold belt. Alternatively, the reflectors comprising the G2 zone might represent the bedding of an older sedimentary package which was either originally laid down on an inclined surface or were tilted in an earlier orogenic event. The overlying B reflector would then represent an angular unconformity and the F2 event at the base of G2 might be a thrust that was activated along the original depositional surface. F2 and F3 may be the deepest thrusts of the Ghanzi-Chobe fold-thrust system, with blind termination within the A2-B sequence. However, there are similarly dipping reflection segments just below F3 which may be cogenetic and thus represent the furthest SW extent of the belt.

Within the sedimentary section the B reflector is offset by one of the previously discussed faults labelled F3 between stations 1572 and 1770. The identification of reflectors above the fold and thrust structure is difficult as their continuity is quite limited and the overall appearance of the sedimentary section on this part of the line is somewhat chaotic. The interval A2 to B appears to thicken over the G2 reflective package between stations 879 to 1473 and suggests that this was an original thickness variation of the A2-B interval itself. Hall *et al.* (1990) point out that since the A2-B sequence is affected by the fold and thrust belt, the age of this interval, at least in part, is pre-thrusting. Also, the fact that the A2-B interval thickens towards the fold belt indicates modest foreland basin development in front of a growing fold belt. Thus the A2-B stratigraphic interval overlaps

with the development of the Ghanzi-Chobe fold belt.

Another noticeable feature is the presence of a series of southeast dipping reflectors located between stations 3156 and 3651 at the SSE end of the profile lying just below the B reflector. These dipping reflectors, labelled "B1", may represent an older sedimentary package, like the G2 package, which has an angular relationship with the overlying B reflector. "B" would then represent an angular unconformity. It is important to note that the SSE end of this profile is intersected by line 91 and it might be possible that the B1 reflectors of line 93 are related to, or part of, the same structure that is indicated by the B1 reflective package on line 91.

Event C is easily recognizable and can be traced over most of the profile beneath the undisturbed portion of the basin. However, beneath the zone near the start of the fold belt deformation ($\approx$ station 1473), it ends abruptly. The exact reason for this is not clear but since the deeper events (i.e. event D) associated with the lower crust do continue under the fold belt, there is no reason to believe that the abrupt change in the reflectivity of event C is due to defocussing caused by the fold belt itself. The internal reflectors below event C show considerable structure in places. Between stations 1869 and 2265, these reflectors take on a synformal appearance. Event D is visible beneath the fold belt structures between stations 681 and 1671. Although it is not completely continuous over this interval, the reflectors that make up its various pieces are strong and show good coherency over their respective lengths. Although it lies at the same crustal level as the depth extensions of faults F1 and F2, it is hard to say whether event D has been involved

in the deformation of the fold belt structures which lie above it.

4.2.5 Line 99

This profile (Figure 4.7) displays many of the same features as line 93 but since it does not extend as far north as its parallel counterpart, the major structures related to the Ghanzi-Chobe fold belt are not imaged to the same extent. However, there is evidence of thrusting near the intersection with line 94 (stations 626 - 725) marked by interpreted fault "F3" to indicate possibly the same fault as labelled on line 93. Above this proposed thrust and within the basin itself, thickening of sedimentary units (A1 to B) is clearly seen. Also present is a thick ($\approx$ 6 km) reflective package, again labelled "G2", which dips to the NNW and may represent the continuance of the G2 package imaged on line 93 to the southeast.

The mid-crustal reflective package C is observable on this profile but certainly not as clearly as it is imaged on line 93. The D event of the lower crust appears to be reasonably defined displaying good continuity and, like the mid to lower crustal reflectors of the other profiles, possesses substantial structure over most of the profile. To illustrate this, a series of NNW dipping reflectors is clearly visible between stations 1220 and 1616. In contrast, the SSE end (stations 2012 - 2507) consists of a series of opposing, SSE dipping reflectors. Also at its NNW end between stations 428 and 928, the D reflector appears to gradually rise up section approaching the same crustal level as the F3 fault which marks the base of the G2 package. Again it is difficult to state whether this portion of event D
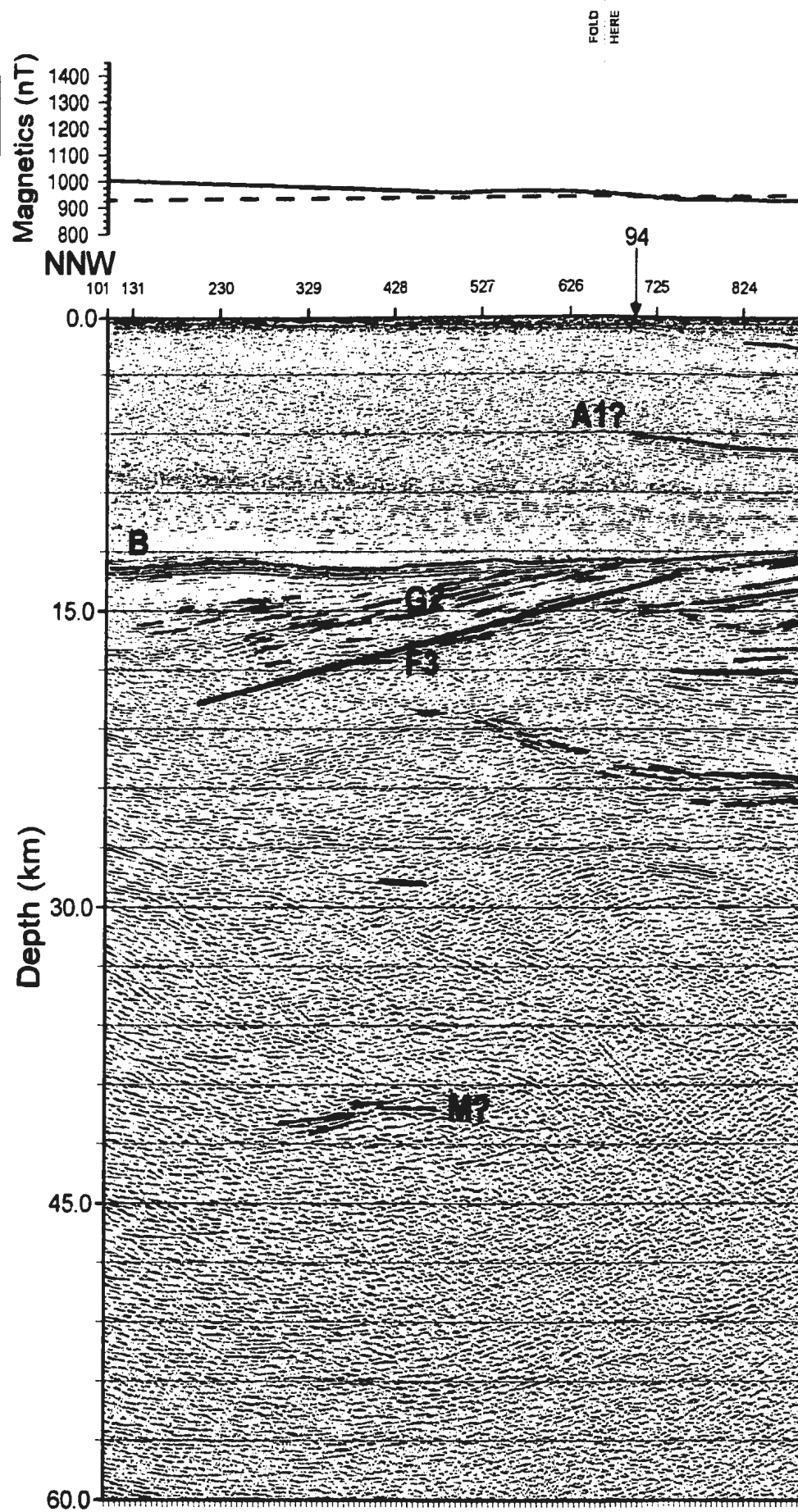
Figure 4.7 Interpreted version of the depth migration for Line 99.
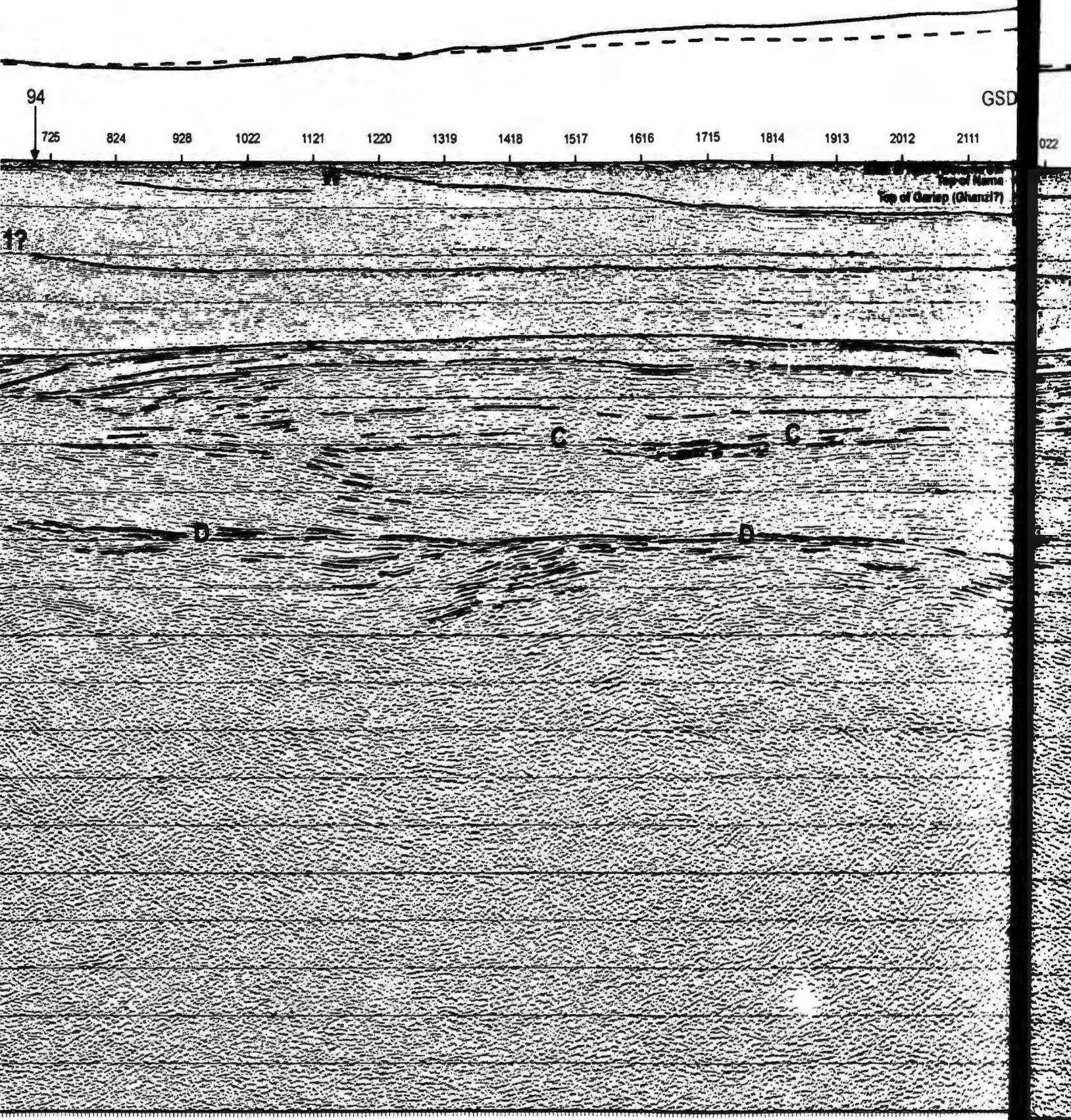
GSD PAN-1

Gravity (mgal)

-90
-100
-110
-120
-130
-140
-150

92

SSE

408 2507 2606 2705 2804 2903 3002 3101

0.0

W

A1?

B

15.0

30.0

Depth (Km)

45.0

60.0
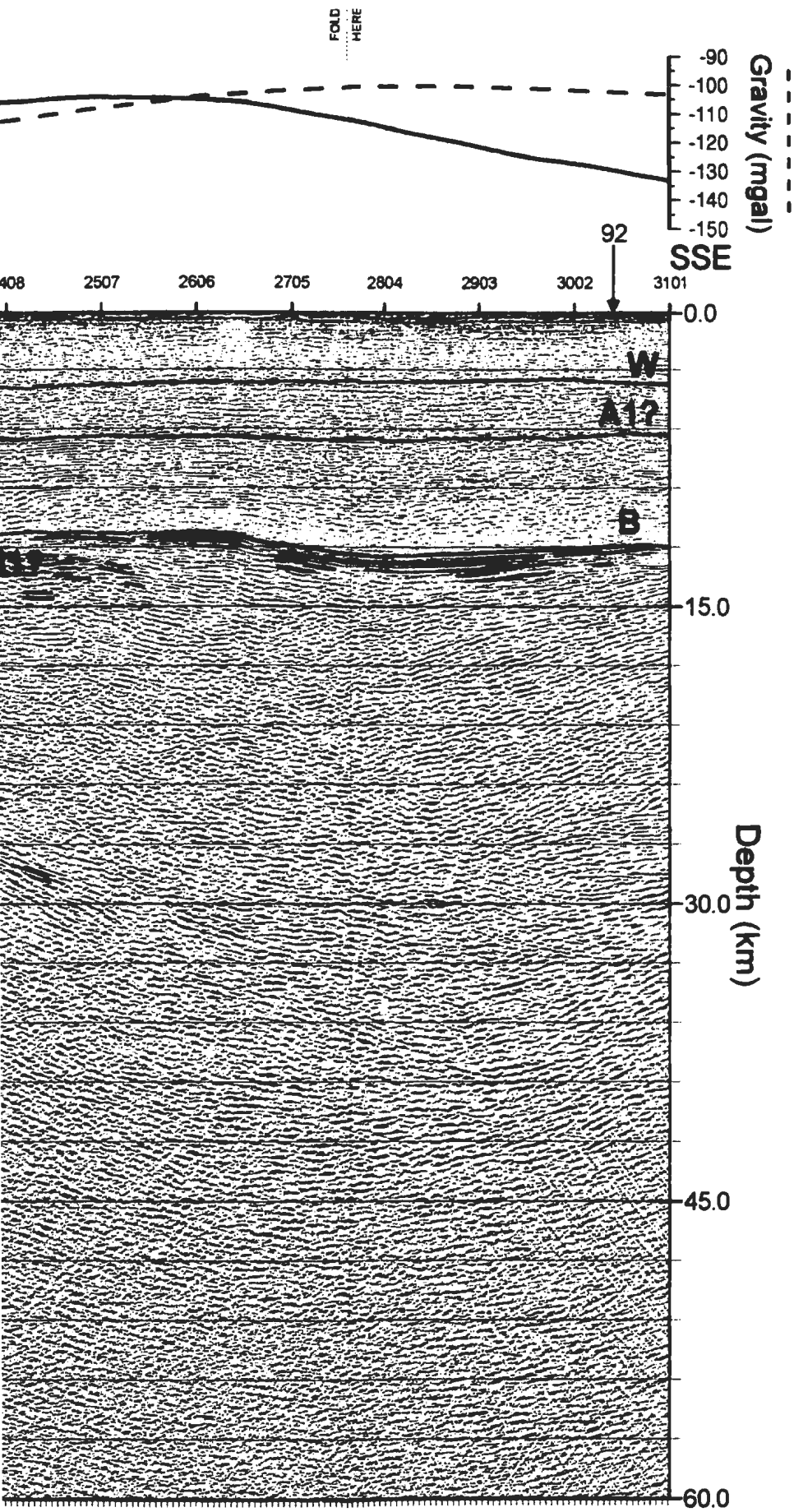
could be involved in the thrusting associated with the deformation of the fold belt that is so clearly imaged on line 93.

4.2.6 Line 91

Line 91 (Figure 4.8) is orientated in a N-S direction and ties with lines 90, 92 and 93. It parallels the Kalahari Line and thus could be considered a "strike" line; indeed the thickness of the sedimentary section is remarkably uniform (10 - 11 km) over the entire profile.

The most noticeable feature of line 91 is the presence of a series of north dipping reflectors located between stations 596 and 992 at a depth of 11 to 15 km just below event B. These dipping reflectors, labelled "B1", may represent a deeper (and probably older) sedimentary package and the angular relationship between them and overlying reflector B may represent an angular unconformity. Augmenting the B1 reflectors is another sequence of reflectors, labelled "B2". Although this reflective package is sparsely observed between stations 893 to 1289 and is a good deal thinner than B1, it does have greater lateral extent and possesses shallower north dips than the B1 reflective package.

The mid to lower crustal reflectors C and D can also be patchily observed on profile 91. It is interesting to note that reflector C, like events B1 and B2, also displays a northward dip along most of its length. However, reflector D for the most part seems to be flat-lying for most of its length and, in fact, exhibits an opposite, shallow, southward dip near its northern end (stations 398 to 794). Situated at a depth of about 30 km below
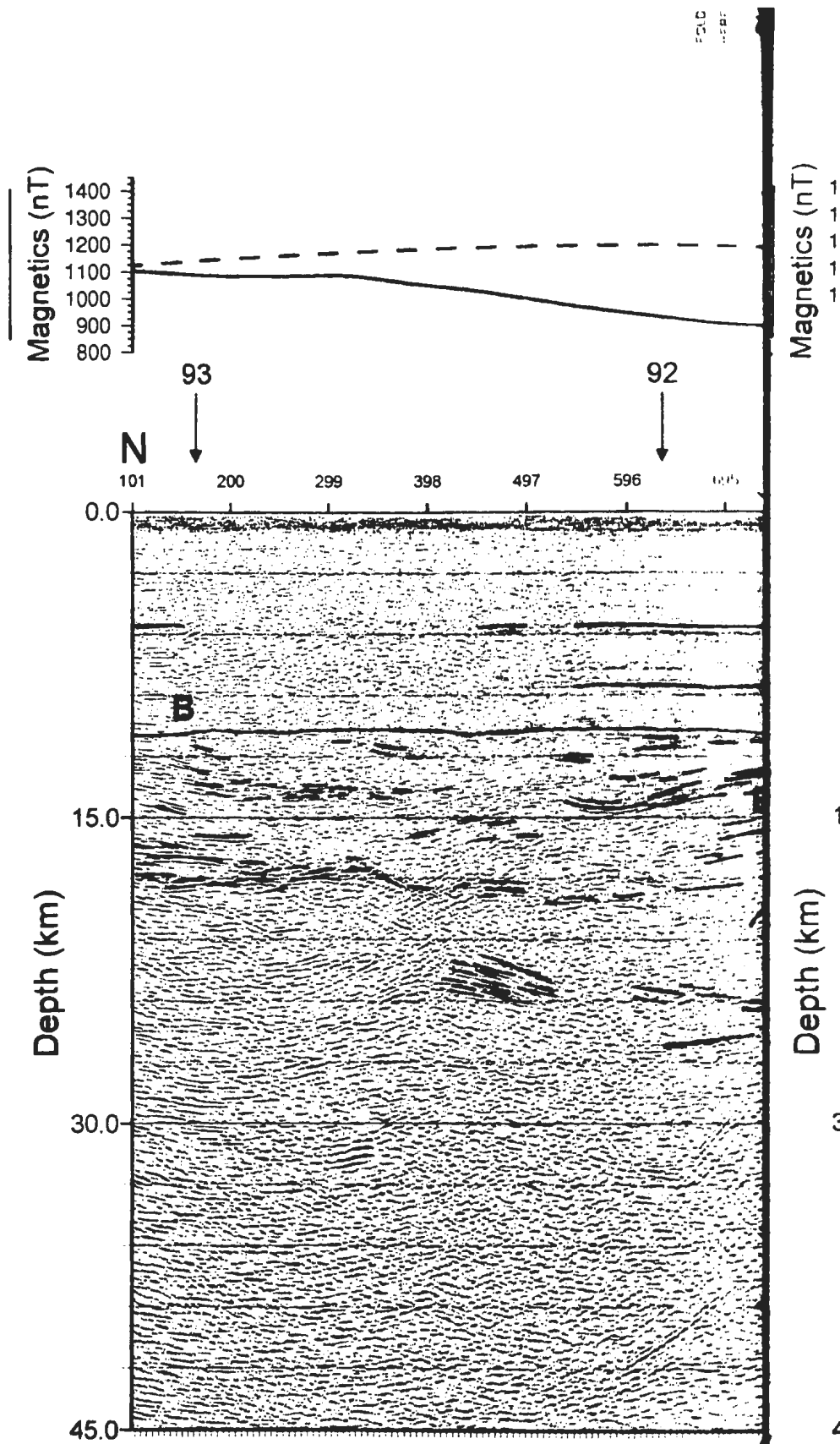
Figure 4.8 Interpreted version of the depth migration for Line 91.

of the depth migration for Line 91.

Gravity (mgal)

-90
-100
-110
-120
-130
-140
-150

90

S

1388   1487   1586   1685   1784   1883   1982   2079

0.0

B

15.0

C   C

D

M?   M?

30.0

Depth (km)

45.0
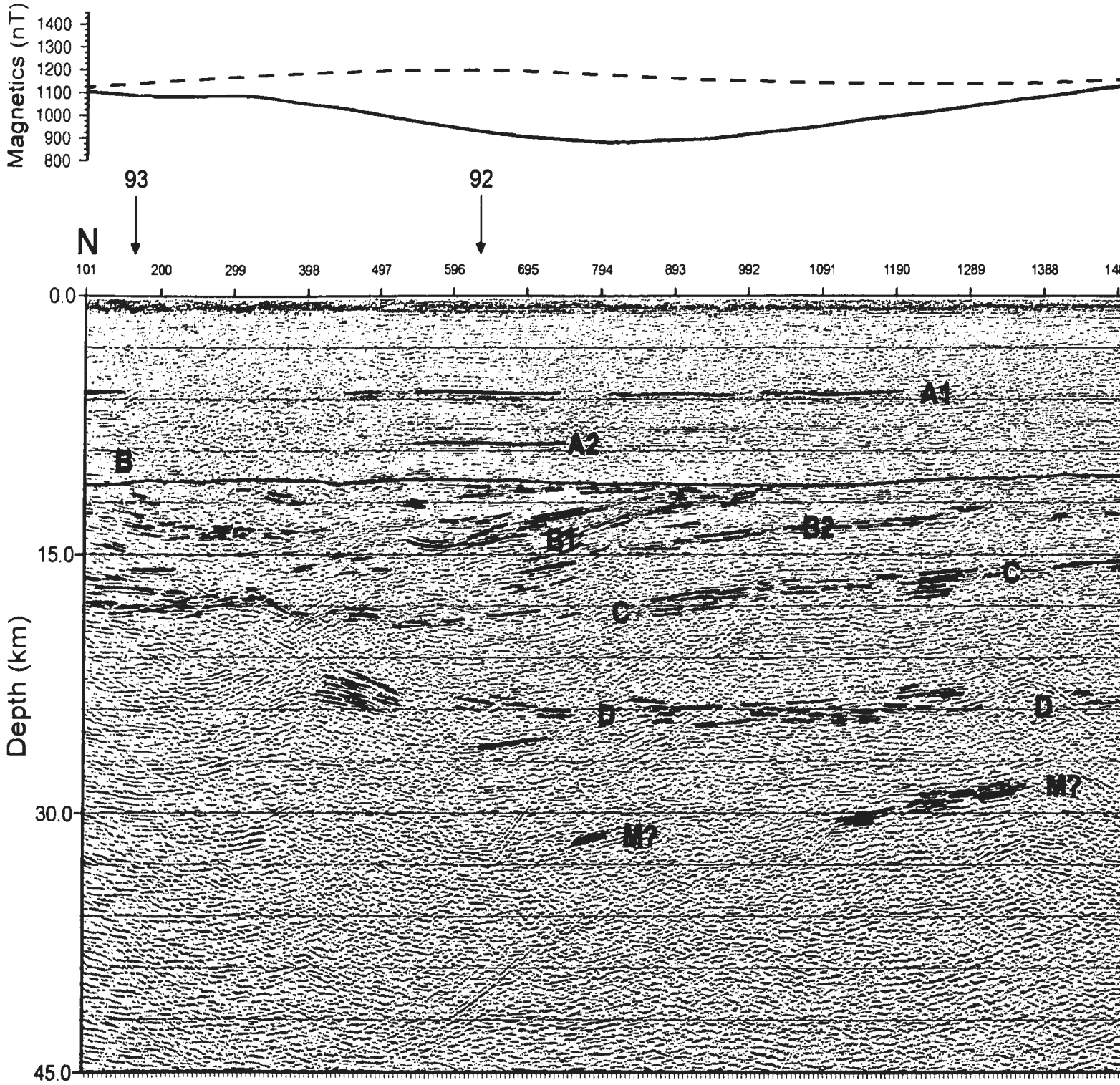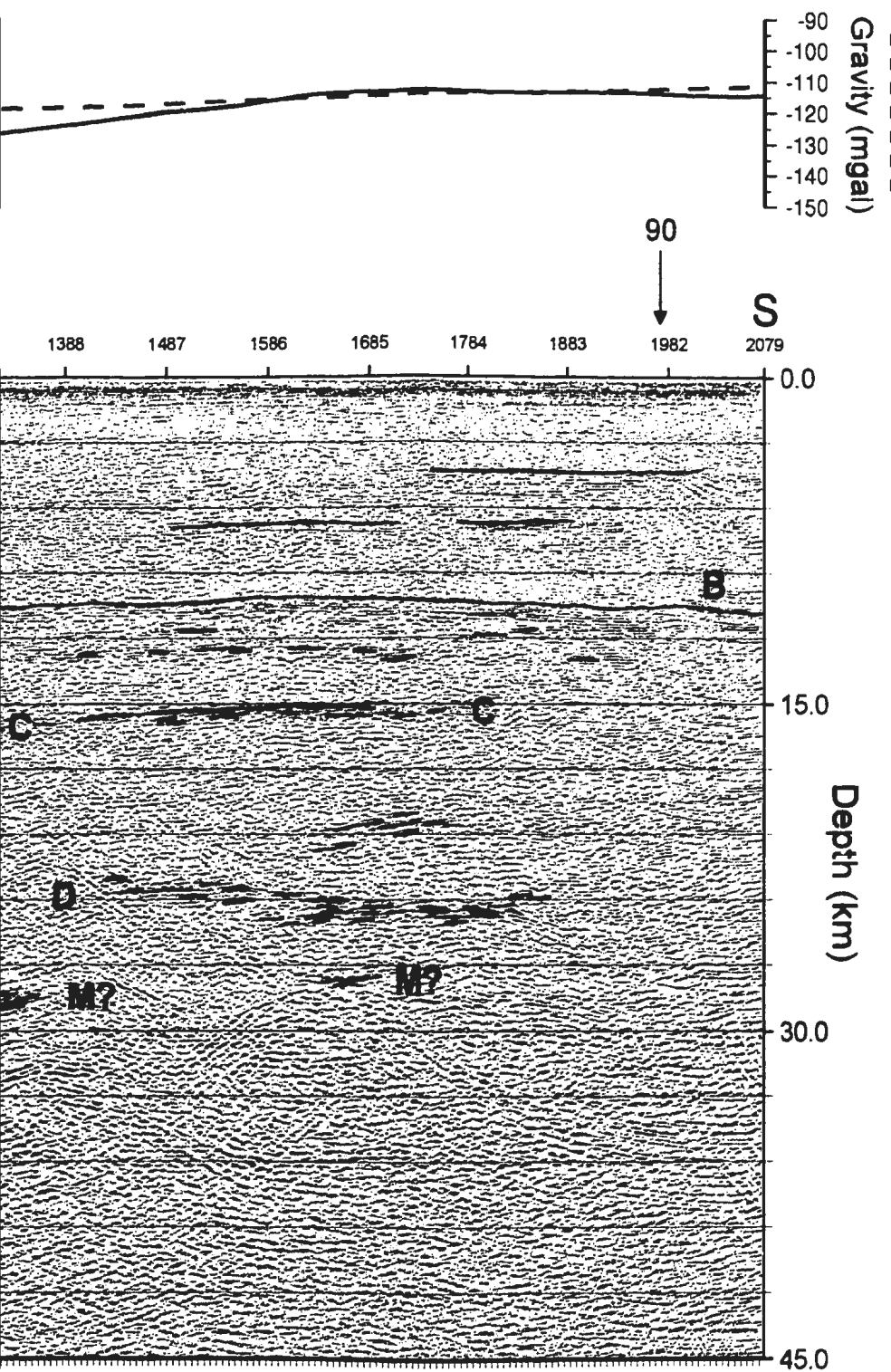
event D between stations 794 to 1685 is another reflective feature labelled M which, like line 90, may represent the base of the crust. Like events B1, B2 and C which occupy higher crustal levels, the M event also displays a noticeable northward dip.

4.2.7 Line 97

Line 97 (Figure 4.9), like line 91, is also orientated in a N-S direction and ties with lines 90 and 92. Being the shortest of all seven profiles ($\approx$ 16 km) and located farther west than line 91, this other "strike" line shows a somewhat thicker and uniform basin fill of approximately 15 km across its length. Other than the A and B reflectors labelled on this profile, this line shows little else with respect to increased reflectivity in the mid to lower crust giving it an appearance similar to line 92.

4.3 Potential Field Data

The gravity and aeromagnetic field data for the Nosop Basin are displayed in Figures 4.10 and 4.11 respectively (rear pocket). As with the seismic data, the right to use these potential field data was obtained from the Government of Botswana by Memorial University's Centre for Earth Resources Research.

The gravity data set provided was originally collected by *Compagnie Generale de Geophysique* (CGG) for the Government of Botswana as a component of the 1987-88 reconnaissance reflection seismic programme. As with the seismic programme, gravity was collected in the Nosop Basin in the southwest as well as the Passarge Basin farther
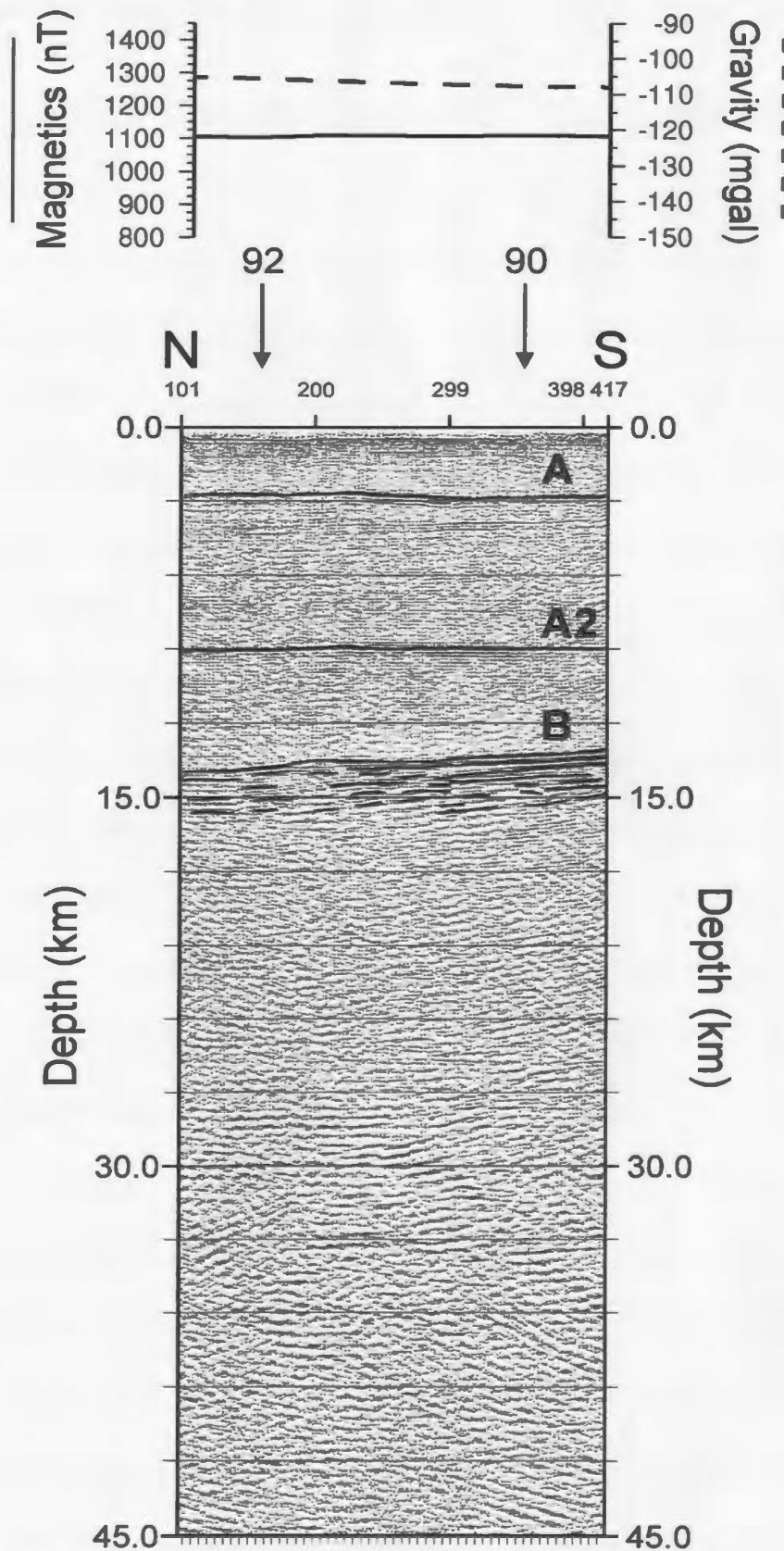
Figure 4.9 Interpreted version of the depth migration for Line 97.

to the northeast. These data were collected on a regularly spaced grid with a station spacing of approximately 3 km along profile lines and an average spacing between adjacent profile lines of approximately 22.5 km. A majority of the grid lines were orientated in a NW-SE direction with their lengths spanning much of the Nosop Basin within the international borders of Botswana's western region as is evident from Figure 4.10.

The gravity data displayed in Figure 4.10 is the Bouguer anomaly map based on a correction density of 2.67 gm/cm^3. These data arrived at Memorial University in a line-oriented, ASCII format and, as such, some processing was required in order to produce the map presented in Figure 4.10. This was accomplished through the use of GEOSOFT$^{\text{℞}}$, a commercially available, microcomputer-based software package that allows the processing and mapping of various types of geophysical data. The primary aim of the processing was to transform the gravity data from a line-oriented, ASCII format to a grid-oriented, binary format which can then be easily displayed in map form. The gridded, binary data consists of cells, usually square in shape, of fixed size with each corner of a cell containing a data value.

A bi-directional method of gridding (GEOSOFT$^®$'s BIGRID program) was utilized to grid the gravity data set. The method is designed to interpolate roughly parallel line-based data and uses linear, minimum curvature or Akima splines to interpolate grid nodes between lines in the direction of the overall trend of the data (Geosoft Inc., 1995). The bi-directional gridding process consists of two principal steps. Each original survey line

is first interpolated along its length to yield data values at the intersection of it with the required grid line. The intersection data values from each grid line are then interpolated along the length of the grid line to produce values at each required grid point. This second interpolation process creates grid lines which are essentially a series of numbers that represent all the values along the various rows in the grid. In the case of the Nosop Basin gravity data set, a 1.2 × 1.2 km cell size was chosen for gridding purposes and a minimum curvature spline was employed for the grid interpolation.

Once the data had been gridded, they were smoothed via 3 passes of a 9-point Hanning filter prior to display (*GEOSOFT*'s GRIDHANN program). The Hanning filter used a 3×3 point kernel filter defined by the following coefficients:

0.06	0.10	0.06
0.10	0.36	0.10
0.06	0.10	0.06

This smoothing was performed in order to improve the cosmetic appearance of the colour contours presented in Figure 4.10.

The total intensity aeromagnetic data presented in Figure 4.11(a) is a subset of the 1975-77 National Reconnaissance Aeromagnetic Survey of Botswana. Unlike the gravity data, this data set was already in a gridded, binary format and consisted of a total of 12 grid files covering the entire country. Two of these grid files cover much of the western half of the country including the Nosop Basin were merged using *GEOSOFT*'s GRIDBOOL program to produce a single grid of the area of interest. This program

applies Boolean functions between two input grids to produce a combined output grid based on the presence or absence of a dummy or null value at a grid point (Geosoft Inc., 1995). In the case of the two western Botswana grids, the resultant output grid contains data values from both grids where either of the two input grids are valid (i.e. non-dummy) and the area of overlap was averaged between the valid data values of the two grids.

This larger, combined grid was then re-gridded, again using BIGRID, in order to resample from the original cell size of 0.6×0.6 km to the 1.2×1.2 km cell size output for the gravity data. When re-gridding grids, BIGRID treats each grid line as an XYZ survey line and performs the same interpolation procedures as were previously discussed (Geosoft Inc., 1995). In order to produce a final grid with the same geographic shape and size as the gravity data set, a multiplier of +1 was applied to this combined and resampled aeromagnetic grid and then added to the gravity grid which had a multiplier of 0 applied. This was accomplished through the use of the GRIDADD program which simply adds two grids together, grid point by grid point, with multiplier factors applied to each grid before the addition. As with the gravity data, the final aeromagnetic grid values were smoothed via three (3) passes of the 9-point Hanning filter prior to display.

In order to facilitate a more rigorous treatment of the aeromagnetic data with respect to its correlation to the deep seismic data, it was necessary to reduce these data to the magnetic pole. This filtering process essentially centres the peaks of the magnetic anomalies over their sources making the data easier to interpret while not losing any geophysical meaning (Geosoft Inc., 1995). Reduction to the magnetic pole was

accomplished using *GEOSOFT*[*]'s 2-D FFT (fast fourier transform) processing system MAGMAP.

For the sake of mathematical convenience and speed, MAGMAP applies filters in the wavenumber or Fourier domain. To do this requires a number of steps, each the responsibility of a separate program in the MAGMAP system. Pre-processing steps involve the preparation of the original space domain grid for filtering and its transform to the wavenumber domain. The filter application step applies the desired filter(s) to the wavenumber grid. Post-processing steps involves returning (inverse fast fourier transform, IFFT) the filtered wavenumber data to the same size and shape as the original space domain grid.

MAGMAP's reduce to the magnetic pole filter, REDP, was applied to the *unsmoothed* total intensity aeromagnetic data for western Botswana as described above. This filter, expressed in the wavenumber domain, has the form:

$$L(\theta) = \frac{1}{[\sin(I_a) - i\cos(I)\cos(D + \theta)]^2}, \; \textit{if } (I_a < I), \; I_a = I$$

where I is the geomagnetic inclination, I_a is the inclination for amplitude correction (never less than I) and D is the geomagnetic declination. For the western Botswana dataset, $I = I_a = -60°$ and $D = 345°$. These reduced to the pole data were also smoothed via three (3) passes of the 9-point Hanning filter prior to display and are presented in Figure 4.11(b).

4.3.1 Correlations with Deep Seismic Data

As is evident from Figures 4.10 and 4.11(b), both the gravity and aeromagnetic data show a series of wide, SW-NE trending anomalies west of the Kalahari Line. These anomalies have wavelengths on the order of 50 km or more and have been appropriately labelled for further discussion. Complementing these map data, the gravity (dashed line) and aeromagnetic (solid line; reduced to the pole) profiles along each of the deep seismic reflection lines are also displayed in Figures 4.3 to 4.9 at the top of the presented sections. The gravity and aeromagnetic profiles along each of the seismic lines were extracted from their respective grids using *GEOSOFT*[®]'s GRIDPROF program. The possible correlation of the major gravity and magnetic anomalies of the Nosop Basin with the various reflectors described from the deep seismic profiles are now discussed in a qualitative manner on anomaly by anomaly basis. The focus of this discussion will be directed towards the nature of the crustal material which may constitute the reflective zones.

4.3.1.1 Anomalies -GA1 and -MA1

The negative[1] gravity anomaly -GA1 and negative aeromagnetic anomaly -MA1 both coincide with the intersection of reflection profiles 93 and 94. Although these anomalies have a large areal extent, their peak intensities occur approximately between stations 1473 - 2285 and stations 695 - 1487 on lines 93 and 94 respectively. Referring to Figures 4.6

---

[1] The term "negative" is used here in a relative fashion as all the gravity data lies in the negative mgal range.

and 4.5 which display reflection profiles 93 and 94, there appears to be no structural relief within the basin itself which might account for these anomalies. It would seem then that the source responsible for these anomalies would be situated at the sub-basin level.

A plausible choice for this deeper source is the mid-crustal C reflector. The lateral extent of this event(s), indicated by the thickened lengths on these two reflection profiles of Figures 4.10 and 4.11(b), shows good correspondence with the gravity and aeromagnetic anomalies. Thus if the C reflective package is the causative body for these potential field anomalies, then it is likely that, at least in this portion of the basin, it is composed of deeper and older, probably Proterozoic sediments. This idea would also be supported by the considerable structure exhibited by the internal reflectors of the mid-crustal C reflective package indicating further sedimentary layering beneath the basin.

4.3.1.2   Makgadikgadi Line (M-M') and Anomalies +MA3 -MA2

The expression of the Makgadikgadi Line is clearly visible on the aeromagnetic data of Figure 4.11(b) and is indicated by the thick solid line labelled M-M'. Defined by the sharp gradient separating the +MA3 and -MA2 anomalies, this magnetic lineament bisects the Nosop Basin in a SW-NE direction. The +MA3 aeromagnetic anomaly, which also follows the dominant SW-NE regional aeromagnetic trend, consists of two strong peaks at its SW and NE ends separated by an intervening saddle.

The Makgadikgadi Line and the +MA3 anomaly are the same features which Reeves (1978) and Hutchins and Reeves (1980) interpreted as a possible structural high which

separated two distinct basins, the Nosop and Ncojane. However, its is clear from the observation of the deep seismic data for lines 93 and 99 presented in Figures 4.6 and 4.7, there is no evidence for the existence of this structural high. There is only one basin of a fairly uniform depth and this observation was originally made by Hall *et al.* (1990) and Wright and Hall (1990).

It would appear then, that the aeromagnetic anomaly patterns may be due to lateral magnetisation contrasts at the mid to lower crustal level. Again referring to the deep seismic data for lines 93 and 99 (see Figures 4.6 and 4.7), line 93 crosses the easterly flank of the NE peak of the +MA3 anomaly between stations 3354 - 3651 while line 99 crosses the same NE peak between stations 2111 - 2804. These locations on profiles 93 and 99 coincide with both the termination of mid-crustal C reflector(s) and the southerly dipping B1 reflective packages indicated on these two profiles. In addition, line 99 at this location also shows the onset of southerly dips of the D reflector(s) and its subsequent termination and, farther to the SSE, the B reflector exhibits a significant downwarp ($\geq$ 1 km) at station 2705. The termination of the C and D reflectors, the onset of southerly dips and the downwarp of the B reflector are all suggestive of crustal scale normal faulting which may have produced a mid to lower crustal "edge". Thus the Makgadikgadi Line, which marks the sharp change between the +MA3 anomaly and its -MA2 complement, may represent the magnetic response to this crustal "edge" or discontinuity.

To test this "edge effect" hypothesis, a least squares inversion was performed using the total field aeromagnetic data extracted along a portion of line 93 (again using

GEOSOFT*'s GRIDPROF program) and beyond following the strike direction of this seismic profile. This inversion was accomplished using the United States Geological Survey's (USGS) potential field modelling software package SAKI and the results are presented in Figure 4.12. A simple prism was used as a starting model with lateral extents (expressed in terms of profile distance) of 5 to 120 km, depth extents of 20 to 30 km and a magnetic susceptibility contrast of $\approx 1.2 \times 10^{-2}$ cgs units. During the inversion process, the vertices defining the causative body (in terms of profile distance and depth) were allowed to vary repeatedly while the magnetization direction remained fixed (i.e. considered induced magnetisation only) until a least squares solution was obtained.

As is evident from Figure 4.12, the depth extents ($\approx 15 - 25$ km) of the causative body generated from the inversion of the total field aeromagnetic data corresponds very well with the mid-crustal C reflective package of line 93. More importantly, however, is that the southern edge of this body matches well with the termination of the C reflective package. Thus the results from the modelling and inversion of the aeromagnetic data would appear to support the existence of a mid-crustal "edge" or discontinuity within this region of the Nosop Basin.

As is apparent from Figure 4.11(b), line 92 tracks just north of the trough of the -MA2 anomaly which, like its +MA3 complement, consists of two strong negative peaks at its SW and NE ends separated by an intervening saddle. Also of note, the +GA2 anomaly of Figure 4.10 appears to be coincident with the Makgadikgadi Line and separates the more negative anomalies (-127 to -148 mgal) in the NNW portion of the
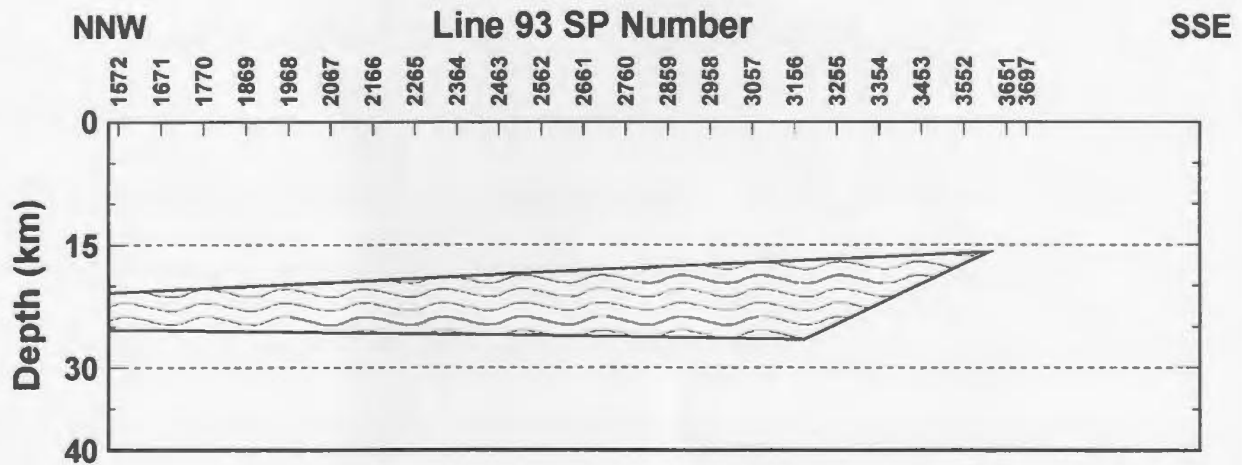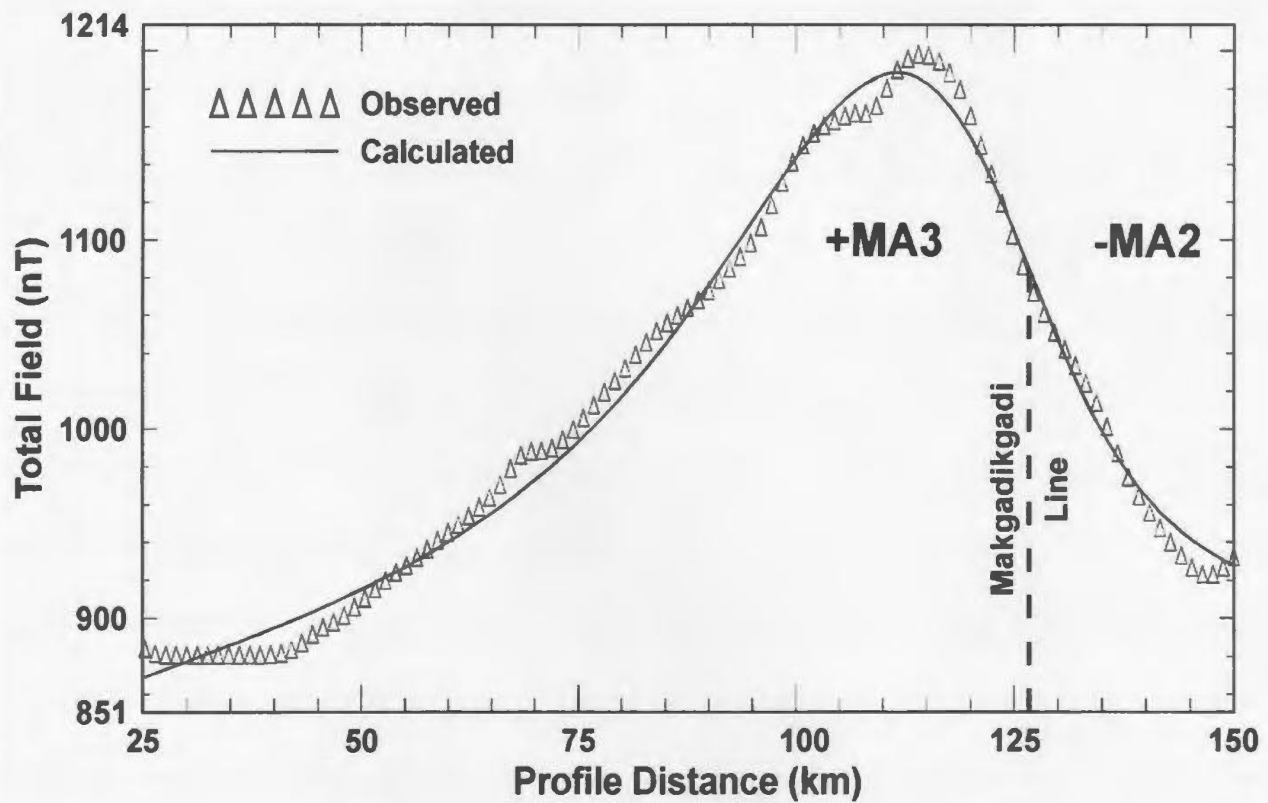
Figure 4.12 Results of least squares inversion of the total field aeromagnetic data extracted along a portion of reflection seismic Line 93.

basin from the less negative anomalies (-95 to -125 mgal) in the SSE. The portion of seismic profiles 92 and 99 which encompass the -MA2 and +GA2 anomalies (stations 2180 - 2972 and stations 2804 - 3101 on 92 and 99 respectively) show little or no pronounced reflectivity in the mid to lower crust. This lack of reflectivity may lend further support to the existence of the mid-crustal structural discontinuity that was introduced in the previous section.

The mid to lower crustal C and D reflective packages so clearly imaged on lines 93, 94 and 99 terminate abruptly at the Makgadikgadi Line (and the +GA2 anomaly) and farther to the south, reflectivity in the mid to lower crust, as indicated by line 92 (Figure 4.4) is generally lacking. Thus the normal faulting which produced this proposed structural discontinuity may have juxtaposed crustal material of notably different reflective character in this region of the Nosop Basin. Although not specifically modelled, the +GA2 anomaly may also represent the gravity response to this crustal edge.

The NE peak of the -MA2 anomaly coincides with the intersection of seismic profiles 91 and 92. This peak is somewhat more negative and has a broader extent than its than its SW complement and shows reasonable correlation with the B1 package on both lines 91 and 92 (Figures 4.8 and 4.4). The lateral extent of the B1 reflectors is indicated by the thickened lengths on these two reflection profiles of Figures 4.10 and 4.11(b). The internal reflectors of the B1 reflective package of line 91, as previously stated, show considerable dips to the N and exhibit a layered character and would again suggest a possible sedimentary origin for the B1 package.

In addition to this, the B1 reflectors of line 93 (stations 3354 - 3552; Figure 4.6) possess opposing southerly dips to the B1 package of line 91. These opposing dips may also give support to the existence of crustal scale normal faulting on the extreme SSE ends of lines 93 and 99. To illustrate this, Figure 4.13 presents a composite of the interpreted depth migrations for lines 93 and 91 joined at their respective cross-overs. As is evident from Figure 4.13, the structural style exhibited by the B1 reflectors of lines 91 and 93 is very reminiscent of a large graben. Thus the intervening area between and below these dipping reflectors may be a down faulted crustal block with the B1 reflectors themselves representing sediment infill into this wide depression.

In summary, the causes of the gravity and magnetic anomalies of the Nosop Basin, west of the Kalahari Line, are most likely attributed to deep sources located beneath the B reflector. The correlation of the deep seismic information with the potential field data re-confirmed that there are not two distinct basins separated by a basement high but rather one broad basin of fairly uniform depth which is referred to as the Nosop Basin. The B1 and C reflectors, because of their considerable internal structure as indicated by the seismics, are interpreted as sedimentary or volcano-sedimentary packages. The Makgadikgadi Line, as defined by the sharp gradient between the +MA3 and -MA2 anomalies, is interpreted as the magnetic response to a mid-crustal "edge" or discontinuity formed by crustal scale normal faulting. This idea is supported by modelling and inversion of the aeromagnetic data as well as the reflection seismic data itself.
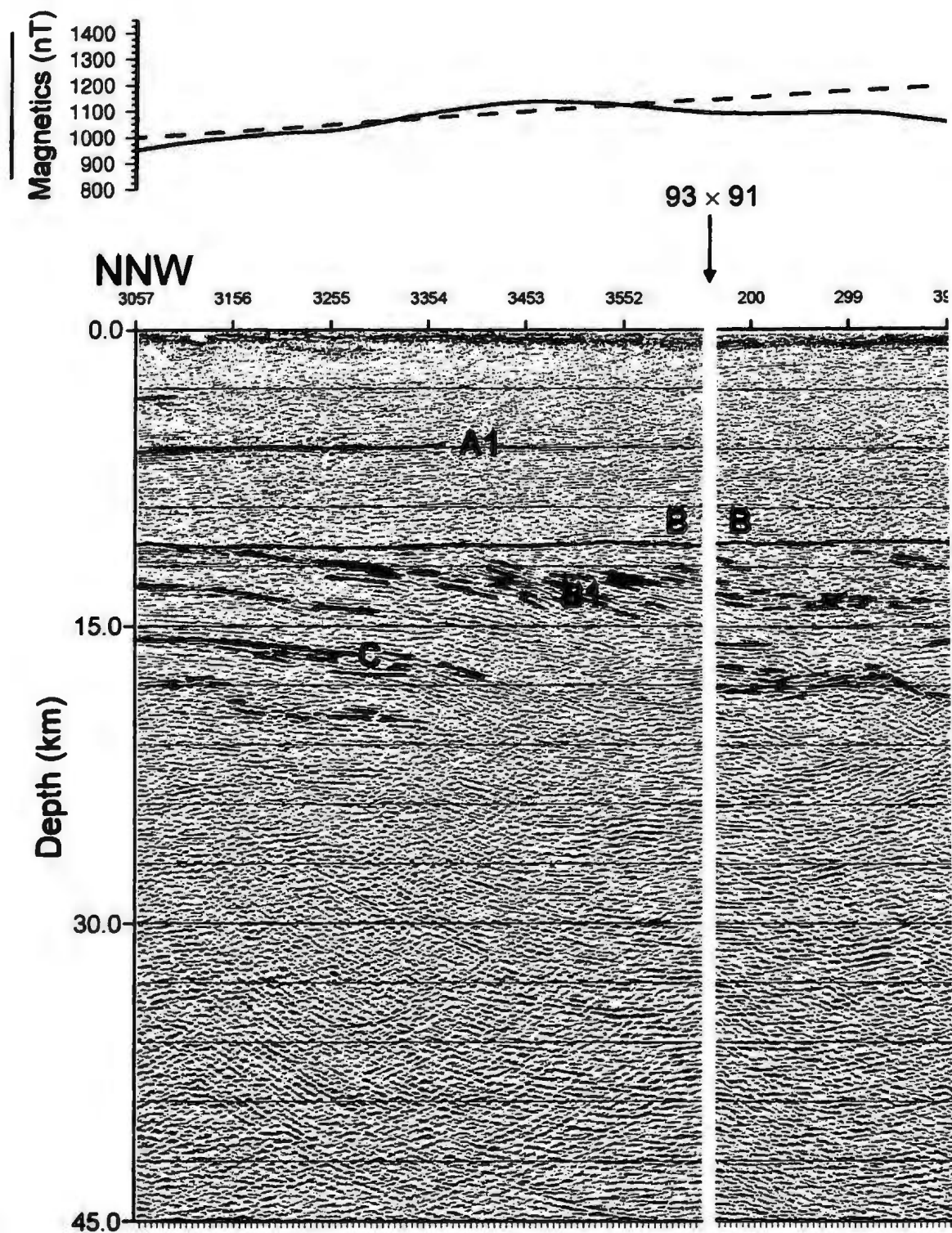
Figure 4.13 Composite of the interpreted depth migrations for Lines 91 and 93.

Gravity (mgal)

-90
-100
-110
-120
-130
-140
-150

93 × 91

92

S

200   299   398   497   596   695   794   893   992   1091

0.0

A1

A2

B   B

B   B2

15.0

C

D

30.0

M?

45.0

Depth (km)

91 and 93.

Interpretation/126
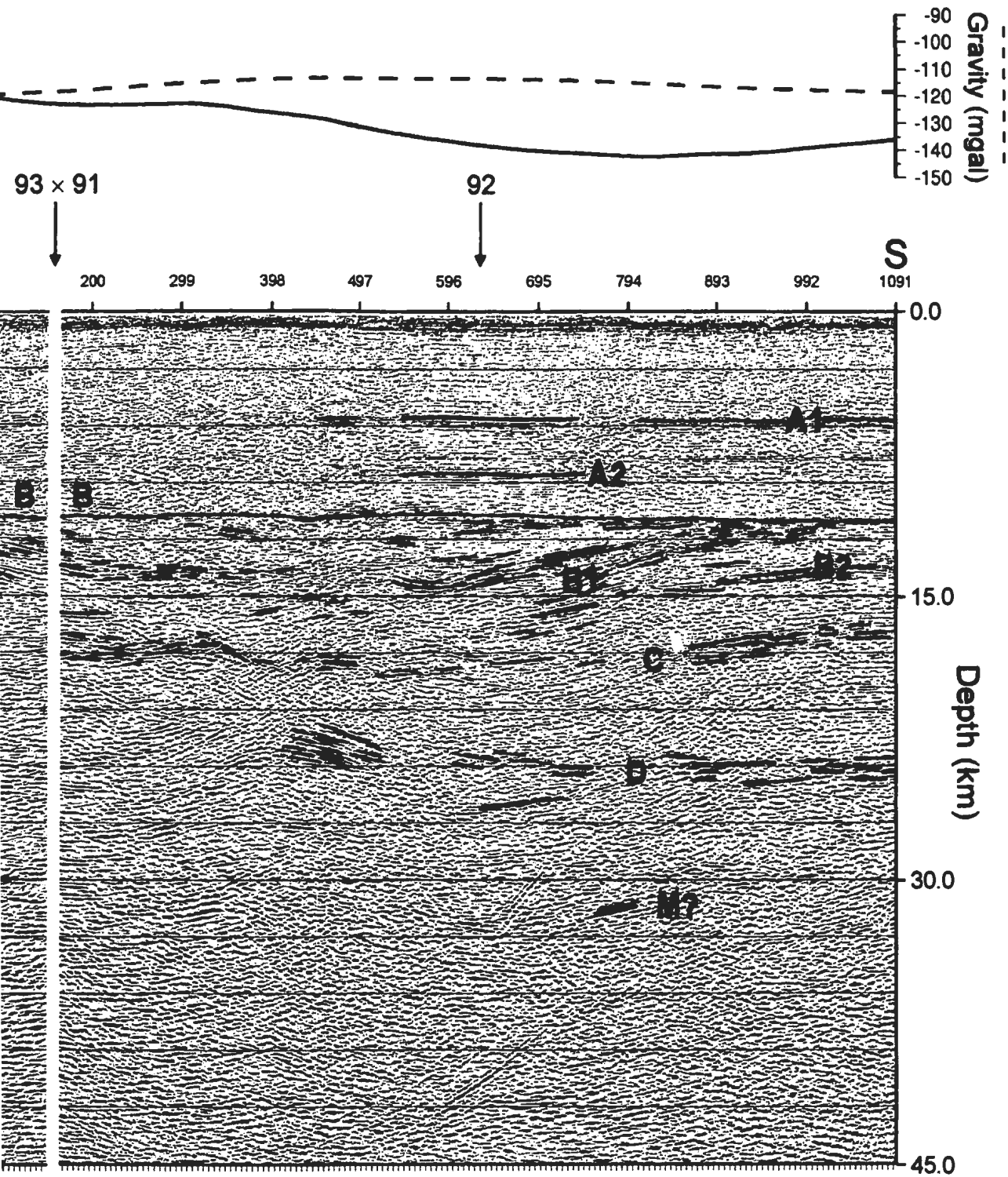
4.4   Discussion

With the seismic reflection profiles adequately described and some of the more prominent reflecting events suitably correlated with the potential field anomalies, it is important to review as to what this information can reveal about the geologic and tectonic history of this area. To do this, the Kalahari Line, the Nosop Basin and the Ghanzi-Chobe fold belt are now discussed individually in light of the seismic data as well as other geophysical and geological information as a means of providing an understanding about the role these three major tectonic elements may have played in the geological evolution of western Botswana.

4.4.1   The Kalahari Line

As has been stated, the Kalahari Line is a major tectonic element of western Botswana. This feature has great lateral extent ($\approx$ 600 km) and is defined geophysically by strong, positive magnetic and gravity anomalies along its length. Drilling has shown these to be caused by shallow ($\leq$ 1 km) mafic bodies such as basalts, gabbros and dolerites. Some of the mafic bodies responsible for producing these strong potential field anomalies have been described in Chapter 2, and the location of the boreholes CKP-8C-1 and CKP-8A which penetrated these causative rocks are shown on both Figures 4.10 and 4.11.

A core sample of the Tshane Complex gabbro recovered from borehole CKP-8C-1 was obtained by Memorial University and hornblendes extracted from this sample have

Table 4.1 ^{40}Ar - ^{39}Ar release data for hornblende extracted from Tshane Complex gabbro recovered from borehole CKP-8C-1, western Botswana.

Temp °C	$\frac{^{40}Ar}{^{39}Ar}$	$\frac{^{37}Ar}{^{39}Ar}$	$\frac{^{36}Ar}{^{39}Ar}$	Moles ^{39}Ar (10^{-12})	^{39}Ar %Total	%^{40}Ar Rad	K/Ca	Age (Ma)
720	95.13	3.412	0.0970	127.8	13.0	70.2	0.143	668.9 ± 6.0
870	113.48	10.477	0.0407	247.6	25.2	90.2	0.046	948.4 ± 8.8
980	117.12	12.792	0.0279	236.8	24.1	93.9	0.038	1003.9 ± 9.2
1020	123.35	16.157	0.0189	86.5	8.8	96.6	0.030	1069.1 ± 9.2
1060	121.80	17.080	0.0146	98.5	10.0	97.7	0.028	1068.3 ± 14.9
1080	122.45	17.469	0.0160	65.2	6.6	97.4	0.028	1070.2 ± 9.1
1130	123.81	18.069	0.0190	57.2	5.8	96.7	0.027	1074.2 ± 8.5
1170	125.06	18.616	0.0241	34.6	3.5	95.6	0.026	1073.2 ± 8.8
1210	129.09	18.393	0.0366	18.6	1.9	92.9	0.026	1075.2 ± 13.1
FUSE	133.44	16.723	0.0810	9.3	0.9	83.2	0.029	1013.0 ± 19.9
TOTAL GAS AGE				982.1	100.0			970.9 ± 9.4
PLATEAU AGE								**1071.7 ± 11.1**

been radiometrically dated by Dr. Daniel Lux of the University of Maine at Orono using the ^{40}Ar - ^{39}Ar technique. The results of his analysis are shown in Table 4.1. Although the data are somewhat discordant, the large jumps in the young ages occurring in the early

temperature increments are associated with a release phase that has a relatively high K/Ca ratio. This is most likely attributed to a biotite impurity that was not removed during the mineral separation procedure (Lux, pers. comm.). Increments 1020°C through 1210°C have consistent ages and consistent K/Ca ratios that are reasonable for hornblende. These increments were used to calculate the plateau age, 1071.0 ± 11.1 Ma, and is probably most representative of the time the gabbro cooled through the closure temperature for hornblende, about 500°C. Although this represents only a single date, the 1,071.7 ± 11.1 Ma plateau age for this gabbro is significant if one considers the position of the Kalahari craton with respect to Laurentia in Hoffman's (1991) proposed late Proterozoic supercontinent of Figure 2.4 presented in Chapter 2.

The continental area encompassing the present day Great Lakes (located on the south central portion of Laurentia, the "proto" North American craton) displays some of the largest potential field anomalies in the interior of the North American continent. These anomalies are associated with the Mid-continent rift system (MRS) which extends along a 2300 km arc northeastward from central Kansas through Lake Superior and southward through Michigan, perhaps into Ohio (Green, 1983). This continental rift system is 1,110 to 1,090 Ma in age (Keweenawan) and marine seismic reflection data from Lake Superior reveal an extraordinary thickness of mafic lavas and sedimentary rocks deposited in a number of discrete mega-grabens/half-grabens (Green *et al.*, 1989). Total vertical thickness of layered Keweenawan strata exceeds 30 km beneath some parts of Lake Superior which may make it the thickest section of continental rift deposits on the planet

(Behrendt *et al.*, 1988). Although this rift was abortive, it represents a major and widespread period of Keweenawan continental extension and subsidence which was accompanied by extrusion of voluminous flood basalts, deposition of minor interflow sediments and intrusion of major igneous bodies including the huge Duluth layered complex (Green *et al.*, 1989). Given its position near the south central margin of the proto-Laurentia continent, it is postulated that Mid-continent rift system (MRS) represents a preserved portion of a precursory 1,110 - 1,090 Ma widespread continental rifting event that may have affected some of the constituent cratons (i.e. Kalahari and Congo cratons) of Hoffman's (1991) proposed supercontinent which bordered Laurentia to the west. Although the breakout of Laurentia probably did not occur until 550 - 500 Ma, this proposed Middle Proterozoic rifting event may represent a gross crustal re-organization of the constituent cratons comprising the late Proterozoic supercontinent prior to the breakout of Laurentia. Thus the 1,071 Ma mafic volcanism associated with the Kalahari Line of western Botswana may be the manifestation of the same rifting event preserved on the Kalahari craton.

Estimates of the thickness of igneous rocks present along the Kalahari Line can be obtained by examining the results of forward modelling of the aeromagnetic data (Zhou, 1988). In order to define the subsurface geometry of the causative bodies, he quantitatively modelled a total of 46 magnetic profiles which cross the Kalahari Line spaced along its entirety from about latitude 23° 30'S to 26° 30'S. Results from the forward modelling of these profiles show that the bodies giving rise to the large positive

magnetic anomalies have a wide variety of geometric shapes and magnetic susceptibilities. Along the southern part of the Kalahari Line between latitudes 25° 00'S and 26° 16'S, the bodies are generally dipping at very low angles to the west. Moving north of latitude 25°S the bodies are much steeper. The widths of these bodies vary from 10 to 40 kilometres with depths-to-top ranging from 1 to 6 kilometres. More importantly, the thicknesses of these bodies vary from 6 to 27 kilometres. It seems evident from the magnetic modelling of the Kalahari Line that the causative bodies producing this feature have considerable depth extent. This represents a significant addition of mafic material to the crust by either extrusive or intrusive igneous activity associated with a continental rifting event of the same scale as that of the Mid-continent rift system.

The presence of major thicknesses of mafic volcanics along the Kalahari Line, and possibly in the Nosop Basin itself, may also be supported by the deep seismic reflection data. Referring to Figure 4.3, the interpreted section for line 90 which crosses the Kalahari Line in a sub-perpendicular orientation, the chaotic nature of the reflectivity seen beneath borehole CKP-8C-1 on the northeastern end of this profile may be an expression of the emplacement of mafic material to mid and upper crustal levels. Also the mid to lower crustal "K" and "F" reflectors of lines 94, 92 and 90 (Figures 4.5, 4.4, and 4.3 respectively) exhibit a layered character nearer the Kalahari Line and, indeed, within the central portion of the basin itself, which may indicate the presence of interbedded mafic lavas and sediments and/or mafic sills which may have been sourced from the Kalahari Line.

In addition to the drilling results, potential field modelling and the pattern of reflectivity, another seismic indicator which provides more evidence of a late middle Proterozoic rifting event affecting the south African sub-continent is the presence of crustal-scale extensional faults. Again referring to lines 90, 92 and 94 of Figures 4.3, 4.4 and 4.5, all three of these profiles were interpreted with crustal faults and/or shear zones, labelled F, at various crustal levels which appear to be listric in shape. Affiliated with these through-going crustal faults are the complementary dipping event(s), labelled "M", which may represent an interrelated shear zone at the base of the crust. As previously stated, the form of these two events, along with the thickening of the basin to the southwest, suggests that the crust beneath a majority of the Nosop Basin may be extended or stretched Kaapvaal craton. If this is so, then it may contradict Hartnady *et al.* (1985)'s nomenclature of the tectonic provinces and Subprovinces of southern Africa, at least in Botswana, that is presented in Figure 2.1 of Chapter 2. This figure shows elements of the larger Kalahari Province, particularly the Rehoboth Subprovince which is somewhat enigmatic in itself, extending west of the Kalahari Line. However, a majority of the "basement" flooring the Nosop Basin may be thinned or attenuated continental crust of the Kaapvaal craton thus throwing the extent of the Rehoboth Subprovince into question.

In summarizing, the Kalahari Line is a major geophysical lineament of western Botswana and drilling has shown that the causative rocks responsible for producing the strong positive gravity and magnetic anomalies associated with it are products of rift-related mafic volcanism. The ^{40}Ar - ^{39}Ar radiometric date of 1071.0 ± 11.1 Ma yielded

from a Kalahari Line gabbro and the juxtaposition of the Kalahari and Laurentia cratons of Hoffman's proposed Proterozoic supercontinent suggest that the North American 1,110 - 1,090 Ma (Keweenawan) Mid-continent rift system and the Kalahari rift proposed here both represent preserved portions of a precursory and widespread late Middle Proterozoic continental rifting event that may have marked the initiation of the breakout of Laurentia from this Proterozoic supercontinent. Forward modelling of the magnetic data demonstrates that considerable thicknesses (6 - 27 km) of mafic material could account for the anomaly pattern(s) exhibited by the Kalahari Line and may represent the addition of significant volumes of intrusive/extrusive mafic volcanics to the continental crust associated with a rifting episode. This idea is also supported by the pattern of reflectivity exhibited by the deep seismic reflection data at or near the Kalahari Line which also shows signs of crustal-scale extensional faulting. These extensional faults along with complementary dipping events at the base of the crust provide further proof that the continental crust of western Botswana witnessed a period of crustal extension during the late Middle Proterozoic.

4.4.2 The Nosop Basin

The Nosop Basin is situated directly west of the Kalahari Line and encompasses a vast area (> 10^4 km^2) of Botswana's western Kalahari region. As previously stated, the basin appears to be uniform in depth with total sediment thicknesses reaching 12 to 15 km and may be even deeper if the reflectors below the B event are considered to be of

sedimentary or volcano-sedimentary origin. The overall form of the Nosop Basin's stratigraphy, as defined by the structure (or its absence) exhibited by the more prominent reflective packages imaged on the seismic profiles, gives it a similar appearance, on a much larger scale, to depositional sequences of younger basins formed on modern rifted continental margins such as the Mesozoic extensional basins of offshore eastern Canada. This is **not** to suggest that the Kalahari region witnessed the development of an "Atlantic-type" rifted, passive margin and full development of oceanic crust but is introduced to demonstrate how seismic sequence stratigraphy, so often used to understand a basin's extensional history, may be applied to the Nosop Basin, at least on a gross scale, to gain similar insights.

The continental margin off eastern Canada is regarded is an "Atlantic-type" margin, where a prism of sediments accumulated in the Mesozoic and Cenozoic as the early ocean widened and deepened. Around Newfoundland the continental margin experienced two episodes of seafloor spreading, and, as such, the region has a complex geological history which is reflected in the regional physiography and changing trends in basement structure (Grant and McAlpine, 1990). Two distinct episodes of rifting are recorded in the extensional basins of the Grand Banks of Newfoundland's offshore region. The northeast-southwest trending basins began to develop during the Late Triassic to Early Jurassic by rifting between North America and Africa. Updoming on the Grand Banks in the latest Jurassic initiated a second period of rifting that culminated in separation of Iberia from the Grand Banks in the late Early Cretaceous.

In the Jeanne d'Arc Basin, probably the most studied of all Grand Banks basins due to its hydrocarbon potential, four major erosional events separate the Mesozoic - Cenozoic stratigraphic record into six depositional sequences (Grant and McAlpine, 1990). These stratigraphic sequences and the erosional events that separate them can be directly related to the geological history of the Newfoundland continental margin and record the initial rift and subsequent drift which occurred between North America and Africa. By analogy, it may be possible to infer something about the geological history of western Botswana by examining the stratigraphy of the Nosop Basin.

Although it would be very difficult to define the stratigraphy of the Nosop Basin in the same detailed way as has been done for the Jeanne d'Arc Basin (Grant and McAlpine, 1990), it may be possible to roughly divide the Nosop's stratigraphy into two depositional megasequences which are illustrated in Figure 4.14. This figure presents an idealized SW-NE geological cross-section of the Nosop Basin based on the structural and stratigraphic styles imaged on line 94. The B reflector, which can be traced with some confidence over a majority of the profiles, appears to divide the basin's sedimentary fill into two distinctive packages based on their internal reflectivity. The pattern of reflectivity which exists below B exhibits considerable structure and coherency and is thought to represent a suite of sedimentary or volcano-sedimentary rocks deposited in a continental rift setting. Above B, the pattern of reflectivity is horizontal to sub-horizontal with a minimum of structure and is consistent with a layer-cake stratigraphy indicative of a period of thermal subsidence which ensued after the major episode of crustal extension had ended. An
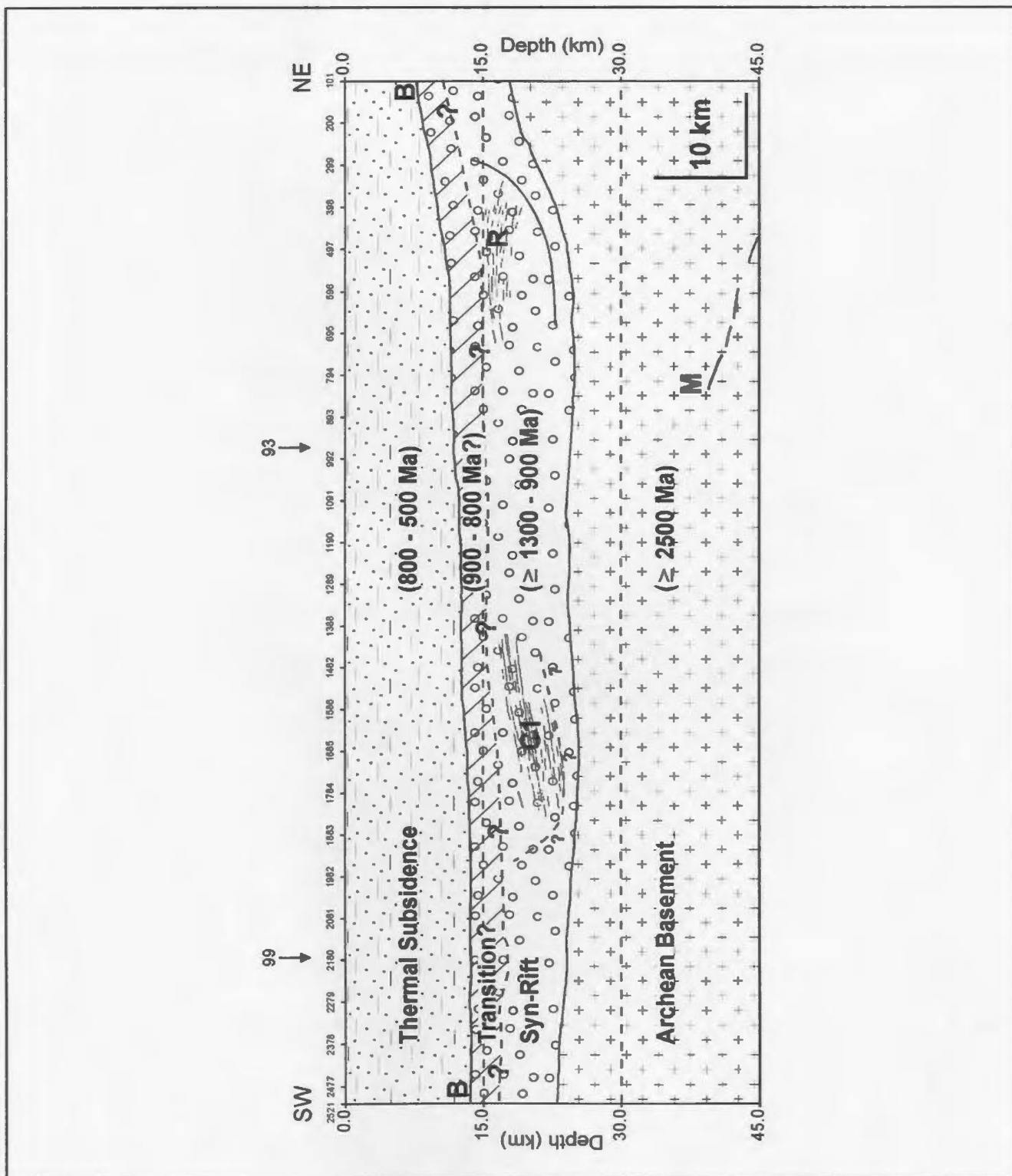
Figure 4.14 Idealized seismo-geological cross-section of Line 94 illustrating the syn-rift and thermal subsidence depositional megasequences proposed for the Nosop Basin.

intermediate depositional sequence separating the syn-rift and thermal subsidence phases is also proposed which would mark the transition from active rifting to thermal relaxation. The existence of this transitory sequence is very loosely based on the presence of horizontal to sub-horizontal reflectors which lie directly below the B reflector and, like the transition sequences of the Jeanne d'Arc Basin, may represent deposition in a rapidly changing tectonic setting and record the rifted of continental crust.

As indicated on Figure 4.14, the presence of the C1 and R reflective packages of line 94 probably provides the strongest seismic evidence in support of a proposed syn-rift sequence. These reflective packages, as previously discussed, exhibit good coherency, significant structure and, more importantly, gentle to moderate dips that may be associated with extensional faulting. The location of these extensional faults, which are interpreted to be listric, are indicated on Figure 4.14 and terminate the C1 and R reflectors to the SW and NE respectively. The geometry of these faults along with the dipping reflectors they bound yields a form reminiscent of large half-grabens. These extensional features are in many cases associated with rifted margins (and indeed aborted rifts in the case of the MRS) and develop early in the rift's history (i.e syn-rift) in response to the onset of crustal extension. In addition to C1 and R reflective sequences of line 94, the B1 reflective package of lines 91 and 93 (Figure 4.13) is also of similar form and may provide further evidence in support of the proposed syn-rift sequence. Thus the sub-B dipping reflective sequences of these three individual profiles may be representative of a thick accumulation of syn-rift sediments of volcano-sedimentary origin that were

deposited early in the development of the proposed late Middle Proterozoic rift which affected the Kalahari area.

If these dipping packages are indeed truly representative of an early syn-rift sequence laid down in grabens and/or half-grabens associated with restrictive, continental rift basins, then they could be linked to the evolution of other similar sequences that border the Kalahari craton to the north and west. Borg (1988) pointed to a number of late middle Proterozoic basins which are aligned along the western and northern margins of the Kalahari craton which contain thick and relatively undeformed volcano-sedimentary sequences with rocks of the previously discussed Ghanzi and Koras Groups comprising two of these major sequences. In the past, many authors have pointed out the lithological and structural similarities of these various basins in an attempt to correlate their lithostratigraphy (Borg, 1988; SACS, 1980; Watters, 1977; Toens, 1974).

Based mainly on the examination of lithostratigraphy, geochronology and regional distribution of volcano-sedimentary assemblages deposited in a number of these basins, Borg (1988) proposed the existence of a late middle Proterozoic continental rift system which developed along the margins of the Kalahari craton. He named this the Koras-Sinclair-Ghanzi (KSG) rift, the names being derived from the locales where these lithological assemblages were originally described. These basins are narrow, fault-bounded continental rift grabens which were depocentres for thick accumulations of coarse clastic continental sediments and distinctly bimodal volcanics which range in thickness from 8,000 to 15,000 metres.

He believed that these basins developed along two branches of a propagating continental rift system - the Koras to Sinclair (SE - NW) distribution forming one active arm of the rift and the Sinclair to Ghanzi (SW - NE) distribution forming the other. A distinct younging along the rift from the southern Koras end (1,300 - 1,200 Ma) to the northeastern Ghanzi end (1,050 - 900 Ma) is indicated from the radiometric ages of volcanic rocks contained within the basins. Borg (1988) interpreted this younging trend as evidence of rift propagation along an older zone of crustal weakness and suggested that the tectonic evolution of the late Proterozoic to early Palaeozoic Damara orogen followed trends established by the earlier KSG rift and was probably caused by the same continuous rifting event. The lack of any significant deformational event marking the transition from the late phase of the KSG rift (1000 - 950 Ma) to the early phase of Damara rifting (950 - 800 Ma) led Borg (1988) to postulate that the mechanism of crustal extension may have been the migration of the African plate over a stationary mantle plume.

Thus the distinct sub-B dipping reflective packages imaged on profiles 91, 93 and 94 of the Nosop Basin may represent buried basinal equivalents of the continental grabens of the Koras-Sinclair-Ghanzi rift system exposed along the northern and western margins of the Kalahari craton. If these dipping structures do have an evolutionary link to Borg's proposed late Middle Proterozoic rift system, then it would seem plausible that this extensional event was somewhat more widespread affecting the whole of the Kalahari craton (stretched Kaapvaal craton?) rather than being confined to its margins. Whatever

the case, it is important to note that, in addition to the deep seismic evidence, there also appears to be ample geological evidence in support of widespread continental rifting of the Kalahari region during the late Middle Proterozoic.

Referring back to the thermal subsidence depositional sequence of Figure 4.14, it would first appear that this sequence records an extraordinarily long history of subsidence ($\geq$ 1,000 Ma) for the Nosop Basin. However, as the drilling results of the PCIAC-GSD Masetlheng Pan-1 well has shown, the stratigraphic record, at least for the upper 4 km of the sequence (the well's $\approx$ T.D.), is by no means continuous. The stratigraphic break at 1,162 m marking the top of the Pre-Karoo strata, which was interpreted as Nama Group, is an obvious major unconformity and represents a substantial portion (Late Proterozoic - Late Carboniferous) of missing geologic time ($\approx$ 300 Ma). Although probably dominated by thermal effects, the magnitude of this unconformity would suggest that the subsidence (and uplift?) history recorded by this thick and seemingly undisturbed sequence (excluding the Ghanzi-Chobe structure) may be somewhat more complex than a simple thermal relaxation in response to rifted continental crust.

The lithological data for the Masetlheng Pan-1 well provides reasonable control on the age and thicknesses of the stratigraphy for the uppermost portion of the proposed thermal subsidence sequence. There are substantial thicknesses (> 1 km) of Karoo, Nama and what are believed to be Ghanzi rather than the originally interpreted Gariep Group rocks recorded in the well. Of course, these thicknesses may change from profile to profile but it would probably be safe to assume that these rocks would still comprise a

majority of at least the upper 4 km of stratigraphy of the thermal subsidence sequence throughout the basin. Given that Litherland (1982) estimated the thickness of the Ghanzi Group to be about 13 km from his mapping of exposures farther to the north peripheral to the basin, it is quite conceivable that a large portion of the deeper stratigraphy (4-15 km) consists solely of Ghanzi Group sediments.

To conclude, the Nosop Basin is broad and encompasses much of the vast Kalahari region of western Botswana and contains considerable thicknesses (> 15 km) of Proterozoic aged sedimentary and/or volcano-sedimentary rock. The gross form of the basin as described by the pattern of the reflectivity seen in the deep seismic reflection profiles may allow its stratigraphy to be divided into two possible depositional megasequences; an early syn-rift sequence located below the prevalent B event and a later thermal subsidence sequence located above it. The reflectivity of the syn-rift sequence is dominated by significant structure and dip and is thought to represent a suite of sedimentary and/or volcano-sedimentary rocks deposited in fault-bounded, continental rift grabens associated with a proposed late Middle Proterozoic extension which affected much of the Kalahari area. In contrast, the thermal subsidence sequence exhibits minimal structure and is indicative of a long period of thermal subsidence which followed after the major episode of extension had ended. This syn-rift sequence may represent buried equivalents of the continental rift sequences of Borg's (1988) proposed late Middle Proterozoic Koras-Sinclair-Ghanzi rift system which are exposed along the western and northern margins of the Kalahari craton. Lithological data from the PCIAC-GSD

Masetlheng Pan-1 well suggests that the uppermost stratigraphy (0-4 km) of the thermal subsidence sequence is probably comprised of rocks from the Karoo Supergroup and Nama and Ghanzi Groups. However, the hiatus of 300 Ma between Nama and Karoo Groups indicates that the Karoo is much younger and unrelated. Given the thickness of the Ghanzi Group measured in outcrop farther north, it is possible that Ghanzi Group sediments comprise a large portion of the lower stratigraphy of this thermal subsidence depositional sequence.

4.4.3 The Ghanzi-Chobe Fold Belt

The buried expression of the Ghanzi-Chobe fold belt imaged on the NNW end of line 93 (less so on line 99) is represented by an impressive fold and thrust structure whose scale is truly enormous. This fold and thrust structure is schematically depicted in Figure 4.15 which presents an idealized NNW-SSE geological cross-section of the Ghanzi-Chobe belt based on the structural and stratigraphic styles imaged on line 93. The wavelengths on these folds are on the order of 25 km and their structural relief is approximately 6 km. Associated with significant crustal shortening, the presence of these compressive structures on these two NNW-SSE trending profiles would seem to be in direct contradiction of the proposed late Middle Proterozoic extensional event set forth in the previous discussions above. However, this contradiction can be resolved if the timing of deformation of the Ghanzi-Chobe fold and thrust structures is examined.

Although exposures of the Ghanzi-Chobe fold belt originally described by Litherland
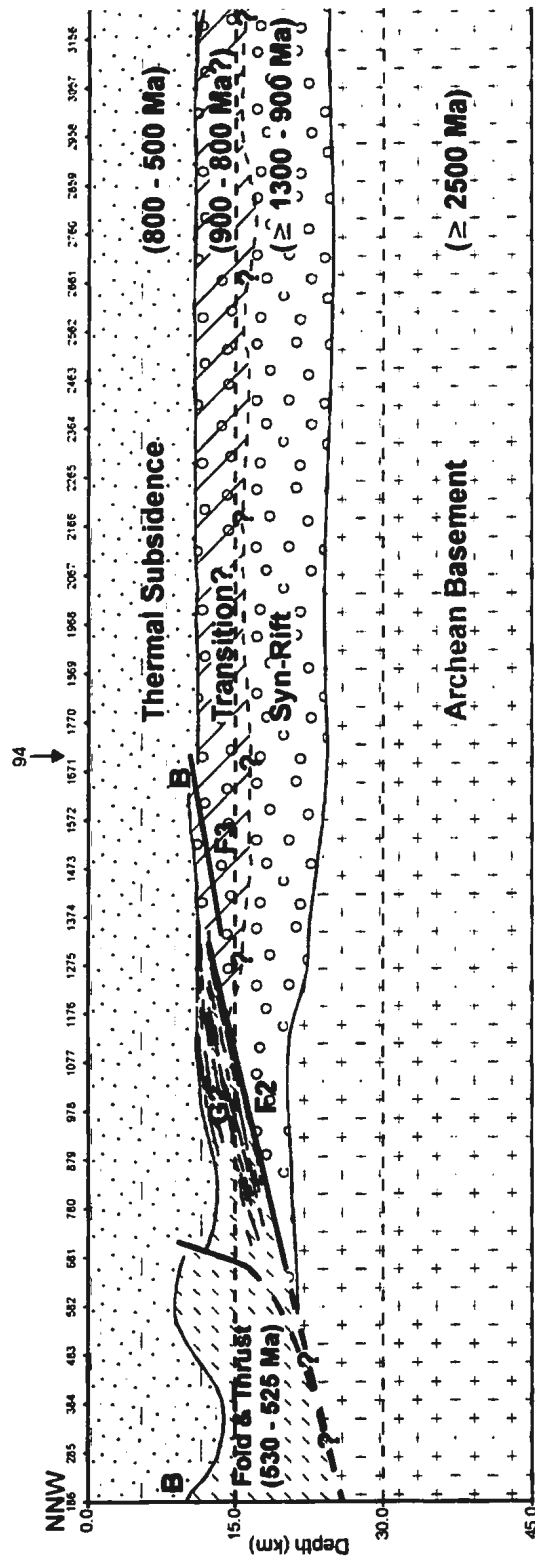
Figure 4.15 Idealized seismo-geological cross-section of Line 93 illustrating the fold and thrust structures associated with the Ghanzi-Chobe belt.

(1982) are confined to the low, narrow Ghanzi ridge of northwest Botswana, regional geophysical surveys have shown that these folded, mid-Proterozoic metasedimentary rocks occupy a 100 km wide zone which extends across much of the northwestern western region of Botswana (Reeves, 1978; Meixner and Peart, 1984). This fold belt is now generally thought to define the southeastern most part of the Damara Province with its deformation being associated with the Damara orogeny (750 - 530 Ma) which produced large open folds with SW-NE trending fold axes (Ramokate *et al.*, 1994; Aldiss and Carney, 1992; Ratsoma *et al.*, 1991; Borg, 1988).

As stated in Chapter 2, published tectonic models for the Damara orogen call for either the development of a limited ocean between the Kalahari and Congo cratons which was later subducted via an Andean-type collision or formation of an intracratonic rift or aulacogen initiated by a zone of high mantle heat flow. Lawrence (1989) proposed a possible scenario for the evolution of a basin system stretching from Namibia through Botswana to Zimbabwe including the Ncojane-Nosop Basin complex which encompasses the Nosop Basin discussed in the preceding section. In attempting to understand the development of this basin complex, Lawrence (1989) utilized the tectonic model of Kasch (1983) which presents a Wilson cycle model (partial ocean opening followed by subduction) for the evolution of the Damara orogen. Lawrence's summary of Kasch's model is presented here to provide a possible insight on the timing of deformation recorded in the Ghanzi-Chobe fold belt.

Initial convergence in the context of evolution of the Damara orogeny is marked by

the onset of subduction of the partial ocean formed by rifting during the late Middle Proterozoic northward beneath the leading edge of the Congo craton. The beginning of this subduction is believed to have occurred between 670 and 650 Ma. Full advancement to an active margin along the edge of the Congo craton is indicated by the formation of the forearc Khomas trough which included the entrainment of ophiolitic "splinters" and accretionary prism development. Collision of the Congo active margin with the passive margin of the Kalahari craton is equated with lower Nama sedimentation in an early foredeep basin of Lawrence's (1989) proposed basin complex. This is believed to have occurred at about 600 Ma. The first major orogenic cycle recorded in the Damara Province is portrayed as a "squashing" of the active margin, later to form the Khomas Subprovince, with the metamorphic - magmatic margin of the Congo craton which later formed the Swakop Subprovince.

The progressive pushing of the active margin against the passive margin heralded the start of the later orogenic cycle recorded in the rocks of the Damara Province. The telescoping of passive margin sediments along low-angle detachments onto the Kalahari foreland marked the development of the Nama foreland basin in the evolutionary scenario of Lawrence's (1989) proposed basin complex. This second orogenic cycle is characterized by considerable crustal shortening and is thought to have started around 570 Ma and culminating with the emplacement of the Naukluft Complex and late stage deformation at about 530-525 Ma.

Thus, given the location of the Ghanzi-Chobe fold belt on the southeastern most edge

of the Damaran structural front, it is likely that the late stages (530 - 525 Ma) of this second orogenic event are responsible for the fold and thrust structures seen at the NNW ends of seismic profiles 93 and 99. It is envisaged that this structural front experienced a slow, southeast migration in response to an increased compressive regime as the convergence between the Congo and Kalahari cratons progressed. Thus more and more of the passive margin sediments of the Kalahari foreland would have been caught up in the deformation associated with the steady, southeastern movement of this structural front.

It would appear then that the time of deformation of the Ghanzi-Chobe structures significantly postdates the late Middle Proterozoic rift proposed in the preceding sections for the Kalahari region (530 - 525 Ma vs. 1,090 - 1,070 Ma). However, it should be noted that line 94, oriented sub-perpendicular to lines 93 and 99, appears to intersect these two lines at the leading edge of the deformational front of the imaged fold and thrust structures at their NNW terminations. Thus it could be that some of the structure seen in the mid to lower crustal levels of line 94 may represent a tectonic overprint of the Ghanzi-Chobe deformation.

Lawrence's (1989) proposal for the development of a foreland basin would certainly have implications on the subsidence history suggested for the thermal subsidence sequence discussed in the preceding Nosop Basin section. Indeed, Hall *et al.*, (1990) also considered foreland basin development as a possible mechanism to explain the substantial subsidence recorded in the Nosop Basin. Hall *et al.* (1990) found it difficult to explain how the 150 km length of line 99 could have subsided by means of flexure associated

with the lithospheric loading by the Ghanzi-Chobe structures alone. There seemed to be no evidence that a majority of the +15 km fill has the asymmetry usually connected with foreland basin flexure. They pointed out that the B event is less than 1 km shallower at the SSE end than the NNW end and would be too little to offer a flexural explanation since it implies that, in order that the whole fill be generated this way, the flexural wavelength would have to be well over 2,000 km, and thus much longer than usually inferred for foreland basins (Beaumont, 1981). Thus, as previously stated, other mechanisms appear to be required to account for the majority of subsidence recorded in the Nosop Basin.

In concluding, the buried expression of the Ghanzi-Chobe fold belt imaged on lines 93 and 99 represent structures of large proportions. The age of deformation of the Ghanzi-Chobe fold and thrust structures is thought to be synchronous with a second, late phase orogenic cycle proposed for the Damara orogeny. This second cycle occurred at 530 - 525 Ma and was characterized by substantial crustal shortening involving the telescoping of passive margin sediments along low-angle detachments onto the Kalahari foreland. This compressive deformational event occurred much later than the late Middle Proterozoic rift proposed for the Kalahari and, as such, the co-existence of compressive and extensional structures on the seismic profiles is not paradoxical. Development of a possible foreland basin in response to lithospheric loading implied by the Ghanzi-Chobe structures cannot alone explain the considerable history of subsidence recorded by the proposed thermal subsidence sequence of the Nosop Basin discussed in the preceding section.

5 CONCLUSIONS

The processing of the seven regional deep seismic reflection profiles recorded in the Nosop Basin of western Botswana was successful in producing images of a deep sedimentary basin (12 - 15 km) underlain by highly reflective mid to lower crust. The quality of these reflection seismic images demonstrates that reconnaissance deep seismic reflection profiling can be utilized early in the investigation of frontier areas to identify a broad base of exploration targets which could be further pursued in greater detail at a later stage in the exploration. Certainly, the deeper crustal structure imaged on these profiles has provided greater insight and understanding of the regional tectonic framework in this region of the south African sub-continent.

The geological information recorded for stratigraphic test well PCIAC-GSD Masetlheng Pan-1 provides a certain degree of control on the age and thicknesses of the lithostratigraphy occupying the upper 4 km of the Nosop Basin. As indicated from the well information, this stratigraphy is represented by significant thicknesses (> 1 km) of Karoo Supergroup, Nama Group and what is believed to be Ghanzi Group rather than the Gariep Group that was originally interpreted from the well. A majority of the well's stratigraphy is late Proterozoic (Ghanzi) to early Cambrian (Nama) in age and the stratigraphic break between the rocks of the Nama Group and those of the Karoo Supergroup, which is Permian to Jurassic in age, is marked by a major unconformity which represents a considerable portion of missing geologic time ($\approx$ 200 - 300 Ma). Given the estimated thickness of the Ghanzi Group exposed farther north along the

Ghanzi ridge, it is quite conceivable that Ghanzi Group sediments comprise a large portion of the lower sediment fill of the Nosop Basin. The major formation depths reported for PCIAC-GSD Masetlheng Pan-1 well tied very well with the depths yielded from the depth migration for line 99 with the difference for all ties being less than 10%. Thus the depth information provided by these migrations is accurate, at least for the stratigraphic interval encompassing the well, and can be reliably used for interpretation purposes.

The broad gravity and magnetic anomalies west of the Kalahari Line appear to be produced by causative sources located beneath the B reflector (> 12 - 15 km) and these anomalies show good correlation with the reflecting events imaged on the seismic profiles at this crustal levels. The correlation of the deep seismic information with the potential field data re-confirmed that, contrary to previous interpretations of the aeromagnetic data alone, there are not two distinct basins separated by a basement high but rather one broad basin of fairly uniform depth which is referred to as the Nosop Basin. Because of the considerable internal seismic structure exhibited by the B1 and C reflectors, these reflective packages are interpreted as sedimentary or volcano-sedimentary packages. The Makgadikgadi Line, as defined by the sharp gradient between the +MA3 and -MA2 anomalies, is interpreted as the magnetic response to a mid-crustal "edge" or discontinuity formed by crustal scale normal faulting. This idea is supported by modelling and inversion of the aeromagnetic data as well as the reflection seismic data itself.

The Kalahari Line is a major tectonic feature of the western Botswana region. Being

defined by a series of strong, positive magnetic and gravity anomalies along its length, drilling has shown that mafic igneous rocks are primarily responsible for producing these strong potential field anomalies. Forward modelling of the magnetic data along the Kalahari Line demonstrates that the causative mafic rocks have considerable depth extent (6 - 27 km) and may represent the addition of significant volumes of mafic material to crust associated with a continental rifting event. The ^{40}Ar-^{39}Ar date of 1,071 ± 11.1 Ma yielded from one of the Kalahari Line gabbros may be significant if considered in light of the paleogeography of Hoffman's (1991) late Proterozoic supercontinent. The south central margin of Laurentia, the proto North American craton, was the site of a major continental rifting event as recorded by the extensive Mid-continent rift system (MRS) which is 1,110 - 1,090 Ma in age (Keweenawan). Given the juxtaposition of the Kalahari and Congo cratons with Laurentia and the 1,071 Ma radiometric age yielded for the Kalahari Line causative mafic rocks, it is postulated that Mid-continent rift system and the proposed Kalahari rift represent preserved portions of a widespread and precursory late Middle Proterozoic rifting event which may have marked the breakout of Laurentia from Hoffman's late Proterozoic supercontinent. This rifting idea is supported by the deep seismic reflection data, particularly the SW-NE profiles, which are orientated sub-perpendicular to the Kalahari Line, as they indicate the possible presence of complementary dipping shear zones which may be the manifestation of crustal-scale extension associated with continental rifting. The form of these complementary shear zones along with the thickening of the sedimentary basin to the SW is suggestive of a

stretched Archean Kaapvaal craton, thinned and attenuated by this proposed late Middle Proterozoic continental rifting event, extending beneath a majority of the Nosop Basin.

The Nosop Basin is a deep and expansive basin which envelops much of the Kalahari region west of the Kalahari Line and contains considerable thicknesses (> 15 km) of Proterozoic and younger sedimentary and/or volcano-sedimentary rock. By comparison to younger extensional basins of rifted continental margins, the gross form of the Nosop Basin may allow its stratigraphy to be divided into two possible depositional megasequences; an early syn-rift sequence and a later thermal subsidence sequence. Significant structure and dip characterizes the reflectivity of the syn-rift sequence and is thus thought to represent a suite of sedimentary and/or volcano-sedimentary rocks deposited in fault-bounded, continental rift grabens associated with a proposed late Middle Proterozoic extension which affected much of the Kalahari area. The thermal subsidence sequence exhibits minimal structure and is indicative of a long period of thermal relaxation which ensued after the major episode of extension had ended. This syn-rift sequence may represent buried equivalents of the continental rift sequences of Borg's (1988) proposed late Middle Proterozoic Koras-Sinclair-Ghanzi rift system which are exposed along the western and northern margins of the Kalahari craton. Borg's proposed rift system provides further geological evidence in support of a widespread late Middle Proterozoic rifting event affecting the Kalahari region.

The buried expression of the Ghanzi-Chobe fold belt imaged on the northwestern edge of the Nosop Basin represent fold and thrust structures of large scale. The age of

deformation of the Ghanzi-Chobe fold and thrust structures is thought to be synchronous with a second, late phase orogenic cycle proposed for the Damara orogeny by Kasch (1983). Characterized by substantial crustal shortening, this second cycle occurred at about 530 - 525 Ma and involved the telescoping of passive margin sediments along low-angle detachments onto the Kalahari foreland. Thus the much later timing of this compressive tectonic event with respect to the proposed late Middle Proterozoic Kalahari rift allows for the co-existence of compressive and extensional structures on the seismic profiles and, as such, is not paradoxical. The considerable history of subsidence (> 1,000 Ma) recorded for the Nosop Basin by the proposed thermal subsidence sequence cannot be explained solely by the development of a possible foreland basin in response to substantial lithospheric loading implied by the Ghanzi-Chobe structures.

REFERENCES

ALDISS, D. T. 1988. The pre-Cainozoic geology of the Okwa Valley near Tswaane borehole. *Geol. Surv. Botswana Bull.,* *34:* *50 pp.*

ALDISS, D. T. AND CARNEY, J. N. 1992. The geology and regional correlation of the Proterozoic Okwa Inlier, western Botswana. *Precamb. Res.,* *38,* *pp. 255-274.*

BALLY, A. W., SCOTESE, C. R. AND ROSS, M. L. 1989. North America; Plate-tectonic setting and tectonic elements in *The Geology of North America - An Overview (Volume A), Bally, A. W. & Palmer, A. R. (editors), Geol. Soc. Am., Boulder, CO, pp. 1-15.*

BARNES, S. J. AND SAWYER, E. W. 1980. An alternative model for the Damara mobile belt: ocean crust subduction and continental convergence. *Precamb. Res.,* *13: pp. 297-336.*

BARTON, E. S. AND BURGER, A. J. 1983. Reconnaissance isotopic investigations in the Namaqua mobile belt and implications for Proterozoic crustal evolution - Upington Geotraverse in *Namaqualand Metamorphic Complex, Botha, B. J. V. (editor). Geol. Soc. S. Afr. Spec. Publ.,* *10: pp. 45-66.*

BEAUMONT, C. 1981. Foreland basins. *Geophysical Journal of the Royal Astronomical Society,* *65: pp. 291-329.*

BEHRENDT, J. C., GREEN, A. G., CANNON, W. F., HUTCHINSON, D. R., LEE, M. W., MILKEREIT, B., AGENA, W. F. AND SPENCER, C. 1988. Crustal structure of the Mid-continent Rift System: Results from GLIMPCE deep seismic reflection profiles. *Geology,* *16,* *pp. 81-85*

BOND, G. C., NICKERSON, P. A. AND KOMINZ, M. A. 1984. Breakup of a supercontinent between 625 Ma and 555 Ma: new evidence and implications for continental histories. *Earth Planet. Sci. Lett.* *70: pp. 325-345.*

BORG, G. 1988. The Koras-Sinclair-Ghanzi rift in Southern Africa; volcanism, sedimentation, age, relationships and geophysical signature of a late middle Proterozoic rift system. *Precamb. Res.,* *38: pp. 75-90.*

BURKE, K., DEWEY, J. F. AND KIDD W. S. F. 1977. World distribution of sutures - the sites of former oceans. *Tectonophysics,* *40: pp. 69-100.*

BURGER, A. J. AND COERTZE, F. J. 1973. Radiometric age measurements on rocks from southern Africa to the end of 1971. *S. Afr. Geol. Surv. Bull., No. 58.*

CADOPPI, P., COSTA, M. AND SACCHI, R. 1987. A cross-section of the Namama thrust belt (Mozambique). *J. African Earth Sci., 6: pp. 493-508.*

CHUN, J. H. AND JACEWITZ, C. 1981. Fundamentals of frequency-domain migration. *Geophysics, 46: pp. 717-732.*

DALZIEL, I. W. D. 1991. Pacific margins of Laurentia and East Antarctica-Australia as a conjugate rift pair: Evidence and implications for an Eocambrian supercontinent. *Geology, 19: pp. 598-601.*

DIX, C. H. 1955. Seismic velocities from surface measurements. *Geophysics, Vol. 20, pp. 68-86.*

FARR, J. L., CHENEY, C. S., BARON, J. H. AND PEART, R. J. 1981. Evaluation of underground water resources. *Geol. Surv. Botswana, GS10 Project Final Report, 290 pp.*

GAZDAG, J. 1978. Wave-equation migration by phase shift. *Geophysics, 43: pp. 124-131.*

GEOSOFT INC., 1995. GEOSOFT℠ Mapping and Processing System, Toronto.

GERMS, G. J. B. 1972. The stratigraphy and palaeontology of the lower Nama Group, South West Africa. *Precamb. Res. Unit, Univ. Cape Town, Bull. 12*

GERMS, G. J. B. 1974. The Nama Group in South West Africa and its relationship to the Pan-African geosyncline. *Jour. Geol. 82: pp. 301-317*

GERMS, G. J. B. 1983. Implications of a sedimentary facies and depositional environmental analysis of the Nama Group in South West Africa/Namibia. *Spec. Publ. Geol. Soc. Afr., 11: pp. 89-114*

GRANT, A. C. AND MCALPINE, K. D. 1990. The continental margin around Newfoundland *in* Geology of the Continental Margin of Eastern Canada, Keen, M. J. and Williams,G. L. (editors); Geological Survey of Canada, Geology of Canada, No. 2, pp. 239-292.

154

GREEN, A. G., CANNON, W.F., MILKEREIT, B., HUTCHINSON, D. R., DAVIDSON, A., BEHRENDT, J. C., SPENCER, C., LEE, M. W., MOREL-À-L'HUISSIER AND AGENA, W.F. 1989. A "GLIMPCE" of the deep crust beneath the Great Lakes in *Properties and Processes of Earth's Lower Crust, Mereu, R. F., Mueller, S. and Fountain, D. M. (editors); Geophysical Monograph 51, IUGG Volume 6, pp. 65-80.*

GREEN, J. C. 1983. Geological and geochemical evidence for the nature and development of the middle Proterozoic (Keweenawan) midcontinent rift of North America. *Tectonophysics 94: pp. 413-437.*

HALL, J., WRIGHT, J. A. AND HOFFE, B. H. 1990. Deep seismic reflection profiling in frontier exploration: an example from basins in Botswana with one billion years of subsidence in *The Potential of Deep Seismic Profiling for Hydrocarbon Exploration, Pinet, B. and Bois, C. (editors), Éditions Technip, Paris, pp. 291-315.*

HALL, J., WRIGHT, J. A. AND HOFFE, B. H. 1989. The deep structure and tectonic setting of sedimentary basins in western Botswana. *Abstract of paper presented at the SEG Annual Meeting, October 29 - November 2, 1989, Dallas, Texas.*

HARTNADY, C. J. H., JOUBERT, P. AND STOWE, C. 1985. Proterozoic crustal evolution in southern Africa. *Episodes, 8: pp. 236-244.*

HATTON, L., WORTHINGTON, M. H. AND MAKIN, J. 1986. *Seismic data processing: theory and practise. Blackwell Scientific Publications, Oxford, 177 pp.*

HAWKESWORTH, C. J., KRAMERS, J. D., MILLER, R. McG. 1981. Old model Nd ages in Namibian Pan-African rocks. *Nature, 289: pp. 278-282.*

HAWKESWORTH, C. J., MENZIES, M. A. AND VAN CALSTEREN, P. 1986. Geochemical and tectonic evolution of the Damara Belt in *Collision Tectonics, Coward, M. P. & Ries, A. C. (editors), Geol. Soc. Spec. Publ., 19: pp. 305-319.*

HENRY, G., CLENDENIN, C. W., STANISTREET, I. G. AND MAIDEN, K. J. 1990. Multiple detachment model for the early rifting stage of the late Proterozoic Damara orogen in Namibia. *Geology, 18: pp. 67-71.*

HOFFMAN, K. H. 1989. New aspects of lithostratigraphic subdivision and correlation of the Late Proterozoic to Early Cambrian rocks of the southern Damaran Belt and their correlation with the central and northern Damaran Belt and the Gariep Belt. *Communs Geol. Surv. Namibia, 5: pp. 59-67.*

HOFFMAN, P. F. 1989. Precambrian geology and tectonic history of North America in *The Geology of North America - An Overview (Volume A), Bally, A. W. & Palmer, A. R. (editors). Geol. Soc. Am., Boulder, CO. pp. 447-512.*

HOFFMAN, P. F. 1991. Did the breakout of Laurentia turn Gondwanaland inside-out? *Science, 252: pp. 1409-1412.*

HUTCHINS, D. G. AND REEVES, C. V. 1980. Regional geophysical exploration of the Kalahari in Botswana. *Tectonophysics, 69: pp. 201-220.*

KASCH, K. W. 1983. Continental collision, suture progradation and thermal relaxation: a plate tectonic model for the Damara orogen in central Namibia. *Geol. Soc. S. Afr. Spec. Publ., 11: pp. 423-429.*

KAŻMIN, V. G. 1988. Tectonic development of the Mozambique zone: from accretion to collision. *Geotectonics, 22: pp. 213-233.*

KEY, R. M. AND RUNDLE, C. C. 1981. The regional significance of new isotopic ages from Precambrian windows through the "Kalahari Beds" in north-western Botswana. *Trans. Geol. Soc. S. Afr., 84: pp. 51-66.*

KRÖNER, A. 1982. Rb-Sr geochronology and tectonic evolution of the Pan-African Damara belt of Namibia, southwestern Africa. *Am. J. Sci., 282: pp. 1471-1507.*

LAWRENCE, S. R. 1989. Prospects for petroleum in late Proterozoic/early Paleozoic basins of southern-central Africa. *Journal of Petroleum Geology, Vol. 12, No. 2: pp. 231-242.*

LEVIN, M. 1981. The geology, hydrology and hydrochemistry of an area between the Kuruman and Orange rivers, northwestern Cape. *Trans. Geol. Soc. S. Afr., 84: pp. 177-190.*

LITHERLAND, M. 1982. The Geology of the Area Around Mamuno and Kalkfontein, Ghanzi District, Botswana. *Geol. Surv. Botswana Dist. Mem., 4: 145 pp.*

MARTIN, H. AND PORADA, H. 1977. The intracratonic branch of the Damara orogen in South West Africa; I. Discussion of geodynamic models. *Precamb. Res., 5: pp. 311-338.*

MEIXNER, H. M. AND PEART, R. J. 1984. The Kalahari Drilling Project: A report on the geological results of follow-up drilling to the aeromagnetic survey of Botswana. *Geol. Surv. Botswana Bull.*, *27*: *224 pp.*

MOORES, E. M. 1991. Southwest U.S. - East Antarctic (SWEAT) Connection: A Hypothesis. *Geology*, *19*: *pp. 425-428.*

PETRO-CANADA 1990. Interpretation of the results of stratigraphic well Masetlheng Pan-1 in the Nosop-Ncojane Basin of SW Botswana. *Petro-Canada International Assistance Corporation (PCIAC) & Geol. Surv. Botswana report, 129 pp.*

RAMOKATE, V., AKANYANG, P., KEY, R. M. AND CAMPBELL, C. 1994. A new lithostratigraphy for the Neoproterozoic Ghanzi Group and Kgwebe formation of western Botswana. *Abstract of paper presented at the joint meeting of IGCP Project 319: "Global Paleogeography of Late Precambrian and Early Paleozoic" and IGCP Project 376: "Laurentian - Gondwana Connections Before Pangea", 2nd Circum-Atlantic/Pacific Terrane Conference, September 25 - 30, Halifax, Nova Scotia.*

RATSOMA, W. M., PIPER, D. P. AND MODIE, B. N. 1991. The structure of the Ghanzi-Chobe belt, NW Botswana, and it relationship to deep sedimentary basins along its southeast flank. *Abstract of paper presented at Inversion Tectonics Meeting, Geol. Soc. S. Afr., December, Cape Town, South Africa.*

RENNE, P. R., ONSTOTT, T. C., D'AGRELLA-FILHO, M. S., PACCA, I. G. AND TEIXEIRA, W. 1990. $^{40}Ar/^{39}Ar$ dating of 1.0-1.1 Ga magnetizations from the São Francisco and Kalahari cratons: tectonic implications for Pan-African and Brasiliano mobile belts. *Earth Planet. Sci. Lett.*, *101*: *pp. 349-370.*

REEVES, C. V. 1978. Reconnaissance aeromagnetic survey of Botswana 1975-77: Final interpretation report. *Botswana Geological Survey Department and Canadian International Development Agency, Terra Job No. 77-20, 199 pp.*

REEVES, C. V. AND HUTCHINS, D. G. 1982. A progress report on the geophysical exploration of the Kalahari in Botswana. *Geoexploration, 20: pp. 209-244.*

REEVES, C. V. AND MISENER, J. D. 1988. New sedimentary basins in continental Africa from gravity and aeromagnetic surveying. *Abstract of paper presented at the 50th annual meeting of the European Association of Exploration Geophysicists, June 6-10, The Hague, The Netherlands.*

157

SACCHI, R., MARQUES, J., COSTA, M. AND CASATI, C. 1984. Kibaran events in the southernmost Mozambique belt. *Precamb. Res.,* *25:* *pp. 141-156.*

SMITH, R.A. 1984. The lithostratigraphy of the Karoo Supergroup in Botswana. *Geol. Surv. Botswana Bull.,* *26:* *239 pp.*

SOUTH AFRICAN COMMITTEE FOR STRATIGRAPHY (SACS). 1980. Stratigraphy of South Africa. Part 1 (Comp. L. E. Kent). Lithostratigraphy of the Republic of South Africa, South West Africa/Namibia, and the Republics of Bophuthatswana, Transkei and Venda. *Handbook Geol. Surv. S. Afr.,* *8:* *690 pp.*

STOLT, R. H. 1978. Migration by Fourier transform. *Geophysics,* *43:* *pp. 23-48*

STOWE, C. W. 1986. Synthesis and interpretation of structures along the northeastern boundary of the Namaqua Tectonic Province, South Africa. *Trans. Geol. Soc. S. Afr.,* *89:* *pp. 185-198.*

TANKARD, A. J., JACKSON, M. P. A., ERIKSON, K. A., HOBDAY, D. K., HUNTER, D. R. AND MINTER, W. E. L. 1982. *Crustal evolution of southern Africa - 3.8 billion years of earth history. Springer-Verlag, New York, 523 pp.*

TEXACO, 1989. *Starpak Processing Manual, Vols. 1, 2 & 3, Houston.*

THOMAS, C. M. 1973. South Ngamiland 1:125,000 geological map and explanation, Sheet Nos. 2022C & D, *Geol. Surv. Botswana.*

TOENS, P. D. 1974. The geology of part of the southern foreland of the Damara orogenic belt in South West Africa and Botswana. *Geol. Rdsch.,* *64:* *pp. 175-193.*

VAN NIEKERK, C. B. AND BURGER, A. J. 1978. A new age for Ventersdorp acidic lavas. *Geol. Soc. S. Afr. Trans.,* *81:* *pp. 155-163.*

WASILENKOFF, J. M. 1988. Geophysical surveys of the Nosop-Ncojane and Passarge Basins, Botswana. *Petro-Canada International Assistance Corporation (PCIAC) & Geol. Surv. Botswana report, 129 pp.*

WATTERS, B. R. 1977. The Sinclair Group: definition and regional correlation. *Trans. Geol. Soc. S. Afr.,* *80:* *pp. 9-16.*

WILLIAMS, H. AND HISCOTT, R. N. 1987. Definition of the Iapetus rift-drift transition in western Newfoundland. *Geology,* *15:* *pp. 1044-1047.*

WILSON, E. J. 1964. Core description, Vreda 281 #1 Stratigraphic Test. *Artnell Exploration Company, 36 pp.*

WRIGHT, J. A. AND HALL, J. 1990. Deep seismic profiling in the Nosop Basin, Botswana: cratons, mobile belts and sedimentary basins. *Tectonophysics, 173: pp. 333-343.*

YILMAZ, Ö, 1987. *Seismic Data Processing, Doherty, S. M. (editor), Society of Exploration Geophysicists, Tulsa, 526 pp.*

ZHOU, Y. 1988. Quantitative aeromagnetic interpretation of the Kalahari Line and the Nosop Basin in S.W. Botswana. *Unpublished M.Sc. thesis, International Institute for Aerospace Survey and Earth Sciences (ITC), Delft, The Netherlands, 67 pp.*
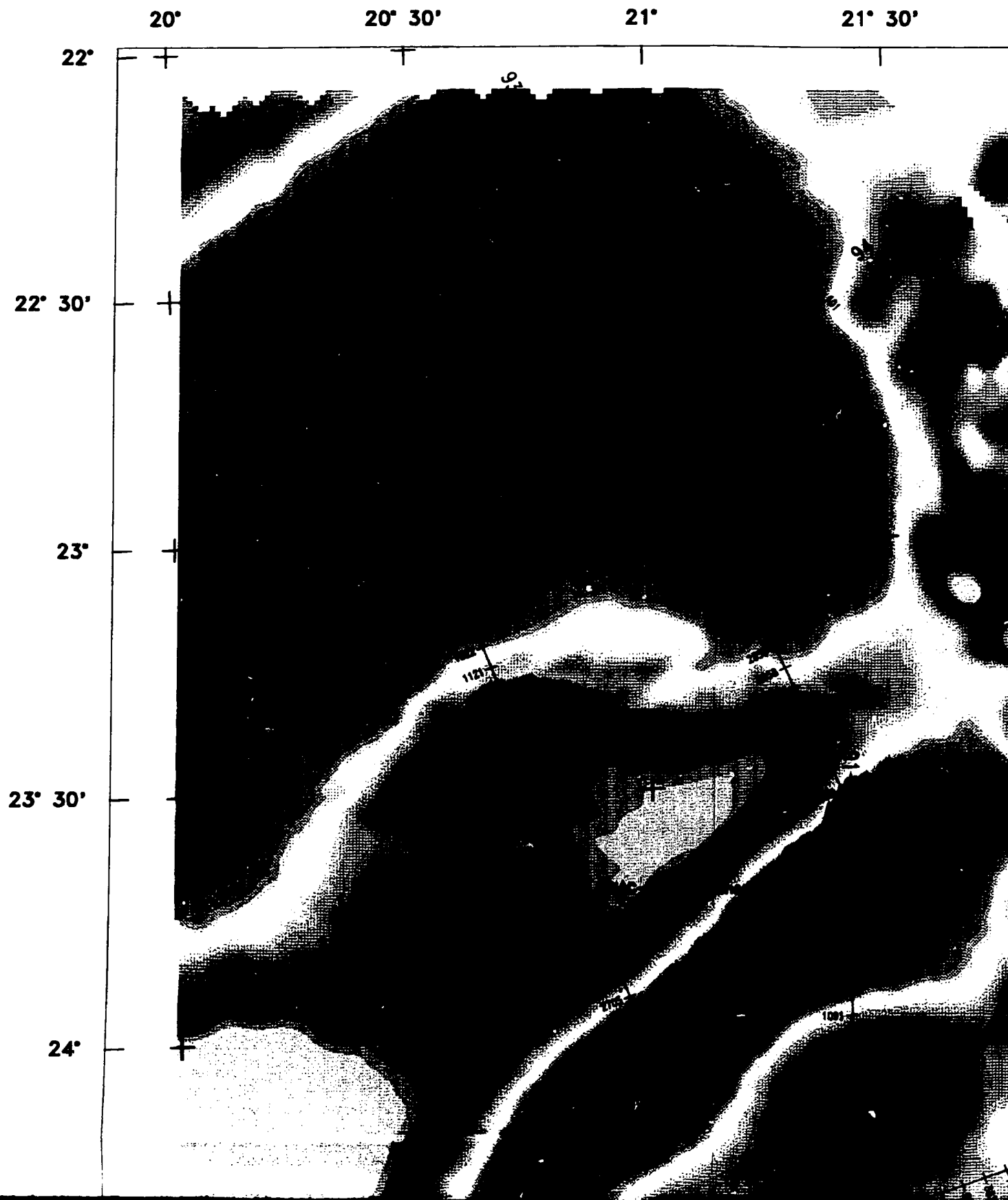
21° 30'	22°	22° 30'

22° 30'

23°

23° 30'

24°

1286
1268
1250
1235
1223
1214
1203
1194
1185
1178
1170
1162
1155
1149
1142
1135
1128
1122
1115
1109
1102
1095
1090
1083
1076
1069
1063
1055
1047
1039
1032

22° 30'

22° 30'

23°

23° 30'

24°

1286	
1268	
1250	
1235	
1223	
1214	
1203	
1194	
1185	
1178	
1170	
1162	
1155	
1149	
1142	
1135	
1128	
1122	
1115	
1109	
1102	
1095	
1090	
1083	
1076	
1069	
1063	
1055	
1047	
1039	
1032	

93

91

22°   22° 30'

22° 30'

23°

M'
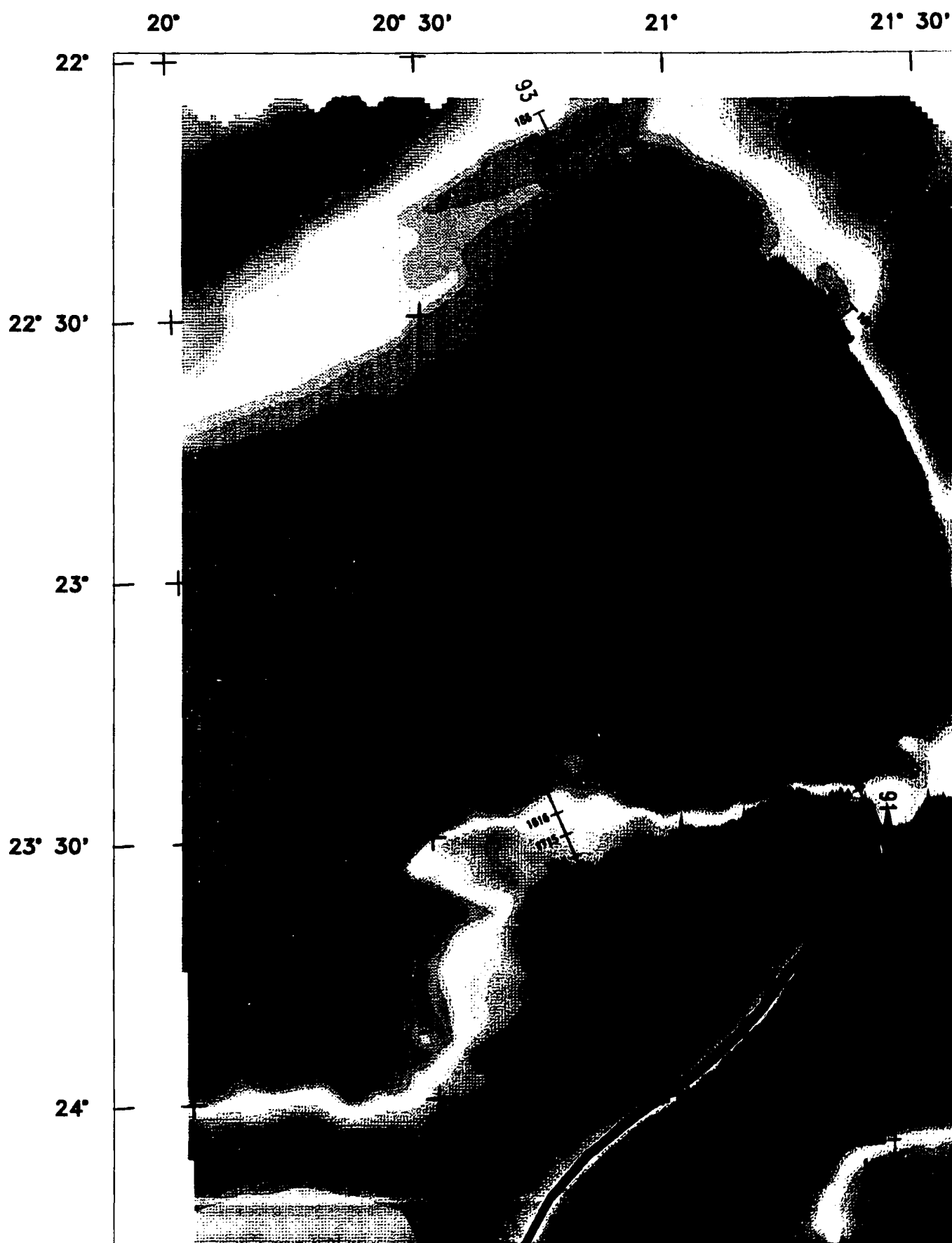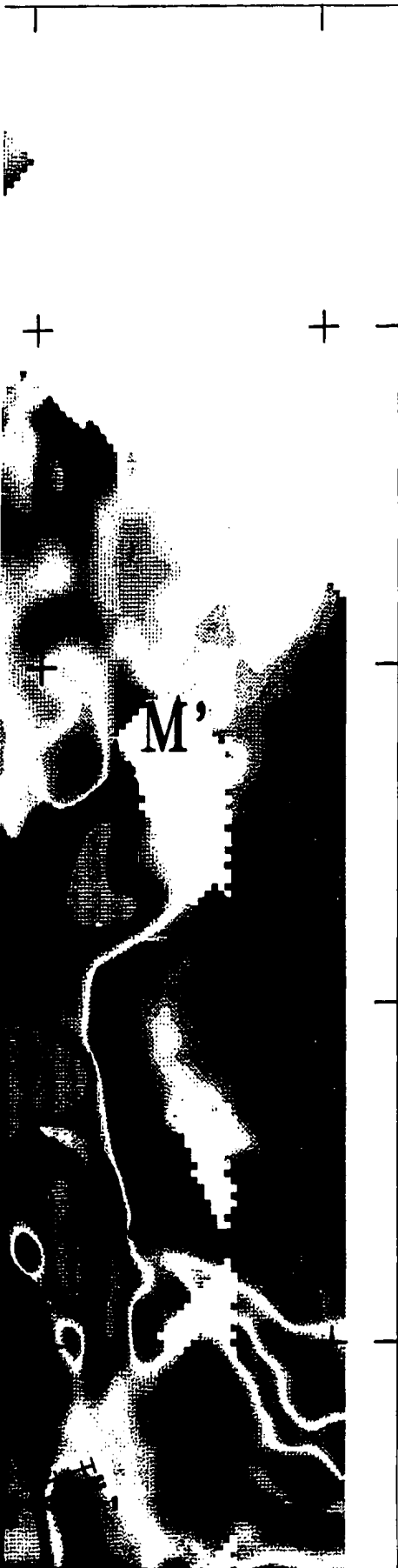
23° 30'

24°

1301
1280
1260
1244
1230
1220
1208
1198
1188
1180
1171
1163
1154
1148
1140
1132
1124
1118
1111
1103
1096
1088
1082
1075
1067
1059
1052
1044
1035
1026
1019
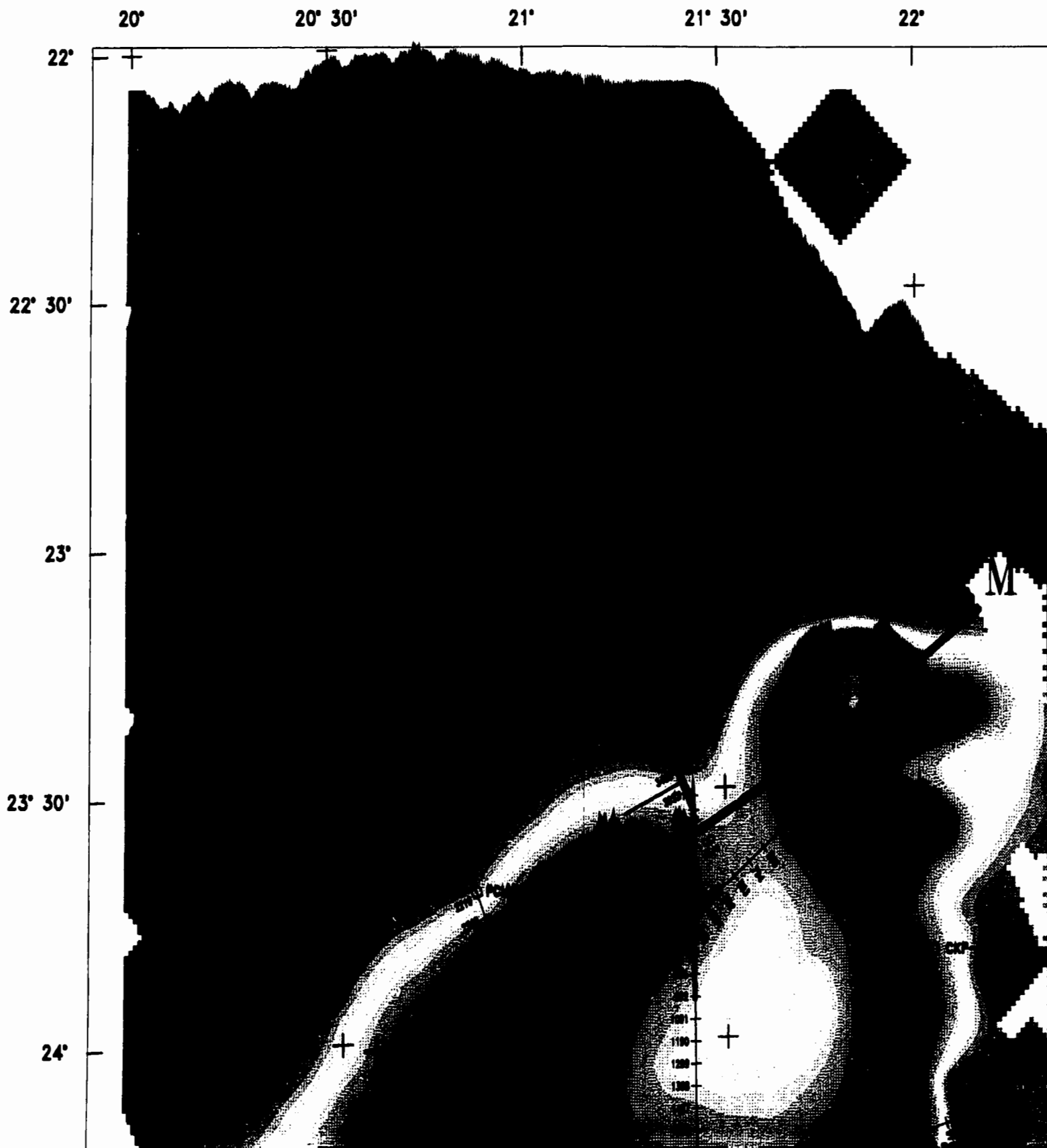
22° 30'

22° 30'

23°

M

23° 30'

24°

-95
-97
-100
-102
-103
-105
-106
-107
-109
-110
-111
-112
-113
-114
-115
-116
-117
-117
-118
-119
-120
-121
-122
-123
-124
-125
-125
-127
-128
-129

22° 30'

22° 30'

23°

M

23° 30'

24°

-95
-97
-100
-102
-103
-105
-106
-107
-109
-110
-111
-112
-113
-114
-115
-116
-117
-117
-118
-119
-120
-121
-122
-123
-124
-125
-125
-127
-128
-129
-130
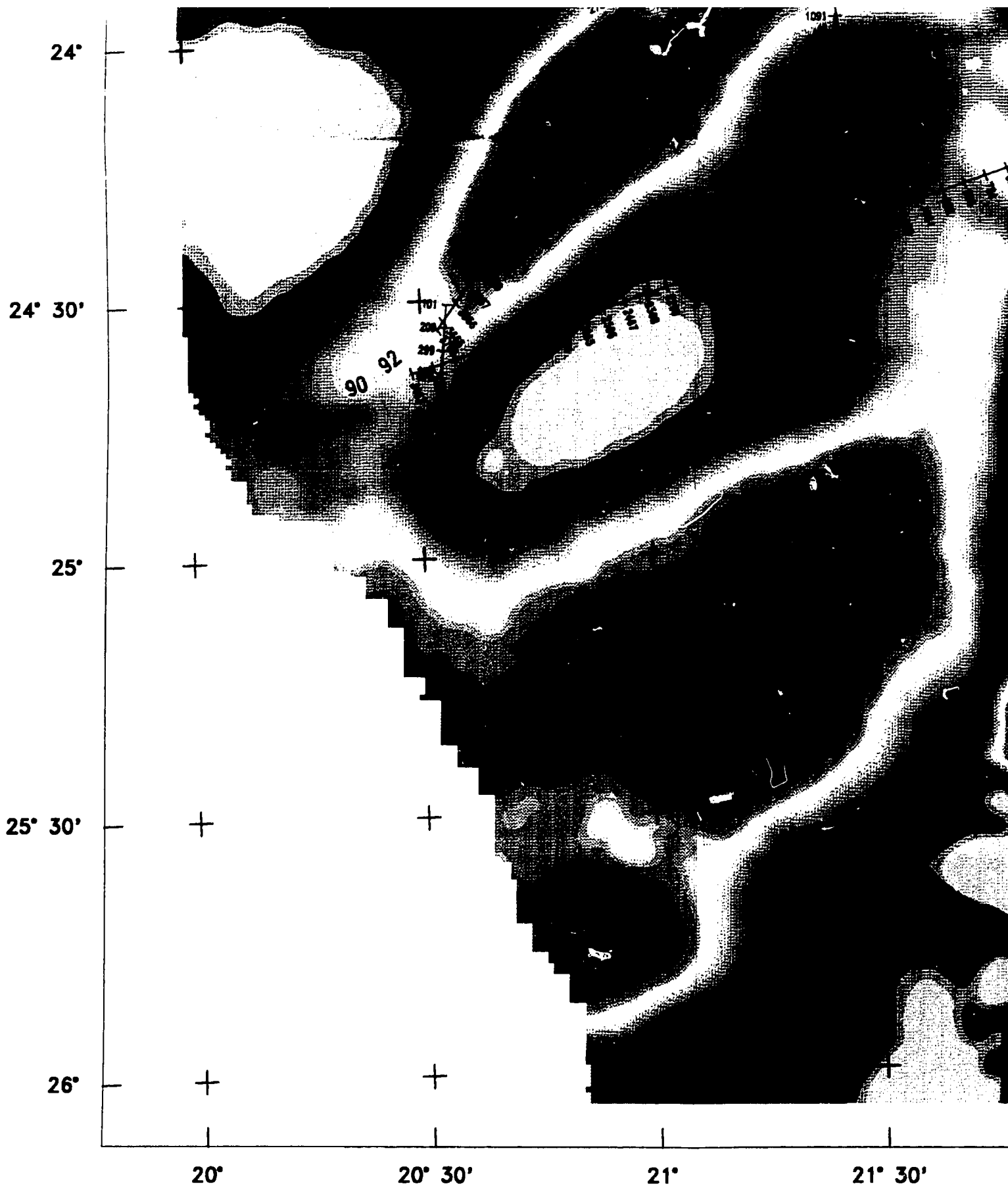
Figure 4.11(a) Magnetic total intensity anomaly map of the Nosop B
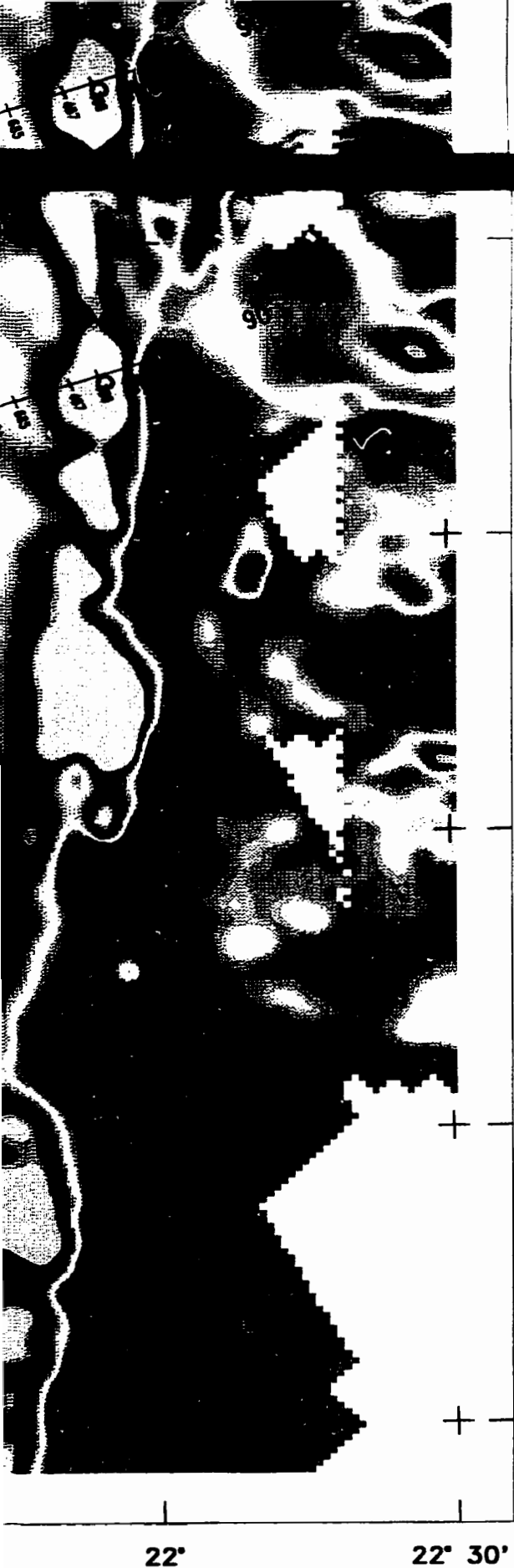
24°

24° 30'

25°

25° 30'

26°

22°   22° 30'

1047
1039
1032

1069
1063
1055
1047
1039
1032
1024
1014
995
982
967
950
931
898
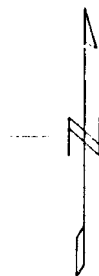
Total Field Intensit
(nT)

Scale 1:1000000

25000   0   25000

(metres)

Basin, western Botswana

24°

24° 30'

25°

25° 30'

22° 30'

26°

Botswana

1055
1047
1039
1032

1076
1069
1063
1055
1047
1039
1032
1024
1014
995
982
967
950
931
898

**Total Field Intensity
(nT)**
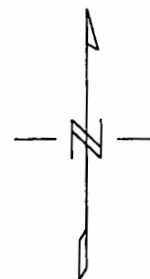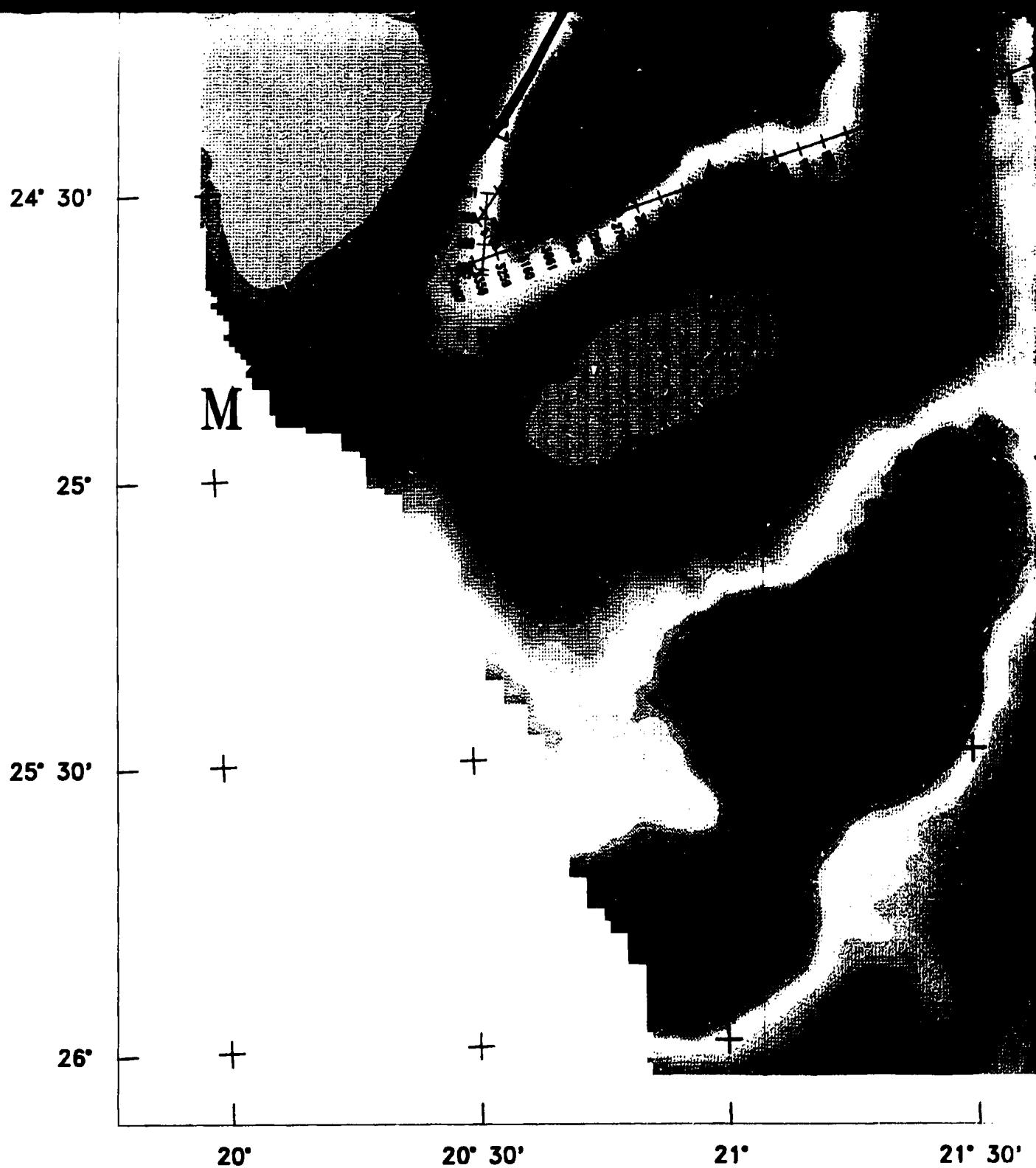
Scale 1:1000000

25000   0   25000   50000

(metres)
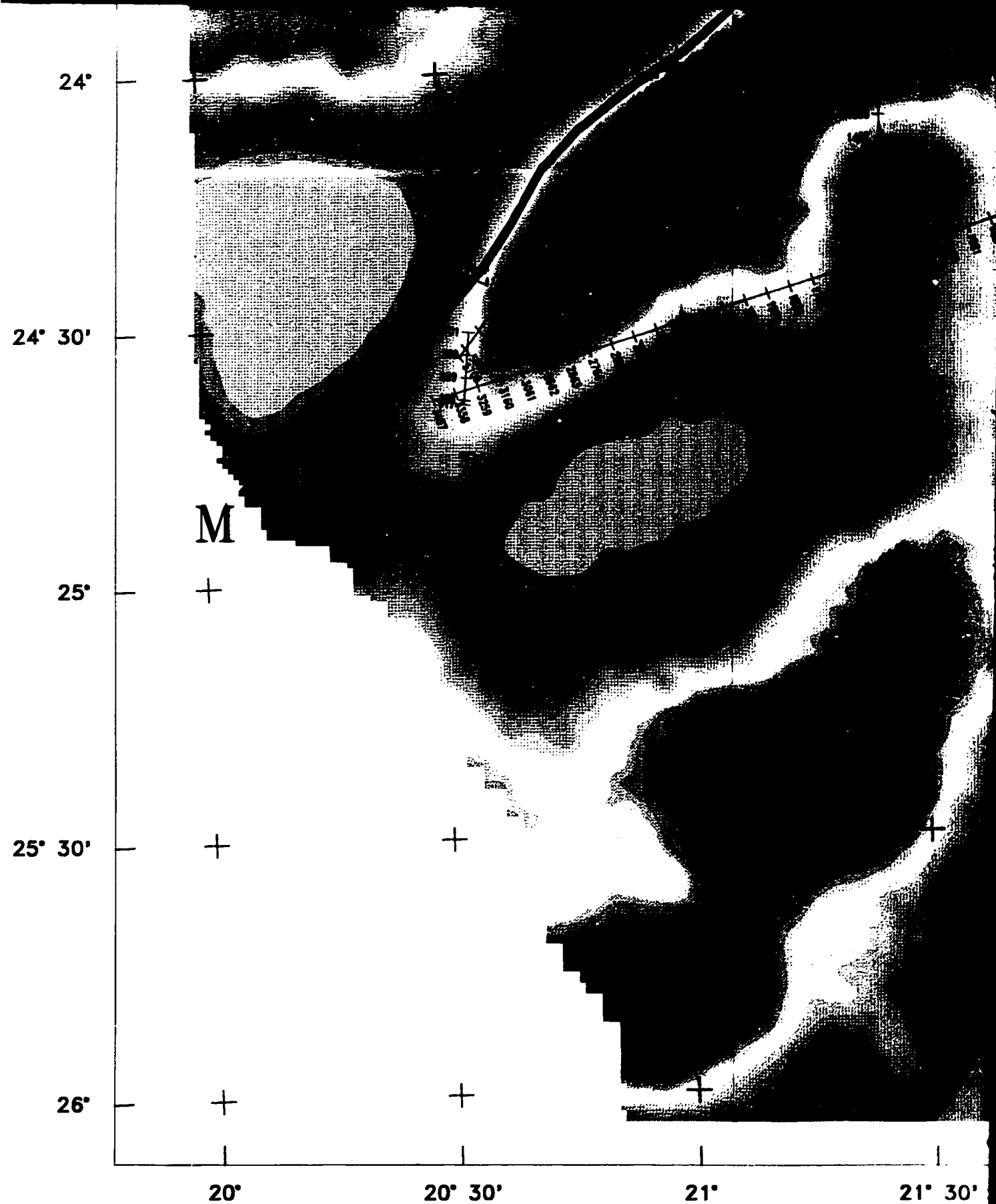
Figure 4.11(b) Reduction to the pole of the magnetic total inte
Nosop Basin, western Botswana; M-M' = Makga
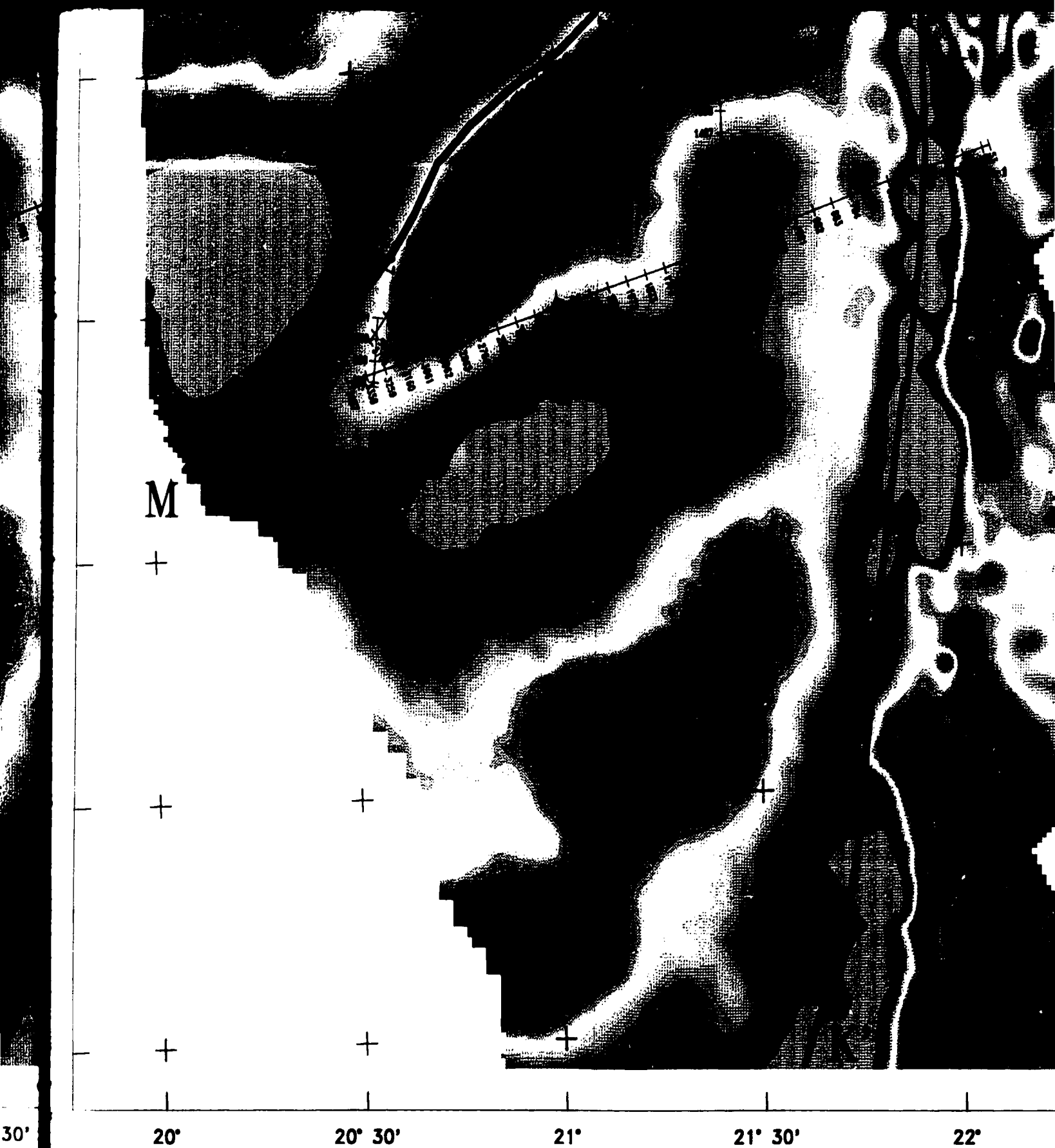
Figure 4.11(b) Reduction to the pole of the magnetic total intensity anomaly map o

Nosop Basin, western Botswana; M–M' = Makgadikgadi Line, K–K' =

24°

24° 30'

25°

25° 30'

26°

22° 30'

1059
1052
1044
1035
1026
1019
1009
998
977
963
946
927
906
869

**Total Field Intensity
(nT)**
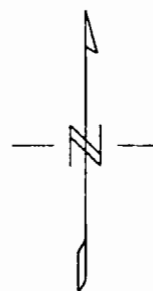
Scale 1:1000000

25000   0   25000   50000

(metres)

p of the

' = Kalahari Line
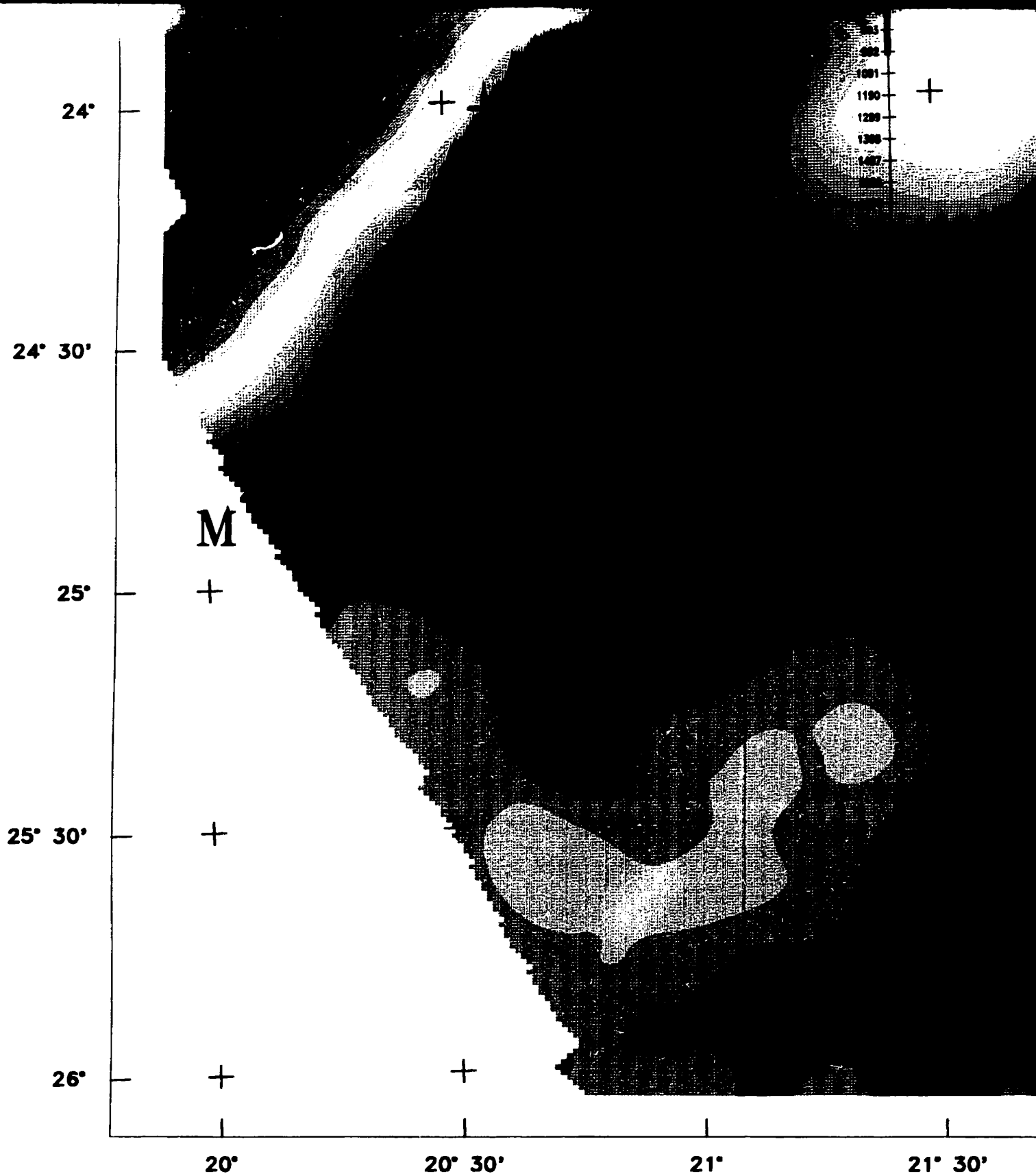
Figure 4.10   Bouguer anomaly map of the Nosop Basin, western
M—M' = Makgadikgadi Line, K—K' = Kalahari Line

Bouger Anomaly
(mgal)

Scale 1:1000000

(density = 2.67);

Figure 4.10   Bouguer anomaly map of the Nosop Basin, western Botswana (density = 2.?
M-M' = Makgadikgadi Line, K-K' = Kalahari Line.

24°

24° 30'

25°

25° 30'

26°

22° 30'

.67);
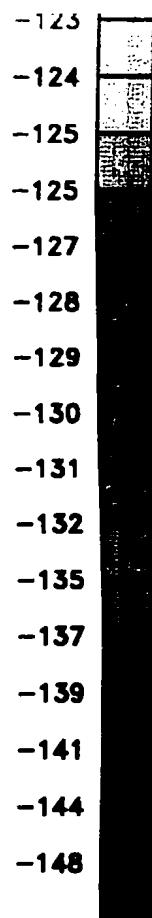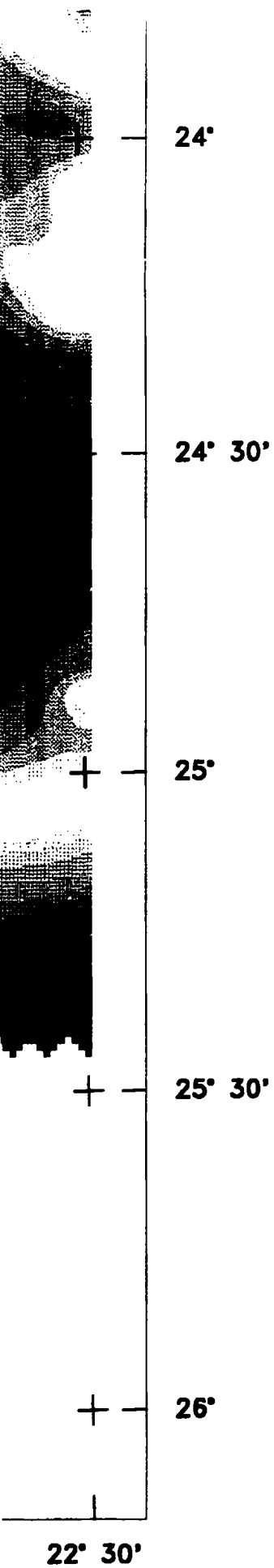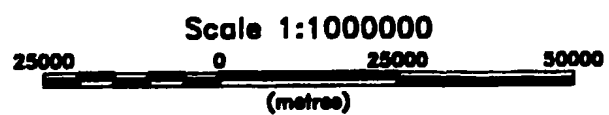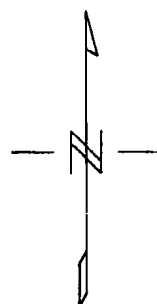
Figure 4.11(a) Magnetic total intensity anomaly map of the Nosop Basin, w

Figure 4.11(a) Magnetic total intensity anomaly map of the Nosop Basin, w

24° 30'

25°

25° 30'

26°

22°　　　　**22° 30'**

1032
1024
1014
995
982
967
950
931
898

Total Field Intensi
(nT)

Scale 1:1000000

25000　　　0　　　25000

(metres)

22° 30'

Botswana

24° 30'

25°

25° 30'

26°

22° 30'

Botswana

1039
1032
1024
1014
995
982
967
950
931
898

Total Field Intensity
(nT)

Scale 1:1000000

25000   0   25000   50000
(metres)

Figure 4.11(b) Reduction to the pole of the magnetic total inter Figu

y map of the

K–K' = Kalahari Line

24° 30'

25°

1026
1019
1009
998
977
963
945
927
906
869

Total Field Intensity
(nT)

25° 30'

26°

22° 30'

Scale 1:1000000

25000   0   25000   50000

(metres)
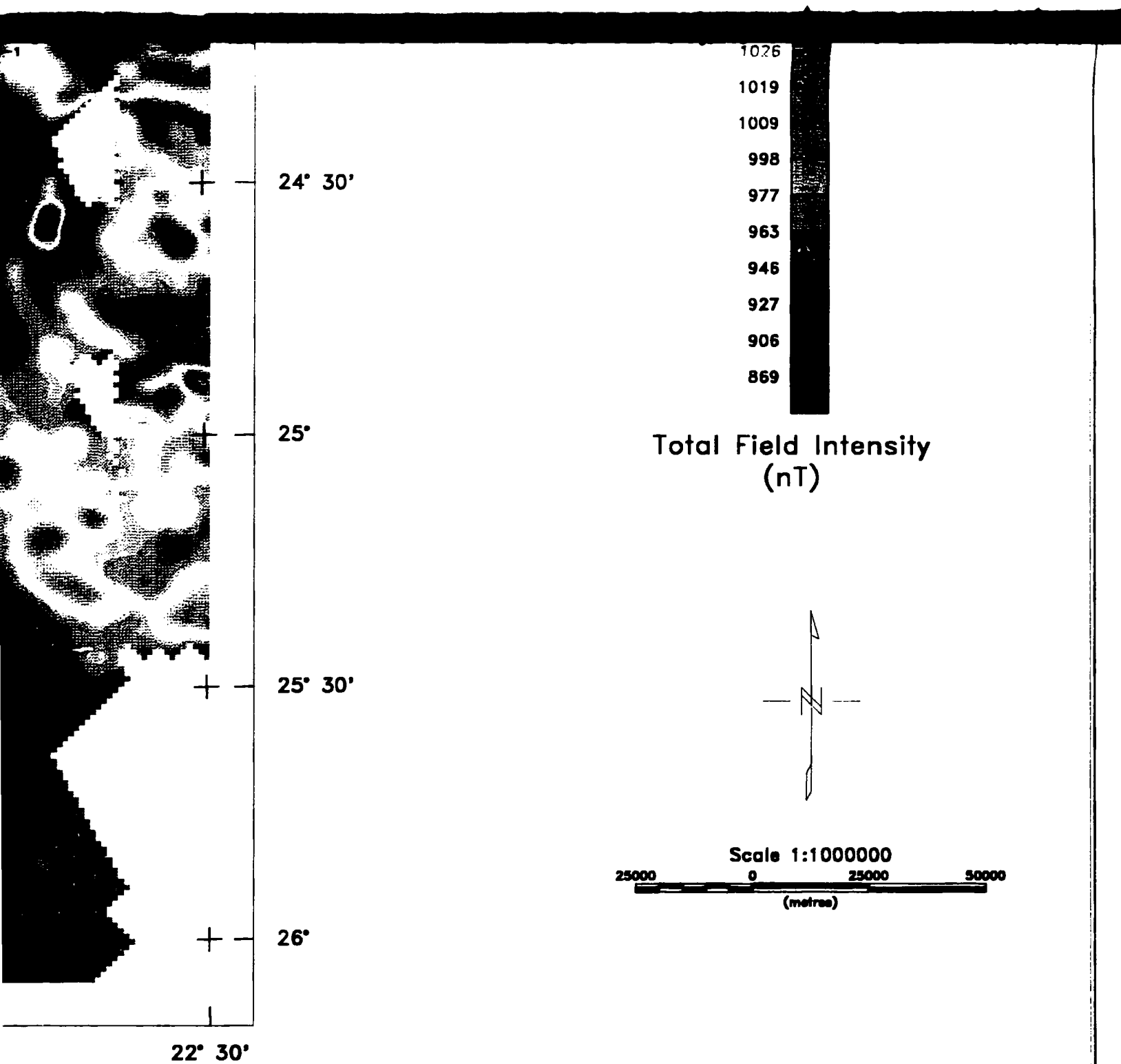
nap of the

-K' = Kalahari Line

Figure 4.10   Bouguer anomaly map of the Nosop Basin, western Botswa

M—M' = Makgadikgadi Line, K—K' = Kalahari Line

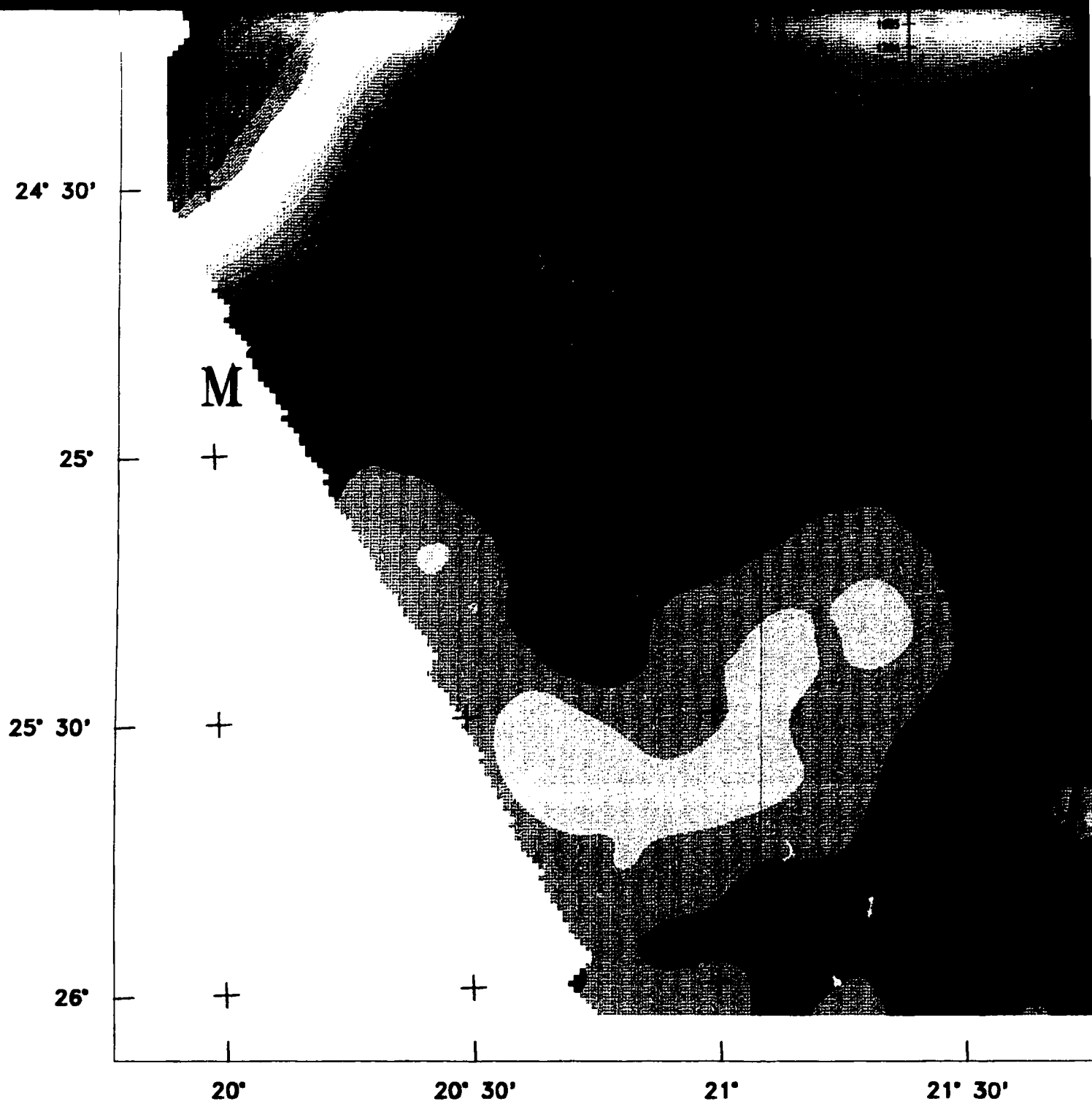Figure 4.10   Bouguer anomaly map of the Nosop Basin, western Bo

M—M' = Makgadikgadi Line, K—K' = Kalahari Line

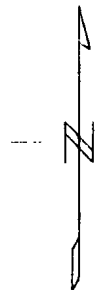otswana (density = 2.67);

24° 30'

−129
−130
−131
−132
−135
−137
−139
−141
−144
−148

Bouger Anomaly
(mgal)

25°

25° 30'

Scale 1:1000000

25000   0   25000

(metres)

26°

n Botswana (density = 2.67);

Figure 4.10   Bouguer anomaly map of the Nosop Basin, western Botswana (den
M–M' = Makgadikgadi Line, K–K' = Kalahari Line